

#27296579

C. 1

LIBRARY Michigan State University



This is to certify that the

dissertation entitled

## NONLINEAR VIBRATIONS OF A FLEXIBLE CONNECTING ROD

presented by

Shang-Rou Hsieh

has been accepted towards fulfillment of the requirements for

Ph.D. degree in Mechanical Engineering

Major professor

Date 7-26-91

MSU is an Affirmative Action/Equal Opportunity Institution

0-12771

PLACE IN RETURN BOX to remove this checkout from your record. TO AVOID FINES return on or before date due.

II _	DATE DUE	DATE DUE
033328		

MSU is An Affirmative Action/Equal Opportunity Institution

# NONLINEAR VIBRATIONS OF A FLEXIBLE CONNECTING ROD

 $\mathbf{B}\mathbf{y}$ 

Shang-Rou Hsieh

#### A DISSERTATION

Submitted to
Michigan State University
in partial fulfillment of the requirements
for the degree of

DOCTOR OF PHILOSOPHY

Department of Mechanical Engineering

#### ABSTRACT

# NONLINEAR VIBRATIONS OF A FLEXIBLE CONNECTING ROD

#### By

#### Shang-Rou Hsieh

An analytical and computer simulation investigation of the dynamic behavior associated with the flexible, uniform connecting rod of an otherwise rigid, in line, planar slider-crank mechanism is presented. The main goal is to analyze the flexural response of the elastic connecting rod and to study how this response depends on the system parameters. Moreover, this work emphasizes nonlinear analyses of the dynamic response and its associated stability.

Two different approaches are used in modeling the flexural vibration of the elastic connecting rod. In the first approach, the model used is general and includes the effects of finite axial and transverse deformations, internal material damping, bearing friction, slider friction, shear deformation and rotary inertia. The axial and the flexural vibrations are described by two nonlinear coupled partial differential equations. In the second approach, the flexural vibration of the connecting rod is described by a single nonlinear ordinary differential equation in the second approach which is obtained from the more general model

by a single mode Galerkin truncation. In deriving this equation, the effects of the shear deformation and rotary inertia are neglected. Moreover, the contribution of axial inertia is neglected in analyzing the acceleration components.

In studying the dynamic response of the connecting rod, the method of multiple scales is employed to solve the equations of motion. The slenderness ratio of the connecting rod is selected as the small scaling parameter. With the method of multiple scales, the solutions of the axial and the transverse deformations are solved as asymptotic series expansions in terms of this scale. In both of the approaches, several resonances, including the primary resonance, the principal parametric resonance, and various super- and sub- harmonic resonances, are investigated in detail. The analytical results are confirmed by the numerical solutions.

The analytical results show that the solutions and their associated stabilities depend in a nontrivial manner on several parameters. They are the ratios of the crank radius to the length of the connecting rod, the ratio of the connecting rod mass to the slider mass, the ratio of the crank speed to the fundamental frequency of flexural vibration, internal material damping, bearing friction and slider friction. The effects of these parameters on the flexural vibration of the connecting rod are investigated analytically and numerically.

To the members of my family.

#### **ACKNOWLEDGEMENTS**

I would like to take this opportunity to express my sincere gratitude to my thesis advisor and teacher, Steven W. Shaw, for his inspiring encouragement, advice and patience.

I would also like to thank the other committee members, Alan G. Haddow, C.Y. Wang and Joseph Whitsell, for their comments and help with this dissertation; and Ki-Yin Chang who helped me in installing the software package AUTO. I am indebted to Rong-Wong Chen for inspiring me to pursue Ph.D. degree in Michigan State University.

Finally, I thank my mother, brother, and my wife Shu-Mei for their support and understanding throughout my graduate study and research.

### **Contents**

1	Intr	roduction	1
	1.1	Description of the Problem	1
	1.2	Literature Survey	2
	1.3	Scope and Purpose	9
	1.4	Organization of Dissertation	10
2	Mat	thematical Modeling	11
	2.1	Basic Assumptions	11
	2.2	Equations of Motion	12
		2.2.1 Deformation	13
		2.2.2 Acceleration Components	15
		2.2.3 Stress-Strain Relation	17
		2.2.4 Equation of Motion	18
		2.2.5 Boundary Conditions	21
	2.3	Comparisons	22
	2.4	Nondimensionalization	25
3	Ana	alysis of the Distributed Parameter Model	29
	3.1	Application of the Method of Multiple Scales (MMS)	30
	3.2	Principal Parametric Resonance	41
	3.3	Primary Resonance $(\Omega pprox \omega_n)$	51

	3.4	Superharmonic Resonance $(\Omega \approx \frac{\omega_n}{2})$	59
	3.5	Superharmonic Resonance $(\Omega \approx \frac{\omega_n}{3})$	64
	3.6	Subharmonic Resonance $(\Omega \approx 3\omega_n)$	68
	3.7	Summary and Conclusion	72
		3.7.1 Effect of the Length Ratio $\xi$	72
		3.7.2 Effect of Mass Ratio S	74
		3.7.3 Effect of Damping Parameters $\mu_2$ , $\mu_3$ and $\mu_4$	77
		3.7.4 Effect of Shear Deformation and Rotary Inertia	83
4	Ana	alysis of the Lumped Parameter Model	86
	4.1	Equation of Motion	87
	4.2	Application of the Method of Multiple Scales	94
	4.3	Principal Parametric Resonance ( $\Omega \approx 2$ )	100
	4.4	Primary Resonance ( $\Omega \approx 1$ )	109
	4.5	Superharmonic Resonance $(\Omega \approx \frac{1}{2}) \dots \dots \dots \dots \dots$	116
	4.6	Superharmonic Resonance $(\Omega \approx \frac{1}{3}) \dots \dots \dots \dots \dots \dots$	119
	4.7	Subharmonic Resonance ( $\Omega \approx 3$ )	124
	4.8	Summary and Discussion	127
		4.8.1 Effect of the Length Ratio $\xi$	127
		4.8.2 Effect of the Frequency Ratio $\Omega$	128
		4.8.3 Effect of the Mass Ratio S	131
		4.8.4 Effect of the Damping Parameters $\mu_2$ and $\mu_4$	134
5	Coı	nparisons between Distributed and Lumped Parameter Models	141
	5.1	Primary Resonance $(\Omega \approx 1)$	141

	5.2	Principal Parametric Resonance $(\Omega \approx 2)$	143
	5.3	Superharmonic Resonance $(\Omega \approx \frac{1}{2}) \dots \dots \dots \dots \dots$	145
	5.4	Superharmonic Resonance $(\Omega \approx \frac{1}{3})$	145
	5.5	Subharmonic Resonance ( $\Omega \approx 3$ )	147
	5.6	Summary	148
6	Nun	nerical Solutions and Comparisons	150
	6.1	Influence of the Length Ratio $\xi$	151
	6.2	Influence of the Mass Ratio S	160
	6.3	Influence of the Friction Parameters $\mu_2$ and $\mu_4$	164
		6.3.1 Effect of the Damping Parameter $\mu_2$	164
		6.3.2 Effect of the Friction Parameter $\mu_4$	168
	6.4	Conclusions	172
7	Sun	nmary and Conclusions	177
A	Con	struction of the Linear Operator	182
В	Sup	erharmonic and Principal Parametric Resonances for $\xi=\epsilon\xi_1$	190
С	Solu	ation Procedure for the Case $\xi=\epsilon^2\xi_2$	194
D	Solu	ation Procedure for the Case $\xi = \epsilon^3 \xi_3$	199
E	Coe	fficients $f_7$ and $f_8$	204

## List of Tables

6.1	Identification of Combinations of Parameters	152
6.2	Comparison of Bifurcation Data	158
6.3	Limits of MMS and AUTO	175

## List of Figures

2.1	Displacement of the beam element	13
2.2	Geometry of the deflection curve	15
2.3	Slider crank mechanism with flexible connecting rod (undeformed state)	15
2.4	Slider crank mechanism with flexible connecting rod (deformed state)	16
2.5	Viscoelastic model (Kelvin-Voigt model)	18
2.6	Free body diagram for beam element	19
3.1	Frequency response equation for the principal parametric resonance	44
3.2	Frequency response equation for the principal parametric resonance	48
3.3	Frequency response equation for the primary resonance	53
3.4	Frequency response equation for the primary resonance	57
3.5	Frequency response equation for superharmonic resonance $(\Omega \approx \frac{\omega_n}{2})$	62
3.6	Influence of mass ratio S on the amplitude of superharmonic resonance $(\Omega \approx \frac{\omega_n}{2})$	64
3.7	Frequency response equation for superharmonic resonance $(\Omega \approx \frac{\omega_n}{3})$	68
3.8	Influence of S on the peak amplitude of the superharmonic resonance $(\Omega \approx \frac{\omega_n}{3})$	69
3.9	Influence of $\xi$ on the primary resonance	73
3.10	Influence of $\xi$ on the main nose of instability	73
3.11	Influence of S on the primary resonance	75
3.12	Influence of S on the main nose of instability	76
3.13	Influence of S on the principal parametric resonance	76
3.14	Influence of $\mu_2$ on the primary resonance	78

3.15	Influence of $\mu_2$ on the main nose of instability	78
3.16	Influence of $\mu_2$ on the principal parametric resonance	79
3.17	Influence of $\mu_3$ on the principal parametric resonance	80
3.18	Influence of $\mu_3$ on the primary resonance	81
3.19	Influence of $\mu_4$ on the superharmonic resonance $(\Omega \approx \frac{\omega_{1n}}{2})$	82
3.20	Influence of $\mu_4$ on the main nose of instability $(\Omega \approx 2\omega_{1n})$	82
3.21	Influence of $\mu_4$ on the principal parametric resonance $(\Omega \approx 2\omega_{1n})$	83
3.22	Influence of $\mu_4$ on primary resonance $(\Omega \approx \omega_{1n})$	84
3.23	Influence of shear deformation and rotary inertia on the primary resonance	85
3.24	Influence of shear deformation and rotary inertia on the principal parametric	
	resonance	85
4.1	Frequency response equation for the principal parametric resonance (equa-	
	tion [4.45])	102
4.2	Frequency response equation for the principal parametric resonance (equa-	
	tion [4.61])	107
4.3	Frequency response equation for the primary resonance (equation $[4.92]$ )	114
4.4	Frequency response equation for superharmonic resonance $(\Omega \approx \frac{1}{2})$	118
4.5	Frequency response equation for the superharmonic resonance $(\Omega\approx\frac{1}{3})$	121
4.6	Influence of $\xi$ on the primary resonance	129
4.7	Influence of $\xi$ on the principal parametric resonance	129
4.8	Influence of S on the primary resonance	131
4.9	Influence of S on the main nose of instability	133
4.10	Influence of S on the principal parametric resonance	133
4.11	Influence of S on superharmonic resonance $(\Omega \approx \frac{1}{2})$	134

4.12	Influence of S on superharmonic resonance $(\Omega \approx \frac{1}{3})$	135
4.13	Influence of $\mu_2$ on the primary resonance (equation [4.92])	136
4.14	Influence of $\mu_2$ on the main nose of instability	136
4.15	Influence of $\mu_2$ on the principal parametric resonance	137
4.16	Influence of $\mu_4$ on the primary resonance $(\Omega \approx 1)$	138
4.17	Influence of $\mu_4$ on superharmonic resonance $(\Omega \approx \frac{1}{2})$	139
4.18	Influence of $\mu_4$ on the main nose of instability $(\Omega \approx 2)$	139
4.19	Influence of $\mu_4$ on the principal parametric resonance $(\Omega\approx 2)$	140
6.1	Frequency response curves from MMS, LSODE and AUTO	151
6.2	Comparison between Analytical result with AUTO (case 5)	153
6.3	Comparison between Analytical result with AUTO (case 6)	153
6.4	Frequency response for cases 1, 4 and 7	154
6.5	Frequency response for cases 2, 5 and 8	156
6.6	Frequency response for cases 3, 6 and 9	156
6.7	Location of points $PD_1$ , $PD_2$ , $LP_1$ and $LP_2$	157
6.8	Comparison between simulation and analytical approximation for case 8	157
6.9	Comparison between simulation and analytical approximation for case $5$	159
6.10	Comparison between simulation and analytical approximation for case 9	159
6.11	Comparison between simulation and analytical approximation for case 6	160
6.12	Frequency response curves from AUTO (cases 4, 5 and 6)	161
6.1 <b>3</b>	Frequency response curves from AUTO (cases 7, 8 and 9)	161
6.14	Simulation results for cases 7 and 8	163
6.15	Nontrivial responses associated with the principal parametric resonance (cases	
	5 and 6)	163

6.16	Amplitude of the response at $\Omega = \frac{1}{2}$	164
6.17	Frequency response curves from AUTO (case 5 and 14)	165
6.18	Frequency response curves from AUTO (case 8 and 17)	165
6.19	Simulation results from LSODE (case 8 and 17)	166
6.20	Nontrivial responses associated with the principal parametric resonance (case	
	5 and 14)	167
6.21	Simulation results for cases 5 and 14	167
6.22	Frequency response curves from AUTO (cases 6 and 21)	168
6.23	Frequency response curves from AUTO (cases 8 and 23)	169
6.24	Nontrivial responses associated with the principal parametric resonance from	
	<b>AUTO</b> (cases 5 and 20)	169
6.25	Nontrivial responses associated with the principal parametric resonance from	
	<b>AUTO</b> (cases 6 and 21)	170
6.26	Frequency response for cases 7 and 22 from LSODE	171
6.27	Analytical approximation and simulation results for case 7	171
6.28	Analytical approximation and simulation results for case 22	172
6.29	Frequency response curve for case 10	173
6.30	Nontrivial responses associated with the principal parametric resonance (case	
	4)	174
6.31	Nontrivial responses associated with the principal parametric resonance (case	
	7)	174

## LIST OF SYMBOLS

A	cross-sectional area of the connecting rod
	the amplitude function of the nth mode of the flexural response
$A_n$	
Å <sub>abs</sub> k'	absolute acceleration of the element on the moving frame
	shear-deflection coefficient
L	the length of the connecting rod
M	resultant bending moment
N	resultant axial force
Q	resultant shear force
S	mass ratio (= slider mass/mass of connecting rod)
$T_0, T_1, T_2$	new time independent variables
u(x,t),v(x,t)	the axial and transverse displacements, respectively
α	angle between the median line and the the x-axis
$lpha_1$	dimensionless parameter related to the slenderness ratio
$lpha_2$	dimensionless parameter related to the effect of shear deformation
$lpha_3$	dimensionless parameter related to the effect of rotary inertia
$\Delta_1, \Delta_4$	dimensionless parameter related to the quadratic nonlinearity
$\Delta_2$ , $\Delta_5$	dimensionless parameter related to the cubic nonlinearity
$\Delta_{3}$	dimensionless parameter related to shear deformation and rotary inertia
$\epsilon$	a small, constant parameter
γ	shear angle
$\eta$	the slenderness ratio of the connecting rod
$\Lambda_1$	amplitude of the particular solution of $v_{1n}$
$\Lambda_{21},\Lambda_{22},\Lambda_{23}$	amplitude of the particular solution of $v_{2n}$
$\mu_b \; (\mu_3)$	bearing damping
$\mu_c \; (\mu_2)$	internal viscoelastic material damping
$\mu_s~(\mu_4)$	friction coefficient
Ω	frequency ratio $\left(=\frac{\omega}{\omega_{1t}}\right)$
$\omega$	operating frequency of the crank shaft
$\omega_{1t}$	first flexural natural frequency of the connecting rod
$\omega_{m{n}}$	the natural frequency of the n-th mode flexural vibration
$\pi$	constant (=3.1415926)
ρ	mass density (mass/volume) of the connecting rod
$\sigma_1,\sigma_2$	detuning parameter of the frequency
$\sigma_{xx},\sigma_{xy}$	normal, shear stresses, respectively
θ	bending angle
$\xi, \xi_1, \xi_2, \xi_3$	length ratio

#### Chapter 1

#### Introduction

#### 1.1 Description of the Problem

In this dissertation, we study the flexural vibration associated with the flexible connecting rod of an otherwise rigid, in-line, planar slide crank mechanism. This problem is equivalent to finding the flexural response associated with a simply supported beam subjected to (1) the motion of foundation which arises from the motion of the crank shaft, (2) axial load arising due to the friction force applied to the slider end and the inertial force of the slider mass, (3) a distributed load which arises from the inertial loading and is applied along the span of the beam, and (4) concentrated frictional moments arising due to the presence of bearing friction.

One of the traditional approaches to the dynamic analysis of mechanisms is based on the assumption that the system is composed of rigid bodies. In fact, a mechanism is defined as "an assembly of rigid bodies, connected by movable joints, to form a closed kinematic chain with one link fixed and having the purpose of transforming motion" [32]. Based on this definition, the early works in the dynamics of mechanisms concerned themselves with deriving the displacements, velocities, accelerations, ... etc, of the mechanism. A basic concept of kinematic analysis is to determine the maximum acceleration of the machine member as a function of the input characteristics. The dynamic analysis includes the derivation of

inertial forces resulting from the rigid-body accelerations found from the kinematic analysis. However, the rigid body assumption may not always hold. As required by modern industry, machinery often needs to operate at high speed while maintaining accurate performance. Due to their inherent flexibility, machine elements deflect when subjected to external loads and/or internal forces. An increase of the operating speed results in increased inertial forces; this increase of the the inertial forces can cause sever deformation of the machine members even without the action of external loads. In other words, inertial loading arising due to the high operating speed can be responsible for link deformation and associated vibrational behavior. Also, link members are being designed to be of smaller mass in order to reduce inertial loads, but this often leads to increased flexibility and thus flexural vibrations. Hence, the traditional rigid linkage analysis is insufficient to provide a satisfactory prediction and description of the function of these mechanisms. Recognizing these shortcomings of rigid body analysis, the idea of kineto-elastodynamics has been introduced [17, 27], which is the study of the motion of mechanisms consisting of elements that deform due to external loads or internal forces. Basically, kineto-elastodyanmics is a field combining kinematics, dynamics and elasticity together. A study of high-speed mechanisms with flexible links requires knowledge of this field. Among the mechanisms commonly used, the slider-crank mechanism may be the simplest. The simplicity of of the structure of the slider-crank makes it useful as a beginning example, especially when only one linkage, the connecting rod, of the mechanism is assumed to be flexible. This mechanism is also of practical interest to the automotive, manufacturing, and agricultural industries.

#### 1.2 Literature Survey

The slider-crank mechanism, in which the connecting rod is considered to be a flexible

member, has been investigated by several authors. In the following, we would like to review some of the fundamental works by previous investigators. For more complete information, please refer to the review articles[27, 17, 26, 45]. The methods employed in studying the elastic mechanism problem can be grouped into the following categories: the finite element method, experimentation and analytical methods.

The basic idea in studying this problem with the finite element method is to model each member of the flexible mechanism as discrete system with a finite number of degrees-offreedom. Therefore, each member can be divided into several small discrete elements. The motion associated with each individual element is described by a set of ordinary differential equations. Finally, each element equation is assembled together and form the global equations of motion describing the motion of the whole mechanism. The advantage of finite element method is that it provides a systematic and easy-to-apply procedure in modeling the mechanism. Winfrey[51, 52] was among the first investigators who applied the finite element methods to study elastic mechanism problem. The application of the finite element method in studying elastic mechanisms was limited by lack of computational powers, in the early 1970s, because of the vast manipulation of the matrices associated with each element and the assembling procedure. With the advent of the high-speed computers, the finite element method has become more popular recently. In order that the finite element method be applied to solve the elastic motion of the mechanisms, the continuous motion of the system is modeled as a sequence of structure configurations at discrete crank angles upon which the inertial loading is imposed. In order to solve these structures with finite element methods, the rigid body motion associated with these instantaneous structures must be removed from the model to avoid singular matrices. Winfrey[51, 52] accomplished this by directly applying the principle of conservation of momentum to the complete mechanism. Imam et al. [25],

Midha et al.[1] and Gandhi et al.[18] considered the crank as a cantilever beam to avoid this complication. Nath and Ghosh [28] removed the rigid-body degree of freedom from the global matrices using a matrix decomposition approach. Concerning the formulation of the equations of motion, two different approaches are employed: the stiffness and the flexibility methods. Winfrey[51, 52] employed the displacement finite element method (the stiffness technique of structural analyses) to study the elastic motion of mechanisms. This approach yields directly the nodal displacements and requires displacement compatibility on interelement boundaries. Midha et al.[2] applied this approach to study the dynamic response of a flexible member of a four-bar linkage. Erdman et al.[4, 3] employed flexibility method of structural analysis to study flexible mechanisms. With this approach, adjacent elements have equilibrating stress distributions on inter-element boundaries and the global degrees of freedom are the stress components. Turcic et al. [48, 47, 13] studied the elastic mechanism problem by using a general procedure in formulating the equations of motion, including the effects of rigid-body motion and elastic coupling terms. Instead of a single type of finite element, they generalized the procedure so that different types of finite elements can be included in the same mechanism. The axial force is solved for by using a quasi-static analysis, and is then included in the transverse component of the equation of motion by the introduction of the geometrical stiffness matrix. The effects of elastic coupling terms are included by adding the geometric stiffness matrix to the element stiffness matrix. This approach is equivalent to modeling the deformation associated with the connecting rod by von Karman's finite deformation theory. Cronin and Liu[12] studied the linear vibration of a connecting rod in a planar slider-crank mechanism by using the finite element analysis software NASTRAN. The steady state responses associated with the connecting rod are investigated with different combinations of parameters. Their results show that superharmonic resonances can be observed when the operating frequency is near to one third or one half of the flexural natural frequencies associated with the connecting rod.

Unlike the finite element method, analytical methods treat each individual flexible member associated with the mechanism as a single continuous system. Assuming that only one of the members is flexible, the motion of the flexible member in an otherwise rigid mechanism is described by a set of partial differential equations which, under some circumstances, can be converted into ordinary differential equations by modal truncation. The major analytical methods applied in these investigations are: Newtonian dynamics[15], Hamiltonian methods[49], variational methods[44, 43, 42] and lumped mass approaches[35, 36, 34]. We note that the last two methodologies, especially the variational principle approach, are equivalent to the finite element method. Some of the related fundamental works are outlined below.

Neubauer, Cohen and Hall[5] examined the transverse deflection of the elastic connecting rod of the slider-crank mechanism by neglecting the longitudinal deformation, the Coriolis, relative tangential, and relative normal components of acceleration. They showed that the amplitude of the transverse vibration increases when the the dynamical axial load approaches the Euler criterion for static buckling of long, slender columns. They also pointed out that a more thorough analysis of the response requires a more complete study which includes the following dimensionless parameters: the ratio of crank speed to natural frequency of flexural vibration, the ratio of connecting rod mass to slider mass, and the ratio of crank radius to connecting rod length. By the Method of Averaging, and assuming a small length ratio, Jasinski, Lee and Sandor[30, 31] investigated the dynamic stability of a flexible connecting rod in a slider-crack mechanism. In the first paper, they studied the slider-crank mechanism for which a concentrated mass is assumed to be attached to one end

of the connecting rod. In the second paper, the connecting rod is assumed to be hinged at each end, an unrealistic assumption. Both longitudinal and transverse deflections are considered, and the coupled linear equations describing the motion are obtained from the force and moment balance of a differential element. Linearization of these equations was accomplished by neglecting the nonlinear coupling terms. Assuming a one-term product solution, they obtain two coupled, nonhomogeneous Mathieu equations. Finally, they use the Routh-Hurwitz criterion investigate the stable regions, and the associated steady-state solutions of the transverse and axial deflections are given. Their results showed that the amplitude of the transverse responses depends upon the frequency ratio quadratically, while the axial response is not so sensitive to this parameter. Moreover, the vibration amplitudes increases as the mass ratio increases. They pointed that future work in this area should include elastic stability analyses using similar asymptotic methods and include the effects of the nonlinear coupling terms. Viscomi and Avre [49] examined the nonlinear bending response of the connecting rod. Assuming that the inertia force from axial deflection is negligible, the axial dynamic force is approximated by solving the so-called reduced equation. With this axial force, the transverse equation is reduced to a single ordinary differential equation by the Galerkin method. The resultant equation is then studied numerically. They showed that, within the frequency range of interest, the second mode is relatively unimportant and the response is closely approximated by the first mode dynamics. By comparing the responses from the linear and nonlinear equations, it was concluded that the system is not adequately defined by the linear form of the equation. Moreover, the existence of multiple steady state solutions was also observed in some parameter regions. They pointed out that the response depends on the following dimensionless parameters: the frequency ratio, the mass ratio, the length ratio, transverse damping and the external piston force. With the same assumptions, Chu and Pan[11] carried out a similar study by use of the Kantorovich method and the method of weighted residual. The final governing equations are studied numerically. Their results show the the effect of small viscous damping on longitudinal vibration is small and can be neglected. Moreover, a sudden increase in the amplitude of the steady state response accompanied with a small increase of the operating frequency, i.e. the jump phenomenon, has also been observed. Using variational principles, Thompson and Ashworth [43] studied a planar slider-crank mechanism mounted on a foundation subjected to a motion normal to the mechanism plane. They found that the combination resonances can be observed when the sum or the difference of the operating and foundation frequencies are approximately equal to the flexural natural frequencies associated with the connecting rod. By applying regular perturbation method to Euler-Bernoulli and Timoshenko beam models, Badlani and Kleinhenz [8] considered the dynamic stability of the undamped elastic connecting rod of an in-line slider-crank, and compared the results from each approach. Their results indicated that new regions of instability exist when both the rotary inertia and the shear deformation are included in the analysis. Tadjbakhsh[41] introduces in a general method for obtaining a single partial differential equation describing the transverse vibration of an undamped elastic link of a mechanism which contains evolutes only, using a two-parameter perturbation approach. The final dimensionless Hill's equation is obtained by assuming a sinusoidal shape function and using Galerkin's method. His result shows that contributions from the second mode and higher mode amount to less than one percent. Zhu and Chen[54] studied the stability of the response of the connecting rod by using a regular perturbation technique. A linear, undamped, nonhomogeneous partial differential equation is used to described the transverse response based on Euler-Bernoulli beam theory. Using this equation and Galerkin's method, they obtain a set of decoupled homogeneous Hill's

equations. After reducing these to Mathieu equations, a first-order Floquet approach was used to obtain the two highest p-periodic and 2p-periodic instability regions. Badlani and Midha[9] studied the effect of internal material damping on the dynamic response behavior of a slider-crank mechanism by using the regular perturbation method. Both steady-state and transient solutions were determined and compared to those results obtained from the undamped connecting rod. They concluded that the viscous internal material damping may have significant influence, both favorable and adverse, on the steady-state and transient transverse responses. Sandor and Zhuang[37] studied a planar four-bar mechanism by using a linearized lumped parameter approach. The effects of rotary inertia and end mass are included in their investigation. A set of nonlinear ordinary differential equations describing the dynamic behavior of the mechanism is derived based on the lumped mass approach. These equations are then linearized and decoupled by using the concept of kinematic influence coefficients. The resultant equations are solved by using a finite difference approach. Their investigation shows that the linearized approach is sufficient in representing the dynamic response, and that the rotary inertia and end mass of the moving link have considerable effect on the elastic response of the mechanisms.

In addition to the analytical and computational works describe above, some experimental works has been carried out [6, 7, 40, 19]. Golebiewski and Sadler[19] determined the bending stress at the midpoint of the elastic connecting rod analytically and experimentally for a model derived by a lumped parameter approach using d'Alembert's principle and Euler-Bernoulli beam theory. They examined the effects of the crank speed, crank length, and slider offset on the maximum bending stress at the midpoint of the connecting rod. Superharmonic responses appeared in both the analytical and experimental results. Sutherland[40] studied a fully elastic planar four-bar mechanism analytically and experimental

mentally. By using Euler-Lagrange formulation and modal analysis with only one mode, the dynamic behavior associated with the mechanism is described by a set of ordinary differential equations with two holonomic constraints. The resultant equations are then simplified by neglecting the shear deformation, rotary inertia, joint frictions, bearing mass and all the external forces except the torque required to keep the mechanism operating at a constant speed. These equations were linearized based on the assumption that the deflections associated with each elastic member are small. Consequently, the resultant equations describing the dynamic behavior associated with the mechanism are three coupled, linear, nonhomogeneous ordinary differential equations with time-varying coefficients. The Method of Harmonic Balance is then applied to solve these equations. He pointed out that length ratios and frequency ratios are the essential dimensionless parameters for this investigation. An experimental study was carried out to support the analytical work. High order superharmonic resonances were observed in the experiments. His results indicated that the modal analysis using only a single mode is sufficient to represent the dynamic response of the mechanism.

#### 1.3 Scope and Purpose

All previous investigations lead to a nonhomogeneous Mathieu equation to describe the transverse vibration, and only linear stability analyses were provided. The existence of superharmonic, subharmonic and combination resonances have been observed both in simulations and experiments [49, 11, 19, 40]. An analytical study of the overall nonlinear response, especially dealing with the superharmonic, subharmonic responses, and their associated stability, is lacking. It is the purpose of this study to provide such an investigation of the vibration associated with the flexible connecting rod of a planar slider-crank mech-

anism. Moreover, this work will focus on the nonlinear analysis of the dynamic response, e.g., primary, principal parametric, superharmonic resonances and their stability.

#### 1.4 Organization of Dissertation

This dissertation is organized as follows. Chapter 2 contains the basic assumptions and the derivation of the partial differential equations used to describe the system. Chapter 3 provides the analysis of the partial differential equations obtained in chapter 2 by using the method of multiple scales. In chapter 4, we simplify the model by using von Karmon's finite deformation theory and obtain an ordinary differential equation describing the flexural vibration associated with the first flexural mode of the connecting rod. We then analyze this ordinary differential equation by using the method of multiple scales. Chapter 5 contains a detailed comparison between the results obtained in chapters 3 and 4. In chapter 6, we compare the results obtained in chapter 4 with numerical simulations. In chapter 7, we close this dissertation with some conclusions and some suggestions for future investigations.

In the course of this study, extensive use was made of the computer assisted symbolic manipulation program  $Mathematica^{TM}$ . This was essential in the lengthy calculations involved in the perturbation procedures.

#### Chapter 2

### **Mathematical Modeling**

In this chapter, equations describing the rotary, axial and transverse dynamic responses associated with a flexible connecting of an otherwise rigid slider crank mechanism are derived. The basic assumptions which are used in deriving these equations of motion are given in section 2.1. Based on these assumptions in section 2.2, we then proceed to derive the equations describing the axial as well as the transverse deflections associated with the connecting rod, and the boundary conditions associated with these equations. In section 2.3, we compare the resultant equations to the models which were used by previous investigators. We then convert the equations of motion and their associated boundary conditions into dimensionless form in order to minimize the number of the system parameters in section 2.4.

#### 2.1 Basic Assumptions

In deriving the equations which describe the axial and the transverse deflections associated with the flexible connecting rod, the following assumption are employed:

- Concerning the connecting rod AB
  - 1. is an elastic member with uniform cross section

- 2. all quantities are assumed to be independent of z, the out-of-plane coordinate
- 3. plane cross section remain plane after deformation
- 4. made of a viscoelastic material
- 5. simply-supported at both ends, with rotary damping at the pivot ends (to model bearing effects)
- 6. point C on rod AB moves to point C', after deformation,
- 7. shear deformation and rotatory inertia are included
- Concerning the crank element OA:
  - 1. perfectly rigid
  - 2. constant crank speed,  $\omega$
- Concerning the slider mass D:
  - 1. no clearance
  - 2. no offset
  - 3. velocity-dependent friction force acting between the slider and its contact surface
  - 4. no external forces applied to the piston.

#### 2.2 Equations of Motion

In the present section, equations describing the axial and transverse deflections associated with the flexible connecting rod are derived based on the assumptions given in section 2.1. This problem is equivalent to a simply supported beam subjected to the inertia forces associated with its motion as specified by the kinematic constraints. These inertia forces are caused by the acceleration associated with the connecting rod. We first analyze the acceleration components of a point located on the flexible connecting rod. We then proceed to derive the equations of motion describing the axial and transverse deformations of the connecting rod following the work of Chow[10]. By combining these results, we obtain the equations describing the axial and transverse deflections associated with the connecting rod subjected to the inertia forces.

#### 2.2.1 Deformation

We now consider a segment of the beam with length  $\Delta x$  taken from the connecting rod as shown in figure 2.1. After deformation, the angle between the median line and the x-axis

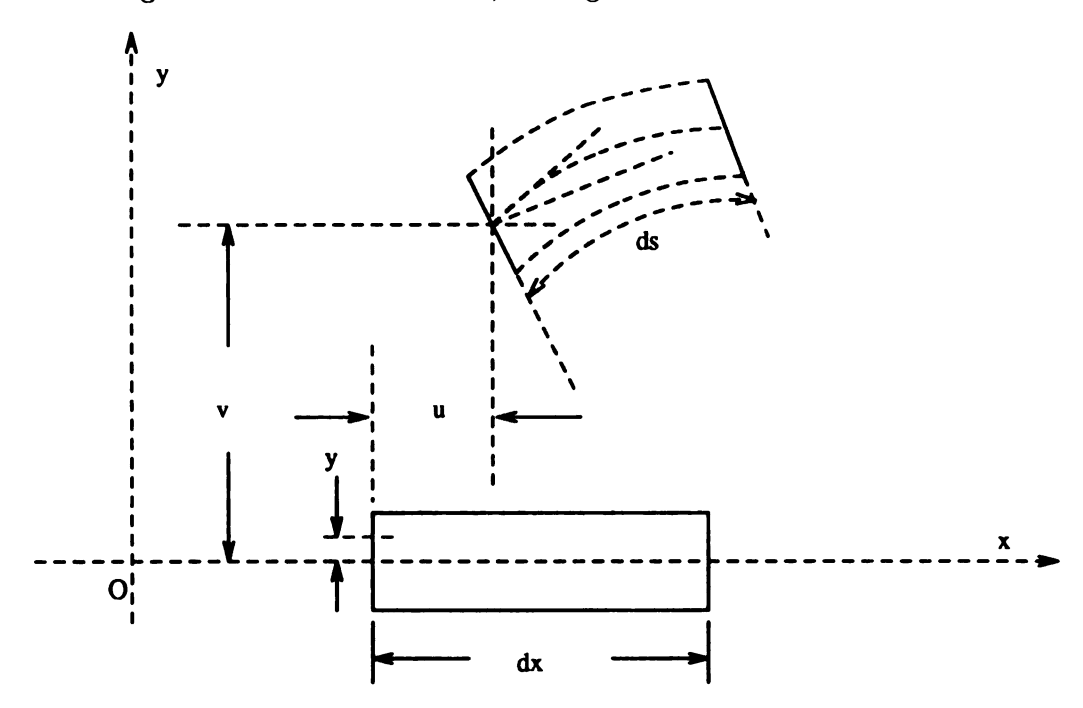


Figure 2.1: Displacement of the beam element

is given as

$$\alpha = \theta + \gamma \tag{2.1}$$

where  $\theta$  = the bending angle and  $\gamma$  = the shear angle. Let a material point located at (x,y)

in the undeformed state move to (x', y') after deformation. Therefore, we have

$$x' = x + u - y \sin \theta \tag{2.2}$$

$$y' = v + y \cos \theta \tag{2.3}$$

where u(x,t) and v(x,t) are the displacements of the median line along the x and y directions, respectively. The length of an undeformed line element (dx,0) in the deformed state is given by

$$ds = \sqrt{dx^2 + dy^2}$$

$$= \sqrt{[v_x + (y\cos\theta)_x]^2 + [1 + u_x - (y\sin\theta)_x]^2} dx \qquad (2.4)$$

where a subscript x stands for the partial derivative of the corresponding function with respect to the spatial variable x. The relative elongation in the x-direction is defined as

$$e = \frac{ds}{dx} - 1 = \sqrt{v_x^2 + (1 + u_x)^2} - 1 - y\theta_x = e_0 - y\theta_x$$
 (2.5)

where  $e_0$  is the relative elongation of the median line. From the geometry of the deflection curve as shown in Figure 2.2, we also have

$$\tan \alpha = \frac{v_x}{1+u_x}, \qquad (2.6)$$

$$\sin \alpha = \frac{v_x}{1+e_0}, \qquad (2.7)$$

$$\cos \alpha = \frac{1+u_x}{1+e_0} \tag{2.8}$$

where  $e_0$  is implicitly defined in equation (2.5).

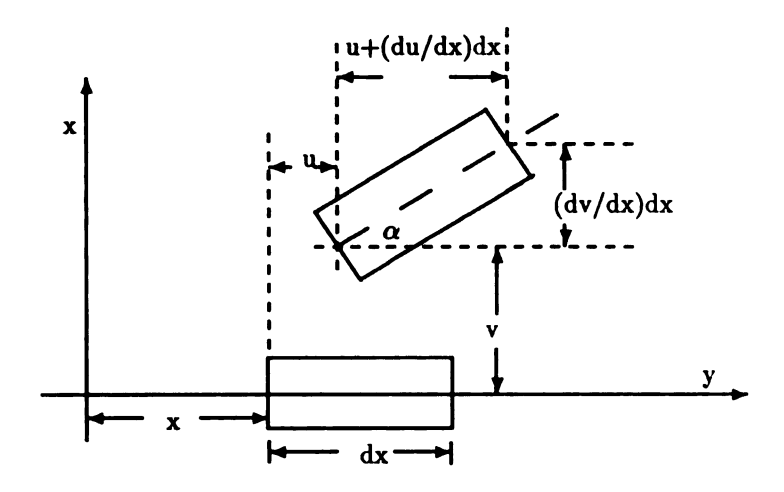


Figure 2.2: Geometry of the deflection curve

#### 2.2.2 Acceleration Components

With the assumptions given in section 2.1, we now proceed to derive equations which describe the axial and transverse vibrations associated with the connecting rod AB. Consider a slider-crank mechanism as shown in Figure 2.3. The reference frames OXY and

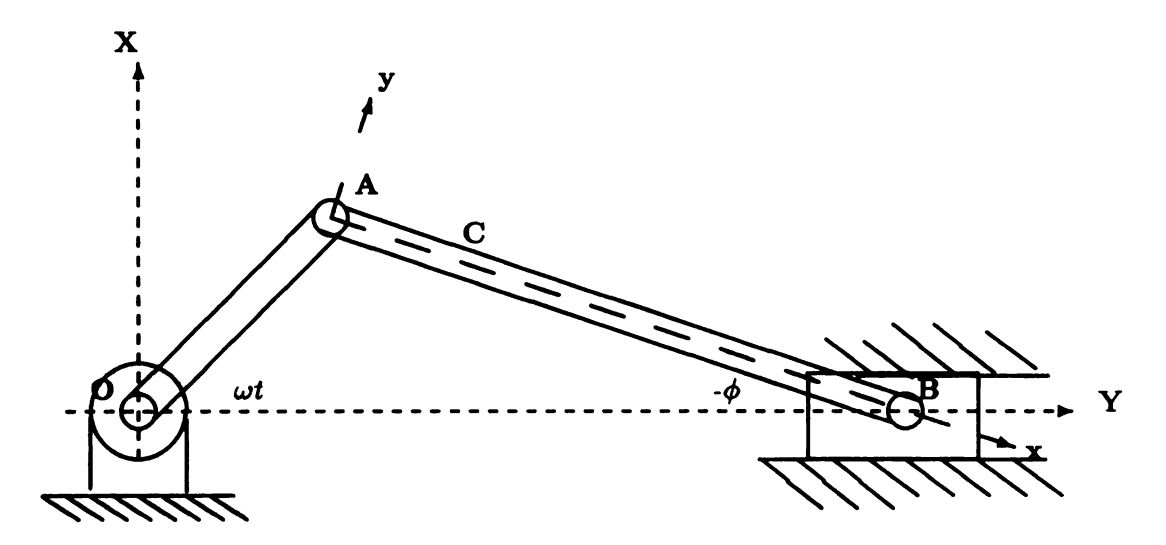


Figure 2.3: Slider crank mechanism with flexible connecting rod (undeformed state)

oxy represent the fixed and moving coordinate systems associated with this slider-crank mechanism, respectively. Let u(x,t) and v(x,t) represent the axial and transverse displace-

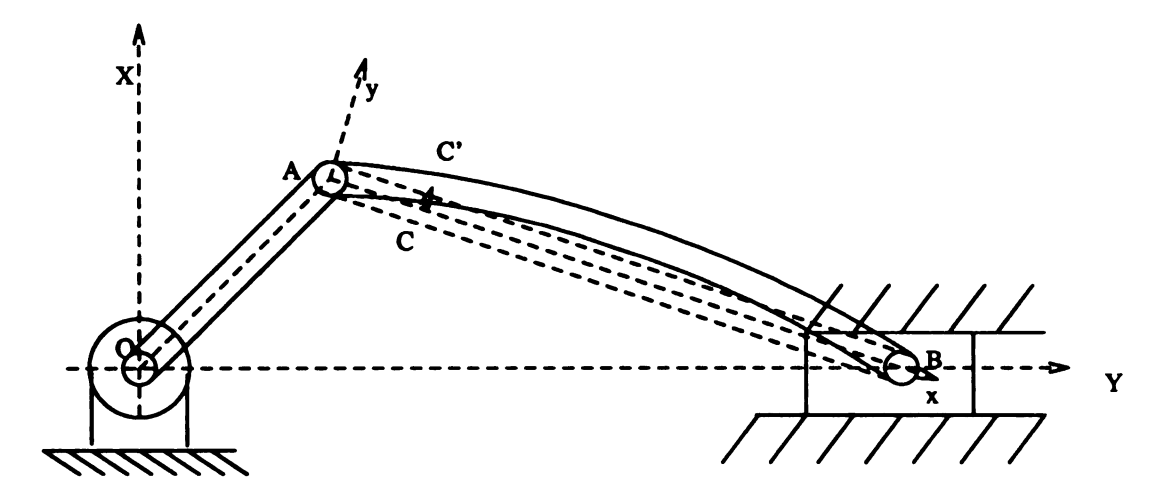


Figure 2.4: Slider crank mechanism with flexible connecting rod (deformed state)

ments of the connecting rod measured in the moving coordinate system, respectively. The moving coordinate system (i.e., oxy) is shown in Figure 2.3 with its origin located at the connecting point on the rigid crank and its x-axis always passing through the ends of the elastic coupler. We now consider a point C located with (x,0) in the moving frame, which moves to point C' after deformation (Figure 2.4). Modeled by the embedded geometric constraint method[33, 53], the position vector  $\bar{\mathbf{r}}$  of point C' can be expressed as

$$\bar{\mathbf{r}} = (x+u)\bar{\mathbf{i}} + v\bar{\mathbf{j}} \tag{2.9}$$

where i and j are the unit vectors along the x- and y-axes, respectively. The deviation of the acceleration components begins with the following well- known result from dynamics[20, 23]:

$$\bar{\mathbf{a}} = \bar{\mathbf{A}}_{abs} + \bar{\omega} \times (\bar{\omega} \times \bar{\mathbf{r}}) + \bar{\omega}_t \times \bar{\mathbf{r}} + \bar{\mathbf{r}}_{tt} + 2\bar{\omega} \times \bar{\mathbf{r}}_t = a_x \bar{\mathbf{i}} + a_y \bar{\mathbf{j}}$$
(2.10)

which allows the absolute acceleration of a point to be written in terms of a moving frame of reference and where

 $\bar{a} = absolute$  acceleration component seen from a fixed coordinate system,

 $\bar{\mathbf{A}}_{abs} = \text{absolute acceleration of the moving frame},$ 

 $\bar{\mathbf{r}}$  = position vector for a particle as reviewed from the moving frame, and is defined in equation (2.9),

 $\bar{\omega}$  = angular velocity of the moving frame.

Substituting equation (2.9) into equation (2.10), we obtain

$$a_x = -r\omega^2 \cos(\omega t - \phi) + u_{tt} - \phi_t v_t - \phi_{tt} v - \phi_t^2 (x + u)$$
 (2.11)

$$a_{y} = -r\omega^{2} \sin(\omega t - \phi) + \phi_{tt}^{2}(x + u) + 2\phi_{t}u_{t} + v_{tt} - \phi_{t}^{2}v$$
 (2.12)

where a subscripts t presents the partial derivative of the corresponding function with respect to the time variable, r is the length of the crank shaft,  $\phi$  represents the angle between OA and OB, measured counter-clockwise,  $a_x$  and  $a_y$  are the acceleration components along the x- and y- axes, respectively.

#### 2.2.3 Stress-Strain Relation

In this section, we consider the relationship between stress and strain. We assume that the connecting rod is made of a viscoelastic material which can be described by models built from discrete elastic and viscous elements. In this work, we assume that the connecting rod is made of a the Kelvin-Voigt material which is modeled as shown in Figure 2.2.3. Therefore, the stress-strain-time relationship for this material is given by

$$\sigma = Ee + \mu_c e_t \tag{2.13}$$

where  $\sigma$  is the normal stress, and e is the strain, E is the elastic spring constant, and  $\mu_c$  is the dashpot coefficient. Based on this, we obtain the following equations for normal stress

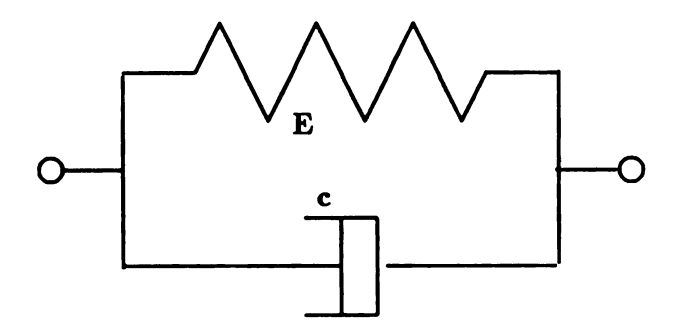


Figure 2.5: Viscoelastic model (Kelvin-Voigt model)

 $\sigma_{xx}$  and shear stress  $\sigma_{xy}$ :

$$\sigma_{xx} = Ee + \mu_c e_t = Ee_0 - Ey\theta_x + \mu_c e_{0t} - \mu_c y \theta_{xt} , \qquad (2.14)$$

$$\sigma_{xy} = G\gamma. (2.15)$$

Now, we express the axial force N, bending moment M and shear force Q according to

$$N = \int_{A} \sigma_{xx} dA = EAe_0 + \mu_c Ae_{0_t}$$
 (2.16)

$$M = \int_{A} \sigma_{xx} y dA = -EI\theta_{x} - \mu_{c} I\theta_{xt} \qquad (2.17)$$

$$Q = \int_{A} \sigma_{xy} dA = k' G A \gamma \qquad (2.18)$$

where A is the cross-sectional area, I is the area moment of the inertia of cross section, k' is the shear-deflection coefficient, a modifying factor introduced by Timoshenko[46].

#### 2.2.4 Equation of Motion

Consider the free body diagram shown in Figure 2.6, from which the equations of motion are obtained by considering the balances of forces and bending moments. From this, we

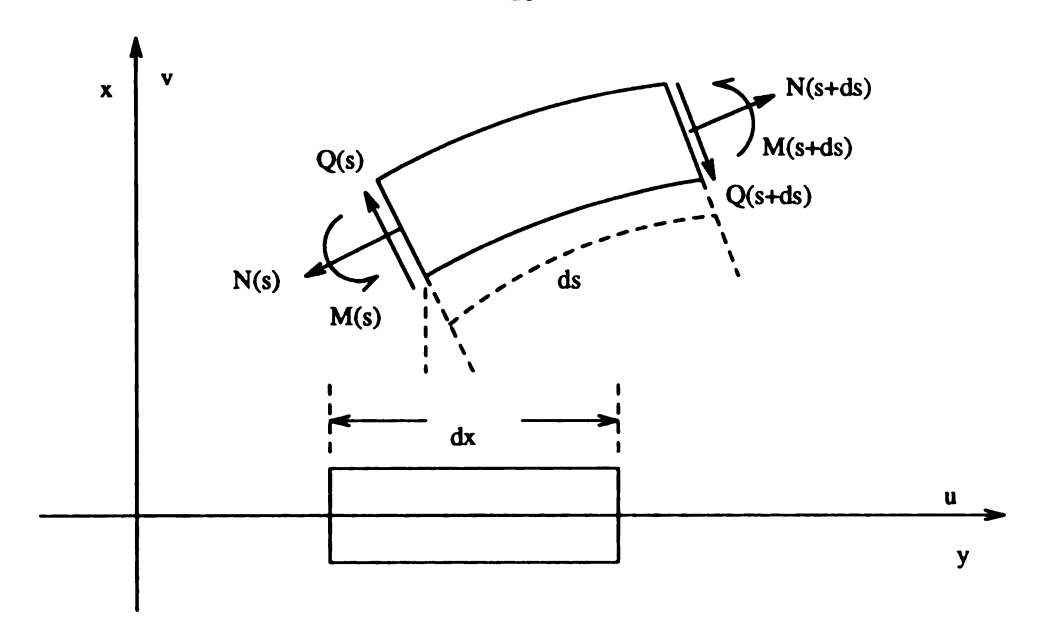


Figure 2.6: Free body diagram for beam element

obtain the following equations:

$$(N\cos\alpha)_x - (Q\sin\theta)_x = \rho A a_x , \qquad (2.19)$$

$$(N \sin \alpha)_x + (Q \cos \theta)_x = \rho A a_y , \qquad (2.20)$$

$$M_x - Q(1+e_0)\cos(\alpha-\theta) = -J\theta_{tt}$$
 (2.21)

where the acceleration components  $a_x$  and  $a_y$  are defined by equation (2.11) and (2.12),  $\rho$  stands for the density (mass per unit volume) of the connecting rod, and J is the mass moment of inertia per unit length. We note the these equations are expressed in terms of eight unknowns, namely N, M, Q,  $\alpha$ ,  $\theta$ , u, v and  $e_0$ . We now proceed to transform these equations into a form in which only the displacements and forces are involved. With equations (2.18), (2.6), (2.7) and (2.8), equation (2.21) reduces to

$$Q = \frac{J\theta_{tt} - EI\theta_{xx} - \mu_c I\theta_{xxt}}{v_x \sin\theta + (1 + u_x)\cos\theta}.$$
 (2.22)

In deriving this equation, we assume that I, E, and  $\mu_c$  are all independent of x. From equation (2.1) and (2.18), we have

$$\alpha = \theta + \gamma = \theta + \frac{Q}{k'AG} \ . \tag{2.23}$$

Equations (2.16) and (2.8) yield

$$N = EAe_0 + \mu_c Ae_{0_t} = EA(\frac{1+u_x}{\cos \alpha} - 1) + \mu_c A(\frac{1+u_x}{\cos \alpha} - 1)_t.$$
 (2.24)

Substituting equations (2.24) and (2.22) into equation (2.19), we obtain

$$EA[(1+u_x) - \frac{1+u_x}{\sqrt{v_x^2+(1+u_x)^2}}]_x + \mu_c A[(1+u_x) - \frac{1+u_x}{\sqrt{v_x^2+(1+u_x)^2}}]_{xt} - \left[\frac{J\theta_{tt} - EI\theta_{xx} - \mu_c I\theta_{xxt}}{v_x + (1+u_x)\cot\theta}\right]_x = \rho Aa_x.$$
 (2.25)

Equations (2.16) and (2.7) yield

$$N = EAe_0 + \mu_c Ae_{0_t} = EA(\frac{v_x}{\sin \alpha} - 1) + \mu_c A(\frac{v_x}{\sin \alpha} - 1)_t.$$
 (2.26)

Substituting equations (2.26) and (2.22) into equation (2.20), we obtain

$$EA[v_{x} - \frac{v_{x}}{\sqrt{v_{x}^{2} + (1 + u_{x})^{2}}}]_{x} + \mu_{c}A[v_{x} - \frac{v_{x}}{\sqrt{v_{x}^{2} + (1 + u_{x})^{2}}}]_{xt} + \left[\frac{J\theta_{tt} - EI\theta_{xx} - \mu_{c}I\theta_{xxt}}{v_{x}\tan\theta + (1 + u_{x})}\right]_{x} = \rho Aa_{y}.$$
(2.27)

Substituting equations (2.24), (2.22) and (2.23) into equation (2.6), we obtain

$$\tan\left(\theta + \frac{J\theta_{tt} - EI\theta_{xx} - \mu_c I\theta_{xxt}}{k'AG[v_x \sin\theta + (1 + u_x)\cos\theta]}\right) = \frac{v_x}{1 + u_x}.$$
 (2.28)

Equations (2.25), (2.27) and (2.28) describe the rotational, axial and transverse defections associated with the flexible connecting rod.

#### 2.2.5 Boundary Conditions

In the present section, we consider the boundary conditions associated with equations (2.25), (2.27) and (2.28). We first consider the boundary conditions applied to the connection point on of the crank shaft. Since the crank shaft is assumed to be perfectly rigid and there is no relative displacement of the connection between the connecting rod and the crank shaft, we must have

$$u(0,t) = 0, (2.29)$$

$$v(0,t) = 0. (2.30)$$

Due to the presence of the frictional moment at point A from the bearing, we have

$$EI\theta_{x}(0,t) + \mu_{b}I\theta_{xt}(0,t) = -M_{A} = \mu_{b}(\omega - \phi_{t} - v_{xt}(0,t))$$
 (2.31)

where  $\mu_b$  represents the friction coefficient, and the moment applied by the bearing is the product of  $\mu_b$  and the relative rotational speed. We now consider the boundary conditions applied to the sliding end to which a mass  $m_4$ , the piston, is attached. At point B, the piston motion is constrained to move along the X direction. Therefore, we have

$$v(L,t) = -u(L,t)\tan\phi. \tag{2.32}$$

Because of the presence of the bearing at point B, there exists a frictional moment at this

point. Therefore, at point B, we have

$$EI\theta_{x}(L,t) + \mu_{b}I\theta_{xt}(L,t) = -M_{B} = \mu_{b}(-\phi_{t} + v_{xt}(L,t)), \qquad (2.33)$$

where the bearing friction law from point A is again employed. We now apply Newton's second law to the slider mass  $m_4$  and obtain the following condition:

$$(N\cos\alpha - Q\sin\theta)\cos(-\phi) + (N\sin\alpha + Q\cos\theta)\sin(-\phi)$$

$$+ m_4 a_x \cos(-\phi) + m_4 a_y \sin(-\phi)$$

$$+ \mu_s Z_t + \mu_s u_t \cos(-\phi) + \mu_s v_t \sin(-\phi) = 0$$
 (2.34)

where  $\mu_s$  is the slider friction coefficient and  $Z_t$  stands for the rigid motion of the slider mass. We note that there are two slider friction forces in equation (2.34). The  $(\mu_s Z_t)$  term represents the friction force caused by rigid body motion, while  $[\mu_s u_t \cos(-\phi) + \mu_s v_t \sin(-\phi)]$  stands for the friction force due to the elastic deformation.

## 2.3 Comparisons

In the present section, we compare the equations of motion obtained in section 2.2 to the models used by other investigators in studying the dynamic response associated with the flexible connecting rod of a slider crank mechanism. Regarding the acceleration components, there is no difference between our approach and other's. Therefore, we shall focus on the beam theory used to model the connecting rod.

If the effect of shear deformation and rotary inertia terms are neglected in our formula-

tion, we have  $\alpha = \theta$  and

$$Q = -EI\theta_{xx} - \mu_c I\theta_{xxt} . (2.35)$$

Moreover, if we assume that the relative elongation of the median lines is very small compared to unity, then equation (2.19) becomes

$$EA[(1+u_x) - \cos \theta]_x + A\mu_c[(1+u_x) - \cos \theta]_x - (Q\sin \theta)_x = \rho Aa_x, \qquad (2.36)$$

and equation (2.20) becomes

$$EA[(1+u_x)\tan\theta-\sin\theta]_x+(Q\cos\theta)_x=\rho Aa_y. \qquad (2.37)$$

Since the relative elongation of the median line is assumed to be very small compared with unity, we also have

$$\sin \theta = v_x \tag{2.38}$$

from equation (2.7). Moreover, we assume that  $\theta$  is very small so that the last equation can be reduced to

$$\theta \approx v_x$$
. (2.39)

Based on this, equation (2.35) becomes

$$Q = -EIv_{xxx} - I\mu_c v_{xxxt}. (2.40)$$

Substituting equations (2.39) and (2.40) into equations (2.36) and (2.37), we obtain the

following equations:

$$\rho A a_x = E A (u_x + \frac{1}{2} v_x^2)_x + A \mu_c (u_x + \frac{1}{2} v_x^2)_x , \qquad (2.41)$$

$$\rho A a_y = E I v_{xxxx} + \mu_c I v_{xxxxt} - (E - \mu_c) A [(u_x + \frac{1}{2}v_x^2)v_x]_x. \qquad (2.42)$$

This derivation is mainly based on the von Karmons finite deformation theory. These two equations were used by previous investigators[9] in studying the dynamic behavior associated with the connecting rod. Viscomi[49] applied this model without considering the effects of internal material damping  $\mu_c$ . In chapter 4, we will use equations (2.41) and (2.42), together with the work by Viscomi to study the flexural response associated with the connecting rod. We now consider the model used by Badlani *et al.*[8]. Linearizing equation (2.1) and neglecting the effects of internal material damping  $\mu_c$ , we obtain

$$\theta + \frac{Q}{k'AG} = v_x \tag{2.43}$$

or

$$Q = k'AG(v_x - \theta). (2.44)$$

Linearizing equation (2.16), we obtain

$$N = EA u_x. (2.45)$$

Substituting equations (2.44) and (2.45) into equations (2.19) to (2.21) and linearizing the resultant equations, we obtain

$$EAu_{xx} = \rho Aa_x, \qquad (2.46)$$

$$Q_x = \rho A a_y, \tag{2.47}$$

$$EI\theta_{xx} + Q = \rho I\theta_{tt} \tag{2.48}$$

where the mass moment of inertia J is expressed as  $J = \rho I$ . Substituting equation (2.44) into equations (2.46) and (2.47), we obtain

$$EI\theta_{xx} + k'AG(v_x - \theta) = \rho I\theta_{tt}, \qquad (2.49)$$

$$k'AG(v_x - \theta)_x = \rho A v_{tt}. \tag{2.50}$$

These two equations were used by Badlani et al.[8] in studying the dynamic behavior associated with the flexible connecting rod. This derivation is mainly based on Timoshenko's beam theory.

### 2.4 Nondimensionalization

We now convert the equations and their associated boundary conditions into dimensionless form in order to minimize the number of system parameters. To achieve this, we introduce the following dimensionless parameters:

$$\begin{split} \bar{u} &= \frac{u}{L}, \ \bar{v} = \frac{v}{L}, \ \bar{x} = \frac{x}{L}, \ \xi = \frac{r}{L}, \ S = \frac{m_4}{\rho A L}, \ \eta^2 = \frac{I}{A L^2}, \\ \omega_{1t}^2 &= \frac{E I \pi^4}{\rho A L^4}, \ \Omega = \frac{\omega}{\omega_{1t}}, \ \bar{t} = \omega_{1t} t, \ \mu_2 = \frac{\mu_c \omega_{1t}}{2E}, \\ \mu_3 &= \frac{\mu_b \pi^4}{2\rho A L^3 \omega_{1t}}, \ \mu_4 = \frac{\mu_s}{2\rho A L \omega_{1t}}, \ \alpha_2 = \frac{E}{k' G}, \alpha_3 = \frac{J}{\rho I}. \end{split}$$

Before we proceed to convert equations (2.25), (2.27) and (2.28) into dimensionless form, let us explain the physical meanings of these parameters. The parameter  $\xi$  is the ratio of

the throw length of the crank shaft to the length of the connecting rod, which is referred to hereafter as the length ratio. The parameter S is the ratio of the mass of the connecting rod to the mass of the slider, and is specified as the mass ratio. The parameter  $\eta$  represents the slenderness ratio of the connecting rod. The parameter  $\alpha_2$  is associated with the effects of shear deformation. The parameter  $\alpha_3$  is associated with the effects of rotary inertia. The parameter  $\Omega$  is the ratio of the operating frequency to the first flexural natural frequency of the connecting rod,  $\omega_{1t}$ , and is referred to as the frequency ratio. The parameter  $\mu_2$  represents the damping effects of the internal material damping acting on the connecting rod. The parameter  $\mu_3$  represents the damping coefficients of the bearing friction applied to the joints at point B and C. The parameter  $\mu_4$  is used to model the friction force acting between the slider and its contact surface. With these dimensionless parameters, equation (2.25) becomes, after dropping the overbars for notational convenience,

$$[(1+u_{x}) - \frac{(1+u_{x})}{\sqrt{(1+u_{x})^{2}+v_{x}^{2}}}]_{x} + 2\mu_{2}[(1+u_{x}) - \frac{1+u_{x}}{\sqrt{(1+u_{x})^{2}+v_{x}^{2}}}]_{xt}$$

$$- \alpha_{3}\eta^{4}\pi^{4}[\frac{\theta_{tt}}{(1+u_{x})\cot\theta+v_{x}}]_{x} + \eta^{2}[\frac{\theta_{xx}}{(1+u_{x})\cot\theta+v_{x}}]_{x}$$

$$+ 2\mu_{2}\eta^{2}[\frac{\theta_{xx}}{(1+u_{x})\cot\theta+v_{x}}]_{xt}$$

$$= \eta^{2}\pi^{4}[-\xi\Omega^{2}\cos(\Omega t - \phi) + u_{tt} - 2\phi_{t}v_{t} - \phi_{tt}v - \phi_{t}^{2}(x+u)], \quad (2.51)$$

equation (2.27) becomes

$$[v_{x} - \frac{v_{x}}{\sqrt{(1+u_{x})^{2}+v_{x}^{2}}}]_{x} + 2\mu_{2}[v_{x} - \frac{v_{x}}{\sqrt{(1+u_{x})^{2}+v_{x}^{2}}}]_{xt}$$

$$+ \eta^{4}\pi^{4}\alpha_{3}[\frac{\theta_{tt}}{(1+u_{x})+v_{x}\tan\theta}]_{x} - \eta^{2}[\frac{\theta_{xx}}{(1+u_{x})+v_{x}\tan\theta}]_{x}$$

$$- 2\mu_{2}\eta^{2}[\frac{\theta_{xx}}{(1+u_{x})+v_{x}\tan\theta}]_{xt}$$

$$= \eta^{2}\pi^{4}[-\xi\Omega^{2}\sin\Omega t - \phi + \phi_{tt}(x+u) + 2\phi_{t}u_{t} - v_{tt} - \phi_{t}^{2}v], \qquad (2.52)$$

and equation (2.28) becomes

$$\tan\left(\theta + \alpha_2 \eta^2 \frac{\alpha_3 \eta^2 \pi^4 \theta_{tt} - \theta_{xx} - 2\mu_2 \theta_{xxt}}{(1 + u_x)\cos\theta + v_x \sin\theta}\right) = \frac{v_x}{1 + u_x}.$$
 (2.53)

We now apply the same procedure to the boundary conditions. We obtain the following conditions at point A:

$$u(0,t) = 0, (2.54)$$

$$v(0,t) = 0, (2.55)$$

$$\theta_x(0,t) = 2\mu_3[\Omega - \phi_t - v_{xt}(0,t)]. \qquad (2.56)$$

While, we have the following conditions at point B:

$$v(1,t) = -u(1,t)\tan\phi, \qquad (2.57)$$

$$\theta_x(1,t) = 2\mu_3[-\phi_t + v_{xt}(1,t)], \qquad (2.58)$$

$$\begin{split} &[(1+u_{x}) \quad - \quad \frac{(1+u_{x})}{\sqrt{(1+u_{x})^{2}+v_{x}^{2}}}] + 2\mu_{2}[(1+u_{x}) - \frac{1+u_{x}}{\sqrt{(1+u_{x})^{2}+v_{x}^{2}}}]_{t} \\ &- \quad \alpha_{3}\eta^{4}\pi^{4}[\frac{\theta_{tt}}{(1+u_{x})\cot\theta+v_{x}}] + \eta^{2}[\frac{\theta_{xx}}{(1+u_{x})\cot\theta+v_{x}}] \\ &+ \quad 2\mu_{2}\eta^{2}[\frac{\theta_{xx}}{(1+u_{x})\cot\theta+v_{x}}]_{t} \\ &+ \quad S\eta^{2}\pi^{4}[-\xi\Omega^{2}\cos(\Omega t - \phi) + u_{tt} - 2\phi_{t}v_{t} - \phi_{tt}v - \phi_{t}^{2}(x+u)] \\ &- \quad [v_{x} - \frac{v_{x}}{\sqrt{(1+u_{x})^{2}+v_{x}^{2}}}]\tan\phi - 2\mu_{2}[v_{x} - \frac{v_{x}}{\sqrt{(1+u_{x})^{2}+v_{x}^{2}}}]_{t}\tan\phi \\ &- \quad \eta^{4}\pi^{4}\alpha_{3}[\frac{\theta_{tt}}{(1+u_{x})+v_{x}\tan\theta}]\tan\phi + \eta^{2}[\frac{\theta_{xx}}{(1+u_{x})+v_{x}\tan\theta}]\tan\phi \\ &+ \quad 2\mu_{2}\eta^{2}[\frac{\theta_{xx}}{(1+u_{x})-v_{x}\tan\theta}]_{t}\tan\phi \end{split}$$

$$- S\eta^{2}\pi^{4} \left[ -\xi \Omega^{2} \sin \Omega t - \phi + \phi_{tt}(x+u) + 2\phi_{t}u_{t} - v_{tt} - \phi_{t}^{2}v \right] \tan \phi$$

$$+ 2\eta^{2}\pi^{4}\mu_{4} \frac{Z_{t}}{\cos \phi} + 2\eta^{2}\pi^{4}\mu_{4} \left[ u_{t} - v_{t} \tan \phi \right] = 0. \qquad (2.59)$$

Equations (2.51) to (2.59) form the basis of the mathematical analysis in the thesis.

## Chapter 3

# Analysis of the Distributed Parameter Model

In the present chapter, we study equations (2.51), (2.52) and (2.53) by applying the Method of Multiple Scales [29]. To apply this method, we must first locate a small, constant parameter which will be used as a basic unit in scaling the response and the other parameters. For the current problem, the slenderness ratio  $\eta$  of the flexible connecting rod is chosen to be the basic measurement unit. The axial and transverse displacements u(x,t)and v(x,t) are expressed in asymptotic series in terms of  $\eta$ . We then expand the partial differential equations describing the dynamical behavior associated with the connecting rod with these assumed solution sequences and obtain a sequence of linear partial differential equations. We then study the dynamic response associated with the elastic connecting rod by solving these equations sequentially. In section 3.1, the Method of Multiple Scales is used to outline each individual resonance case. In section 3.2, we study the case of the principal parametric resonance. In section 3.3, we study the case of primary resonance. Superharmonic resonances of order 1/2 and 1/3 are studied in sections 3.4, and 3.5, respectively. Section 3.6 contains the analysis for the case of the order two subharmonic resonance. We summarize the results and provide a detailed parameter study in section 3.7.

### 3.1 Application of the Method of Multiple Scales (MMS)

To apply MMS, we need to introduce a set of new independent time variables  $T_n$  according to

$$T_n = \epsilon^n t \tag{3.1}$$

where  $\epsilon$  is a small constant parameter which is related to the slenderness ratio of the connecting rod. Because the connecting rod is assumed to made of a slender beam, its slenderness ratio  $\eta = \sqrt{\frac{I}{AL^2}}$  is small. Based on this, we choose this quantity as a basic measurement unit of the parameters that are used to model the problem. Therefore, we scale the slenderness ratio of the connecting rod by letting

$$\eta^2 = \alpha_1 \epsilon^2 \ . \tag{3.2}$$

Moreover, the length ratio  $\xi$  is scaled according to

$$\xi = \epsilon \xi_1 \ . \tag{3.3}$$

It follows that the derivatives with respect to t become expansions in terms of the partial derivatives with respect to  $T_n$  according to

$$\frac{d}{dt} = \frac{\partial}{\partial T_0} + \epsilon \frac{\partial}{\partial T_1} + \epsilon^2 \frac{\partial}{\partial T_2} + \dots = D_0 + \epsilon D_1 + \epsilon^2 D_2 + \dots$$
 (3.4)

$$\frac{d^2}{dt^2} = D_0^2 + 2\epsilon D_0 D_1 + \epsilon^2 (D_1^2 + 2D_0 D_2) + \dots$$
 (3.5)

where  $D_j$  stands for the derivatives with respect to the independent time variable  $T_j$ . We next assume that the solutions u(x,t) and v(x,t) can be represented by expansions having

the forms:

$$u(x,t) = \epsilon u_1(x,T_0,T_1,T_2) + \epsilon^2 u_2(x,T_0,T_1,T_2) + \epsilon^3 u_3(x,T_0,T_1,T_2) + \dots, \quad (3.6)$$

$$v(x,t) = \epsilon v_1(x, T_0, T_1, T_2) + \epsilon^2 v_2(x, T_0, T_1, T_2) + \epsilon^3 v_3(x, T_0, T_1, T_2) + \dots$$
 (3.7)

Note that the number of independent time scales  $T_j$  needed depends upon the order to which the expansion are carried out. For the present problem, it is sufficient to expand the solutions up to  $O(\epsilon^3)$ . Therefore, only the first three time scales are used in the expansions. There are three damping parameters  $\mu_2$ ,  $\mu_3$  and  $\mu_4$  involved in equations (2.51), (2.52) and (2.53). Basically, these damping parameters are rescaled in such a way that they will show up in the final resonant condition together with the detuning parameter which is related to the nearness of the frequency ratio  $\Omega$  to a resonance condition. A trial and error approach is used to show that the damping parameter  $\mu_2$  must be of order  $O(\epsilon^2)$ ,  $\mu_3$  of order  $O(\epsilon^2)$  and  $\mu_4$  is of order O(1). This leads to the following ordering of these damping coefficients in terms of  $\epsilon$ :

$$\mu_2 = \epsilon^2 \mu_{2_2} \,, \tag{3.8}$$

$$\mu_3 = \epsilon^2 \mu_{3_2} \,, \tag{3.9}$$

$$\mu_4 = \mu_{4_0} \,. \tag{3.10}$$

Substituting equations (3.2) to (3.10) into equation (2.5), expanding and equating the coefficients of the like-power terms in  $\epsilon$ , we obtain the following expansions for the elongation  $e_0$  of the median line along the connecting rod:

$$e_0 = \epsilon e_{0_1} + \epsilon^2 e_{0_2} + \epsilon^3 e_{0_3} + \epsilon^4 (e_{0_4} - 4e_{0_2}v_{1x}^2) + O(\epsilon^5)$$

$$= \epsilon u_{1_x} + \epsilon^2 (u_{2_x} + \frac{v_{1_x}^2}{2}) + \epsilon^3 (u_{3_x} + v_{1_x} v_{2_x})$$

$$+ \epsilon^4 [(u_{4_x} + \frac{v_{1_x}^4}{8} + \frac{v_{2_x}^2}{2} + v_{1_x} v_{3_x}) - 4(u_{2_x} + \frac{v_{1_x}^2}{2}) v_{1_x}^2] + O(\epsilon^5)$$
(3.11)

where  $e_{0j}$  represents the j-th order term in the expansion of  $e_0$ . Applying the same procedure to equations (2.51), (2.52) and (2.53), we obtain the following equations:

Order  $\epsilon$ 

$$u_{1_{xx}} = (e_{0_1})_x = 0, (3.12)$$

Order  $\epsilon^2$ 

$$(u_{2x} + \frac{v_{1x}^2}{2})_x = (e_{0x})_x = 0, (3.13)$$

Order  $\epsilon^3$ 

$$(u_{3x} + v_{1x}v_{2x})_x = (e_{0x})_x = -\alpha_1 \pi^4 \xi_1 \Omega^2 \cos \Omega T_0, \qquad (3.14)$$

$$\alpha_1 \pi^4 D_0^2 v_1 + \alpha_1 v_{1_{xxxx}} = (e_{0_2} v_{1_x})_x + \alpha_1 \pi^4 \xi_1 \Omega^2 (1 - x) \sin \Omega T_0, \qquad (3.15)$$

Order  $\epsilon^4$ 

$$(e_{0_4})_x + 2\mu_{2_2}(D_0e_{0_2})_x - (e_{0_2}v_{1x}^2)_x + \alpha_1(v_{1x}v_{1xxx})_x = \alpha_1\pi^4[D_0^2u_2 - \xi_1\Omega^2v_1\sin\Omega T_0$$
  
$$-\xi_1\Omega^2v_1\sin\Omega T_0 + 2\xi_1\Omega(D_0v_1)\cos\Omega T_0 + \xi_1^2\Omega^2\sin^2\Omega T_0 - \xi_1^2\Omega^2x\cos^2\Omega T_0], \qquad (3.16)$$

$$\alpha_1 \pi^4 D_0^2 v_2 + \alpha_1 v_{2xxxx} = (e_{0_3} v_{1x})_x + (e_{0_2} v_{2x})_x - 2\alpha_1 \pi^4 (D_0 D_1 v_1)$$

$$+ \alpha_1 \pi^4 \xi_1^2 \Omega^2 \cos \Omega T_0 \sin \Omega T_0, \qquad (3.17)$$

Order  $\epsilon^5$ 

$$\alpha_{1}\pi^{4}D_{0}^{2}v_{3} + \alpha_{1}v_{3xxxx} = -\alpha_{1}^{2}\alpha_{2}v_{1xxxxxx} - 2\mu_{22}\alpha_{1}D_{0}v_{1xxxx} + \alpha_{1}(e_{02}v_{1xxx})_{x}$$

$$- \alpha_{1}(v_{1x}v_{1xx}^{2})_{x} + (e_{02}v_{3x})_{x} + (e_{03}v_{2x})_{x} - \frac{1}{2}(e_{02}v_{1x}^{3})_{x}$$

$$+ 2\mu_{22}D_{0}(e_{02}v_{1x})_{x} + (e_{04}v_{1x})_{x} - (e_{02}^{2}v_{1x})_{x} + \alpha_{1}^{2}\alpha_{3}\pi^{4}D_{0}^{2}v_{1xx}$$

$$- \alpha_{1}\pi^{4}(2D_{0}D_{1}v_{2} + 2D_{0}D_{2}v_{1} + D_{1}^{2}v_{1}) + \alpha_{1}\pi^{4}\xi_{1}^{2}\Omega^{2}v_{1}\cos^{2}\Omega T_{0}$$

$$+ 2\alpha_{1}\pi^{4}\xi_{1}\Omega(D_{0}u_{2})\cos\Omega T_{0} - \alpha_{1}\pi^{4}\xi_{1}\Omega^{2}u_{2}\sin\Omega T_{0}$$

$$- \alpha_{1}\pi^{4}\xi_{1}^{3}\Omega^{2}\frac{(1+x)}{2}\sin^{3}\Omega T_{0} + \alpha_{1}\pi^{4}\xi_{1}^{3}\Omega^{2}x\cos^{2}\Omega T_{0}\sin\Omega T_{0}.$$
 (3.18)

Applying the same procedure to the boundary conditions, we obtain the following boundary conditions:

Order  $\epsilon$ 

$$u_1 = v_1 = v_{1xx} = 0$$
, at  $x = 0$ , (3.19)

$$u_{1x} = v_1 = v_{1xx} = 0$$
, at  $x = 1$ , (3.20)

Order  $\epsilon^2$ 

$$u_2 = v_2 = v_{2xx} = 0$$
, at  $x = 0$ , (3.21)

$$(u_{2x} + \frac{v_{1x}^2}{2}) = v_2 = 0, v_{2xx} = -2\mu_{3x}\Omega, \text{ at } x = 1,$$
 (3.22)

Order  $\epsilon^3$ 

$$u_3 = v_3 = 0,$$

$$v_{3xx} = -\alpha_1 \alpha_2 v_{1xxxx} - v_{1x}^2 \frac{v_{1xx}}{2} - 2\mu_{3_2} D_0 v_{1x} - 2\mu_{3_2} \xi_1 \Omega \cos \Omega T_0 , \text{ at } x = 0 , \quad (3.23)$$

$$v_3 = -u_2 \xi_1 \sin \Omega T_0 ,$$

$$(u_{3x} + v_{1x} v_{2x}) = S\alpha_1 \pi^4 \xi_1 \Omega^2 \cos \Omega T_0 + 2\alpha_1 \pi^4 \mu_{4_0} \xi_1 \Omega \sin \Omega T_0 ,$$

$$v_{3xx} = -\alpha_1 \alpha_2 v_{1xxxx} - v_{1x}^2 \frac{v_{1xx}}{2} - 2\mu_{3_2} D_0 v_{1x} + 2\mu_{3_2} \xi_1 \Omega \cos \Omega T_0 , \text{ at } x = 1 , \quad (3.24)$$

#### Order $\epsilon^4$

$$e_{0_{4}} + \alpha_{1}v_{1x}v_{1xxx} = -2\mu_{2_{2}}D_{0}e_{0_{2}} + \alpha_{1}\pi^{4}\xi_{1}^{2}\Omega\mu_{4_{0}}\sin(2\Omega T_{0})$$

$$+ \alpha_{1}\pi^{4}\xi_{1}^{2}\Omega^{2}S(\cos^{2}\Omega T_{0} - \sin^{2}\Omega T_{0}) - \alpha_{1}\pi^{4}S(D_{0}^{2}u_{2})$$

$$+ \alpha_{1}\pi^{4}\xi_{1}\Omega^{2}Sv_{1}\sin\Omega T_{0} - 2\alpha_{1}\pi^{4}\xi_{1}\Omega S(D_{0}v_{1})\cos\Omega T_{0}$$

$$- \alpha_{1}\pi^{4}\xi_{1}S(D_{0}^{2}v_{1})\sin\Omega T_{0} - (e_{0_{2}}v_{1x})\xi_{1}\sin\Omega T_{0} + (e_{0_{2}}v_{1x}^{2})$$

$$+ \alpha_{1}\xi_{1}v_{1xxx}\sin\Omega T_{0} - 2\alpha_{1}\pi^{4}\mu_{4}(D_{0}u_{2}), \text{ at } x = 1.$$
(3.25)

In the following, we show that  $u_1(x, T_0, T_1, T_2) = 0$  and hence we drop all the terms involving products with  $u_1(x, T_0, T_1, T_2)$ . To show that  $u_1(x, T_0, T_1, T_2) = 0$ , we solve equation (3.12) to obtain the general solution of  $u_1(x, T_0, T_1, T_2)$ , which takes the following form:

$$u_1(x, T_0, T_1, T_2) = b_1(T_0, T_1, T_2)x + b_2(T_0, T_1, T_2)$$
(3.26)

where  $b_1(T_0, T_1, T_2)$  and  $b_2(T_0, T_1, T_2)$  can be determined by the boundary conditions associated with  $u_1$ . By applying equations (3.19) and (3.20), we determine that  $b_1 = b_2 = 0$ . Hence,  $u_1$  must be zero. This indicates that, for simply-supported slender beam, the axial deformation is much smaller than the transverse one. Next, we consider equation (3.13) and its associated boundary condition (3.22). Together, they reveal that

$$\left(u_{2x} + \frac{v_{1x}^2}{2}\right) = e_{02} = 0. {(3.27)}$$

Consequently, equation (3.15) reduces to

$$\alpha_1 \pi^4 (D_0^2 v_1) + \alpha_1 v_{1xxxx} = \alpha_1 \pi^4 \xi_1 \Omega^2 (1 - x) \sin \Omega T_0$$
 (3.28)

which can be converted into the following equations:

$$(D_0^2 \hat{v}_{1n}) + \omega_n^2 \hat{v}_{1n} = \frac{2}{n\pi} \xi_1 \Omega^2 \sin \Omega T_0$$
 (3.29)

by Galerkin's procedure with  $v_1 = \hat{v}_{1n}(\sin n\pi x)$ , where  $\omega_n^2 = n^4$  for n = 1, 2, 3, ... In analyzing the particular solution of  $\hat{v}_{1n}$ , we need to consider the following cases separately: (1)  $\Omega$  is near to  $\omega_n$  and (2)  $\Omega$  is away from  $\omega_n$ . The case in which  $\Omega$  is near to  $\omega_n$  corresponds to the primary resonance and will be investigated in section 3.3. At the present time, we assume that  $\Omega$  is away from  $\omega_n$  and continue our analysis to consider the equation of higher order. When  $\Omega$  is away from  $\omega_n$ , the general solution of  $\hat{v}_{1n}$  is given as

$$\hat{v}_{1n} = A_n(T_1, T_2) exp(j\omega_n T_0) + \Lambda_1 \sin \Omega T_0 + c.c.$$
 (3.30)

where c.c. stands for the complex conjugate of the preceding term, and

$$\Lambda_1 = \left(\frac{2}{n\pi}\right) \frac{\xi_1 \Omega^2}{(\omega_n^2 - \Omega^2)} \tag{3.31}$$

represents the amplitude of the particular solution. The function  $A_n(T_1, T_2)$  in equa-

tion (3.30) is a complex function of time scales  $T_1$  and  $T_2$ , which represents the amplitude of the homogeneous solution. The second term of equation (3.30) represents the particular solution. Since the frequency ratio  $\Omega$  is assumed to be away from  $\omega_n$ , the magnitude of the particular solution is finite (equation [3.31]). Note that, according to the linear theory, the homogeneous solution will decay to zero due to the presence of the damping parameters. However, as we will find out later on, due to nonlinear effects, this is not always true. When certain conditions are met, the homogeneous solution may not decay to zero and hence must be included. Equation (3.14), together with its boundary condition (3.23), leads to

$$e_{0_3} = (u_{3x} + v_{1x}v_{2x}) = \alpha_1 \pi^4 (1 - x + S)\xi_1 \Omega^2 \cos \Omega T_0 + 2\alpha_1 \pi^4 \xi_1 \Omega \mu_{4_0} \sin \Omega T_0$$
 (3.32)

which represents the third order expansion of the axial elongation of the median line along the connecting rod. Substituting equation (3.27) and (3.32) into equation (3.17), we obtain

$$\alpha_{1}\pi^{4}D_{0}^{2}v_{2} + \alpha_{1}v_{2xxx} = \alpha_{1}\pi^{4}\xi_{1}\Omega^{2}[(1-x+S)v_{1x}]_{x}\cos\Omega T_{0} - 2\alpha_{1}\pi^{4}D_{0}D_{1}v_{1}$$

$$+ \alpha_{1}\pi^{4}\xi_{1}^{2}\Omega^{2}\cos\Omega T_{0}\sin\Omega T_{0} + 2\alpha_{1}\pi^{4}\mu_{4_{0}}\xi_{1}\Omega v_{1xx}\sin\Omega T_{0}$$
(3.33)

which can be converted into the following equation:

$$D_0^2 \hat{v}_{2n} + \omega_n^2 \hat{v}_{2n} = -2j\omega_n (D_1 A_n) exp(j\omega_n T_0) + (\frac{1 - \cos n\pi}{n\pi}) \xi_1^2 \Omega^2 \sin(2\Omega T_0)$$

$$-\frac{1}{4} (1 + 2S)(n\pi)^2 \xi_1 \Omega^2 [A_n exp(j\omega_n T_0 + j\Omega T_0) + \bar{A}_n exp(-j\omega_n T_0 + j\Omega T_0)]$$

$$-\mu_{4_0} \xi_1 \Omega [(n\pi)^2 \bar{A}_n exp(j\Omega T_0 - j\omega T_0 - j\pi/2) - \frac{(n\pi)^2}{2} \Lambda_1 exp(2j\Omega T_0)]$$

$$-\frac{1}{4} (1 + 2S)(n\pi)^2 \Lambda_1 \xi_1 \Omega^2 \sin(2\Omega T_0)$$
(3.34)

with  $v_2 = \hat{v}_{2n}(\sin n\pi x)$ , where an overbar stands for the complex conjugate of the corre-

sponding term. Now, in analyzing the solution of this equation, we need to distinguish between the following cases: (1)  $2\Omega$  is near to  $\omega_n$ , (2)  $\Omega$  is near to  $2\omega_n$  and (3)  $\Omega$  is away from  $2\omega_n$  and  $\frac{\omega_n}{2}$ . The first case corresponds a superharmonic resonance, and will be investigated in section 3.4. The second case corresponds the principal parametric resonance which will be investigated in section 3.2. At the present time, we assume that  $\Omega$  is away from  $2\omega_n$  and  $\frac{\omega_n}{2}$ . Under this condition, we must have

$$D_1 A_n = 0 \tag{3.35}$$

in order to remove the secular term from the particular solution of  $\hat{v}_{2n}$ . This implies that the amplitude  $A_n$  of the free oscillation term in the general solution of  $v_1$  (equation [3.30]) must be independent of the time scale  $T_1 = \epsilon t$ . The particular solution of  $\hat{v}_{2n}$  is then given as

$$\hat{v}_{2n} = \Lambda_{21} \sin 2\Omega T_0 + \Lambda_{22} exp(j\Omega T_0 + j\omega_n T_0) + \Lambda_{23} exp(j\Omega T_0 - j\omega_n T_0) + \Lambda_{24} exp(2j\Omega T_0) + \Lambda_{25} exp(j\Omega T_0 - j\omega_n T_0 - j\pi/2) + c.c.$$
(3.36)

where

$$\Lambda_{21} = \frac{1 - \cos n\pi}{n\pi} \frac{\xi_1^2 \Omega^2}{(\omega_n^2 - 4\Omega^2)} - \frac{1}{4} (1 + 2S) (n\pi)^2 \Lambda_1 \frac{\xi_1 \Omega^2}{\omega_n^2 - 4\Omega^2} , \qquad (3.37)$$

$$\Lambda_{22} = -\frac{(1+2S)}{4} (n\pi)^2 \xi_1 \Omega^2 \frac{A_n}{[\omega_n^2 - (\omega_n + \Omega)^2]}, \qquad (3.38)$$

$$\Lambda_{23} = -\frac{1}{4}(1+2S)(n\pi)^2 \xi_1 \Omega^2 \frac{\bar{A}_n}{[\omega_n^2 - (\omega_n - \Omega)^2]}, \qquad (3.39)$$

$$\Lambda_{24} = \frac{\Lambda_1}{2} \frac{(n\pi)^2}{\omega_n^2 - 4\Omega^2} \,, \tag{3.40}$$

and

$$\Lambda_{25} = -\mu_{4_0} \xi_1 \Omega(n\pi) \frac{\bar{A}_n}{\omega_n^2 - (\Omega - \omega_n)^2} . \tag{3.41}$$

From the expression  $u_{2x} + \frac{v_{1x}^2}{2} = 0$ , we solve  $u_2(x, T_0, T_1, T_2)$  and obtain

$$u_2 = -\frac{1}{4}(n\pi)^2 \hat{v}_{1n}^2 \left(x + \frac{\sin 2n\pi x}{2n\pi}\right) \tag{3.42}$$

where  $\hat{v}_{1n}$  is given by equation (3.30). With this information, equation (3.16) reduces to

$$e_{0_4} + \alpha_1(v_{1x}v_{1xxx})_x = \alpha_1\pi^4 [D_0^2u_2 - \xi_1\Omega^2v_1\sin\Omega T_0 + 2\xi_1\Omega(D_0v_1)\cos\Omega T_0 + \xi_1^2\Omega^2\sin^2\Omega T_0 - \xi_1^2\Omega^2x\cos^2\Omega T_0]$$
(3.43)

subjected to the following boundary conditions:

$$e_{0_4} + \alpha_1(v_{1x}v_{1xxx}) = -S\alpha_1\pi^4 [D_0^2u_2 + \xi_1^2\Omega^2\sin^2\Omega T_0 - \xi_1^2\Omega^2\cos^2\Omega T_0]$$

$$- \alpha_1\pi^4\mu_{4_0}\xi_1\Omega\sin2\Omega T_0 + \alpha_1\xi_1v_{1xxx}\sin\Omega T_0$$

$$+ \alpha_1\pi^4\mu_{4_0}(n\pi)^2(D_0\hat{v}_{1n})\hat{v}_{1n}, \text{ at } x = 1.$$
(3.44)

With these two equations, we solve for  $e_{0_4}$  and obtain

$$e_{0_{4}} = \left(u_{4x} + \frac{v_{1x}^{4}}{8} + \frac{v_{2x}^{2}}{2} + v_{1x}v_{3x}\right)$$

$$= -\alpha_{1}v_{1x}v_{1xxx} + \alpha_{1}\pi^{4}\xi_{1}^{2}\Omega^{2}(\frac{1}{2} - \frac{x^{2}}{2} + S)\cos^{2}\Omega T_{0} + \alpha_{1}\pi^{4}\xi_{1}^{2}\Omega^{2}(x - 1 - S)\sin^{2}\Omega T_{0}$$

$$+\alpha_{1}\pi^{4}\xi_{1}(\frac{\cos n\pi x - \cos n\pi}{n\pi})[\Omega^{2}\hat{v}_{1n}\sin\Omega T_{0} - 2\Omega(D_{0}\hat{v}_{1n})\cos\Omega T_{0}]$$

$$+\alpha_{1}\pi^{4}\frac{D_{0}^{2}\hat{v}_{1n}^{2}}{8}[(n\pi)^{2}(1 + 2S - x^{2}) - \sin^{2}n\pi x] + \alpha_{1}\pi^{4}\mu_{4_{0}}\xi_{1}^{2}\Omega\sin2\Omega T_{0}$$

$$-\alpha_{1}\xi_{1}(n\pi)^{3}\cos n\pi\sin\Omega T_{0} + \alpha_{1}\pi^{4}\mu_{4_{0}}(n\pi)^{2}(D_{0}\hat{v}_{1n})\hat{v}_{1n}. \tag{3.45}$$

With these results, equation (3.18) reduces to

$$\alpha_{1}\pi^{4}D_{0}^{2}v_{3} + \alpha_{1}v_{3xxxx} = -\alpha_{1}^{2}\alpha_{2}v_{1xxxxxx} - 2\alpha_{1}\mu_{2}D_{0}v_{1xxxx}$$

$$+ (e_{0_{3}}v_{2x})_{x} - \alpha_{1}(v_{1x}v_{1xx}^{2})_{x} + (e_{0_{4}}v_{1x})_{x} + \alpha_{1}^{2}\alpha_{3}\pi^{4}D_{0}^{2}v_{1xx}$$

$$- \alpha_{1}\pi^{4}(2D_{0}D_{2}v_{1} + 2D_{0}D_{1}v_{2} + D_{1}^{2}v_{1}) + \alpha_{1}\pi^{4}\xi_{1}^{2}\Omega^{2}v_{1}\cos\Omega T_{0}$$

$$+ 2\alpha_{1}\pi^{4}\xi_{1}\Omega(D_{0}u_{2})\cos\Omega T_{0} - \alpha_{1}\pi^{4}\xi_{1}\Omega^{2}u_{2}\sin\Omega T_{0}$$

$$- \alpha_{1}\pi^{4}\xi_{1}^{3}\Omega^{2}\frac{(1+x)}{2}\sin^{3}\Omega T_{0} + \alpha_{1}\pi^{4}\xi_{1}^{3}\Omega^{2}x\cos^{2}\Omega T_{0}\sin\Omega T_{0}$$

$$+ \alpha_{1}\pi^{4}\mu_{4_{0}}(n\pi)^{2}(D_{0}\hat{v}_{1n})\hat{v}_{1n}v_{1xx}$$

$$(3.46)$$

subjected to boundary conditions (3.23) and (3.24). We note that equation (3.46), together with its associated boundary conditions (3.23) and (3.24), represent a simply supported beam subjected to (1) motion of its foundation and (2) external moments applied to its both ends. It is not a straightforward procedure to reduce this partial differential equation into ordinary differential equation. Here, we use the variational approach[16, 46] to compensate for the effects of the nonhomogeneous boundary conditions and obtain an equivalent system to which the Galerkin's method can be applied directly. Appendix A contains the detailed approach regarding this procedure. At this moment, we only present the final result as below:

$$\begin{split} D_0{}^2\hat{v}_{3n} &+ \omega_n^2\hat{v}_{3n} = -2j\omega_n(D_2A_n + \mu_{2_1}n^4A_n)exp(j\omega_nT_0) \\ &+ (\alpha_1\alpha_3 + \alpha_1\alpha_2)A_n(n\pi)^2n^4exp(j\omega_nT_0) + j\frac{2}{\pi^2}n^4\mu_{3_2}A_nexp(j\omega_nT_0) \\ &- (n\pi)^2n^4[\frac{8}{15} - (\frac{1}{3} + S)(n\pi)^2]A_n^2\bar{A}_nexp(j\omega_nT_0) + f_1\xi_1^2A_nexp(j\omega_nT_0) \\ &+ jf_2\xi_1^3exp(3j\Omega T_0) + jf_3\xi_1\bar{A}_n^2exp(j\Omega T_0 - 2j\omega_nT_0) \end{split}$$

$$- j\omega_{n}\mu_{4_{0}}(n\pi)^{4}A_{n}^{2}\bar{A}_{n}exp(j\omega_{n}T_{0}) - j\frac{1}{2}\mu_{4_{0}}A_{n}(n\pi)^{4}\omega_{n}\Lambda_{1}^{2}exp(j\omega_{n}T_{0})$$

$$+ \frac{1}{8}(n\pi)^{4}\mu_{4_{0}}\Lambda_{1}^{3}\Omega exp(3j\Omega T_{0}) + (n\pi)^{4}\mu_{4_{0}}\Lambda_{1}\bar{A}_{n}^{2}(\omega_{n} - \frac{\Omega}{2})exp(j\Omega T_{0} - 2j\omega_{n}T_{0})$$

$$+ N.S.T. + c.c. \qquad (3.47)$$

where N.S.T. represents those terms which have no effect when we consider the secular terms in the particular solution of  $\hat{v}_{3n}$ . In analyzing the particular solution of equation (3.47), there are three cases which need to be considered separately: (1)  $\Omega$  is near to  $3\omega_n$ , (2)  $\Omega$  is near to  $3\omega_n$ , and (3)  $\Omega$  is away from  $3\omega_n$  and  $3\omega_n$ . The case in which  $\Omega$  is near to  $3\omega_n$  corresponds to a subharmonic resonance and will be investigated in section 3.6. The case in which  $\Omega$  is near to  $3\omega_n$ , corresponds to a superharmonic resonance and will be investigated in section 3.5.

At this point, we pause and discuss some general features of this pattern of analysis. After a small, constant parameter  $\epsilon$  has been located, the solutions are expressed in uniform expansions based on this parameter. By using these assumed solution sequences, the equations describing the transverse and the axial deflection can be converted into a sequence of partial differential equations which can be solved easily, since they are linearized by the nature of the perturbation expansions. We note that in solving every sequential order for the flexible vibration associated with the flexible connecting rod, we are considering a simply supported beam subjected to the following generalized forces: (1) a distributed load, which comes form the inertia force associated with the gross beam motion, applied along the span of the beam, (2) concentrated moments, which are caused by the presences of the bearing damping  $\mu_b$ , shear deformation and rotary inertia, (3) motion of the foundation which comes from the motion of the crank, and (4) axial loading which comes from the inertia force associated with the slider mass and its friction force. In order to make the

analysis as clear as possible, we provide a general procedure for solving this kind of problem in Appendix A. In solving these equations for the flexural vibration associated with the connecting rod, the primary resonance arises first and then the principal parametric resonance. After these two resonances, several secondary resonances arise. In principle, it is possible to extend this analysis to study even higher order resonances, for instance the subharmonic resonance which occurs when  $\Omega$  is near to  $5\omega_n$ . However, this involves an unreasonable amount of computational work. As a matter of fact, the present results are accomplished with a great deal help from a Macintosh version of the computer symbolic manipulation program  $Mathematica^{TM}$ . Although the primary resonance occurs first, in the analysis, we investigate the principle parametric resonance first rather than the primary one, since this pattern will simplify the analysis and make it more easily understood. After

### 3.2 Principal Parametric Resonance

In analyzing the particular solution of equation (3.34), when the frequency ratio  $\Omega$  is near to  $2\omega_n$ , the principal parametric resonance takes place. To describe the nearness of  $\Omega$  to  $2\omega_n$ , we express  $\Omega$  as

$$\Omega = 2\omega_n + 2\epsilon\sigma_1 \tag{3.48}$$

where  $\sigma_1$  is the detuning parameter. At the same time, the damping parameter  $\mu_2$  is rescaled according to

$$\mu_2 = \epsilon \mu_{2_1},\tag{3.49}$$

so that it will show up in the final resonance equation, together with detuning parameter  $\sigma_1$ . We first expand equations (2.51), (2.52) and (2.53) with these new ordering relations, and then carry out the same procedure as described in the last section. Since the computational work is routine, we only present a few essential results in the following analysis. For a detailed solution, refer to Appendix B. Following the same procedure as described in the last section, the first order flexural vibration associated with the connecting rod is described by equation (3.29). Consequently, the general solution of  $\hat{v}_{1n}$  is given in equation (3.30). When we try to solve the second order equation for the flexural vibration, we obtain the following equation:

$$D_0^2 \hat{v}_{2n} + \omega_n^2 \hat{v}_{2n} = -2j\omega_n (D_1 A_n) exp(j\omega_n T_0) - 2j\mu_{2_1} A_n n^4 \omega_n exp(j\omega_n T_0)$$

$$- (1 + 2S)(n\pi)^2 \omega_n^2 \bar{A}_n \xi_1 exp(j\omega_n T_0 + 2j\sigma_1 T_1)$$

$$- 2\mu_{4_0} (n\pi)^2 \omega_n \bar{A}_n \xi_1 exp(j\omega_n T_0 + 2j\sigma_1 T_1 - j\frac{\pi}{2}) + N.S.T. + c.c.$$
 (3.50)

where N.S.T. stands for those terms which have no effects in considering the secular term in the particular solution of  $\hat{v}_{2n}$ . Therefore, we must have

$$-2j\omega_{n}(D_{1}A_{n}) - 2j\mu_{2_{1}}\omega_{n}A_{n}n^{4} - (1+2S)(n\pi)^{2}\omega_{n}^{2}\bar{A}_{n}\xi_{1}exp(2j\sigma_{1}T_{1})$$
$$- 2\mu_{4_{0}}(n\pi)^{2}\omega_{n}\bar{A}_{n}\xi_{1}exp(2j\sigma_{1}T_{1} - j\frac{\pi}{2}) = 0, \tag{3.51}$$

in order to remove the secular term from the particular solution of  $\hat{v}_{2n}$ . In solving this equation, the unknown complex function  $A_1(T_1, T_2)$  will be expressed in polar form

$$A_n(T_1 T_2) = \frac{a}{2} exp(j\Psi) .$$
 (3.52)

Expanding equation (3.50) with this expression, and separating the resultant equation into

the real and imaginary parts, we obtain

$$a' = -\mu_{2_1} n^4 a - 2a\xi_1 \Delta_1 \sin(2\Phi_1) + a(n\pi)^2 \xi_1 \mu_{4_0} \cos(2\Phi_1)$$
 (3.53)

$$a\Phi_1' = \sigma_1 a - 2a\xi_1 \Delta_1 \cos(2\Phi_1) - a(n\pi)^2 \xi_1 \mu_{40} \sin(2\Phi_1)$$
 (3.54)

where the phase angle  $\Phi_1$  and  $\Delta_1$  are defined by

$$\Phi_1 = \sigma_1 T_1 - \Psi , \qquad (3.55)$$

$$\Delta_1 = \frac{(1+2S)}{4} (n\pi)^2 n^2 \tag{3.56}$$

and the prime indicate derivatives with respect to the time scale  $T_1$ . Periodic steady state conditions can be achieved whenever  $a' = a\Phi'_1 = 0$ , these yields the following conditions:

$$n^{4}\mu_{2_{1}}a = -2a\xi_{1}\Delta_{1}\sin(2\Phi_{1}) + a(n\pi)^{2}\xi_{1}\mu_{4_{0}}\cos(2\Phi_{1}),$$

$$\sigma_{1}a = 2a\xi_{1}\Delta_{1}\cos(2\Phi_{1}) + a(n\pi)^{2}\xi_{1}\mu_{4_{0}}\sin(2\Phi_{1}). \tag{3.57}$$

Squaring these equations and adding them together, we obtain the frequency response equation which takes the form:

$$\left[\sigma_1^2 + n^8 \mu_{2_1}^2 - (2\xi_1 \Delta_1)^2 - (n\pi)^4 \mu_{4_0}^2 \xi_1^2\right] a^2 = 0. \tag{3.58}$$

From this frequency response equation, we note that the trivial solution a=0 is always the steady state response for this resonance. To determine the stability associated with this trivial solution, we transform equation (3.50) into Cartesian coordinate by substituting  $A_n = (B_R + jB_I) \exp(j\sigma_1 T_1 + \gamma T_1)$ , and then separating the resultant equation into the

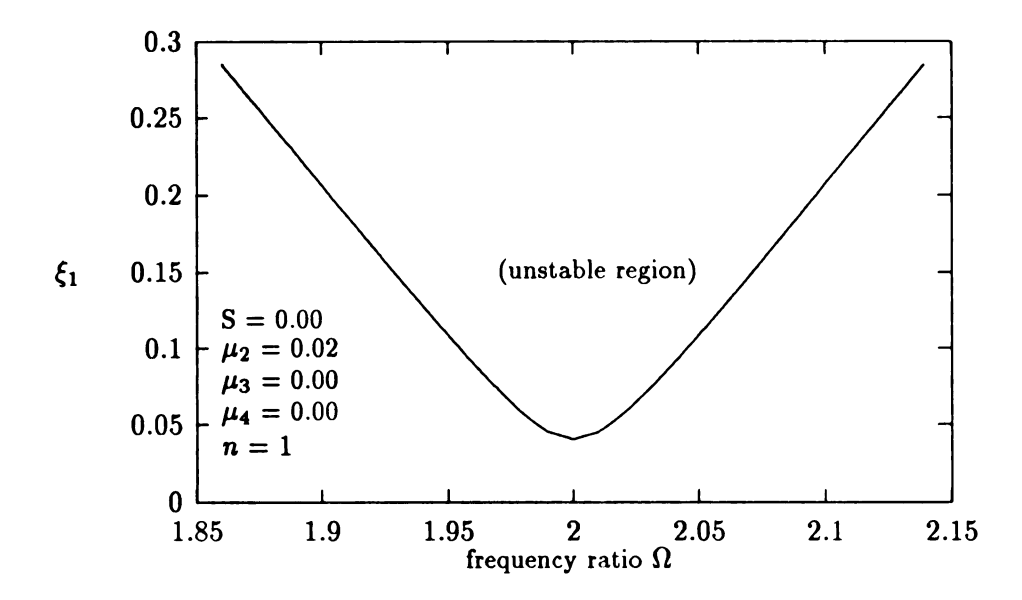


Figure 3.1: Frequency response equation for the principal parametric resonance

real and imaginary part to obtain two equations. From these two equations, we solve for the nontrivial solutions of  $B_R$  and  $B_I$ . From this, we determine that when

$$\sigma_1^2 + n^8 \mu_{2_1}^2 > \xi_1^2 \left[ 4\Delta_1^2 - (n^2 \pi^2 \mu_{4_0})^2 \right]$$
 (3.59)

the trivial solution is unstable. Otherwise, it is stable. Figure 3.2 shows an example of a stability boundary in the  $\xi$ - $\Omega$  plane.

In order to capture the effects of the nonlinearities, we need to rescale either the solutions or the parameters, so that the nonlinearity will then be included in the final equation describing the resonant condition. This problem is equivalent to a simply supported beam subjected to both the transverse and the axial force coming from the same source. We note that this force source arises because of the inertial force acting on the the connecting rod. Moreover, these inertial forces are proportional to the length ratio  $\xi$ . Because the magnitude of this force source is proportional to the length ratio  $\xi$ , we rescale the length

ratio in order to extend our analysis to include the nonlinearity. Therefore, we restart our analysis by letting

$$\xi = \epsilon^2 \xi_2 \tag{3.60}$$

and keeping the orders of damping parameter  $\mu_2$ ,  $\mu_3$  and  $\mu_4$  be the same as given in equations (3.8), (3.9) and (3.10). Expanding equations (2.51), (2.52) and (2.53) with this new length ratio, and equating the coefficient of like-power terms, we will obtain a new sequence of linear partial differential equations. Carrying the same procedure for the boundary conditions, we obtain a sequence of boundary conditions associated with these linear partial differential equations. We then follow the same procedure as that described in the last section. Because the computational work is tedious and routine, we only present a few results which are essential to our work in the following analysis. For a complete solution procedure, refer to Appendix C. The equation describing the first order flexural vibration becomes

$$D_0^2 \hat{v}_{1n} + \omega_n^2 \hat{v}_{1n} = 0 (3.61)$$

which admits the following solution

$$\hat{v}_{1n} = A_n exp(j\omega_n T_0) + c.c. \qquad (3.62)$$

We then obtain the following ordinary differential equation describing the second order flexural vibration:

$$D_0^2 \hat{v}_{2n} + \omega_n^2 \hat{v}_{2n} = \frac{2}{n\pi} \xi_2 \Omega^2 \sin \Omega T_0 - 2j\omega_n (D_1 A_n) \exp(j\omega_n T_0) + c.c.$$
 (3.63)

In analyzing the particular solution of  $\hat{v}_{2n}$ , we need to distinguish the following two cases:

(1)  $\Omega$  is near to  $\omega_n$  and (2)  $\Omega$  is away from  $\omega_n$ . The first case is referred to as the the primary resonance which will be investigated in section 3.3. At the present time, we continue our analysis to consider the third order flexural vibration with the assumption that  $\Omega$  is away from  $\omega_n$ . Under this condition, we must have  $D_1A_n=0$  in order to remove the secular term from the particular solution of equation (3.63). This implies that the amplitude  $A_n$  must be independent of the time scale  $T_1$ . Based on this, we assume that all the higher order flexural response  $\hat{v}_{1n}$  also independent of  $T_1$ . Therefore, we obtain the following equation describing the third order flexural vibration:

$$D_{0}^{2}\hat{v}_{3n} + \omega_{n}^{2}\hat{v}_{3n} = -2j\omega_{n}(D_{2}A_{n})exp(j\omega_{n}T_{0}) - 2j\omega_{n}n^{4}\mu_{2_{2}}A_{n}exp(j\omega_{n}T_{0})$$

$$+ \left[\alpha_{1}\alpha_{2} + \alpha_{1}\alpha_{3}\right](n\pi)^{2}n^{4}A_{n}exp(j\omega_{n}T_{0}) + 2j\omega_{n}\mu_{3_{2}}\frac{n^{2}}{\pi^{2}}A_{n}exp(j\omega_{n}T_{0})$$

$$+ \xi_{2}(n\pi)^{2}\mu_{4_{0}}\Omega\bar{A}_{n}exp(j\Omega T_{0} - j\omega_{n}T_{0} - j\pi/2)$$

$$- \frac{1}{4}(2S+1)(n\pi)^{2}\xi_{2}\Omega^{2}\bar{A}_{n}exp(j\Omega T_{0} - j\omega_{n}T_{0})$$

$$- \left[\frac{15}{8} - (\frac{1}{3} + S)(n\pi)^{2}\right](n\pi)^{2}n^{4}A_{n}^{2}\bar{A}_{n}exp(j\omega_{n}T_{0})$$

$$- j\mu_{4_{0}}(n\pi)^{4}A_{n}^{2}\bar{A}_{n}\omega_{n}exp(j\omega_{n}T_{0}) + N.S.T. + c.c. . \tag{3.64}$$

To describe the nearness of  $\Omega$  to  $2\omega_n$ , we express  $\Omega$  as

$$\Omega = 2 + 2\epsilon^2 \sigma_2 \ . \tag{3.65}$$

Hence, we must have

$$-2j\omega_{n}(D_{2}A_{n})-2j\omega_{n}n^{4}\mu_{2_{2}}A_{n}+2j\frac{n^{4}}{\pi^{2}}A_{n}\mu_{3_{2}}-j(n\pi)^{4}\mu_{4_{0}}A_{n}^{2}\bar{A}_{n}\omega_{n}$$

$$+\xi_{2}(n\pi)^{2}\mu_{4_{0}}\Omega\bar{A}_{n}exp(2j\sigma_{2}T_{1}-j\pi/2)+A_{n}(n\pi)^{2}n^{4}[\alpha_{1}\alpha_{2}+\alpha_{1}\alpha_{3}]$$

$$-\frac{1}{4}(1+2S)(n\pi)^{2}\xi_{2}\Omega^{2}\bar{A}_{n}exp(2j\sigma_{2}T_{1})$$

$$-\left[\frac{15}{8}-\left(\frac{1}{3}+S\right)(n\pi)^{2}\right](n\pi)^{2}n^{4}A_{n}^{2}\bar{A}_{n}=0$$
(3.66)

in order to remove the secular term from the particular solution of  $\hat{v}_{3n}$ . Expanding this equation with  $A_n = \frac{a}{2} exp(j\Psi)$ , and separating the resultant equation into the real and imaginary parts, we obtain

$$a' = -n^4 \mu_{2_2} a + -\frac{1}{8} (n\pi)^4 \mu_{4_0} n^2 a^3 + \frac{n^2}{\pi^2} \mu_{3_2} a - 2a \xi_2 \Delta_1 \sin(2\Phi_2) ,$$

$$+a \mu_{4_0} \xi_2 (n\pi)^2 \cos(2\Phi_2) , \qquad (3.67)$$

$$a\Phi_2' = \sigma_2 a + \Delta_3 a - \Delta_2 a^3 - 2a\Delta_1 \xi_2 \cos(2\Phi_2) - a\mu_{4_0} \xi_2 (n\pi)^2 \sin(2\Phi_2)$$
 (3.68)

where

$$\Delta_2 = \frac{1}{8} (n\pi)^2 n^2 \left[ \frac{15}{8} - \left( \frac{1}{3} + S \right) (n\pi)^2 \right], \qquad (3.69)$$

$$\Delta_3 = \frac{n^2}{2} (n\pi)^2 (\alpha_1 \alpha_2 + \alpha_1 \alpha_3) , \qquad (3.70)$$

$$\Phi_2 = \sigma_2 T_2 - \Psi \tag{3.71}$$

and primes indicate derivatives with respect to the time scale  $T_2$ . The steady state condition can be obtained by letting  $a' = a\Phi_2' = 0$ , which leads to

$$-a\xi_{2}[2\Delta_{1}\sin{(2\Phi_{2})}-\mu_{4_{0}}(n\pi)^{2}\cos{(2\Phi_{2})}] = an^{2}[\mu_{2_{2}}n^{2}+\frac{\mu_{4_{0}}}{8}(n\pi)^{4}a^{2}-\frac{\mu_{3_{2}}}{\pi^{2}}](3.72)$$

$$a[2\Delta_1\xi_2\cos(2\Phi_2) + \mu_{4_0}\xi_2(n\pi)^2\sin(2\Phi_2)] = a[\sigma_2 + \Delta_3 - \Delta_2a^2].$$
 (3.73)

Squaring these equations and adding them together, we obtain

$$a^{2}[(n^{4}\mu_{2_{2}} + \frac{1}{8}(n\pi)^{4}\mu_{4_{0}}\omega_{n}a^{2} - \frac{n^{2}}{\pi^{2}}\mu_{3_{2}})^{2} + (\sigma_{2} - \Delta_{2}a^{2} + \Delta_{3})^{2} - (2\xi_{2}\Delta_{1})^{2} - (n\pi)^{4}\xi_{2}^{2}\mu_{4_{0}}^{2}] = 0 \quad (3.74)$$

which is the frequency response equation for this parametric resonance. An example of this frequency response equation is plotted in Figure 3.2. From equation (3.74), we solve for the

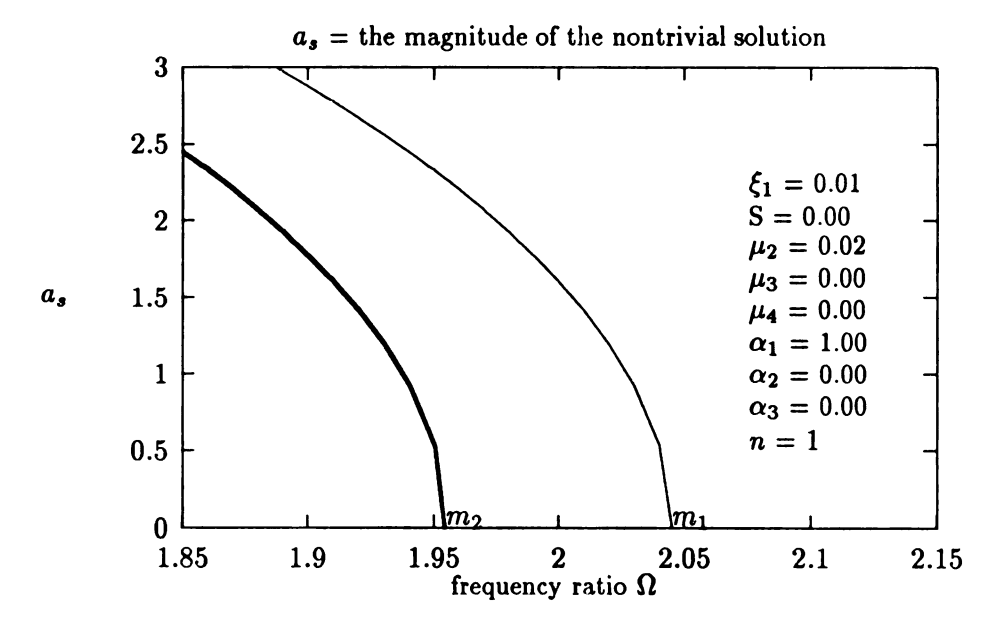


Figure 3.2: Frequency response equation for the principal parametric resonance

nontrivial solution of  $a^2$  and obtain

$$(a_2)^2 = (\frac{1}{k})[-l + \sqrt{l^2 - km}], \qquad (3.75)$$

$$(a_3)^2 = (\frac{1}{k})[-l - \sqrt{l^2 - km}]$$
 (3.76)

where

$$k = \left[ \left( \frac{\mu_{4_0}}{8} \right) (n\pi)^4 \right]^2 + \Delta_2^2, \tag{3.77}$$

$$l = \left(\frac{\mu_{4_0}}{8}\right)(n\pi)^4 \left[n^4\mu_{2_2} - \left(\frac{n}{\pi}\right)^2\mu_{3_2}\right] - (\sigma_2 - \Delta_3)\Delta_2, \qquad (3.78)$$

$$m = \left[ n^4 \mu_{2_2} - \left( \frac{n}{\pi} \right)^2 \mu_{3_2} \right]^2 + (\sigma_2 - \Delta_3)^2 - 4\xi_2^2 \Delta_1^2 - (n\pi)^4 \xi_2^2 \mu_{4_0}^2 . \tag{3.79}$$

For the existence of these real amplitudes  $a_1$ ,  $a_2$  and  $a_3$ , the term inside the radical sign must be positive or zero. This implies that, in order to produce a sustained nontrivial steady state response, the magnitude of the forcing must be large enough to overcome the effect of the energy dissipated. Moreover, we must have

$$\sigma_2 + \Delta_3 < \sqrt{(2\xi_2\Delta_1)^2 + (n\pi)^4 \xi_2^2 \mu_{4_0}^2 - [\mu_{2_2} n^4 - (\frac{n}{\pi})^2 \mu_{3_2}]^2}$$
 (3.80)

for the existence of  $(a_2)^2$ , and

$$\sigma_2 + \Delta_3 < -\sqrt{(2\xi_2\Delta_1)^2 + (n\pi)^4 \xi_2^2 \mu_{4_0}^2 - (\mu_{2_2} n^4 - (\frac{n}{\pi})^2 \mu_{3_2})^2}$$
 (3.81)

for the existence of  $(a_3)^2$ . In order to determine the stability associated with these steady state responses, we compute the the Jacobian matrix associated with equations (3.68) and (3.68) and obtain

$$\begin{bmatrix} -(\frac{a^2}{4})n^2(n\pi)^4\mu_{4_0} & -2(\sigma_2 - \Delta_2 a^2 + \Delta_3)a \\ -2\Delta_2 a & -2n^4\mu_{2_2} - \mu_{4_0}(n\pi)^4n^2(\frac{a^2}{4}) + (\frac{n}{\pi})^2\mu_{3_2} \end{bmatrix}.$$
(3.82)

After we compute the eigenvalues of this matrix, we obtain the following conclusions:

(1) when 
$$\sigma_2 > -\Delta_3 + \sqrt{(2\xi_2\Delta_1)^2 + (n\pi)^4\xi_2^2\mu_{4_0}^2 - (\mu_{2_2}n^4 - (\frac{n}{\pi})^2\mu_{3_2})^2}$$
, there is only one

response: the trivial one, and it is stable,

(2) when  $\sigma_2 < -\Delta_3 + |\sqrt{(2\xi_2\Delta_1)^2 + (n\pi)^4\xi_2^2\mu_{4_0}^2 - (\mu_{2_2}n^4 - (\frac{n}{\pi})^2\mu_{3_2})^2}|$ , the trivial solution becomes unstable, while  $a_2$  exists and is stable,

(3) when  $\sigma_2 < -\Delta_3 - \sqrt{(2\xi_2\Delta_1)^2 + (n\pi)^4\xi_2^2\mu_{4_0}^2 - (\mu_{2_2}n^4 - (\frac{n}{\pi})^2\mu_{3_2})^2}$ ,  $a_3$  exists and is unstable, while the trivial solution and  $a_2$  are stable.

Remark: Before leaving this section, there are few points to make. We first compare the linear and nonlinear results. If we neglect the effects of shear deformation  $\alpha_2$ , rotary inertia  $\alpha_3$ , the friction force introduced by elastic deformation ( $\mu_4 a^3$  term) and bearing damping  $\mu_3$ , then equations (3.68) and (3.68) become

$$a' = -n^4 \mu_{2_2} a - 2a \xi_2 \Delta_1 \sin(2\Phi_2) + a \mu_{4_0} \xi_2 (n\pi)^2 \cos(2\Phi_2) , \qquad (3.83)$$

$$a\Phi_2' = \sigma_2 a - \Delta_2 a^3 - 2a\Delta_1 \xi_2 \cos(2\Phi_2) - a\mu_{4_0} \xi_2 (n\pi)^2 \sin(2\Phi_2).$$
 (3.84)

In consequence, the frequency response equation becomes

$$a^{2}[(n^{4}\mu_{2})^{2} + (\sigma_{2} - \Delta_{2}a^{2})^{2} - (2\xi_{2}\Delta_{1})^{2} - (n\pi)^{4}\xi_{2}^{2}\mu_{4}^{2}] = 0.$$
 (3.85)

It is clear that equations (3.58) and (3.85) coincide with each other in their linear parts. To show this, we substitute  $\mu_{2_2} = \epsilon \mu_{2_1}$ , and  $\xi_2 = \epsilon \xi_1$ , into equation (3.85). Then equation (3.85) reduces to equation (3.58) when a approaches zero. Moreover, the equation describing the variation of the amplitude of the response (equations [3.53] and [3.84]) are in the same form. The difference between the linear and nonlinear analyses appears in the equation describing the variation of the phase angle  $\Phi_2$  (equations [3.54] and [3.84]). This implies that the direct effect of the nonlinearity is to affect the phase angle. From another point of

view, the nonlinearity affects the rate at which energy is pumped into the system. In the absence of nonlinearity, the response is unstable when the parameters are located inside the unstable regions. According the linear theory, the amplitude of response will grow without limit. However, this increasing response amplitude will be accompanied with a change of phase angle because of the presence of nonlinearity. A new steady state condition will then be achieved when the energy put into the system is balanced by the energy dissipated by the damping. Furthermore, let us consider the main nose of instability, a region in which the trivial solution becomes unstable. If we substitute the trivial solution a = 0 into equation (3.85) then we will obtain equation (3.58). From the conclusion obtained from the nonlinear analysis, we obtain the same region of instability regarding the trivial solution.

We next consider the effects of the shear deformation and the rotary inertia which are included in the parameter  $\Delta_3$  in this work. It is clear that these effects can only be found in the nonlinear analysis. These nonlinearities affect the response by shifting the stability region along the frequency axis to the left. In other words, the main nose of instability in which the trivial response becomes unstable will be centered to the left of  $\Omega = 2\omega_n$ . We note that the effect of  $\Delta_3$  is of higher order. Therefore, its effect is included in the analysis by using rescaling relation (3.60). In other words, its effect on the response may not be significant.

# 3.3 Primary Resonance $(\Omega \approx \omega_n)$

In this section, we consider the case in which the frequency  $\Omega$  is near to  $\omega_n$ . This is referred to as the primary resonance. To begin our analysis, let us reconsider equation (3.63) in section 3.2, and assume that  $\Omega$  is near to  $\omega_n$ . Moreover, the damping parameters  $\mu_2$  and  $\mu_4$  are rescaled by equations (3.49) and (3.10). In order to make the analysis clear, we

redefine  $\sigma_1$  to quantitatively represent the nearness of  $\Omega$  to  $\omega_n$ . Hence, we let

$$\Omega = \omega_n + \epsilon \sigma_1 \tag{3.86}$$

in equation (3.63). Under this condition, we must have

$$-2j\omega_n(D_1A_n) - \frac{\xi_2}{n\pi}\Omega^2 exp(j\sigma_1T_1 - j\frac{\pi}{2}) - 2j\mu_{2_1}n^4A_n\omega_n = 0$$
 (3.87)

in order to remove the secular term from the particular solution of  $\hat{v}_{2n}$ . Expanding this equation with  $A_n = \frac{a}{2} exp(j\Psi)$ , and separating the resultant equation into real and imaginary parts, we obtain

$$a' = -\mu_{2_1} n^4 a - \frac{n\xi_2}{\pi} \cos \Phi_1 , \qquad (3.88)$$

$$a\Phi_1' = \sigma_1 a + \frac{n\xi_2}{\pi} \sin \Phi_1 \tag{3.89}$$

where  $\Phi_1$  is given in equation (3.55). The steady state condition can be achieved when  $a'=a\Phi_1'=0$ . Therefore, we obtain

$$n^4 \mu_{2_1} a = -\frac{n\xi_2}{\pi} \cos \Phi_1 , \qquad (3.90)$$

$$\sigma_1 a = -\frac{n\xi_2}{\pi} \sin \Phi_1 . \qquad (3.91)$$

Squaring these two equations and adding them together, we obtain the following frequency response equation:

$$(n^8 \mu_{2_1}^2 + \sigma_1^2) a^2 = (\frac{n\xi_2}{\pi})^2 . (3.92)$$

Therefore, solution of the flexural vibration is approximated by

$$v(x,t) = \epsilon v_1(x,t) + O(\epsilon^2)$$

$$= \epsilon [a\cos(\Omega T_0 - \Phi)] \sin n\pi x + O(\epsilon^2)$$
(3.93)

where a and  $\Phi$  are described by equations (3.88) and (3.89), respectively. The steady state value of the phase angle  $\phi$  is described by

$$\tan \Phi_s = \left(\frac{\sigma_1}{\mu_{2_1}}\right). \tag{3.94}$$

Equation (3.92) is the frequency response of the primary resonance. We note that it does

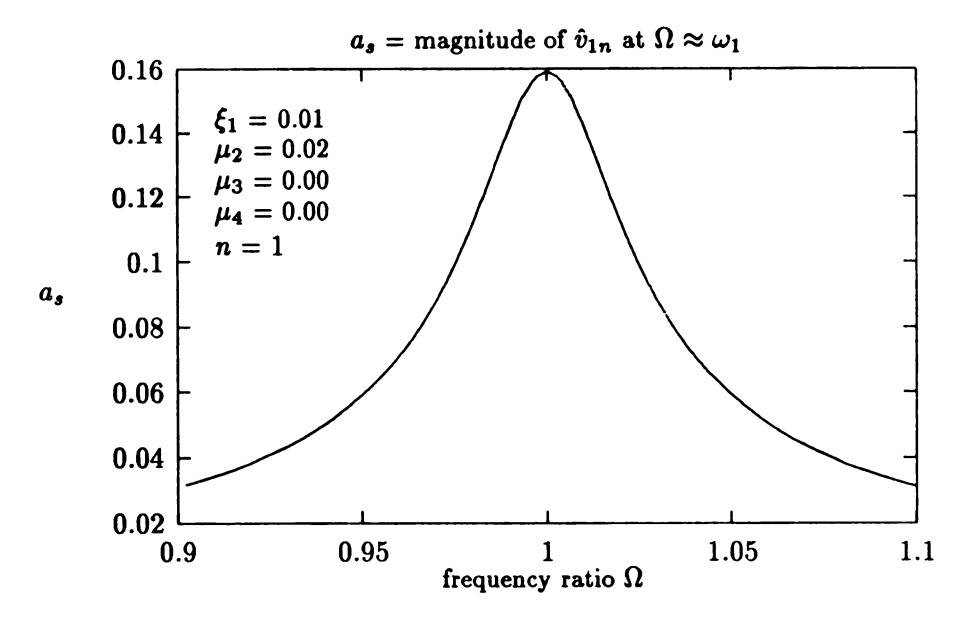


Figure 3.3: Frequency response equation for the primary resonance

not contain any nonlinearity, and hence corresponds to the frequency response condition for a linear oscillator. Figure 3.3 provides an example for this frequency response equation. All these imply that the ordering relation (equation [3.60]) fails to capture the nonlinearity in the analysis. In order to extend our analysis to includes the nonlinearity, we rescale the

length ratio  $\xi$  by letting

$$\xi = \epsilon^3 \xi_3 \,. \tag{3.95}$$

Moreover, we rescale the damping parameters  $\mu_2$ ,  $\mu_3$  and  $\mu_4$  according to equation (3.8), (3.9) and (3.10), respectively. Expanding equations (2.51), (2.52) and (2.53) with these new ordering relations, and equating the coefficients of the like-power terms, we will obtain a sequence of partial differential equations. Applying the same procedure to the boundary conditions, we will obtain a sequence of boundary condition associated with these equations. We then solve these equations by following the same procedure as described in the previous sections. Because this procedure is routine and tedious, we only present a few essential results in the following analysis. For a complete solution procedure, refer to Appendix D. The equation describing the first order flexural vibration is given in equation (3.61). In consequence, the solution of the first order flexural vibration is given by equation (3.62). The equation describing the second order flexural vibration of the connecting rod is given as

$$D_0^2 \hat{v}_{2n} + \omega_n^2 \hat{v}_{2n} = -2j\omega_n (D_1 A_n) exp(j\omega_n T_0) - \frac{2}{n\pi} \mu_{3_2} \Omega \cos n\pi + c.c.$$
 (3.96)

where  $\left(-\frac{2}{n\pi}\mu_{3_2}\Omega\cos n\pi\right)$  comes form the nonhomogeneous boundary conditions. The elimination of the secular terms requires that  $(D_1A_n)=0$ . This implies that the amplitude function of the transverse response is independent of the time scale  $T_1$ . The third order term for the flexural vibration of the connecting rod is described by the following equation:

$$D_0^2 \hat{v}_{3n} + \omega_n^2 \hat{v}_{3n} = -2j\omega_n (D_1 A_n) exp(j\omega_n T_0) + 2j\frac{n^4}{\pi^2} \mu_{3_2} A_n exp(j\omega_n T_0)$$

$$- \left[ \frac{15}{8} - (\frac{1}{3} + S)(n\pi)^2 \right] (n\pi)^2 n^4 A_n^2 \bar{A}_n exp(j\omega_n T_0)$$

$$+ A_n (n\pi)^2 n^6 (\alpha_1 \alpha_2 + \alpha_1 \alpha_3) exp(j\omega_n T_0) - j(n\pi)^4 \mu_{4_0} \omega_n A_n^2 \bar{A}_n exp(j\omega_n T_0)$$

$$-2j\omega_{n}n^{4}\mu_{2}A_{n}exp(j\omega_{n}T_{0})-j\frac{\xi_{3}}{n\pi}exp(j\Omega T_{2})+N.S.T.+c.c.$$
 (3.97)

To describe the nearness of the frequency ratio  $\Omega$  to  $\omega_n$ , we express  $\Omega$  as

$$\Omega = \omega_n + \epsilon^2 \sigma_2 \,. \tag{3.98}$$

Therefore, we must have

$$-2j\omega_{n}(D_{1}A_{n}) + A_{n}(n\pi)^{2}n^{6}(\alpha_{1}\alpha_{2} + \alpha_{1}\alpha_{3}) - 2j\omega_{n}n^{4}\mu_{2_{2}}A_{n} - j(n\pi)^{4}\omega_{n}\mu_{4_{0}}A_{n}^{2}\bar{A}_{n}$$

$$+2j\frac{n^{4}}{\pi^{2}}\mu_{3_{2}}A_{n} - \left[\frac{15}{8} - (\frac{1}{3} + S)(n\pi)^{2}\right](n\pi)^{2}n^{4}A_{n}^{2}\bar{A}_{n} - j\frac{\xi_{3}}{n\pi}exp(j\sigma_{2}T_{2}) = 0$$
(3.99)

in order to remove the secular term from the particular solution of  $\hat{v}_{3n}$ . Expanding this equation with  $A_n = \frac{a}{2} exp(j\Psi)$ , and separating the resultant equation into real and imaginary parts, we obtain

$$a' = -n^4 \mu_{2_2} a - \frac{1}{8} (n\pi)^4 \mu_{4_0} \omega_n a^3 + \frac{n^2}{\pi^2} \mu_{3_2} a - \frac{\xi_3}{n\pi} \cos \Phi_2 , \qquad (3.100)$$

$$a\Phi_2' = \sigma_2 a - \Delta_2 a^3 + \Delta_3 a + \frac{\xi_3}{n\pi} \Omega^2 \sin \Phi_2$$
 (3.101)

where  $\Phi_2$  is defined by equation (3.71),  $\Delta_2$  is defined by equation (3.69) and  $\Delta_3$  is defined by equation (3.70). The steady state condition for these equations can be achieved when  $a'=a\Phi_2'=0$ . This leads to

$$-\left(\frac{n}{\pi}\right)\xi_3\cos\Phi_2 = n^4\mu_{2_2}a + \frac{1}{8}(n\pi)^4\mu_{4_0}\omega_n a^3 - \frac{n^2}{\pi^2}\mu_{3_2}a, \qquad (3.102)$$

$$-(\frac{n}{\pi})\xi_3 \sin \Phi_2 = \sigma_2 a - \Delta_2 a^3 + \Delta_3 a . \qquad (3.103)$$

Squaring these equations and adding them together, we obtain the following frequency response equation:

$$a^{2}[(\sigma_{2} - \Delta_{2}a^{2} + \Delta_{3})^{2} + (n^{4}\mu_{2} + \frac{1}{8}(n\pi)^{4}\mu_{4}\omega_{n}a^{2} - 2\frac{n^{2}}{\pi^{2}}\mu_{3})^{2}] = (\frac{n\xi_{3}}{\pi})^{2}.$$
 (3.104)

Consequently, the frequency response curves take the following form when solved for the detuning parameter:

$$\sigma_2 = \left[\Delta_2 a^2 - \Delta_3\right] \pm \sqrt{\left(\frac{n\xi_3}{a\pi}\right)^2 - \left[n^4 \mu_{2_2} + \frac{1}{8}(n\pi)^4 \mu_{4_0} \omega_n a^2 - \frac{n^2}{\pi^2} \mu_{3_2}\right]^2} \ . \tag{3.105}$$

This equation indicates that the steady-state response can reach its maximum amplitude described by

$$\left(\frac{n\xi_3}{\pi}\right)^2 - a_p^2 \left[n^4 \mu_{2_2} + \frac{1}{8}(n\pi)^4 \mu_{4_0} \omega_n a_p^2 - \frac{n^2}{\pi^2} \mu_{3_2}\right]^2 = 0 \tag{3.106}$$

which occurs at the frequency

$$\Omega = \omega_n + \epsilon \sigma_p = \omega_n + \epsilon^2 (\Delta_2 a_p^2 - \Delta_3) . \tag{3.107}$$

Since  $\Delta_2 < 0$  and  $\Delta_3 > 0$  for each individual mode, we have  $\sigma_p < 0$ . Therefore, the frequency response curves bend to the left. Figure 3.4 provides an example for this frequency response equation. To determine the stability of these steady state responses, we compute the Jacobian matrix associated with equations (3.100) and (3.101), which takes the form:

$$\begin{bmatrix} -n^{4}\mu_{2_{2}} - \frac{3}{8}(n\pi)^{4}\omega_{n}\mu_{4_{0}}a^{2} + \frac{n^{2}}{\pi^{2}}\mu_{3_{2}} & -(\sigma_{2} - \Delta_{2}a^{2} + \Delta_{3})a \\ (\sigma_{2} + 3\Delta_{2}a^{2} + \Delta_{3})/a & -n^{4}\mu_{2_{2}} + \frac{n^{2}}{\pi^{2}}\mu_{3_{2}} - \frac{1}{8}(n\pi)^{4}\omega_{n}\mu_{4_{0}}a^{2} \end{bmatrix} . \quad (3.108)$$

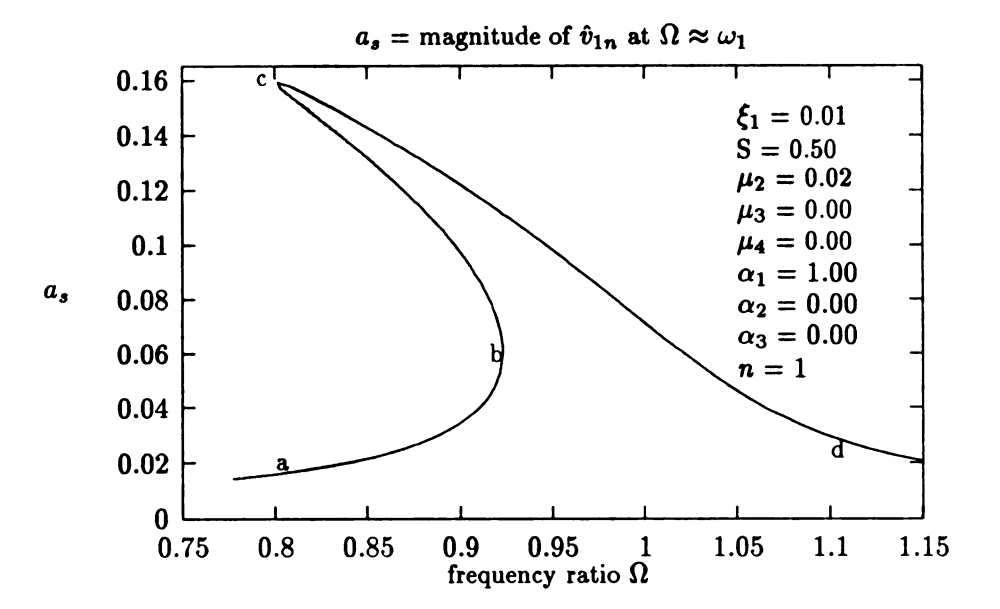


Figure 3.4: Frequency response equation for the primary resonance

By computing the eigenvalues of this matrix, we determine that when

$$[n^{4}\mu_{2_{2}} + \frac{3}{8}(n\pi)^{4}\omega_{n}\mu_{4_{0}}a^{2} - \frac{n^{2}}{\pi^{2}}\mu_{3_{2}}][n^{4}\mu_{2_{2}} + \frac{1}{8}(n\pi)^{4}\omega_{n}\mu_{4_{0}}a^{2} - \frac{n^{2}}{\pi^{2}}\mu_{3_{2}}] + (\sigma_{2} - \Delta_{2}a^{2} + \Delta_{3})(\sigma_{2} - 3\Delta_{2}a^{2} + \Delta_{3}) < 0$$
(3.109)

these steady state responses are unstable. Otherwise, they are stable. The solution v(x,t) of the flexural vibration of the connecting rod can be approximated by

$$v(x,t) = \epsilon v_1(x,t) + O(\epsilon^2)$$

$$= \epsilon \left[ a \cos(\Omega T_0 - \Phi) \right] \sin n\pi x + O(\epsilon^2)$$
(3.110)

where a and  $\Phi$  are described by equations (3.100) and (3.101), respectively. The steady state value of the phase angle is described by

$$\tan \Phi_s = \left(\frac{\sigma_2 - \Delta_2 a^2 + \Delta_3}{\mu_{2_2} n^4 + \frac{1}{8} (n\pi)^4 \omega_n \mu_{4_0} a^2 - \frac{n^2}{\pi^2} \mu_{3_2}}\right). \tag{3.111}$$

From Figure 3.4, it is clear that, when  $\Omega$  is located between point b and c, there exists more than one steady state response. Those steady state responses located along the bc portion of the response curve are unstable, and hence will not be observed either in simulations or experiments. Moreover, for frequences between point b and c in Figure 3.4, the initial conditions will decide the steady state response. In other words, the initial conditions will decide whether the response shall appear along the ab curve or the cd portion. To be more precise, there is a saddle node bifurcation[50, 21] associated with points b and c in Figure 3.4. For each stable steady state response, there is one corresponding basin of attraction. The response is then determined by the location of the initial conditions.

Remark: Before proceeding to the next section, there are few points which need to be made. We first compare the results from the linear and nonlinear analyses. By neglecting the effects of shear deformation, rotary inertia, the friction parameters  $\mu_{3_2}$  and  $\mu_{4_0}$  associated with equations (3.100) and (3.101), we obtain

$$a' = -n^4 \mu_{2_2} a - \frac{n\xi_3}{\pi} \cos \Phi_2 , \qquad (3.112)$$

$$a\Phi_2' = \sigma_2 a + \Delta_2 a^3 + \frac{n\xi_3}{\pi} \sin \Phi .$$
 (3.113)

The resultant frequency response equation takes the form:

$$a^{2}[(\sigma_{2}-\Delta_{2}a^{3})^{2}+(n^{4}\mu_{2_{2}})^{2}]=(\frac{n\xi_{3}}{\pi})^{2}. \tag{3.114}$$

Basically, the equations describing the variation of the amplitude of the response (equations [3.88] and [3.100]) are exactly the same. The only difference between linear and nonlinear analyses shows up in the equations describing the variation of the phase angle

(equations [3.89] and [3.101]). Moreover, equations (3.92) and (3.114) coincide with each other in their linear parts. To show this, we substitute  $\mu_{22} = \epsilon \mu_{21}$ ,  $\xi_3 = \epsilon \xi_2$  and  $\sigma_2 = \epsilon \sigma_1$  into equation (3.114). Then equation (3.114) will reduce to equation (3.92) as a approaches zero. This implies that when the amplitude of response is small, linear theory works well. However, as the amplitude of response increases, the nonlinearity affects the system by changing the rate at which energy is pumped into the system. As a consequence, a new "equilibrium" will be reached when the rate at which energy put into the system is balanced by the rate of energy dissipated.

It is clear that the shear deformation and the rotary inertia do not affect the linear response, because they are not included in the resonance condition. In consequence, they will not affect the peak amplitude of the primary resonance. The shear deformation and the rotary inertia affect the primary resonance by shifting the location of the frequency at which the primary resonance reaches its peak amplitude to the left by a small amount of order  $O(\epsilon^2)$ . In other words, the backbone curve, which is the locus of the peak amplitude associated with the frequency response curves, will not originate from  $\Omega = \omega_n$ . However, the effect of  $\Delta_3$  is independent of the response and is of order  $O(\epsilon^2)$ . Hence, we may expect that  $\Delta_3$  affects the linear approximation by a very small amount.

# 3.4 Superharmonic Resonance $(\Omega \approx \frac{\omega_n}{2})$

Recalling that in analyzing the particular solution of  $\hat{v}_{2n}$  in section 3.1, we assumed that the frequency ratio  $\Omega$  is away from  $2\omega_n$  and  $\frac{\omega_n}{2}$ , and then proceeded to analyze the equations of higher order. The case in which  $\Omega$  is near to  $2\omega_n$  corresponds to the principal parametric resonance and has been studied in section 3.2. In the current section, we investigate a superharmonic resonance case in which the frequency ratio  $\Omega$  is near to  $\frac{\omega_n}{2}$ . To consider

this case, let us express the frequency ratio  $\Omega$  as

$$\Omega = \frac{1}{2}(\omega_n + \epsilon \sigma_1) . \tag{3.115}$$

The damping parameters  $\mu_2$  and  $\mu_4$  are rescaled according to equations (3.49) and (3.10), so that they will show up, together with detuning parameter  $\sigma_1$ , in the final resonant condition. We then expand equations (2.51), (2.52) and (2.53) with these ordering relations, and follow the same procedure as described in section 3.2. Again, we only present a few results which are essential to our work. For a completed analysis, please refer to Appendix B. Following the same procedure as described in the last section, the first order flexural vibration associated with the connecting rod is described by equation (3.29). Consequently, the general solution of  $\tilde{v}_{1n}$  is given in equation (3.30). The equation describing the second order flexural vibration becomes

$$\begin{split} D_0{}^2\hat{v}_{2n} &+ \omega_n^2\hat{v}_{2n} = -2j\omega_n(D_1A_n)exp(j\omega_nT_0) - 2j\mu_{2_1}\omega_nn^4A_nexp(j\omega_nT_0) \\ &+ \frac{(n\pi)^2}{2}\mu_{4_0}\xi_1\Omega\Lambda_1exp(2j\Omega T_0) + \frac{1-\cos n\pi}{n\pi}\xi_1^2\Omega^2exp(2j\Omega T_0 - j\frac{\pi}{2}) \\ &- \frac{1}{4}(1+2S)(n\pi)^2\Lambda_1\xi_1\Omega^2exp(2j\Omega T_0 - j\frac{\pi}{2}) + N.S.T. + c.c. . \end{split}$$
(3.116)

Therefore, in order to remove the secular terms from the particular solution of  $\hat{v}_{2n}$ , we must have

$$-2j\omega_{n}(D_{1}A_{n})-2jn^{4}\mu_{2_{1}}\omega_{n}A_{n}+\frac{\mu_{4_{0}}}{6}\xi_{1}^{2}(n\pi)\omega_{n}exp(j\sigma_{1}T_{1})$$

$$+\left(\frac{\xi_{1}^{2}}{n\pi}\right)\left(\frac{\omega_{n}^{2}}{4}\right)\left[\frac{1-\cos n\pi}{2}-\frac{1}{6}(1+2S)(n\pi)^{2}\right]exp(j\sigma_{1}T_{0}-j\frac{\pi}{2})=0.$$
 (3.117)

Expanding this equation with  $A_n = \frac{a}{2} exp(j\Psi)$ , and then separating the resultant into the

real and imaginary parts, we obtain the following equations:

$$a' = -n^4 \mu_{2_1} a + \frac{\mu_{4_0}}{6} (n\pi) \xi_1^2 \sin \Phi_1 - \frac{\xi_1^2 \omega_n}{24n\pi} [3(1 - \cos n\pi) - 2\frac{\Delta_1}{n^2}] \cos \Phi_1, (3.118)$$

$$a\Phi_1' = \sigma_1 a + \frac{\mu_{40}}{6} (n\pi) \xi_1^2 \cos \Phi_1 + \frac{\xi_1^2 \omega_n}{24n\pi} [3(1 - \cos n\pi) - 2\frac{\Delta_1}{n^2}] \sin \Phi_1$$
 (3.119)

where  $\Phi_1$  is given in equation (3.55), and  $\Delta_1$  is defined by equation (3.56). The steady state condition of these equations can be obtained by letting  $a' = a\phi'_1 = 0$ , which yields

$$n^4 \mu_{2_1} a = \frac{\mu_{4_0}}{6} (n\pi) \xi_1^2 \sin \Phi_1 - \frac{\xi_1^2 \omega_n}{24n\pi} [3(1 - \cos n\pi) - 2\frac{\Delta_1}{n^2}) \cos \Phi_1, \qquad (3.120)$$

$$-\sigma_1 a = \frac{\mu_{4_0}}{6} (n\pi) \xi_1^2 \cos \Phi_1 + \frac{\xi_1^2 \omega_n}{24n\pi} [3(1 - \cos n\pi) - 2\frac{\Delta_1}{n^2}) \sin \Phi_1. \tag{3.121}$$

Squaring these steady state responses and adding them together, we obtain the following equation:

$$a^{2}(n^{8}\mu_{2_{1}}^{2} + \sigma_{1}^{2}) = \xi_{1}^{4}\left[\frac{\mu_{4_{0}}}{6}(n\pi)\right]^{2} + \frac{\omega_{n}^{2}}{(24n\pi)^{2}}\left[3(1-\cos n\pi) - 2\frac{\Delta_{1}}{n^{2}}\right]^{2}$$
(3.122)

which is the frequency response equation for this superharmonic resonance. Figure 3.4 provides an example for this frequency response equation. Therefore, when  $\Omega$  is near to  $\frac{\omega_2}{2}$ , the response of the flexural vibration can be approximated by

$$v(x,t) = \epsilon v_1(x, T_0, T_1, T_2) + O(\epsilon^2)$$

$$= \epsilon \left[ \Lambda_1 \sin \Omega T_0 + a \cos (2\Omega T_0 - \Phi) \right] \sin n\pi x + O(\epsilon^2)$$
(3.123)

where  $\Lambda_1$  is given in equation (3.31), while a and the phase angle  $\Phi$  are described by

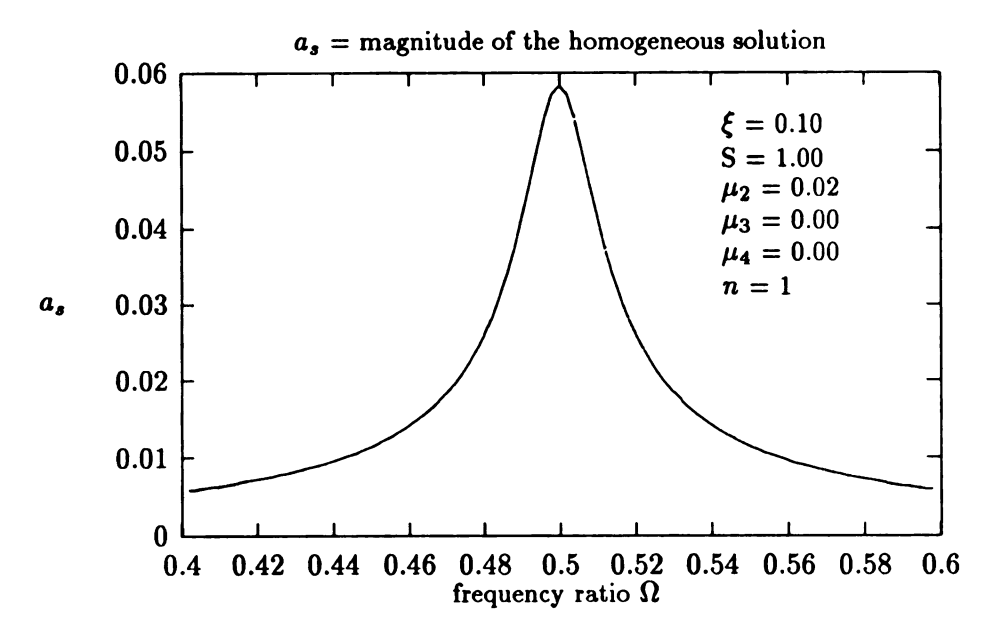


Figure 3.5: Frequency response equation for superharmonic resonance  $(\Omega \approx \frac{\omega_n}{2})$ 

equations (3.119) and (3.119). The steady state value of the phase angle  $\Phi_1$  is given as

$$\tan \Phi_s = \frac{-4\mu_{4_0}\mu_{2_1}(n\pi)^2 + \sigma_1\omega_n[3(1-\cos n\pi) - 2\frac{\Delta_1}{n^2}]}{4\mu_{4_0}\sigma_1(n\pi) + \omega_n[3(1-\cos n\pi) - 2\frac{\Delta_1}{n^2}]}.$$
 (3.124)

Remark: Equation (3.123) is the first order approximate solution to the flexural vibration associated with the connecting rod. Note that this solution consists of two parts: the homogeneous and the particular solutions. A simple calculation of the eigenvalues associated with these steady state responses indicates that the homogeneous solution is stable for  $\mu_{2_1} > 0$ . Hence, a steady state superharmonic resonance exists for all conditions and the solution is composed of two periodic functions. The particular solution is, of course, of the same frequency as the the operating frequency. While the homogeneous solution oscillates with twice the frequency of the operating frequency. Therefore, for this superharmonic resonance, the homogeneous solution of  $\hat{v}_{1n}$  interacts in  $\hat{v}_{2n}$ , and hence does not decay to zero. This indicates that the presence of this non-vanishing homogeneous solution is the

character of the nonlinearity possessed by the system. Moreover, the magnitude of this homogeneous solution is proportional to the square of the length ratio  $\xi_1$ . This implies that the homogeneous solution vanishes more rapidly than the particular solution as the length ratio  $\xi$  approaches zero.

Remark: The mass ratio S has a very interesting effect on the overall flexural response. To analyze this point, we consider the frequency response equation (3.122). We note that the right hand side of this equation represents the magnitude of the external force and is always positive. Therefore, a local minimum will imply a local minimum value of magnitude of the force, and hence a local minimum value of the amplitude of the homogeneous solution. Figure 3.6 shows the influence of S on the magnitude of the homogeneous solution. We note that  $a_s$  decreases when S increases from zero to about 0.11, and then  $a_s$  increases as S increases beyond 0.11. Based on this, we find that  $a_s$  reaches a minimum when

$$2\Delta_1 - 3n^2(1 - \cos n\pi) = 0. (3.125)$$

This implies that a proper choice of the mass ratio will help in suppressing (but not totally eliminating) the peak amplitude associated with this superharmonic resonance (Figure 3.6). Figure 3.6 shows the variation of the peak amplitude  $a_s$  with respect to the mass ratio S. As shown in this figure, the peak amplitude  $a_s$  decreases as S increases from 0 to 0.11, and then it increases as S increases beyond 0.11. We note that the presence of the damping parameter  $\mu_{4_0}$  in the right hand side of the frequency response equation (3.122) indicates that the an increase in  $\mu_{4_0}$  will increase the amplitude of response. It can be interpreted as follows. The presence of  $\mu_{4_0}$  implies the presence of the friction force acting on the slider end, and hence increasing  $\mu_{4_0}$  corresponding to increasing the axial load acting on

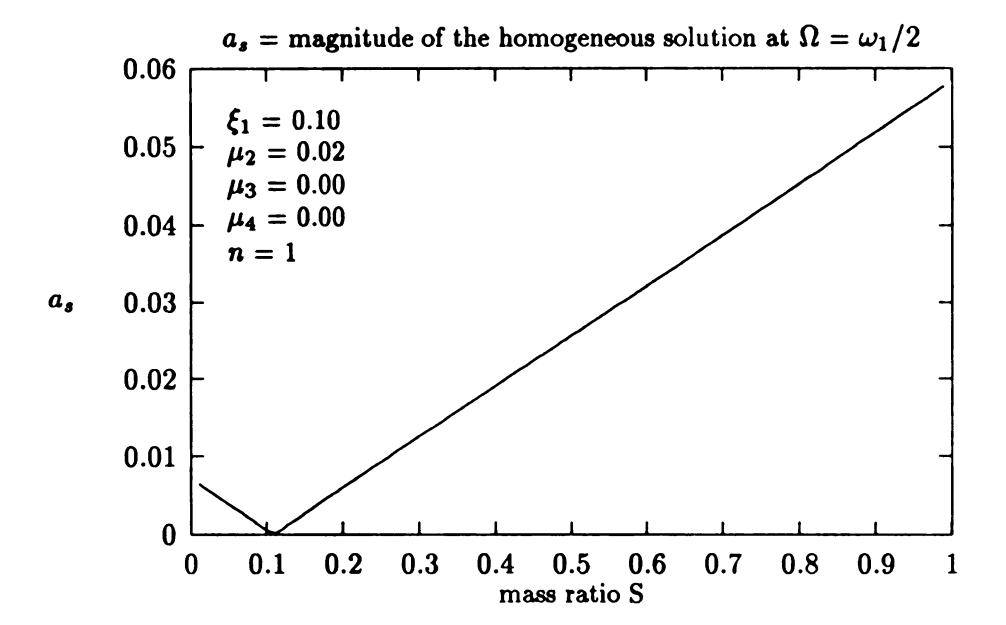


Figure 3.6: Influence of mass ratio S on the amplitude of superharmonic resonance  $(\Omega \approx \frac{\omega_n}{2})$  the connecting rod. As a consequence, the amplitude of response will increase.

## 3.5 Superharmonic Resonance $(\Omega \approx \frac{\omega_n}{3})$

In analyzing the particular solution of equation (3.47), a superharmonic resonance takes place when  $\Omega$  is near to  $\frac{\omega_n}{3}$ . Under this condition, equation (3.47) reduces to

$$D_{0}^{2}\hat{v}_{3n} + \omega_{n}^{2}\hat{v}_{3n} = -2j\omega_{n}(D_{2}A_{n} + n^{4}\mu_{2}A_{n})exp(j\omega_{n}T_{0})$$

$$+ 2j\frac{n^{4}}{\pi^{2}}A_{n}\mu_{3}exp(j\omega_{n}T_{0}) + A_{n}(\alpha_{1}\alpha_{2} + \alpha_{1}\alpha_{3})(n\pi)^{2}n^{4}exp(j\omega_{n}T_{0})$$

$$- \left[\frac{15}{8} - (\frac{1}{3} + S)(n\pi)^{2}\right]n^{6}A_{n}^{2}\bar{A}_{n}exp(j\omega_{n}T_{0}) + \frac{(n\pi)}{1536}\omega_{n}\mu_{4_{0}}\xi_{1}^{3}exp(j\omega_{n}T_{0} + j\sigma_{2}T_{2})$$

$$- j\omega_{n}(n\pi)^{4}\mu_{4_{0}}A_{n}^{2}\bar{A}_{n}exp(j\omega_{n}T_{0}) - j(\frac{1}{32})\mu_{4_{0}}(n\pi)^{2}A_{n}\omega_{n}\xi_{1}^{2}exp(j\omega_{n}T_{0})$$

$$+ f_{1_{1}}\xi_{1}^{2}A_{n}exp(j\omega_{n}T_{0}) + jf_{2_{1}}\xi_{1}^{3}exp(j\omega_{n}T_{0} + j\sigma_{2}T_{2}) + N.S.T. + c.c.$$
 (3.126)

where  $f_{1_1}$  and  $f_{2_1}$  are given in Appendix A. Therefore, we must have

$$-2j\omega_{n}(D_{1}A_{n}) - 2j\omega_{n}n^{4}\mu_{2_{2}}A_{n} + 2j\frac{n^{4}}{\pi^{2}}A_{n}\mu_{3_{2}} - j\omega_{n}(n\pi)^{4}\mu_{4_{0}}A_{n}^{2}\bar{A}_{n}$$

$$+ (\alpha_{1}\alpha_{2} + \alpha_{1}\alpha_{3})(n\pi)^{2}n^{4}A_{n} - \left[\frac{15}{8} + (\frac{1}{3} + S)(n\pi)^{2}\right]n^{6}A_{n}^{2}\bar{A}_{n} + f_{1_{1}}A_{n}\xi_{1}^{2}$$

$$- j(\frac{1}{32})\mu_{4_{0}}(n\pi)^{2}A_{n}\omega_{n}\xi_{1}^{2} + \left[\frac{(n\pi)}{1536}\omega_{n}\mu_{4_{0}}\xi_{1}^{3} + jf_{2_{1}}\xi_{1}^{3}\right]exp(j\sigma_{2}T_{2}) = 0$$
 (3.127)

in order to remove the secular term from the particular solution. Since the leading coefficient of  $\mu_{4_0}exp(j\sigma_2T_2)$  is very small, we neglect this term in the following analysis. Expanding equation (3.127) with  $A_n = \frac{a}{2}exp(j\Psi)$ , and separating the resultant equation into real and imaginary parts, we obtain

$$a' = -an^{2} \left[ \mu_{2_{2}}n^{2} + \frac{\mu_{4_{0}}}{8}(n\pi)^{4}a^{2} + \frac{\mu_{4_{0}}}{64}\mu_{4_{0}}(n\pi)^{2}\xi_{1}^{2} - \frac{\mu_{3_{2}}}{\pi^{2}} \right] + \frac{f_{2_{1}}}{n^{2}}\xi_{1}^{3}\cos\Phi_{2}, (3.128)$$

$$a\Phi'_{1} = a\left[\sigma_{2} + \frac{f_{1_{1}}}{2n^{2}}\xi_{1}^{2} + \Delta_{3} - \Delta_{2}a^{2}\right] - \frac{f_{2_{1}}}{n^{2}}\xi_{1}^{3}\sin\Phi_{2}$$

$$(3.129)$$

where  $\Delta_2$  is defined in equation (3.69) and  $\Delta_3$  is defined in equation (3.70). The steady state conditions can be achieved by letting  $a'=a\Phi_2'=0$ . This yields

$$\frac{f_{2_1}}{n^2}\xi_1^3\cos\Phi_2 = a\left[\mu_{2_2}n^4 + \frac{\mu_{4_0}}{8}(n\pi)^4n^2a^2 + (\frac{\mu_{4_0}}{64})(n\pi)^2n^2\xi_1^2 - \frac{n^2}{\pi^2}\mu_{3_2}\right], \quad (3.130)$$

$$\frac{f_{2_1}}{n^2}\xi_1^3\sin\Phi_2 = \left[\sigma_2 + \frac{f_{1_1}}{2n^2}\xi_1^2 + \Delta_3 - \Delta_2a^2\right]. \quad (3.131)$$

Squaring these equations and adding them together, we obtain the following equation:

$$[(\mu_{2_2}n^4 + \frac{\mu_{4_0}}{8}(n\pi)^4n^2a^2 + (\frac{\mu_{4_0}}{64})(n\pi)^2n^2\xi_1^2 - \frac{n^2}{\pi^2}\mu_{3_2})^2 + (\sigma_2 + \frac{f_{1_1}}{2n^2}\xi_1^2 + \Delta_3 - \Delta_2a^2)^2]a^2 = (\frac{f_{2_1}}{n^2}\xi_1^3)^2$$
(3.132)

which is the frequency response equation for this superharmonic resonance. We then solve the values of  $\sigma_2$  and obtain the following frequency response curves:

$$\sigma_{2} = -\frac{f_{1_{1}}}{2n^{2}}\xi_{1}^{2} + \Delta_{2}a^{2} - \Delta_{3}$$

$$\pm \sqrt{\left(\frac{f_{2_{1}}}{n^{2}a}\xi_{1}^{3}\right)^{2} - n^{4}\left[\mu_{2_{2}}n^{2} + \frac{\mu_{4_{0}}}{8}(n\pi)^{4}a^{2} + \left(\frac{\mu_{4_{0}}}{64}\right)(n\pi)^{2}\xi_{1}^{2} - \frac{\mu_{3_{2}}}{\pi^{2}}\right]^{2}}. (3.133)$$

Thus, despite the presence of the damping parameters, the homogeneous solution does not decay to zero. Furthermore, the steady state response takes the form:

$$v(x,t) = \epsilon v_1(x,t) + O(\epsilon^2)$$

$$= \epsilon [\Lambda_1 \sin \Omega T_0 + a \cos (3\Omega T_0 - \Phi)] \sin n\pi x + O(\epsilon^2)$$
(3.134)

where a and the phase angle  $\Phi$  are described by equations (3.128) and (3.129). The steady state value of the phase angle  $\Phi$  is described by

$$\tan \Phi_s = \left[ \frac{\sigma_2 + \frac{f_{1_1}}{2n^2} \xi_1^2 + \Delta_3 - \Delta_2 a^2}{\mu_{2_2} n^4 + (\frac{\mu_{4_0}}{8})(n\pi)^4 n^2 a^2 + (\frac{\mu_{4_0}}{64})(n\pi)^2 n^2 \xi_1^2 - (\frac{n^2}{\pi^2})\mu_{3_2}} \right]. \tag{3.135}$$

By computing the eigenvalues of the Jacobian matrix associated with equations (3.128) and (3.129), we determine that when

$$(n^{4}\mu_{2_{2}} + \frac{\mu_{4_{0}}}{8}(n\pi)^{4}n^{2}a^{2} + (\frac{\mu_{4_{0}}}{64})(n\pi)^{2}n^{2}\xi_{1}^{2} - \frac{n^{2}}{\pi^{2}}\mu_{3_{2}})$$

$$(n^{4}\mu_{2_{2}} + \frac{3\mu_{4_{0}}}{8}(n\pi)^{4}n^{2}a^{2} + (\frac{\mu_{4_{0}}}{64})(n\pi)^{2}n^{2}\xi_{1}^{2} - \frac{n^{2}}{\pi^{2}}\mu_{3_{2}})$$

$$+(\sigma_{2} + \frac{f_{1_{1}}}{2n^{2}}\xi_{1}^{2} - \Delta_{2}a^{2} + \Delta_{3})(\sigma_{2} + \frac{f_{1_{1}}}{2n^{2}}\xi_{1}^{2} - 3\Delta_{2}a^{2} + \Delta_{3}) < 0$$
(3.136)

these steady state responses are unstable. Otherwise they are stable.

Remark: According to this analysis, the free oscillation term does not decay to zero, despite the presence of the damping parameter. Therefore, the steady state response is composed of two periodic functions. The particular solution oscillates with the same frequency as that of the external frequency, while homogeneous solution oscillates with the frequency that is three times the operating frequency  $\Omega$ . We note that the amplitude of the particular solution is of order  $O(\xi)$ , and the homogeneous solution is of order  $O(\xi^3)$ . This indicates that the free oscillation term vanishes more rapidly than the forcing oscillation as  $\xi$  approaches zero. From the frequency response curves and the stability analysis, we know that within a certain frequency region, there exists more than one steady state response. We note that the homogeneous solution possesses a peak amplitude  $a_p$  described as

$$(f_{2_1}\frac{\xi_1^3}{n^2})^2 - a_p^2[\mu_{2_2}n^4 + n^2(n\pi)^4\mu_{4_0}\frac{a_p^2}{8} + \frac{xi_1^2}{64}n^2(n\pi)^2\mu_{4_0} - \frac{n^2}{\pi^2}\mu_{3_2}]^2 = 0$$
 (3.137)

which occurs at

$$\sigma_{2_p} = -\frac{f_{1_1}}{2n^2} \xi_1^2 + \Delta_2 a_p^2 - \Delta_3 . \qquad (3.138)$$

We note that  $\Delta_2 < 0$  in the last equation. This indicates that the frequency response curves bends to the left corresponding a superharmonic resonance with softening type of nonlinearity. Figure 3.7 provides an example for the frequency response equation for this superharmonic resonance. Note that, in Figure 3.7, there is almost no bending associated with the response curve. This implies that, to observe higher order superharmonic resonances, the bending effect may require a larger length ratio as well as a larger mass ratio. In other words, it is necessary to have strong nonlinearity and a large response amplitude of response in order to achieve a significant bending in the response curve. Another interesting phenomenon accompanying this superharmonic resonance is the influence of the mass ratio

on the peak amplitude  $a_p$ . The numerator of equation (3.137) is the force applied to this superharmonic resonance, and it is a quadratic function in terms of S. A proper choice of the mass ratio S will minimize the magnitude of the force and hence minimize the amplitude of the response. Figure 3.8 shows the influence of the mass ratio on the peak amplitude associated with the superharmonic resonance. From this figure, we see that the amplitude of the response will decrease when S is increases from zero to a critical value; while the peak amplitude will increase when S is beyond this critical value.

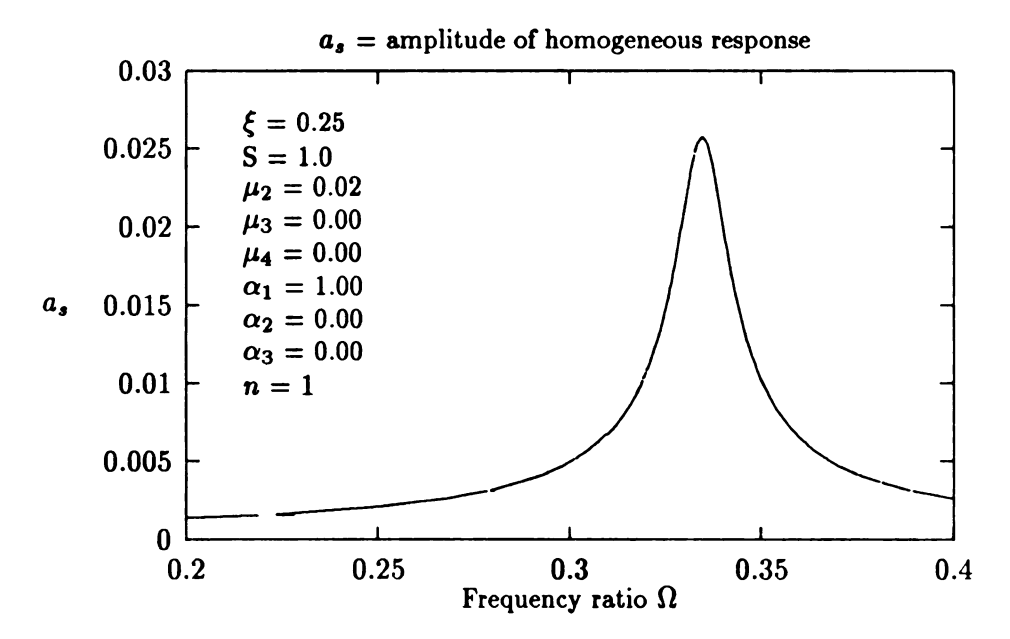


Figure 3.7: Frequency response equation for superharmonic resonance  $(\Omega \approx \frac{\omega_n}{3})$ 

## 3.6 Subharmonic Resonance $(\Omega \approx 3\omega_n)$

In this section, we consider the case in which  $\Omega$  is near to  $3\omega_n$ . Under this condition, the system is potentially in a state of subharmonic resonance. To analyze this subharmonic resonance, we express  $\Omega$  as

$$\Omega = 3(\omega_n + \epsilon^2 \sigma_2). \tag{3.139}$$

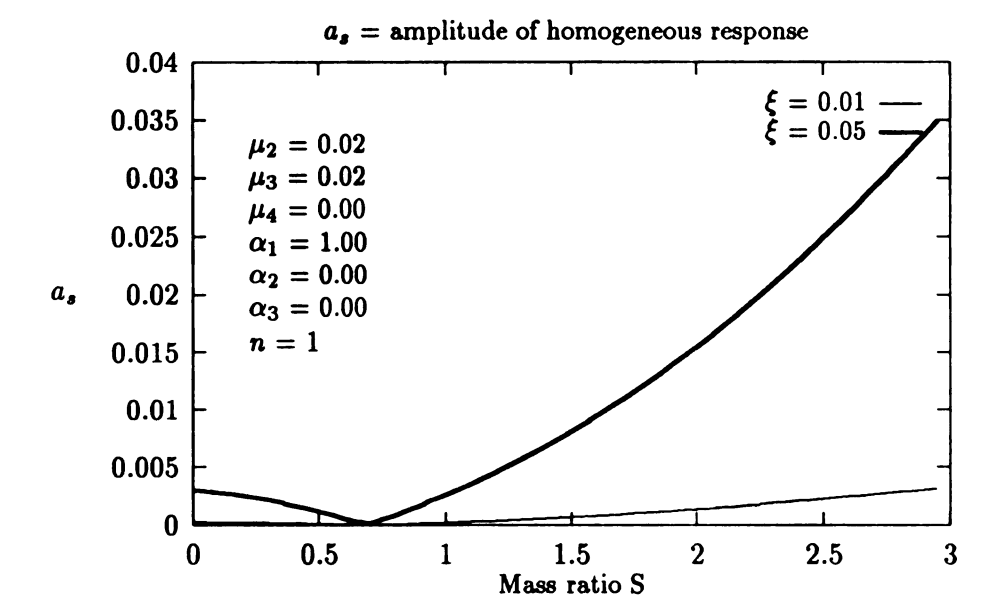


Figure 3.8: Influence of S on the peak amplitude of the superharmonic resonance  $(\Omega \approx \frac{\omega_n}{3})$ Then equation (3.47) reduces to

$$D_{0}^{2}\hat{v}_{3n}^{2} + \omega_{n}^{2}\hat{v}_{3n} = -2j\omega_{n}\left[\mu_{22}n^{4} + D_{2}A_{n} + j\mu_{40}(n\pi)^{4}A_{n}^{2}\bar{A}_{n}\right]exp(j\omega_{n}T_{0})$$

$$+ f_{12}\xi_{1}^{2}A_{n}exp(j\omega_{n}T_{0}) + \left[jf_{31}\xi_{1}\bar{A}_{n}^{2} + (\frac{9}{8})\mu_{40}(n\pi)^{3}\omega_{n}\xi_{1}\bar{A}_{n}^{2}\right]exp(3j\sigma_{2}T_{2} + j\omega_{n}T_{0})$$

$$+ (\alpha_{1}\alpha_{2} + \alpha_{1}\alpha_{3})(n\pi)^{2}n^{4}A_{n}exp(j\omega_{n}T_{0}) + j(\frac{81}{32})\mu_{40}\xi_{1}^{2}(n\pi)^{2}A_{n}exp(j\omega_{n}T_{0})$$

$$- (n\pi)^{2}\left[\frac{15}{8} - (\frac{1}{3} + S)(n\pi)^{2}\right]n^{4}A_{n}^{2}\bar{A}_{n}exp(j\omega_{n}T_{0})$$

$$+ 2j\frac{n^{4}}{\pi^{2}}\mu_{32}A_{n}exp(j\omega_{n}T_{0}) + N.S.T. + c.c. \tag{3.140}$$

where c.c. represents the complex conjugate term of the proceeding terms, and an overbar stands for the complex conjugate term of the corresponding function. Hence, we must have

$$-2j\omega_{n}(\mu_{22}n^{4}+D_{2}A_{n})+2j\frac{n^{4}}{\pi^{2}}\mu_{32}A_{n}+(\alpha_{1}\alpha_{2}+\alpha_{1}\alpha_{3})(n\pi)^{2}n^{4}A_{n}$$

$$-(n\pi)^{2}\left[\frac{15}{8}-(\frac{1}{3}+S)(n\pi)^{2}\right]n^{4}A_{n}^{2}\bar{A}_{n}+f_{12}\xi_{1}^{2}A_{n}exp(j\omega_{n}T_{0})$$

$$-j\omega_{n}\mu_{40}\left[(n\pi)^{4}A_{n}^{2}\bar{A}_{n}+(\frac{81}{32})(n\pi)^{2}\xi_{1}^{2}A_{n}\right]$$

+ 
$$\left[jf_{3_1}\xi_1\bar{A}_n^2 + (\frac{9}{8})\mu_{4_0}(n\pi)^3\omega_n\xi_1\bar{A}_n^2\right]exp(3j\sigma_2T_2) = 0$$
 (3.141)

in order to remove the secular term from the particular solution. Expanding equation (3.141) with  $A_n = \frac{a}{2} exp(j\Psi)$ , and separating the resultant equation into real and imaginary parts, we obtain

$$a' = -a \left[ n^4 \mu_{2_2} - \left( \frac{n}{\pi} \right)^2 \mu_{3_2} + \frac{\mu_{4_0}}{8} \omega_n (n\pi)^4 a^2 + \left( \frac{81}{64} \right) \mu_{4_0} (n\pi)^2 \omega_n \right]$$

$$+ \left( \frac{f_{3_1} \xi_1}{4n^2} \right) a^2 \cos \left( 3\Phi_2 \right) , \qquad (3.142)$$

$$a\Phi_2' = \sigma_2 a + \frac{f_{1_2}}{2n^2} \xi_1^2 a - \frac{\xi_2}{4n^2} f_{3_1} a^2 \sin(3\Phi_2) + \Delta_3 a - \Delta_2 a^3$$
 (3.143)

The steady state conditions can be obtained by letting  $a' = a\Phi_2' = 0$ , these yield

$$(\frac{f_{3_1}\xi_1}{4n^2})a^2\cos(3\Phi_2) = a[n^4\mu_{2_2} - \frac{n^2}{\pi^2}\mu_{3_2} + \mu_{4_0}n^2(n\pi)^4(\frac{a^2}{8}) + (\frac{81}{64})(n\pi)^2n^2a\xi_1^2[3.144)$$

$$\frac{\xi_2}{4n^2}f_{3_1}a^2\sin(3\Phi_2) = \sigma_2a + \frac{f_{1_2}}{2n^2}\xi_1^2a + \Delta_3a - \Delta_2a^3.$$

$$(3.145)$$

We obtain the frequency response equation which takes the form:

$$a^{2}[(\mu_{2_{2}}n^{4} - \frac{n^{2}}{\pi^{2}}\mu_{3_{2}} + \mu_{4_{0}}n^{2}(n\pi)^{4}(\frac{a^{2}}{8}) + (\frac{81}{64})(n\pi)^{2}n^{2}a\xi_{1}^{2})^{2} + (\sigma_{2} + \frac{f_{1_{2}}}{2n^{2}}\xi_{1}^{2} + \Delta_{3} - \Delta_{2}a^{2})^{2} - (\frac{f_{3_{1}}\xi_{1}}{4n^{2}})^{2}a^{2}] = 0 \quad (3.146)$$

by squaring equations (3.144) and (3.145), and adding them together. From equation (3.146), we know that the trivial solution for a is always a steady state response. Due to the complexity of this equation, we neglect the effect of  $\mu_{40}$  in the following analysis. We solve

equation (3.146) for the nontrivial values of  $a^2$  and obtain

$$(a_{2,3})^2 = (\frac{1}{2\Delta_2^2})[p \pm \sqrt{p^2 - 4q}]$$
 (3.147)

where coefficients p and q are

$$p = 2\Delta_2(\sigma_2 + \frac{f_{1_2}}{2n^2}\xi_1^2 + \Delta_3) + (\frac{f_{3_1}}{4n^2}\xi_1)^2, \qquad (3.148)$$

$$q = (\mu_{2_2}n^4 - \frac{n^2}{\pi^2}\mu_{3_2})^2 + (\sigma_2 + \frac{f_{1_2}}{2n^2}\xi_1^2 + \Delta_3)^2. \tag{3.149}$$

We note that q is always positive. Therefore, these nontrivial free oscillations exist only if  $p \ge 0$  and  $p^2 - 4q \ge 0$ . When these conditions hold, it is possible for the system to respond in such a way that the homogeneous oscillation does not decay to zero, in spite of the presence of damping parameters. In consequence, the steady state response can be approximated by

$$v(x,t) = \epsilon v_1 + O(\epsilon^2) = \epsilon (a_s \cos(\frac{\Omega}{3}T_0 - \frac{\Phi_s}{3}) + \Lambda_1 \sin\Omega T_0) + O(\epsilon^2)$$
 (3.150)

where  $a_s$  is described by equation (3.147),  $\Lambda_1$  is defined by equation (3.31), and the phase angle  $\Phi_s$  is given by

$$\tan \Phi_s = \left(\frac{\sigma_2 + \frac{f_{12}}{2n^2}\xi_1^2 + \Delta_3}{n^4\mu_{22} - \frac{n^2}{\pi^2}\mu_{32}}\right). \tag{3.151}$$

Remark: We note that the response of the system is described as follows. When the initial conditions are selected in such a way that the resulting steady state corresponds to a stable nontrivial solution of  $a_s$ , then the magnitude of the free oscillation term does not equal to zero. Under this condition, the first order flexural response associated with the connecting rod contains frequencies of  $\Omega$  and  $\frac{\Omega}{3}$ . Otherwise, the first term of equation (3.150) will be

zero, only particular solution will exist, and the response contains only the frequency  $\Omega$ . Friction parameter  $\mu_4$ , which is used of model the friction force acting between the slider mass and its contact surface, has a favorable effect in reducing the amplitude of response. This is caused by the friction force introduced by the elastic deformation, which behaves as a resistance to prevent the connecting rod from further deformation.

### 3.7 Summary and Conclusion

In this section, we summarize the results obtained in previous sections. Based on the observations from previous investigators[11, 49] and the analytical results obtained in the previous sections, we select in turn the length ratio  $\xi$ , the frequency ratio  $\Omega$ , the mass ratio S, and the damping parameters  $\mu_2$ ,  $\mu_3$  and  $\mu_4$  and then provide a detailed discussion regarding the effect of each individual parameter on the overall response.

## 3.7.1 Effect of the Length Ratio $\xi$

As we mentioned in the introductory section, the increase of the inertial force is primarily responsible for the failure of the traditional dynamic analysis of mechanisms. In this problem, the acceleration components  $a_x$  and  $a_y$  are proportional to the length ratio  $\xi$  (equations [2.11] and [2.12]). Consequently, the inertial force is proportional to this parameter. The general solution of the first order flexural vibration is given as a combination of the particular and homogeneous solutions. The magnitude of the particular solution is proportional to  $\xi$ . If no resonance occurs, the free oscillation term will decay to zero, and hence steady state response contains the particular solution only. In consequence, the amplitude of the response will be proportional to the length ratio. In the case of primary resonance, the amplitude of the resonance is proportional to  $\xi$  (equation[3.106]). Figure 3.9

shows the effect of  $\xi$  on the amplitude of the primary resonance. Moreover, the frequency at which this peak amplitude is observed depends upon the square of the magnitude of the particular solution, which in turn depends on  $\xi^2$ .

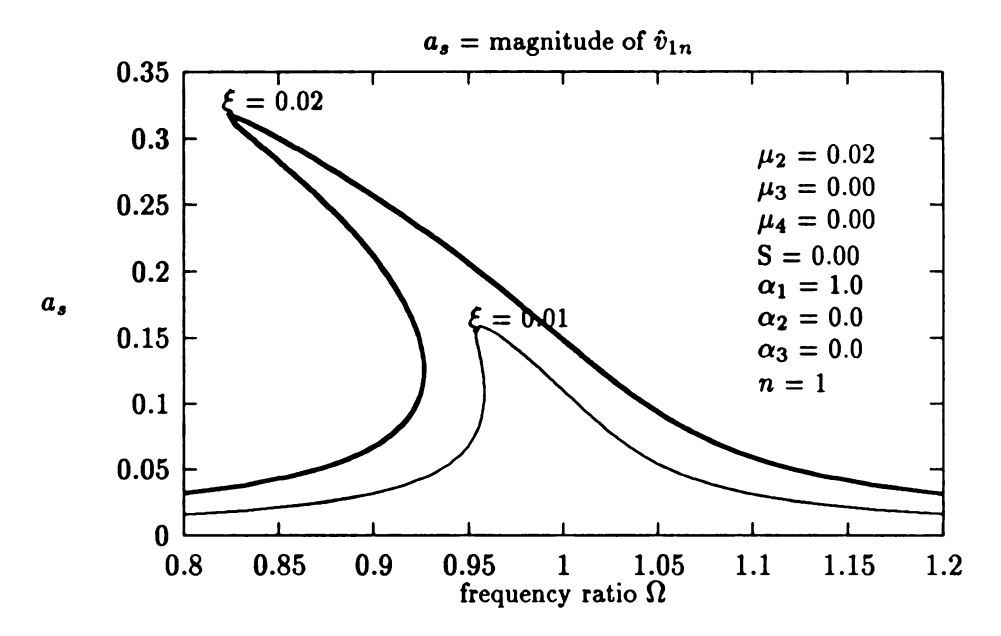


Figure 3.9: Influence of  $\xi$  on the primary resonance

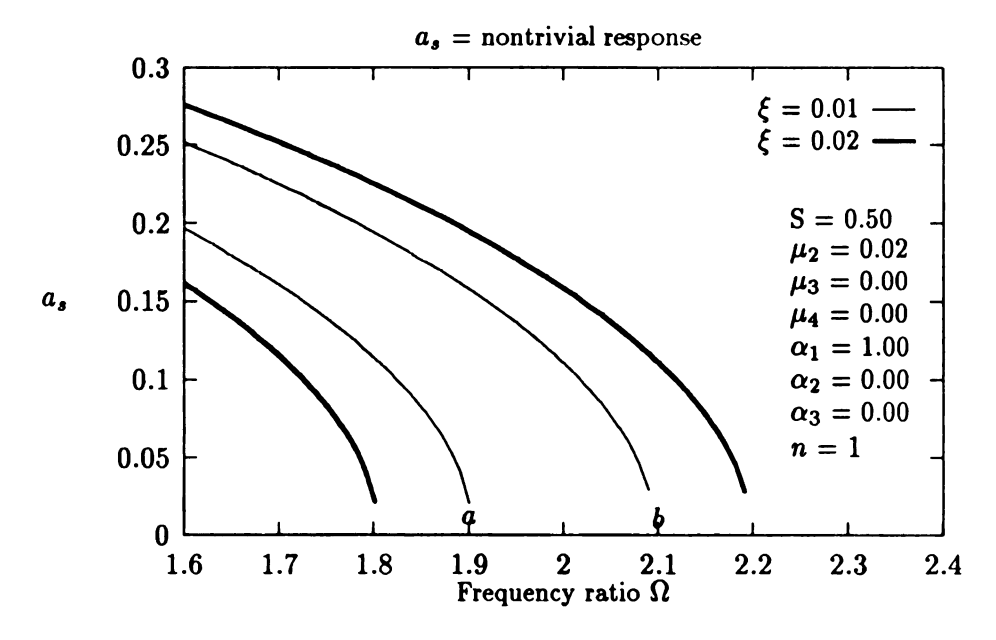


Figure 3.10: Influence of  $\xi$  on the main nose of instability

In the case of the principal parametric resonance, the width of the frequency region in which the trivial response becomes unstable also depends on  $\xi$  (equation[3.59]). In other

words, the width of main nose of instability is proportional to  $\xi$ . Figure 3.6 shows the effect of the length ratio on the main nose of instability. We note that, in Figure 3.6, the width between the transition curves increases when  $\xi$  increases. Figure 3.10 shows the effect of the length ratio on the amplitude of the nontrivial responses. We note that, in Figure 3.10, the region between points a and b indicates the region in which the trivial response becomes unstable. In the case of superharmonic resonances, the magnitude of the non-zero homogeneous solution also depends on  $\xi$ . To be more precise, when  $\Omega$  is near to  $\omega_n/2$ , the magnitude of the non-zero free oscillation term is of order  $O(\xi^2)$ ; when  $\Omega$  is near to  $\omega_n/3$ , while the magnitude of the non-zero free oscillation term is of order  $O(\xi^3)$ . Hence, the contribution of the non-zero homogeneous solution depends on the order of  $\xi$ . All these imply that the length ratio is the primary parameter for the current problem.

#### 3.7.2 Effect of Mass Ratio S

The effect of this parameter is not immediately clear. Generally speaking, it acts as the nonlinearity associated with the system. In order to make our discussion as clear as possible, we need to consider each resonance case separately. In the case of primary resonance case, a slight increase of S will cause a significant increase of the value of  $\sigma_p$ , the value of detuning at which the peak amplitude occurs. To make this point more clear, let us consider the following cases: S = 0 and S = 1. When there is no mass attached to the slider end, the value of  $\sigma_p$  is given as

$$(\sigma_p)_{S=0} = (\frac{\pi^2}{3} - \frac{15}{8})\frac{\pi^2}{8}$$
 (3.152)

for the first mode (n=1). In consequence, the frequency at which the peak amplitude associated with the primary resonance can be observed will shift to the left by an amount  $\epsilon^2 \sigma_p$  with the value of  $\sigma_p$  being given by equation (3.152). Now, we consider the case in

which S = 1. When S = 1, the value of  $\sigma_p$  becomes

$$(\sigma_p)_{S=1} = (\frac{\pi^2}{3} - \frac{15}{8})\frac{\pi^2}{8} - \frac{\pi^4}{8} = (\sigma_p)_{S=0} - \frac{\pi^4}{8}$$
 (3.153)

A rough estimate of the difference between these two values of  $\sigma_p$  shows that  $(\sigma_p)_{S=1}$  is about eight times the value of  $(\sigma_p)_{S=1}$ . Moreover, this ratio will increase as the value of S increases. This implies that the value of  $\sigma_p$  is very sensitive to the value of S. A slight change of S will cause a significant change of  $\sigma_p$ . Figure 3.11 shows the influence of the mass ratio S on the primary resonance.

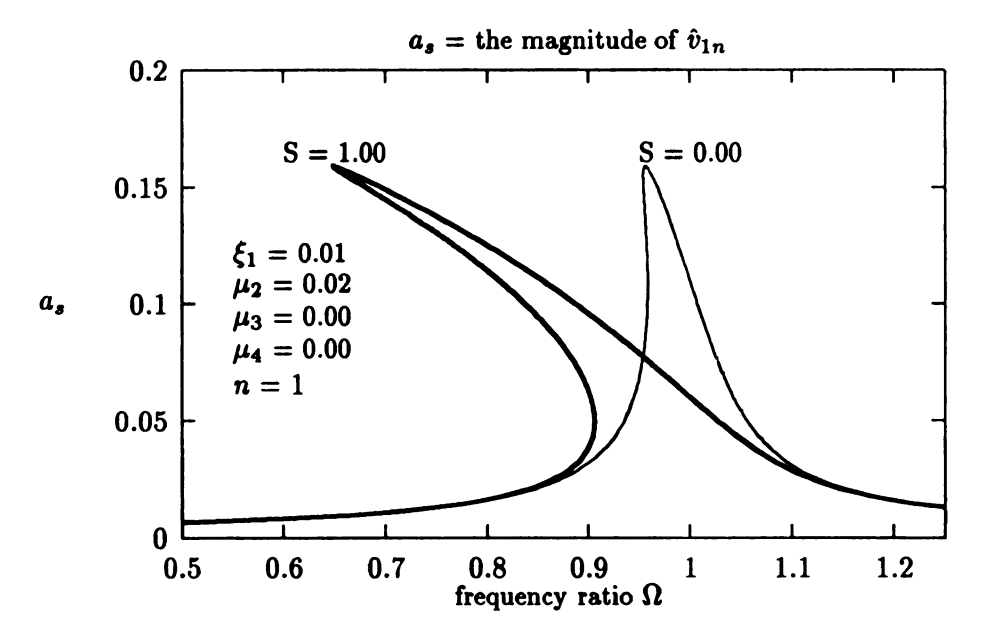


Figure 3.11: Influence of S on the primary resonance

The mass ratio S affects the principal parametric resonance by increasing the width of the main noise of instability. Figure 3.12 shows the influence of S to the main nose of instability. From this figure, it is very clear that the distance between two transition curves increases when the mass ratio S increases. Figure 3.13 shows the amplitude of the nontrivial homogeneous response associated with the principal parametric resonance.

In all the superharmonic resonances, S has a very interesting effect on the response. We

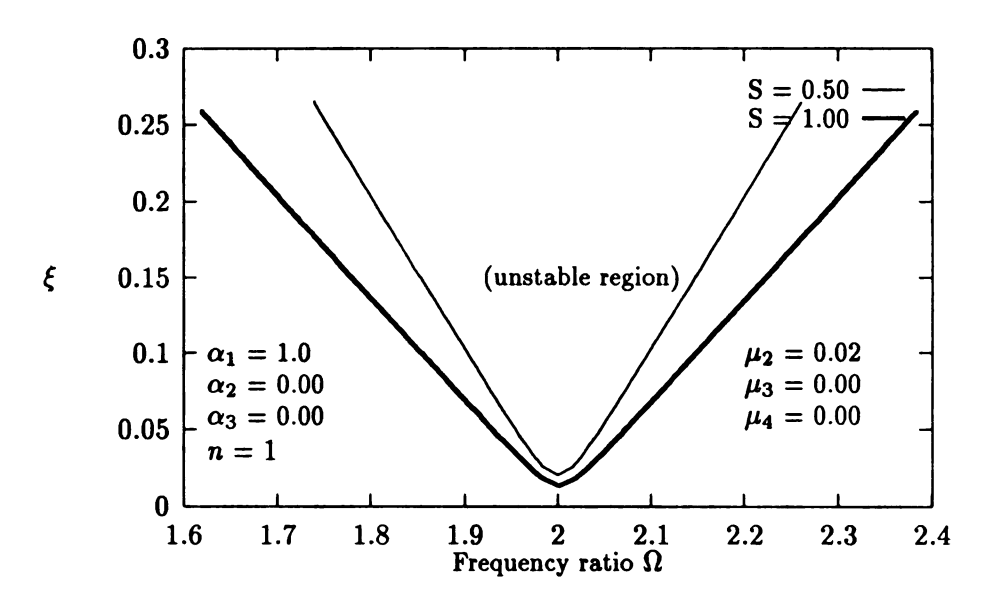


Figure 3.12: Influence of S on the main nose of instability

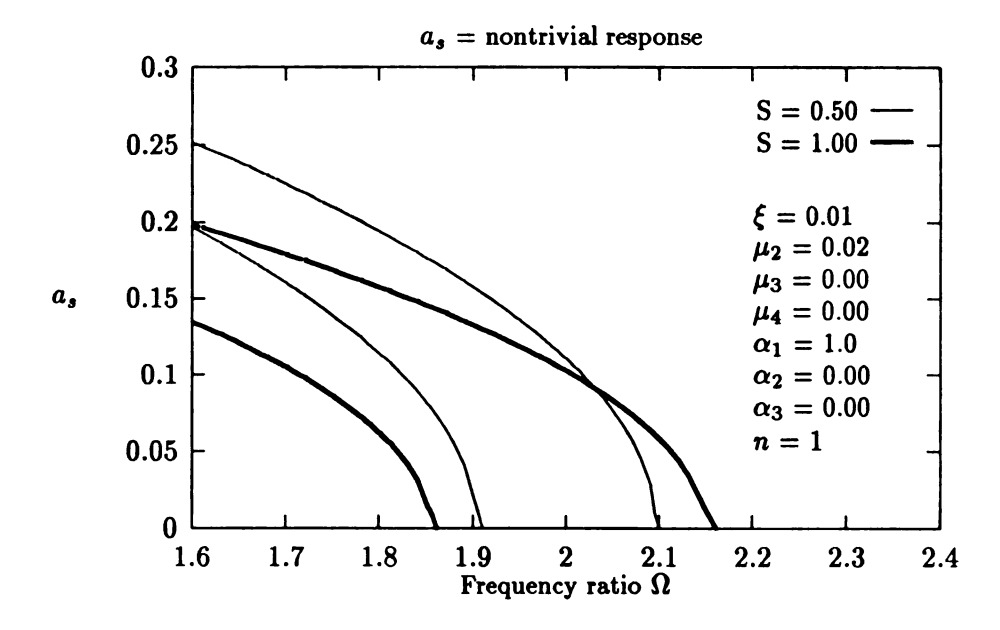


Figure 3.13: Influence of S on the principal parametric resonance

first consider the case in which  $\Omega$  is near to  $\frac{\omega_n}{2}$ . When this resonance occurs, the steady state response is composed of particular and homogeneous solutions. The magnitude of the free oscillation component depends on the value of S. It is interesting to find that the magnitude of the free oscillation term decreases as S increases from zero up to a critical value, while the magnitude increases as S is increased beyond this critical value (which is the root of equation (3.125)). Hence, the magnitude of the overall response follows the same trend as the homogeneous solution (Figure 3.6). This implies that a proper choice of the mass ratio S can aid in decreasing the amplitude of superharmonic resonances. This may have important practical implication for the design of slider crack mechanisms.

#### 3.7.3 Effect of Damping Parameters $\mu_2$ , $\mu_3$ and $\mu_4$

The internal material damping  $\mu_2$  has a favorable effect on the overall response of the system. In the primary resonance case, the presence of  $\mu_2$  in the frequency response equations (3.104) and (3.92) will reduce the peak amplitude of the system. The amplitude of this resonance will decrease as  $\mu_{2_2}$  is increased (Figure 3.14). In the principal parametric resonance, the width of the main nose of instability will decrease as we increase the value of  $\mu_{2_1}$  in equation (3.58). Moreover, the amplitude of the response decreases as we increase the value of  $\mu_{2_2}$  in equation (3.74). Figure 3.15 shows the effect of the damping parameter  $\mu_2$  on the width of the main nose of instability. We note that, in Figure 3.15, the presence of  $\mu_2$  will cause the upward vertical movement of the transition curve. Therefore, the width of the main nose of instability will decrease. As a matter of fact, the shrinking accompanied with the presence of  $\mu_2$  may be so large that the width of the main nose of instability reduces to zero for a specific value of  $\xi$ . Figure 3.16 shows the influence of  $\mu_2$  on the branches of the nontrivial responses associated with the principal parametric resonance. The am-

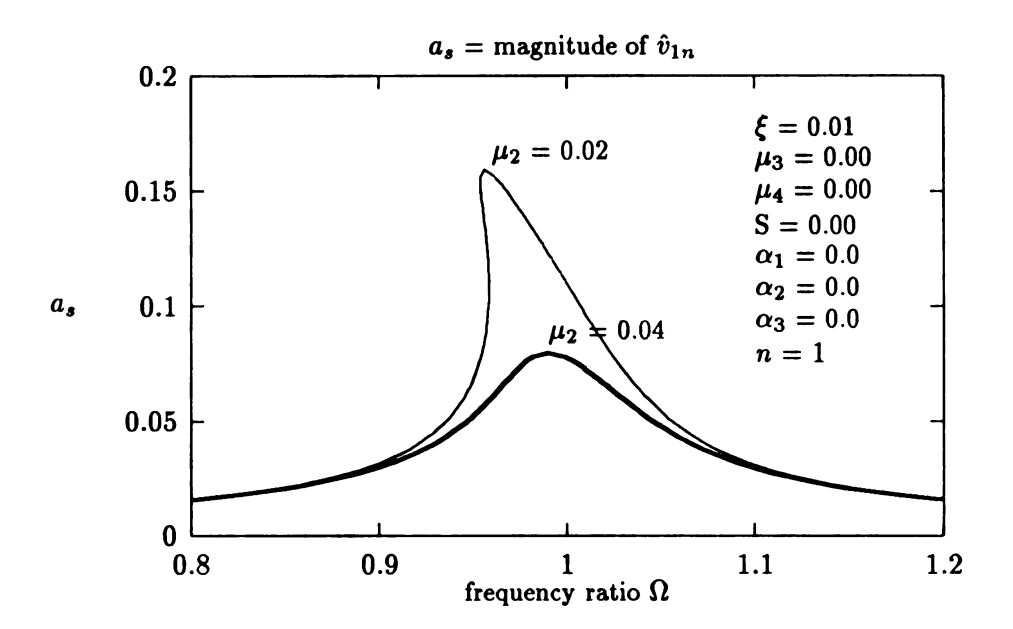


Figure 3.14: Influence of  $\mu_2$  on the primary resonance

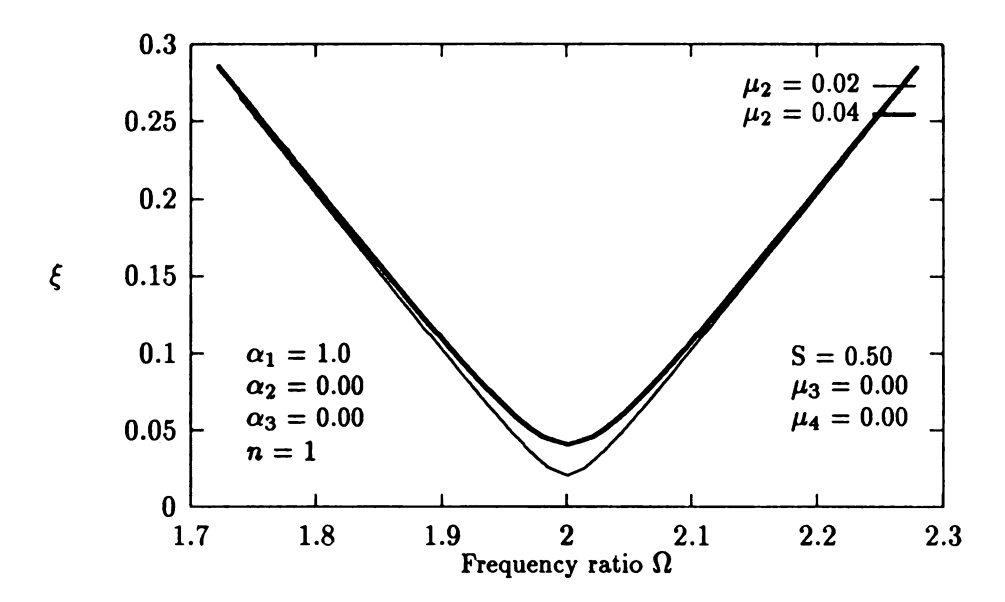


Figure 3.15: Influence of  $\mu_2$  on the main nose of instability

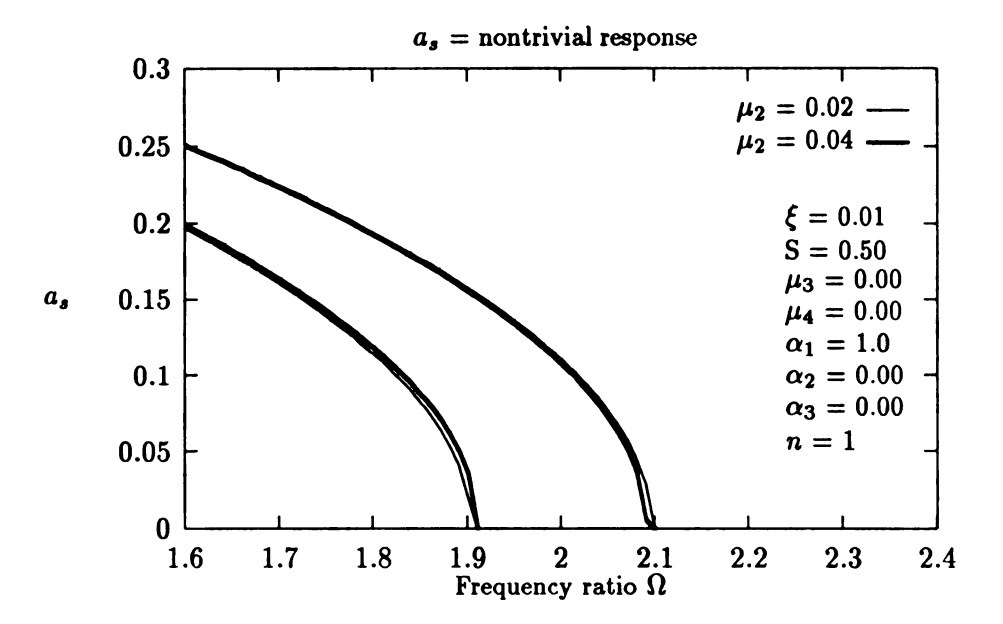


Figure 3.16: Influence of  $\mu_2$  on the principal parametric resonance

plitude of the nontrivial responses associated with the parametric resonance will decrease as  $\mu_2$  increases. The parameter  $\mu_2$  is a measure of the system's ability to dissipate energy through material damping. Hence, in order to produce a sustained nontrivial steady-state response, the magnitude of the external force must be large enough to overcome the energy dissipated. Therefore, for a given system, the width of the main nose of instability shrinks as the value of  $\mu_2$  is increased. In both of the superharmonic resonances, the amplitude of the free oscillation term will decrease as we increase the value of  $\mu_{22}$  (equations [3.122], [3.132]). These observations show that the presence of  $\mu_2$  has a favorable effect on the overall response.

The bearing friction  $\mu_3$  has an adverse effect on the overall response of the system. To show this, let us consider the sign associated with parameter  $\mu_3$  in the frequency response equation of each resonance case. The negative sign associated with parameter  $\mu_3$  in every frequency response equation indicates that the presence of this parameter has an adverse effect on the system. From another point of view, the presence of this parameter implies a

constant positive energy flux and hence increase the amplitude of the response. Figure 3.17 shows the influence of  $\mu_3$  on the amplitude of the nontrivial response associated with the principal parametric resonance. We note that  $\mu_3$  does not affect the main nose of instability associated with the principal parametric resonance. From this figure, it is seen that the effect of  $\mu_3$  on the nontrivial response is not very significant. Figure 3.18 shows the influence of  $\mu_3$  on the primary resonance. From these two figures, it is very clear that the influence of  $\mu_3$  on each resonance case is not very significant, although  $\mu_3$  has an adverse effect. The reason for this is that the relative angular motion associated with each joint point (A and B) is constant in the first order. The presence of  $\mu_3$  will cause a constant friction moment acting on each joint. These friction moments will enlarge the transverse deformation.

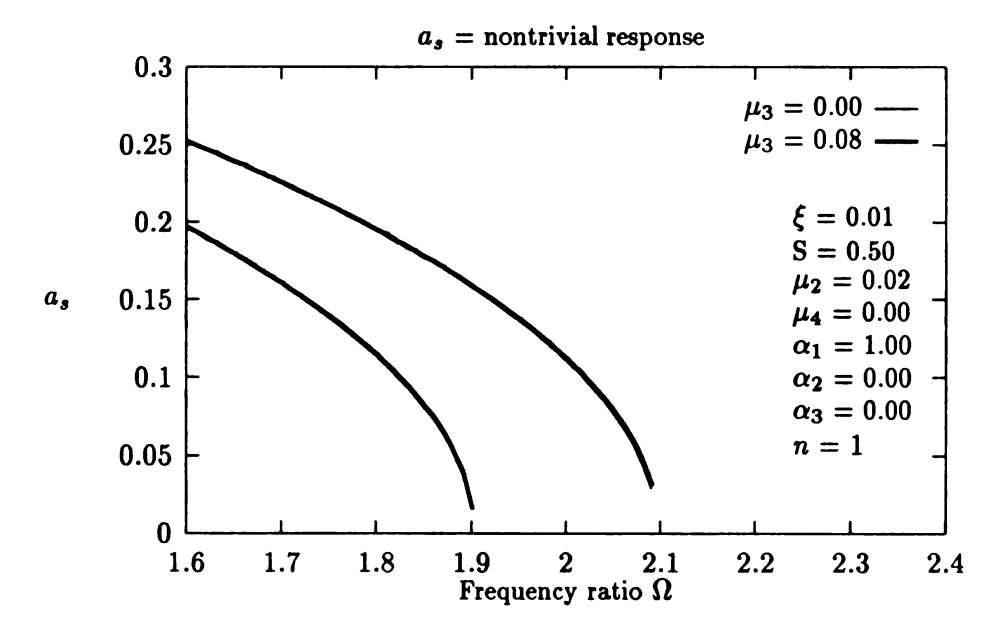


Figure 3.17: Influence of  $\mu_3$  on the principal parametric resonance

The effect of the friction parameter  $\mu_4$ , which is used to model the friction between the slider mass and its contact surface, is complicated. In order to have a clear picture regarding the effect of  $\mu_4$  on the response, one must consider the nature of this friction force. The slider friction force is composed of the actions of the rigid body motion as

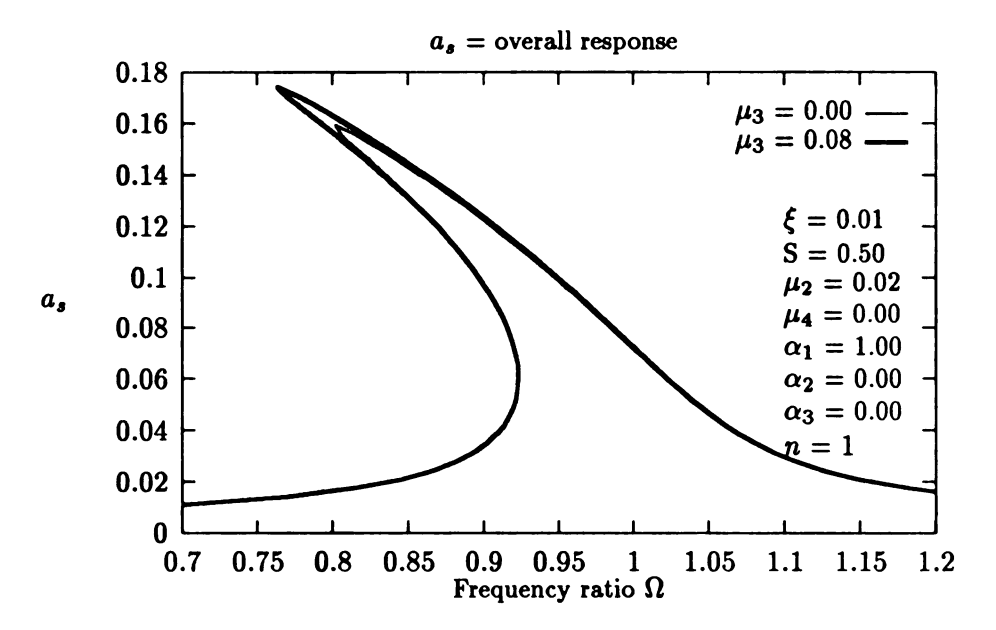


Figure 3.18: Influence of  $\mu_3$  on the primary resonance

well as the elastic deformation. When the response amplitude is small, slider friction is mainly composed of the friction introduced by rigid body motion. As the value of  $\mu_4$  increases, slider friction increases. This results an increase in the axial force acting on the connecting rod. Consequently, the response amplitude increases. From this,  $\mu_4$  has an adverse effect on the response. This can be observed in the second order superharmonic  $(\Omega \approx \frac{1}{2})$  resonance (Figure 3.19). Moreover, the width of the main nose of instability associated with the principal parametric resonance resonance increases as we increase the value of  $\mu_4$  (Figure 3.20).

The increase of the amplitude of response implies an increase of the foreshortening. This results an increase in the friction force introduced by elastic deformation. The friction force introduced by foreshortening acts as resistance which prevents the connecting rod from further deformation and hence has a favorable effect. In general, the slider friction is composed of two friction forces with compatible magnitude, and the system reaches dynamic equilibrium. This can be observed in the principal parametric resonance (Figure 3.21). Figure 3.21

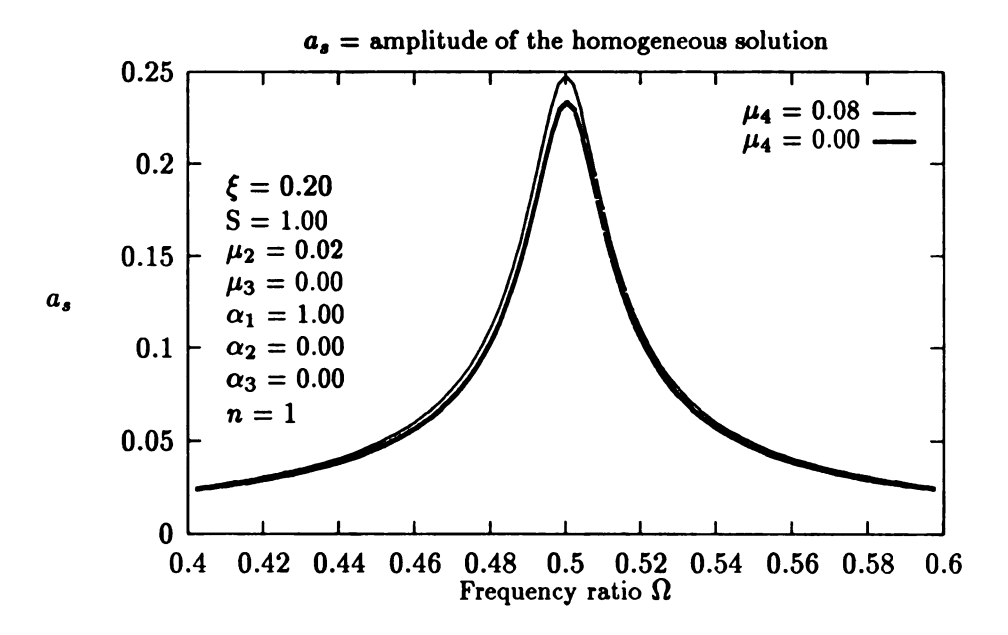


Figure 3.19: Influence of  $\mu_4$  on the superharmonic resonance  $(\Omega \approx \frac{\omega_{1n}}{2})$ 

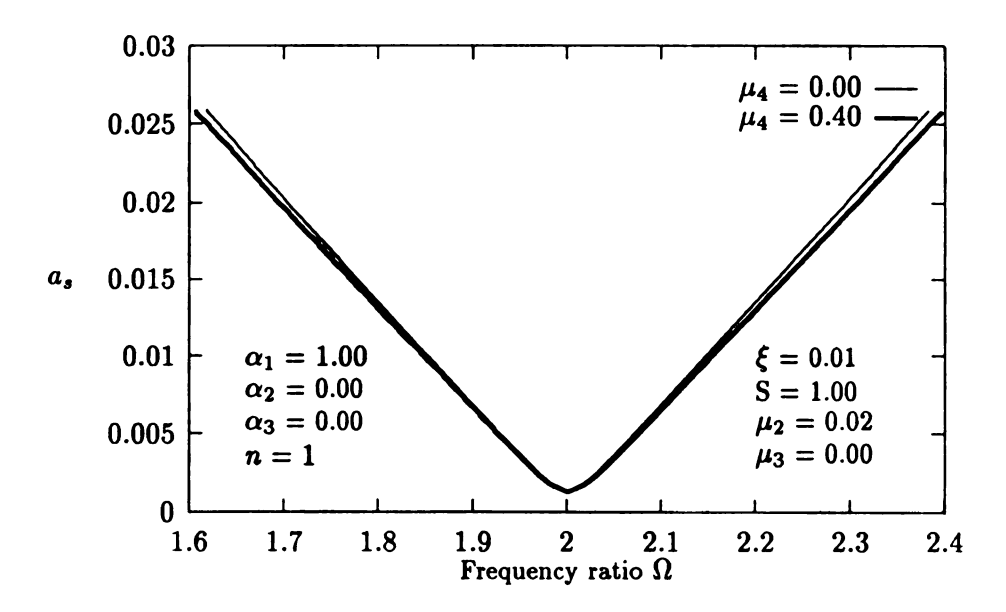


Figure 3.20: Influence of  $\mu_4$  on the main nose of instability  $(\Omega \approx 2\omega_{1n})$ 

shows branches of response originating from the main nose of instability associated with the principal parametric resonance. From this figure, we find that  $\mu_4$  has a favorable effect on the outgoing response by reducing the response amplitude; while it also has a tendency to increase the width of the main nose of instability.

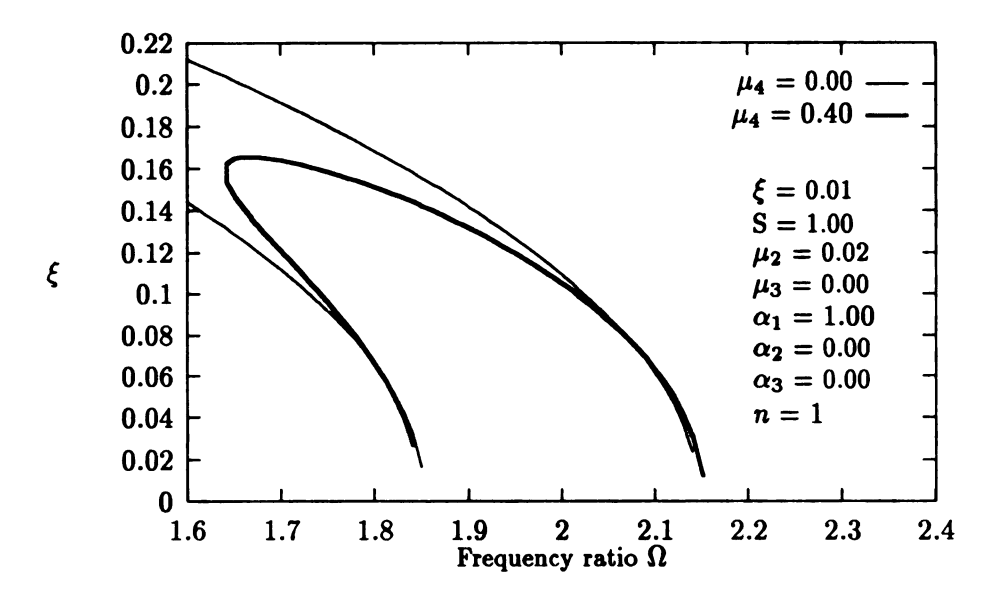


Figure 3.21: Influence of  $\mu_4$  on the principal parametric resonance  $(\Omega \approx 2\omega_{1n})$ 

Figure 3.22 shows the frequency response curve for the primary resonance. From this figure, it is clear that friction parameter  $\mu_4$  has a favorable effect on the primary resonance by reducing the amplitude of response. This is caused by the friction force introduced by large elastic deformation.

#### 3.7.4 Effect of Shear Deformation and Rotary Inertia

In this work, the effects of shear deformation and rotary inertia are included in the parameter  $\Delta_3$ . In the primary resonance, the presence of shear deformation and rotary inertia affect the frequency response curve in such a way that the locus of the peak amplitude, i.e., the backbone curve, will not originate from  $\omega_n$ . The origin of the backbone curve is shifted to the left by an amount of order  $O(\epsilon^2)$ . Figure 3.23 shows the effects of shear deformation

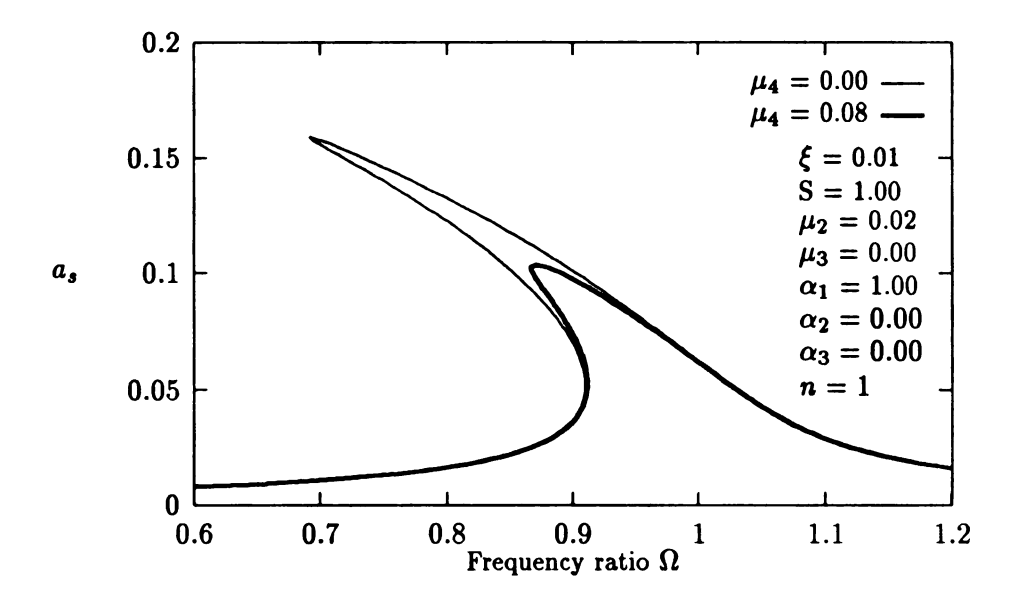


Figure 3.22: Influence of  $\mu_4$  on primary resonance  $(\Omega \approx \omega_{1n})$ 

and rotary inertia to the primary resonance. We note that there is no difference in the profile of the frequency response equations, while the shift between these curves is caused by the presence of shear deformation and rotary inertia ( $\alpha_2 = \alpha_3 = 1$ ). In the principal parametric resonance, the presence of  $\Delta_3$  causes a shift of the center of the main nose of instability (Figure 3.24). In other words, the center of the region in which the trivial solution becomes unstable will shift to the left by an amount of order  $O(\epsilon^2)$ , while the width of this region remains unchanged. Figure 3.24 shows the effect of shear deformation and rotary inertia on the principal parametric resonance. We note that the profiles associated with the nontrivial responses for these two cases are very similar, while the shift of these nontrivial responses is caused by the presence of shear deformation and rotary inertia ( $\alpha_2 = \alpha_3 = 1$ ).

Shear deformation and rotary inertia do not affect the superharmonic resonance in which  $\Omega$  is near to  $\frac{\omega_n}{2}$ . In the superharmonic resonance in which  $\Omega$  is near to  $\frac{\omega_n}{3}$ , these two terms affect the response of the system in a way similar to the primary resonance. In other words, the backbone curve will not originate from the point  $\Omega = \frac{\omega_n}{3}$ . It shifts to the left by an

amount of order  $O(\epsilon^2)$ .

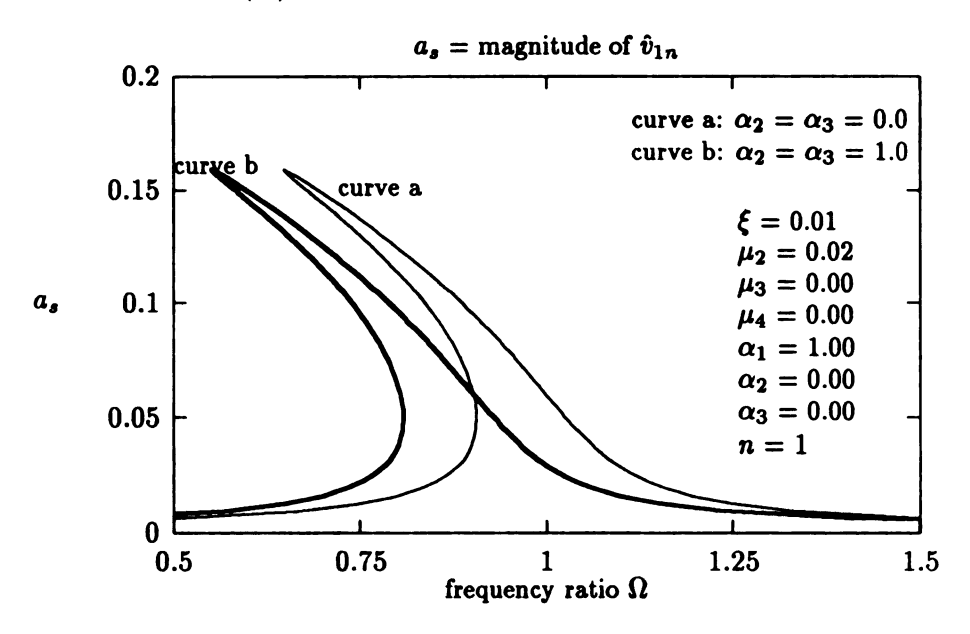


Figure 3.23: Influence of shear deformation and rotary inertia on the primary resonance

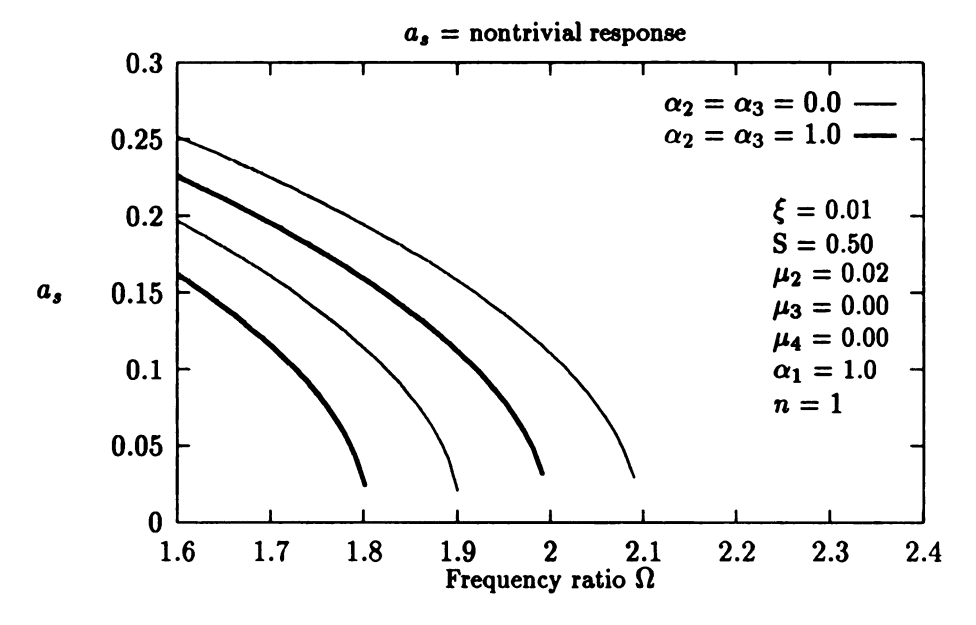


Figure 3.24: Influence of shear deformation and rotary inertia on the principal parametric resonance

## Chapter 4

## **Analysis of the Lumped Parameter Model**

In the present chapter, we consider an alternative approach to the problem under investigation. Instead of a set of partial differential equations, the dynamic behavior of the connecting rod is modeled by a single ordinary differential equation. This approach is based on extending the work by Viscomi and Ayre[49] by the inclusion of internal material damping, bearing friction and sliding friction. In this chapter, we also demonstrate how an active piston force can be incorperated in this model. Based on the assumptions given in section 2.1, except that the effects of the shear deformation and rotary inertia are neglected, the elastic response of the connecting rod is modeled by two coupled nonlinear partial differential equations. Based on the first order approximation, the equation describing the axial component is first solved to obtain the time-varying axial force. Using this axial force and neglecting the axial displacement, the equation describing the flexural response becomes a single uncoupled partial differential equation. This equation is then converted into a single ordinary differential equation by Galerkin's method with a single mode. We first consider the linearized model and obtain the corresponding response curve. The Method of Multiple Scales is then employed to locate the conditions in which the linear approximation fails to provide a satisfactory prediction. Improved approximations are also obtained by the Method of Multiple Scales. In section 4.2, the equation describing the elastic response associated with the connecting rod is derived, and converted into dimensionless form. Section

4.2 contains the main outline of the analysis, and several resonance cases are introduced. The principal parametric resonance is investigated in section 4.3. Section 4.4 contains the analysis for the primary resonance. Two superharmonic resonances in which the operating frequency is near to one half and one third of the fundamental natural flexural frequency are studied in section 4.5 and section 4.6, respectively. In section 4.7, we consider the subharmonic resonance of order three. In section 4.8, we summarize the results and provide a detailed parameter study.

## 4.1 Equation of Motion

In this section, an equation describing the flexural vibration associated with the connecting rod of an otherwise rigid slider-crank mechanism is derived. After this equation is obtained, it is then transformed into dimensionless form in order to minimize the number of system parameters.

The basic equations describing the motion along the transverse direction are derived based on the assumptions given in section 2.1, except that the the effects of shear deformation and rotary inertia are neglected. In other words, we model the connecting rod using the Euler-Bernoulli beam theory. With these assumptions, we proceed to derive equations which describe the flexural vibration associated with the connecting rod AB. Consider a slider-crank mechanism as shown in Figure 2.3. The OXY coordinate system represents a fixed inertial reference frame with its origin being attached on the crank shaft. The oxy coordinate system represents the moving reference frame with its origin being attached on joint A. The ox axis passes through the idea pin joints at the ends of the elastic connecting rod and makes an angle  $-\phi$  with the OX axis. Let u(x,t) and v(x,t) represent the axial and transverse displacements of the connecting rod, respectively. The equations of motion

in the oxy coordinate system are described by force and moment balance and are given by

$$\frac{\partial P(x,t)}{\partial x} = EA(u_x + \frac{1}{2}v_x^2)_x + A\mu_c(u_x + \frac{1}{2}v_x^2)_{xt} = \rho Aa_x , \qquad (4.1)$$

$$EIv_{xxxx} + I\mu_c v_{xxxxt} - EA[(u_x + \frac{1}{2}v_x^2)_x v_x]_x - \mu_c A[(u_x + \frac{1}{2}v_x^2)_t v_x]_x = \rho Aa_y.$$
 (4.2)

where P(x,t) = axial force acting on the connecting rod,

 $\rho$  = mass density (mass per unit volume) of the connecting rod,

A = cross-sectional area of the connecting rod, and

 $a_x(x,t)$  and  $a_y(x,t)$  are acceleration components given by

$$a_x = -r\omega^2 \cos(\omega t - \phi) + \frac{\partial^2 u}{\partial t^2} - 2\frac{\partial \phi}{\partial t} \frac{\partial v}{\partial t} - \frac{\partial^2 \phi}{\partial t^2} v - (\frac{\partial \phi}{\partial t})^2 (x + u) , \qquad (4.3)$$

$$a_{y} = -r\omega^{2}\sin(\omega t - \phi) + \frac{\partial^{2}\phi}{\partial t^{2}}(x + u) + 2\frac{\partial\phi}{\partial t}\frac{\partial u}{\partial t} + \frac{\partial^{2}v}{\partial t^{2}} - (\frac{\partial\phi}{\partial t})^{2}v. \qquad (4.4)$$

The axial strain  $e_0$  at the median line of the connecting rod is approximated by

$$e_0 = \frac{\partial u}{\partial x} + \frac{1}{2} (\frac{\partial v}{\partial x})^2 . \tag{4.5}$$

From the analysis in chapter 3, we know that the axial displacement is small compared to the transverse displacement. Therefore, we neglect the contribution of the axial displacement on the inertia forces  $\rho a_x$  and  $\rho a_y$ . Equation (4.1) then becomes

$$\frac{\partial P}{\partial x} = EA(u_x + \frac{1}{2}v_x^2)_x + +A\mu_c(u_x + \frac{1}{2}v_x^2)_{xt}$$

$$= \rho A[-r\omega^2\cos(\omega t - \phi) - 2(\frac{\partial \phi}{\partial t})(\frac{\partial v}{\partial t}) - \frac{\partial^2 \phi}{\partial t^2}v - (\frac{\partial \phi}{\partial t})^2x], \qquad (4.6)$$

and equation (4.2) becomes

$$EIv_{xxxx} + I\mu_c v_{xxxxt} - EA[(u_x + \frac{1}{2}v_x^2)v_x]_x - A\mu_c[(u_x + \frac{1}{2}v_x^2)_t v_x]_x =$$

$$= -\rho A[-r\omega^2 \sin(\omega t - \phi) + \frac{\partial^2 \phi}{\partial t^2} x + \frac{\partial^2 v}{\partial t^2} - (\frac{\partial \phi}{\partial t})^2 v]. \qquad (4.7)$$

Integrating equation (4.1) from 0 to x, we obtain

$$P(x,t) = P(0,t) + \rho A \int_0^x a_x dz$$
 (4.8)

where P(0,t) stands for the force applied to the end to which the end mass  $m_4$  attached. If the axial load acting along the connecting rod is known, then this equation is a partial differential equation describing the transverse displacement v(x,t). Using the free body diagram as shown in Figure 2.4 and summing forces along the x-direction, we can determine the time-varying axial force P(x,t) to be of the form

$$P(x,t) = \rho A \int_{L}^{x} a_{x} dz + m_{4} \ddot{\delta} + (M_{A} + M_{B}) \frac{\tan \phi}{L} + \mu_{s} \dot{\delta} + \rho A \frac{\tan \phi}{L} \int_{0}^{L} (a_{y} x - a_{x} v) dx + \frac{F(t) - m_{4} \ddot{Z} - \mu_{s} \dot{Z}}{\cos \phi}$$
(4.9)

where the overdot represents the time derivatives, F(t) is the active piston force,  $\ddot{Z}$  represents the piston acceleration from the rigid body motion of the mechanism,  $\mu_s \dot{Z}$  is the friction force acting on the slider due to rigid body motion,  $\delta$  is the foreshortening due the bending deflection of the rod, and the  $\mu_s \dot{\delta}$  term represents the slider friction due to elastic deformation.

In order to determine the piston acceleration  $\ddot{Z}$ , let us digress and consider the rigid body kinematic analysis. From Figure 2.4, in order to retain the motion of the piston end

along the X-direction, we must have

$$L\sin\left(-\phi\right) = r\sin\omega t\tag{4.10}$$

which can be written in the following dimensionless form:

$$\sin \phi = -\xi \sin \omega t \tag{4.11}$$

where  $\xi$  represents the ratio of the effective radius of the crank shaft to the length of the connecting rod and is specified as the length ratio. With this geometrical relation, the piston displacement function can be expressed as

$$Z(t) = r\cos\Omega t + L\cos\phi = L(\xi\cos\Omega t + \cos\phi). \tag{4.12}$$

The foreshortening due to the bending deflection of the connecting rod can be approximated by

$$\delta = \int_0^L \sqrt{1 + (\frac{\partial v}{\partial x})^2} dx - L \approx \frac{1}{2} \int_0^L (\frac{\partial v}{\partial x})^2 dx . \tag{4.13}$$

This approximation of the foreshortening effect is based on the small transversal deformation assumption. Hence, we keep only the first order term of the foreshortening effect. Substituting equation (4.6) into equation (4.7), we obtain the following equation

$$EIv_{xxxx} + \mu_c Iv_{xxxxt} - [P(x,t)v_x]_x =$$

$$\rho A[-r\omega^2 \sin(\omega t - \phi) + \frac{\partial^2 \phi}{\partial t^2} x + \frac{\partial^2 v}{\partial t^2} - (\frac{\partial \phi}{\partial t})^2 v]$$
(4.14)

where P(x,t) is given by equation (4.9). Equation (4.14) describes the transverse deflection

of the connecting rod.

We now consider the boundary conditions for the connecting rod. Since the crank shaft is assumed to be perfectly rigid and there is no relative displacement of the connection between the connecting rod and the crank shaft, we have

$$v(0,t) = 0. (4.15)$$

Also, at x = L, the piston motion is constrained to move along the X direction. Thus, we have

$$v(L,t) = u(L,t)\tan(-\phi). \tag{4.16}$$

Again, equation (4.5) implies that the axial displacement u(x,t) is much smaller than the transverse one. It is shown in [9] that this boundary condition can be approximated by v(L,t) = 0. Due to the presence of the fictional moments on points A and B due to bearings, we have the following boundary conditions:

$$EIv_{xx}(0,t) = -M_A = \mu_b[\omega - \dot{\phi} - v_{xt}(0,t)],$$
 (4.17)

$$EIv_{xx}(L,t) = -M_B = \mu_b[\dot{\phi} - v_{xt}(L,t)],$$
 (4.18)

where  $\mu_b$  represents the friction coefficient such that the moment applied by the bearings is the product of  $\mu_b$  and the *relative* rotational speed. We assume the value of the friction coefficient  $\mu_b$  is very small compared to the length ratio so that these reaction moments can be neglected for the first order approximation. Therefore, with the first order approximation, the reaction moments acting on points A and B are zero. Based on these observations

and assumptions, the solution v(x,t) can be approximated as

$$v(x,t) = \sum_{n=1}^{n} \bar{v}_n(t) \sin\left(\frac{n\pi x}{L}\right)$$
 (4.19)

where  $\bar{v}_n(t)$  represents the amplitude of the displacement at the midpoint of the beam, and  $\sin \frac{n\pi x}{L}$  are the natural modes of transverse vibrations of a uniform beam with pinned ends. Previous work[49] has shown that higher order modes have insignificant influence on the transverse response of the connecting rod for the region in which the model is valid. Hence, we assume that the solution of v(x,t) can be approximated by a single mode  $(\bar{v}_1(t)\sin(\frac{\pi x}{L}))$ . Substituting this assumed solution into equation (4.14) and projecting the equations onto the first mode, we obtain the following equation:

$$\frac{2\rho A L \ddot{\phi}}{\pi} - \frac{4\rho A r \sin(\omega t - \phi)\omega^{2}}{\pi} + \frac{E I \pi^{4} v}{L^{4}} - \frac{5\rho A \dot{\phi}^{2} v}{4} + \frac{\rho A \pi^{2} \dot{\phi}^{2} v}{3} \\
+ \frac{\pi^{2} \mu_{s} v \dot{\phi} \sin \phi}{\cos \phi L} - \frac{\pi^{2} \mu_{b} v \dot{\phi} \tan \phi}{L^{3}} + \frac{\rho A \pi^{2} v \ddot{\phi} \tan \phi}{3} + \frac{\pi^{2} \mu_{s} r \omega v \sin \omega t}{L^{2} \cos \phi} \\
+ \frac{\pi^{2} \mu_{b} \omega v \tan \phi}{L^{3}} + \frac{\rho A r \pi^{2} \omega^{2} v \cos(\omega t - \phi)}{2L} - \frac{\rho A r \pi^{2} \omega^{2} v \tan \phi \sin(\omega t - \phi)}{2L} \\
+ \frac{\pi^{2} \dot{\phi}^{2} m_{4} v}{L} + \frac{\pi^{2} m_{4} \ddot{\phi} v \sin \phi}{L \cos \phi} + \frac{\pi^{2} m_{4} r v \omega^{2} \cos \omega t}{L^{2} \cos \phi} + \frac{\pi^{2} v F(t)}{L \cos \phi} \\
+ (\frac{\rho A \pi \ddot{\phi}}{L} + \frac{2\rho A r \pi \omega^{2} \tan \phi \cos(\omega t - \phi)}{L^{2}}) v^{2} + \frac{\rho A \pi^{2} \ddot{\phi} v^{3} \tan \phi}{L^{2}} \\
+ \frac{\pi^{4} I \mu_{c} \dot{v}}{L^{4}} + \frac{2\rho A \pi \dot{\phi} v \dot{v}}{L} + \frac{\rho A \pi^{2} \dot{\phi} \tan \phi \dot{v} v^{2}}{L^{2}} + \frac{\pi^{4} m_{4} v \dot{v}^{2}}{2L^{3}} + \frac{\mu_{s}}{4L^{2}} \pi^{4} v^{2} \dot{v} \\
+ (\rho A + \frac{\rho A \pi v \tan \phi}{L} + \frac{\pi^{4} m_{4} v^{2}}{2L^{3}}) \ddot{v} = 0 \tag{4.20}$$

which is a single nonlinear ordinary differential equation describing the flexural vibration associated with the connecting rod of a slider-crank mechanism under the assumptions given above. In the following analyses, we only consider the cases in which there is no external force acting on the piston, i.e., F(t) = 0 in equation (4.20). We note that these

simplifications (equations [4.15] to [4.18]) are essential in truncating equations (4.14) with the linear mode shape function (equation [4.19]) and obtaining equation (4.20). With the same dimensionless parameters as those described in section 2.4, equation (4.20) can be written into the following dimensionless form:

$$(1 + \pi v \tan \phi + \frac{S}{2} \pi^4 v^2) \ddot{v} + 2\mu_2 \dot{v} + \frac{2}{\pi} (\ddot{\phi} - 2\xi \Omega^2 \sin (\Omega t - \phi))$$

$$+ v \left[ 1 + \ddot{\phi} \pi^2 (S + \frac{1}{3}) \tan \phi + \dot{\phi}^2 (\frac{\pi^2}{3} + \pi^2 S - \frac{5}{4}) + (\frac{1}{2} + S) \xi \Omega^2 \pi^2 \frac{\cos \Omega t}{\cos \phi} \right]$$

$$+ v \left[ 2\mu_3 (\Omega - 2\dot{\phi}) \pi^2 \tan \phi + 2\mu_4 (\dot{\phi} - \Omega) \pi^2 \tan \phi \right]$$

$$+ v^2 \left[ \pi \ddot{\phi} + 2\pi \xi \Omega^2 \tan \phi \cos (\Omega t - \phi) \right] + 2\pi \dot{\phi} \dot{v} v \tan \phi$$

$$+ v^3 (\frac{\pi^2}{2} \ddot{\phi} \tan \phi) + (\frac{\pi^4}{2}) S \dot{v}^2 v + v^2 \dot{v} (\pi^2 \dot{\phi} \tan \phi + \mu_4 \pi^4) = 0$$

$$(4.21)$$

where all the overdots represent the derivatives with respect to time,  $\bar{v}_1$  is replaced by v and all the overbars have been dropped for notational simplification. Equation (4.21) is a second order differential equation describing the flexural response associated with the connecting rod. We note that it contains the following features: (1) nonlinear inertial terms, (2) external as well as parametric forces arising from inertial forces, (3) dissipation effects, and (4) time-dependent quadratic and cubic nonlinearities. Despite of its complexities, each term of equation (4.21) has its own physical source. All the terms involving the parameter S, except  $(\frac{S}{2}\pi^4v^2\ddot{v})$  and  $(\frac{S}{2}\pi^4v\dot{v}^2)$ , which represent the foreshortening effect, arise because of the inertial force associated with the slider mass  $m_4$ . The forcing term,  $[\frac{2}{\pi}(\ddot{\phi}-2\xi\Omega^2\sin{(\Omega t-\phi)})]$ , arises because of the action of the transverse acceleration component  $a_y$  on the connecting rod. The following terms arise because of the effects of bending moments caused by the actions of  $a_x$  and  $a_y$ :  $\pi v\ddot{v}\tan\phi$ ,  $\frac{\ddot{\phi}}{3}\pi^2v\tan\phi$ ,  $v\dot{\phi}^2$ ,  $\frac{\xi}{2}\Omega^2\pi^2v\frac{\cos{\Omega t}}{\cos\phi}$ ,  $2\pi\xi\Omega^2v^2\tan\phi\cos{(\Omega t-\phi)}$ ,  $\frac{\pi^2}{2}v^3\ddot{\phi}\tan\phi$  and  $\pi^2v^2\dot{v}\dot{\phi}\tan\phi$ . All the terms involving the parameters  $\mu_3$  and  $\mu_4$  arise from

the actions of the bearing friction and friction force on slider mass, respectively.

Now, let us reconsider equation (4.11). Since in most of the applications, the length ratio is smaller than one, we expand equation (4.11) in terms of the length ratio  $\xi$  to obtain the following asymptotic series:

$$\phi = \sin^{-1}(\sin \Omega t)$$

$$= -(\xi \sin \Omega t) - \frac{(\xi \sin \Omega t)^3}{6} - \frac{(\xi \sin \Omega t)^5}{120} + \dots$$

$$x = -(\xi + \frac{3\xi^3}{4} + \dots) \sin \Omega t - (\frac{3\xi^3}{4} + \dots) \sin 3\Omega t - (\frac{\xi^5}{16} + \dots) \sin 5\Omega t + \dots$$
 (4.22)

This equation indicates that the excitation provided to the connecting rod is a superposition of harmonic inputs at frequencies which are multiples the crank rotation speed. Note that the force amplitudes associated with higher harmonics are of small magnitude.

#### 4.2 Application of the Method of Multiple Scales

Before applying MMS (Method of Multiple Scales) to study equation (4.21), let us first consider a solution to the linearized model of equation (4.21). To achieve this end, we expand the original equation (4.21), with the help of equations (4.11) and (4.22), and retain all the first order terms in  $\xi$ , v and its time derivatives. This results in the equation

$$\ddot{v}(t) + 2\mu_2 \dot{v}(t) + v(t) = \frac{2}{\pi} \xi \Omega^2 \sin \Omega t \qquad (4.23)$$

which represents a linear oscillator subjected to an external excitation. The response of this equation is given as

$$v(t) = X\sin(\Omega t - \varphi) \tag{4.24}$$

where

$$X = (\frac{2}{\pi}) \frac{\xi \Omega^2}{\sqrt{(1 - \Omega^2)^2 + 4\mu_2^2 \Omega^2}}$$
 (4.25)

and

$$\varphi = \tan^{-1}\left(\frac{2\mu_2\Omega}{1-\Omega^2}\right). \tag{4.26}$$

Equation (4.24) represents the response curve of the linearized system for small length ratios. From equation (4.25), we see that, to first order, the amplitude of the steady-state response is proportional to the length ratio  $\xi$  as well as the square of the frequency ratio  $\Omega$ . However, this estimate may not be sufficient to capture the true response under certain conditions. In the current section, we use the Method of Multiple Scales[29] to locate these conditions, while we will improve our approximation in the subsequent sections for each individual condition.

To apply MMS, we need to introduce a set of new independent time variables  $T_n$  and, in addition, reorder some parameters, such as the length ratio  $\xi$  and the damping parameters  $\mu_2$ ,  $\mu_3$  and  $\mu_4$ . The new independent time variables  $T_n$  are introduced according to  $T_n = \epsilon^n t$ . It follows that the derivatives with respect to t become expansions in terms of the partial derivatives with respect to  $T_n$  according to equations (3.4) and (3.5). Moreover, we assume that the length ratio  $\xi$  can be ordered by  $\xi = \epsilon \xi_1$ . Since the amplitude of the response is proportional to the length ratio  $\xi$ , we assume that the solution v(t) can be represented by an expansion taking the following form

$$v(t) = \epsilon v_1(T_0, T_1, T_2) + \epsilon^2 v_2(T_0, T_1, T_2) + \epsilon^3 v_3(T_0, T_1, T_2) + \dots$$
 (4.27)

The damping parameters  $\mu_2$ ,  $\mu_3$  and  $\mu_4$  are treated in the same way as described in chapter 3.

In other words, the ordering of  $\mu_3$  is fixed to of order  $O(\epsilon^2)$ , the ordering of  $\mu_4$  is fixed to be of order O(1), and  $\mu_2$  is reordered according to the order of  $\sigma$ , the detuning parameter.

Substituting equations (3.1), (3.4), (3.5), (3.8), (3.9) and (3.10) into equation (4.21), expanding and equating the coefficients of the like-power terms we obtain the following equations:

Order  $\epsilon$ 

$$D_0^2 v_1 + v_1 = (\frac{2}{\pi}) \xi_1 \Omega^2 \sin \Omega T_0 , \qquad (4.28)$$

Order  $\epsilon^2$ 

$$D_0^2 v_2 + v_2 = -2D_0 D_1 v_1 - (S + \frac{1}{2}) \xi_1 \pi^2 \Omega^2 v_1 \cos \Omega T_0 + (\frac{2}{\pi}) \Omega^2 \xi_1^2 \sin 2\Omega T_0 , (4.29)$$

Order  $\epsilon^3$ 

$$D_0^2 v_3 + v_3 = -2D_0 D_1 v_2 - 2\mu_{2_2} D_0 v_1 - D_1^2 v_1 - 2D_0 D_2 v_1 - \pi^2 (S + \frac{1}{2}) \xi_1 \Omega^2 v_2 \cos \Omega T_0$$

$$- (\frac{\pi^2}{3} + \pi^2 S - \frac{5}{4}) \xi_1^2 v_1 \Omega^2 \cos \Omega T_0^2 + (\frac{1}{3} + S) \xi_1^2 \Omega^2 v_1 \sin \Omega T_0^2$$

$$- 2\pi^2 \mu_{4_0} \Omega \xi_1 v_1 \sin \Omega T_0 + 2\xi_1 \Omega \pi (D_0 v_1) v_1 \cos \Omega T_0 - \frac{\pi^4}{2} S(D_0 v_1)^2 v_1$$

$$- \frac{\pi^4}{2} S(D_0^2 v_1) v_1^2 + \pi \xi_1 [D_0 (D_0 v_1^2)] \sin \Omega T_0 - \mu_{4_0} \pi^4 (D_0 v_1) v_1^2 . \tag{4.30}$$

In obtaining the general solution of  $v_1(T_0, T_1, T_2)$  from equation (4.28), we need to distinguish between the following special cases: (1)  $\Omega$  is near to unity and (2)  $\Omega$  is away from unity. The case in which  $\Omega$  is near to one corresponds to the primary resonance. When this occurs, the linear estimate (equations [4.24]) fails to provide a good prediction of the response. Section 4.4 contains a complete analysis of the primary resonance. At the present

time, let us assume that  $\Omega$  is away from one and continue our analysis. Under this condition, the general solution of  $v_1(T_0, T_1, T_2)$  is given as the combination of the homogeneous and particular solutions,

$$v_1(T_0, T_1, T_2) = A_1(T_1, T_2) exp(jT_0) + \Lambda_4 \sin \Omega T_0 + c.c.$$
 (4.31)

where  $A_1$  is an unknown complex function which will be determined later,  $\Lambda_4$  is given as

$$\Lambda_4 = (\frac{2}{\pi}) \frac{\xi_1 \,\Omega^2}{1 - \Omega^2} \tag{4.32}$$

and c.c. stands for the complex conjugate terms of the preceding terms on the right hand side of equation (4.31). Note that, according to the linear theory, the homogeneous part of solution (4.31), i.e.  $A_1exp(jT_0)$  term, will decay to zero due the presence of the damping parameters. Thus, the homogeneous solution is not included in the steady- state response of the linear system (equation [4.24]). At the present moment, we include the homogeneous solution in this general solution and proceed to find the conditions in which this homogeneous solution will not decay to zero. Substituting the solution  $v_1(T_0, T_1, T_2)$  into equation (4.29), we obtain

$$D_0^2 v_2 + v_2 = -2j(D_1 A_1) exp(jT_0) + (\frac{1}{\pi}) \xi_1^2 \Omega^2 exp(2j\Omega T_0 - j\frac{\pi}{2})$$

$$- (S + \frac{1}{2}) \xi_1 \Omega^2 \pi^2 \frac{\Lambda_1}{4} exp(2j\Omega T_0 - j\frac{\pi}{2})$$

$$- (S + \frac{1}{2}) \xi_1 \Omega^2 \pi^2 \frac{A_1}{2} exp(j\Omega T_0 + jT_0)$$

$$- (S + \frac{1}{2}) \xi_1 \Omega^2 \pi^2 \frac{\bar{A}_1}{2} exp(j\Omega T_0 - jT_0) + c.c. . \tag{4.33}$$

In analyzing the particular solution of equation (4.33), there are three cases which need to

be considered separately: (1)  $\Omega$  is near to  $\frac{1}{2}$ , (2)  $\Omega$  is near to 2 and (3)  $\Omega$  is neither near to  $\frac{1}{2}$  nor to 2. The first case corresponds to a superharmonic resonance, while the second one corresponds to a subharmonic resonance, or the principle parametric resonance. Both of these cases will be studied in detail and improved approximations will be provided later on. For the present, let us assume that  $\Omega$  is away from  $\frac{1}{2}$  and 2, and continue our analysis. When  $\Omega$  is away from  $\frac{1}{2}$  and 2, we must have

$$D_1 A_1(T_1, T_2) = 0 (4.34)$$

in order to remove the secular term from the particular solution of  $v_2$ . This implies that the unknown amplitude function  $A_1(T_1, T_2)$  must be independent of the time variable  $T_1$ . As a consequence, all the higher order solutions are assumed to be independent of the time variable  $T_1$ . Thus, all the derivatives with respect to time variable  $T_1$  are zero. The particular solution of  $v_2(T_0, T_2)$  is then given as

$$v_{2} = \frac{1}{1 - 4\Omega^{2}} \left[ \frac{\xi_{1}^{2}\Omega^{2}}{\pi} - \left( \frac{S}{4} + \frac{1}{8} \right) \xi_{1}\pi^{2}\Omega^{2}\Lambda_{1} \right] exp(2j\Omega T_{0} - j\frac{\pi}{2})$$

$$- \frac{1}{1 - (1 + \Omega)^{2}} \left( \frac{S}{2} + \frac{1}{4} \right) \xi_{1}\Omega^{2}\pi^{2}A_{1}exp(j\Omega T_{0} + jT_{0})$$

$$- \frac{1}{1 - (1 - \Omega)^{2}} \left( \frac{S}{2} + \frac{1}{4} \right) \xi_{1}\Omega^{2}\pi^{2}\bar{A}_{1}exp(j\Omega T_{0} - jT_{0}) + c.c. . \tag{4.35}$$

Substituting  $v_1(T_0, T_2)$  and  $v_2(T_0, T_2)$  into equation (4.30), we obtain

$$\begin{array}{lll} D_0{}^2v_3+v_3&=&-2j\mu_{2_2}A_1exp(jT_0)-j\mu_{4_0}\pi^4A_1^2\bar{A}_1exp(jT_0)-2j(D_2A_1)exp(jT_0)\\ \\ &+&\pi^4SA_1^2\bar{A}_1exp(jT_0)+f_7\xi_1^2A_1exp(jT_0)+jf_8\xi_1^3exp(3j\Omega T_0)\\ \\ &+&2j\pi\Omega\xi_1\bar{A}_1^{\ 2}exp(j\Omega T_0-2jT_0)-j(\frac{\mu_{4_0}}{2})\pi^4A_1\Lambda_4^2exp(jT_0) \end{array}$$

$$+ \frac{\pi^4}{8} \Lambda_1^3 \Omega \mu_{40} exp(3j\Omega T_0) + \mu_{40} \pi^4 \Lambda_4 (1 - \frac{\Omega}{2}) \bar{A}_1^2 exp(j\Omega T_0 - 2jT_0)$$

$$+ N.S.T. + c.c. \tag{4.36}$$

where N.S.T. represents those terms which will not produce secular term in the particular solution of  $v_3$ . In analyzing the particular solution of equation (4.36), there are three cases which need to be considered separately: (1)  $\Omega$  is near to 3, (2)  $\Omega$  is near to  $\frac{1}{3}$ , and (3)  $\Omega$  is away from 3 and  $\frac{1}{3}$ . The first case corresponds to a subharmonic resonance, while the second case corresponds to a superharmonic resonance. These two cases will be investigated in sections 4.6 and 4.7, respectively, in order to obtain better approximations.

At this point, we pause and briefly consider some of the general features of this analysis procedure. By using the assumed solution sequence, the equation describing the transverse vibration of the connecting rod can be transformed into a sequence of ordinary differential equations which can be solved quite easily, since they are linearized by the nature of perturbation expansion. In solving these sequential equations, several resonant conditions arise. The primary resonance appears first, and then the principle parametric resonance. After these two resonances, some secondary resonances of subharmonic and superharmonic types arise. When these occur, the linear approximation is insufficient to provide a good estimate of the response of the system.

For simplicity, we follow the same analysis pattern as described in the last chapter. The principal parametric resonance is examined first in section 3.2. The primary resonance is investigated in section 3.3. After these two resonances, secondary resonances are examined case by case.

### 4.3 Principal Parametric Resonance ( $\Omega \approx 2$ )

Recalling that in analyzing the particular solution of equation (4.33) in section 4.2, when the frequency ratio  $\Omega$  is near to 2, a principle parametric resonance takes place. To describe the dynamics when the frequency ratio is close to 2, we express  $\Omega$  as

$$\Omega = 2 + 2\epsilon \,\sigma_1 \tag{4.37}$$

where  $\sigma_1$  is the detuning parameter. The damping parameter  $\mu_4$  is reordered by  $\mu_4 = \mu_{40}$ . Moreover, the damping parameter  $\mu_2$  is rescaled according to  $\mu_2 = \epsilon \mu_{21}$  so that it will show up, together with detuning parameter  $\sigma_1$ , in the final resonant condition. After carrying out the same procedure as that described in the last section, equation (4.29) reduces to

$$D_0^2 v_2 + v_2 = -2j(D_1 A_1) exp(jT_0) - 2j\mu_{2_1} A_1 exp(jT_0)$$

$$- (\frac{S}{2} + \frac{1}{4}) \dot{\xi}_1 \Omega^2 \pi^2 \bar{A}_1 exp(jT_1 + 2j\sigma_1 T_0)$$

$$- \xi_1 \Omega \pi^2 \mu_{4_0} \bar{A}_1 exp(2j\sigma_1 T_1 - j\frac{\pi}{2}) + N.S.T. + c.c.$$
(4.38)

where N.S.T. represent those terms which will not produce the secular terms in the particular solution of  $v_2(T_0, T_1, T_2)$ . In order to eliminate the secular terms, the following must hold

$$-2j(D_1 A_1) - 2j\mu_{2_1} A_1 - 4(\frac{S}{2} + \frac{1}{4})\xi_1 \pi^2 \bar{A}_1 exp(2j\sigma_1 T_0)$$

$$-2\pi^2 \mu_{4_0} \xi_1 \bar{A}_1 exp(2j\sigma_1 T_1 - j\frac{\pi}{2}) = 0.$$
(4.39)

Expanding equation (4.39) with  $A_1 = (\frac{a}{2})exp(j\Psi)$ , and separating the resultant equation

into real and imaginary parts, we obtain

$$a' = -\mu_2, a - 2a\xi_1\Delta_4\sin 2\Phi_1 + a\pi^2\mu_{40}\xi_1\cos 2\Phi_1, \qquad (4.40)$$

$$a\Phi_1' = \sigma_1 a - 2a\xi_1 \Delta_4 \cos 2\Phi_1 - a\pi^2 \mu_{4_0} \xi_1 \sin 2\Phi_1 \tag{4.41}$$

where  $\Phi_1 = \sigma_1 T_1 - \Psi$  and  $\Delta_4$  are defined by

$$\Delta_4 = (2S+1)(\frac{\pi^2}{4}) \tag{4.42}$$

and the primes indicate derivatives with respect to  $T_1$ . The steady state response conditions are obtained by letting a'=0 and  $\Phi_1'=0$ , which yield

$$\mu_{2_1}a = -2a\xi_1\Delta_4\sin 2\Phi_1 + a\pi^2\xi_1\mu_{4_0}\cos 2\Phi_1, \qquad (4.43)$$

$$\sigma_1 a = 2a\xi_1 \Delta_4 \cos 2\Phi_1 + a\pi^2 \xi_1 \mu_{40} \sin 2\Phi_1 . \qquad (4.44)$$

Squaring these equations, and adding them together, we obtain

$$\left[\sigma_1^2 + \mu_{2_1}^2 - (2\xi_1 \Delta_4)^2 - (\pi^2 \xi_1 \mu_{4_0})^2\right] a^2 = 0. \tag{4.45}$$

Equation (4.45) is an equation for the amplitude of the response as a function of the detuning parameter, the damping parameters and the length ratio. From this equation, we see that the trivial solution a=0 is the unique steady state response for the current resonant condition. To determine the stability of this solution, we substitute  $A_1=(B_R+jB_I)exp(j\sigma_1T_1+\gamma T_1)$  into equation (4.39), in which  $B_R$  and  $B_I$  are two constants, and separate the resultant equations into real and imaginary parts to obtain two equations.

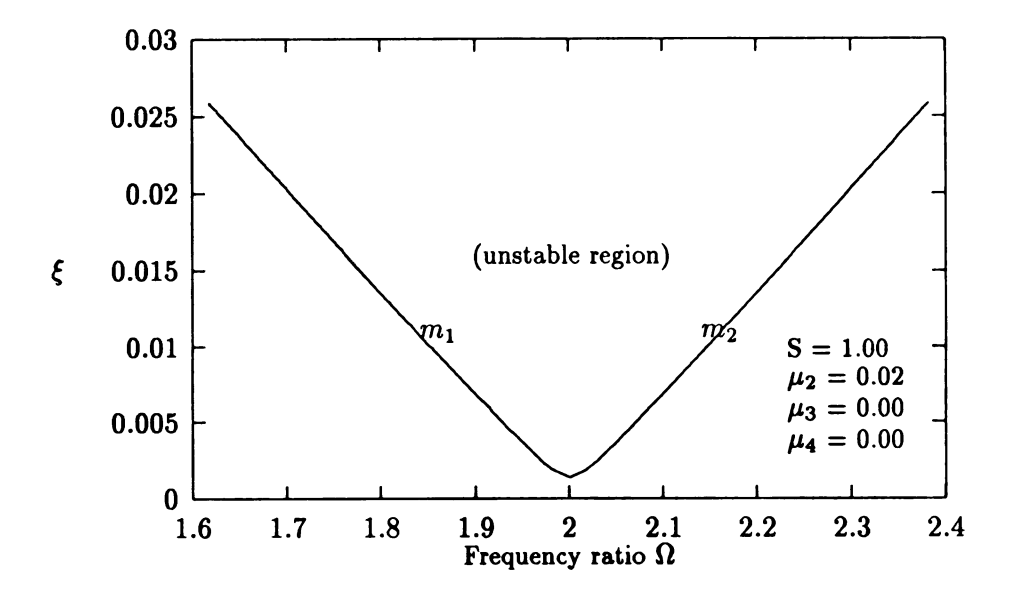


Figure 4.1: Frequency response equation for the principal parametric resonance (equation [4.45])

We then solve the nontrivial constant solutions of  $B_R$  and  $B_I$  from these two equations. From this, we determine that when

$$\sigma_1^2 + \mu_{2_1}^2 < \xi_1^2 (4\Delta_4^2 + \pi^4 \mu_{4_0}^2)$$
 (4.46)

this trivial solution become unstable. It is clear that  $\sigma_1^2 + \mu_{21}^2 = \xi_1^2 (4\Delta_4^2 + \pi^4 \mu_{40}^2)$  represents the transition curve which is the solid curve shown in Figure 4.1. Along this curve, the eigenvalues associated with the responses are either +1 or -1. In the unstable region, any disturbance, no matter how small, applied to the steady-state response results an unbounded growth in the response amplitude of the linear model. However, as the amplitude of the response becomes large, the nonlinear terms can no longer be neglected. In the remaining part of this section, we extend our analysis to investigate these nonlinear effects. In stable regions, equation (4.24) can be used to predict the response, since the trivial response is

stable and will remain zero. Thus, the steady state response can be approximated by

$$v(t) = \epsilon v_1(T_0, T_1, T_2) + O(\epsilon^2) = \epsilon \Lambda_1 \sin \Omega T_0 + O(\epsilon^2). \tag{4.47}$$

When the response is unstable, any small disturbance applied to the trivial response will grow unbounded, and then dominate the response curve. This is an example of parametric resonance.

In order to capture the effects of nonlinearities, it is necessary to reorder either the solution or the parameters so that the nonlinearities will be included in the equation describing the resonant condition. For the present problem, the amplitude of the response is shown to be proportional to the length ratio (equation [4.24] in section 4.2). Therefore, a reordering of the length ratio is equivalent to the reordering of the solution. To carry out the nonlinear analysis, we reorder the length ratio  $\xi$  according to  $\xi = \epsilon^2 \xi_2$ . Expanding equation (4.21) with this new length ratio, and equating the coefficients of the like-power terms in  $\epsilon$ , we obtain

Order  $\epsilon$ 

$$D_0^2 v_1 + v_1 = 0 , (4.48)$$

Order  $\epsilon^2$ 

$$D_0^2 v_2 + v_2 = -2D_0 D_1 v_1 + (\frac{2}{\pi}) \xi_2 \Omega^2 \sin \Omega T_0, \qquad (4.49)$$

Order  $\epsilon^3$ 

$$D_0^2 v_3 + v_3 = -2D_0 D_2 v_1 - 2\mu_{2_2} D_0 v_1 - \pi^4 S(D_0^2 v_1^3) - 2\mu_{4_0} \pi^2 \xi_2 \Omega v_1 \sin \Omega T_0$$

$$- D_1^2 v_1 - 2D_0 D_1 v_2 - \pi^2 (S + \frac{1}{2}) \xi_2 \Omega^2 v_1 \cos \Omega T_0 - \pi^4 \mu_{4_0} (D_0 v_1) v_1^2 . \quad (4.50)$$

Equation (4.48) admits the solution

$$v_1(T_0, T_1, T_2) = A(T_1, T_2)exp(jT_0) + c.c. (4.51)$$

Substituting this solution into equation (4.49), we obtain

$$D_0^2 v_2 + v_2 = -2j(D_1 A_1) exp(jT_0) + (\frac{2}{\pi}) \xi_2 \Omega^2 \sin \Omega T_0 + c.c.$$
 (4.52)

In analyzing the solution of this equation, we need to distinguish between these two cases: (1)  $\Omega$  is near to one and (2)  $\Omega$  is away from one. The first case is referred to as the primary resonance and will be investigated in next section. At this moment, let us consider case (2). When  $\Omega$  is away from one, we have  $D_1 A_1 = 0$  which implies the independence of  $A_1$  to the time variable  $T_1$ . Therefore, all the higher order solutions are assumed to be independent of  $T_1$ . With this assumption, equation (4.50) reduces to

$$D_0^2 v_3 + v_3 = -2j\mu_{2_2}A_1exp(jT_0) - 2j(D_1A_1)exp(jT_0) - j\mu_{4_0}\pi^4A_1^2\bar{A}_1exp(jT_0)$$

$$- (S + \frac{1}{2})\xi_2\Omega^2\pi^2(\frac{\bar{A}_1}{2})exp(j\Omega T_0 - jT_0) - 2\mu_{4_0}\pi^2\xi_2\bar{A}_1exp(j\Omega T_0 - j\frac{\pi}{2})$$

$$+ \pi^4SA_1^2\bar{A}_1exp(jT_0) + N.S.T. + c.c.$$
(4.53)

which describes the third order term in the flexural response associated with the connecting rod. To describe the nearness of  $\Omega$  to 2, we express  $\Omega$  as

$$\Omega = 2 + 2\epsilon^2 \sigma_2 \ . \tag{4.54}$$

Hence, we must have

$$-2j\mu_{2_2}A_1 - 2j(D_2A_1) - 4\xi_2\Delta_4\bar{A}_1exp(2j\sigma_2T_2) + \pi^4SA_1^2\bar{A}_1$$
$$- 2\mu_{4_0}\pi^2\xi_2\bar{A}_1exp(2j\sigma_2T_2 - j\frac{\pi}{2}) - j\mu_{4_0}\pi^4A_1^2\bar{A}_1 = 0$$
(4.55)

in order to remove the secular terms from the particular solution of  $v_1$ . Substituting  $A_1 = (\frac{a}{2})exp(j\Psi)$  into equation (4.55) and separating the resultant equation into real and imaginary parts, we obtain

$$a' = -\mu_{2_2}a - \mu_{4_0}\pi^4 \frac{a^3}{8} - 2\xi_2\Delta_4 a \sin 2\Phi_2 + \xi_2\pi^2\mu_{4_0}a \cos 2\Phi_2, \qquad (4.56)$$

$$a\Phi_2' = \sigma_2 a - 2\xi_2 \Delta_4 a \cos 2\Phi_2 - \xi_2 \pi^2 \mu_{4_0} a \sin 2\Phi_2 + \Delta_5 a^3$$
 (4.57)

where  $\Phi_2 = \sigma_2 T_2 - \Psi$  and  $\Delta_5$  is defined by

$$\Delta_5 = \frac{1}{8} \pi^4 S \tag{4.58}$$

and the primes represent the derivatives with respect to the time scale  $T_2$ . The steady state conditions for these equations are given as

$$\mu_{2_2}a + \mu_{4_0}\pi^4 \frac{a^3}{8} = -2\xi_2 a \Delta_4 \sin 2\Phi_2 + \xi_2 \pi^2 \mu_{4_0} a \cos 2\Phi_2 , \qquad (4.59)$$

$$\sigma_2 a + \Delta_5 a^3 = 2\xi_2 a \Delta_4 \cos 2\Phi_2 + \xi_2 \pi^2 \mu_{4_0} a \sin 2\Phi_2. \tag{4.60}$$

The frequency response equation takes the following form

$$a^{2}[(\mu_{2_{2}} + \mu_{4_{0}}\pi^{4}\frac{a^{2}}{8})^{2} + (\sigma_{2} + \Delta_{5}a^{2})^{2} - (2\xi_{2}\Delta_{4})^{2} - (\pi^{2}\xi_{2}\mu_{4_{0}})^{2}] = 0.$$
 (4.61)

From this equation, we solve for the nontrivial solution of  $a^2$  and obtain

$$(a_2)^2 = (\frac{1}{k})[-l + \sqrt{l^2 - km}], \qquad (4.62)$$

$$(a_3)^2 = (\frac{1}{k})[-l - \sqrt{l^2 - km}], \qquad (4.63)$$

where

$$k = \left[ \left( \frac{1}{8} \right) \mu_{4_0} \pi^4 \right]^2 + \Delta_5^2 , \qquad (4.64)$$

$$l = (\frac{1}{8})\mu_{4_0}\mu_{2_2}\pi^4 + \Delta_5\sigma_2, \qquad (4.65)$$

$$m = \mu_{2_2}^2 + \sigma_2^2 - (2\xi_2\Delta_4)^2 - (\pi^2\xi_2\mu_{4_0})^2. \tag{4.66}$$

Figure 4.2 shows an example for these frequency response curves. From equations (4.62) and (4.63), we know that  $a_2$  and  $a_3$  exist only when

$$l^2 - km > 0. (4.67)$$

This implies that the magnitude of the forcing term must be large enough in order to produce a sustained nontrivial steady-state response. Furthermore, we need

$$\sigma_2 < \sqrt{(2\xi_2\Delta_4)^2 + (\pi^2\xi_2\mu_{4_0})^2 - \mu_{2_2}^2} \tag{4.68}$$

for the existence of  $a_2$ , and

$$\sigma_2 < -\sqrt{(2\xi_2\Delta_4)^2 + (\pi^2\xi_2\mu_{4_0})^2 - \mu_{2_2}^2} \tag{4.69}$$

for the existence of  $a_3$ .

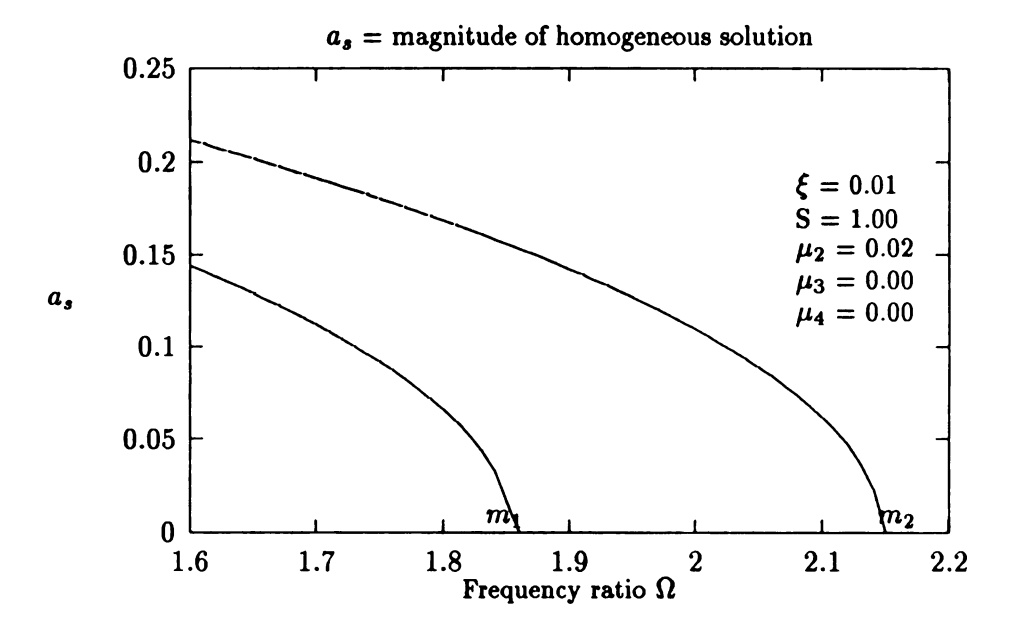


Figure 4.2: Frequency response equation for the principal parametric resonance (equation [4.61])

In order to determine the stability of these steady-state responses, we compute the Jacobian matrix associated with equations (4.56) and (4.57), which takes the form,

$$\begin{bmatrix} -(\frac{\mu_{4_0}}{4})\pi^2 a^2 & -2(\sigma_2 + \Delta_5 a^2)a \\ 2\Delta_5 a & -2\mu_{2_2} - (\frac{\mu_{4_0}}{4})\pi^2 a^2 \end{bmatrix} . \tag{4.70}$$

The eigenvalues associated with this matrix are

$$\lambda_{1,2} = -(\mu_{2_2} + \frac{\mu_{4_0}}{4}\pi^2a^2) \pm \sqrt{(\frac{\mu_{4_0}}{8}\pi^2a^2)(\mu_{2_2} + \frac{\mu_{4_0}}{8}\pi^2a^2) + \Delta_5a^2(\sigma_2 + \Delta_5a^2)}.$$
 (4.71)

Thus, the stability of each individual steady-state response is decided by the sign of the term inside the radical sign. When this quantity is negative, we have a stable steady state response. Otherwise, it is unstable. Thus, the following conclusion is obtained:

(1) when  $\sigma_2 > \sqrt{(2\xi_2\Delta_4)^2 + (\pi^2\xi_2\mu_{4_0})^2 - \mu_{2_2}^2}$ , only the trivial solution is possible, and it is stable.

(2) when  $\sigma_2 < |\sqrt{(2\xi_2\Delta_4)^2 + (\pi^2\xi_2\mu_{4_0})^2 - \mu_{2_2}^2}|$ , the trivial solution becomes unstable, while  $a_2$  exists and is stable, and  $a_3$  does not exist.

(3)when  $\sigma_2 < -\sqrt{(2\xi_2\Delta_4)^2 + (\pi^2\xi_2\mu_{4_0})^2 - \mu_{2_2}^2}$ ,  $a_3$  exists and is unstable, and  $a_2$  and  $a_1$  are stable.

Remark: Before leaving this section, a few points need to be made. First, let us compare linear resonant equations (equations [4.40] and [4.41]) with the nonlinear version (equations [4.56] and [4.57]). Basically, they coincide with each other in the linear part. The difference in equations describing the variation of the amplitude is the nonlinear term  $(\frac{1}{8})\mu_{4_0}a^3$ . We note that  $(\frac{1}{8})\mu_{4_0}a^3$  arises because of the slider friction introduced by elastic deformation. The difference in equations describing the variation of phase angle is the  $\Delta_5 a^3$  term in equation (4.57). Next, let us compare the frequency response equations obtained from the linear and nonlinear analyses. Again, they coincide with each other in the linear part. The influence of the nonlinearity on the response can be determined by a direct comparison. In absence of the nonlinearity, the response is unstable when the parameters located inside the unstable regions. According to linear theory, the amplitude of the response grows without limit. Due to the nonlinear effects, this increasing response amplitude will be accompanied with an increase of the resistance force and a change of the phase angle. The resistance force arises because of the foreshortening introduced by elastic deformation. As the amplitude of the response increases, this resistance force whose magnitude is proportional to the foreshortening also increases. The amplitude of response reaches its equilibrium state when this resistance compensates the effect of the slider friction introduced by the rigid body motion. We now consider the effect of the nonlinear terms in the equation describing the variation of phase angle. Due the effects of nonlinearity, the increase of the amplitude of response will accompany with a change of the phase angle. This implies a change in the rate at which energy is pumped into the system. When the energy put into the system is balanced by the energy dissipated by the system, the system reaches its steady state.

## 4.4 Primary Resonance ( $\Omega \approx 1$ )

From equations (4.31) and (4.32) in section 4.2, it is clear that the amplitude of the particular solution approaches infinity as  $\Omega$  approaches one. This phenomenon is referred to as the primary resonance. Let us reconsider equation (4.49), and now assume that  $\Omega$  is near to one. To make the analysis more clear, let us express  $\Omega$  as

$$\Omega = 1 + \epsilon \sigma_1 \ . \tag{4.72}$$

In addition, the damping parameter  $\mu_2$  is rescaled according to equation (3.49). With these arrangements, equation (4.49) becomes

$$D_0^2 v_2 + v_2 = -2D_0 D_1 v_1 + (\frac{2}{\pi}) \xi_2 \Omega^2 \sin \Omega T_0 - 2\mu_{2_1} D_0 v_1$$
 (4.73)

by following the same procedure as that described in section 4.3. To retain the periodicity of the solution, the following must hold

$$-2j(D_1A_1)-2j\mu_{2_1}A_1-(\frac{\xi_2}{\pi})\Omega^2 exp(j\sigma_1T_0-j\frac{\pi}{2})=0$$
 (4.74)

after substituting  $v_1 = A_1 exp(jT_0)$  into equation (4.73). Expanding the last equation with  $A_1 = (\frac{a}{2}) exp(j\Psi)$  and separating the the resultant equation into the real and imaginary

parts, we obtain

$$a' = -\mu_{2_1} a - (\frac{\xi_2}{\pi}) \cos \Phi_1 , \qquad (4.75)$$

$$a\Phi_1' = \sigma_1 a + (\frac{\xi_2}{\pi})\sin\Phi_1 \tag{4.76}$$

where  $\Phi_1$  is given in equation (3.55). After solving these equations, solution v(t) of the original equation is approximated by

$$v(t) = \epsilon v_1 + O(\epsilon^2) = \epsilon a \cos(\Omega T_0 - \Phi) + O(\epsilon^2)$$
(4.77)

where the magnitude of the steady state response  $a_s$  is described by

$$a_s = \frac{\xi_1}{\pi} \frac{1}{\sqrt{\mu_{2_1}^2 + \sigma_1^2}} \tag{4.78}$$

and the steady state value of the phase angle  $\Phi_s$  is given by

$$\tan \Phi_s = \left(\frac{\sigma_1}{\mu_{2s}}\right). \tag{4.79}$$

It is interesting, and not surprising, to find that equation (4.77) is the first order approximation of equation (4.24) which is the response for linearized model when  $\Omega$  is near to one. The local equivalence between equations (4.77) and (4.24) can be shown as below:

$$X = \left(\frac{2}{\pi}\right) \frac{\xi \Omega^2}{\sqrt{(1-\Omega^2)^2 + 4\mu_2^2 \Omega^2}} \approx \left(\frac{2}{\pi}\right) \frac{\epsilon^2 \xi_2}{\sqrt{4\epsilon^2 \sigma_1^2 + 4\epsilon^2 \mu_{2_1}^2}} = \left(\frac{1}{\pi}\right) \frac{\epsilon \xi_1}{\sqrt{\sigma_1^2 + \mu_{2_1}^2}} = \epsilon a_s , \quad (4.80)$$

while angles  $\varphi$  and  $\phi$  are related by

$$\tan \varphi = \frac{2\mu_2\Omega}{1-\Omega^2} \approx \frac{2\epsilon\Omega}{-2\epsilon\sigma_1} = -\cot \Phi_1. \tag{4.81}$$

Hence, equations (4.77) and (4.24) are within  $O(\epsilon^2)$  in an  $\epsilon$ -neighborhood of  $\Omega=1$ . This shows that the reordering relation (3.60) can not help us in including the nonlinearity in our analysis. Based on this fact, let us rescale the length ratio  $\xi$  according to  $\xi=\epsilon^3\xi_3$ . Substituting this reordering relation into equation (4.21), expanding and equating the coefficients of the like-power terms, we obtain

Order  $\epsilon$ 

$$D_0^2 v_1 + v_1 = 0 , (4.82)$$

Order  $\epsilon^2$ 

$$D_0^2 v_2 + v_2 = -2D_0 D_1 v_1 , (4.83)$$

Order  $\epsilon^3$ 

$$D_0^2 v_3 + v_3 = -2D_0 D_2 v_1 - 2D_0 D_1 v_2 - D_1^2 v_1 - 2\mu_{2_2} D_0 v_1$$
$$- \pi^4 S(D_0^2 v_1^3) + (\frac{2}{\pi}) \xi_3 \Omega^2 \sin(\Omega T_0) - \mu_{4_0} \pi^4 v_1^2 (D_0 v_1) . \tag{4.84}$$

The solution of equation (4.82) is given by equation (4.51). Also, from equation (4.83), we know that  $A_1$  must be independent of the time scale  $T_1$  in order to eliminate the secular term from the particular solution of  $v_2$ . With this, equation (4.84) can be reduced to

$$\begin{split} D_0{}^2v_3 &+ v_3 = -2j(D_2A_1)exp(jT_0) - 2j\mu_{2_2}A_1exp(jT_0) \\ &+ (\frac{1}{\pi})\xi_3\Omega^2exp(j\Omega T_0 - j\pi/2) - j\mu_{4_0}\pi^4A_1^2\bar{A}_1exp(jT_0) \end{split}$$

+ 
$$\pi^4 A_1^2 \bar{A}_1 exp(jT_0) + N.S.T. + c.c.$$
 (4.85)

Therefore, we must have

$$-2j(D_2A_1)-2j\mu_{2_2}A_1-j\mu_{4_0}\pi^4A_1^2\bar{A}_1+(\frac{1}{\pi})\xi_3\Omega^2exp(j\sigma_2T_2-j\pi/2)+\pi^4A_1^2\bar{A}_1=0 \quad (4.86)$$

in order to eliminate the secular terms from the particular solution of  $v_3$ . Expanding equation (4.86) with  $A_1 = (\frac{a}{2})exp(j\Psi)$ , and separating the resultant equation into real and imaginary parts, we obtain

$$a' = -\mu_{2_2}a - \mu_{4_0}\pi^4 \frac{a^3}{8} - \frac{\xi_3}{\pi}\cos\Phi_2, \qquad (4.87)$$

$$a\Phi_2' = \sigma_2 a + \Delta_5 a^3 + \frac{\xi_3}{\pi} \sin \Phi_2 \tag{4.88}$$

where  $\Phi_2$  is given in equation (3.71),  $\Delta_5$  is given in equation (4.58) and the frequency ratio  $\Omega$  is expressed as

$$\Omega = 1 + \epsilon^2 \sigma_2 \ . \tag{4.89}$$

The steady-state response can be obtained by letting  $a' = \Phi'_2 = 0$  in equations (4.87) and (4.88), which gives

$$\mu_{2_2}a + \mu_{4_0}\pi^4 \frac{a^3}{8} = -\frac{\xi_3}{\pi}\cos\Phi_2, \qquad (4.90)$$

$$\sigma_2 a + \Delta_5 a^3 = -\frac{\xi_3}{\pi} \sin \Phi_2 . {(4.91)}$$

The frequency response equation is then given by

$$a^{2}[(\mu_{2_{2}} + \mu_{4_{0}}\pi^{4}\frac{a^{2}}{8})^{2} + (\sigma_{2} + \Delta_{5}a^{2})^{2}] = (\frac{\xi_{3}}{\pi})^{2}. \tag{4.92}$$

and the frequency response curve as

$$\sigma_2 = -\Delta_5 a^2 \pm \sqrt{(\frac{\xi_3}{a\pi})^2 - (\mu_{2_2} + \mu_{4_0} \pi^4 \frac{a^2}{8})^2} . \tag{4.93}$$

Figure 4.3 provides an example of the frequency response equation associated with the primary resonance. To find the peak amplitude  $a_p$  of the steady-state response, we need to solve the following equation:

$$\left(\frac{\xi_3}{\pi}\right)^2 - a_p^2 \left[\mu_{2_2} + \left(\frac{1}{8}\right)\mu_{4_0}\pi^4 a_p^2\right]^2 = 0 \tag{4.94}$$

which is a cubic equation in terms of  $a_p^2$ . Moreover, the steady-state response achieves its maximum amplitude at frequency  $\Omega = 1 + \epsilon^2 \sigma_{2p}$  where

$$\sigma_{2p} = -\Delta_5 a_p^2 \tag{4.95}$$

where  $a_p$  represents the solution of equation (4.94). The negative sign in the last equation implies that the response curve reaches this peak amplitude at a frequency of less than one. Moreover, over a region of  $\Omega$  values, there exist more than one steady-state response (Figure 4.3). The frequency response curve bends to the left, corresponding to a softening type of nonlinearity. The stability of these steady-state responses can be decided by computing the eigenvalues of the Jacobian matrix associated with equations (4.87) and (4.88) which takes the form

$$\begin{bmatrix} -\mu_{2_2} - (\frac{3\mu_{4_0}}{8})\pi^4 a^2 & -(\sigma_2 + \Delta_5 a^2)a \\ (\sigma_2 + 3\Delta_5 a^2)/a & -\mu_{2_2} - (\frac{\mu_{4_0}}{8})\pi^4 a^2 \end{bmatrix}. \tag{4.96}$$

From its eigenvalues, we determine that when

$$\left[\mu_{2_2} + \left(\frac{1}{8}\right)\mu_{4_0}\pi^4a^2\right]\left[\mu_{2_2} + \left(\frac{3}{8}\right)\mu_{4_0}\pi^4a^2\right] + (\sigma_2 + \Delta_5a^2)(\sigma_2 + 3\Delta_5a^2) < 0 \tag{4.97}$$

the steady-state responses are unstable. Otherwise, they are stable. The solution v(t) can approximated by

$$v(t) = \epsilon v_1(T_0, T_1, T_2) + O(\epsilon^2) = \epsilon a \cos(\Omega T_0 - \Phi) + O(\epsilon^2)$$
(4.98)

where a and  $\Phi$  are described by equations (4.87) and (4.88). The steady state value of the phase angle  $\Phi$  is given by

$$\Phi_s = \tan^{-1}\left(\frac{\sigma_2 + \Delta_5 a^2}{\mu_{2_2} + \frac{1}{8}\mu_{4_0} \pi^4 a^2}\right). \tag{4.99}$$

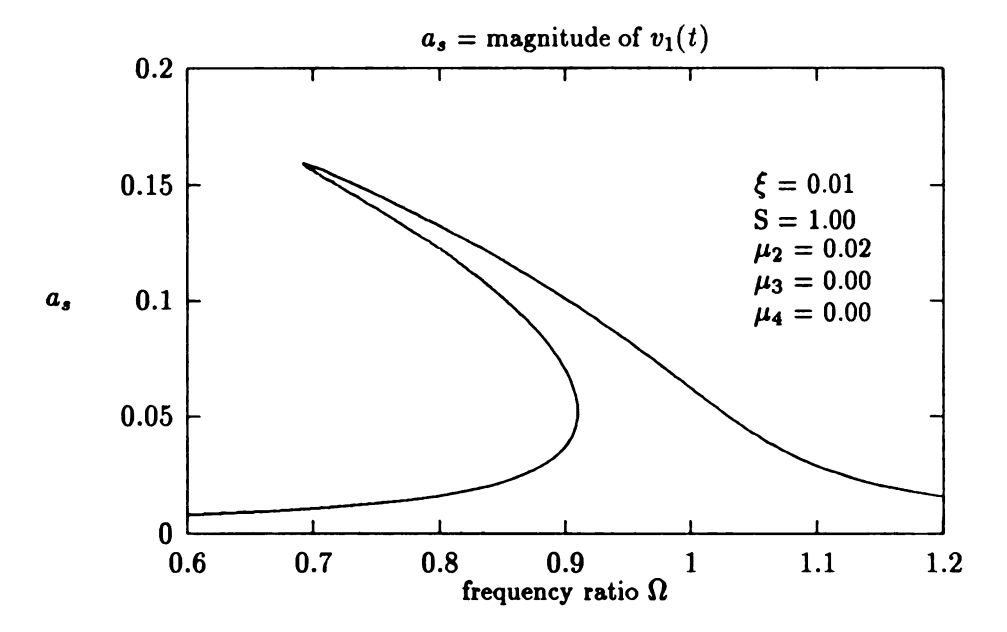


Figure 4.3: Frequency response equation for the primary resonance (equation [4.92])

Remark: Before leaving this section, a few points need to be mentioned. First, let us neglect the effect of  $\mu_{4_0}$  and then compare the final equations describing the resonant conditions between linear and nonlinear analyses. We note that the amplitude function a is described by equations of the same type (equations [4.87] and [4.75]), while the equations describing the phase angles  $\Phi_1$  and  $\Phi_2$  (equations [4.76] and [4.88]) are coincident in the linear part. The only difference between these two analyses is the existence of the nonlinear term  $\Delta_5 a^2$  in the equation describing  $\Phi_2$  (equation [4.88]). This implies that the nonlinear affects the response of the system by changing the phase angle  $\Phi_2$ . Therefore, there is a change in the rate at which energy is pumped into the system accompanying this phase change as a varies. The system achieves its steady state amplitude when the energy dissipated by the system is balanced by the energy pumped into the system. This implies that the magnitude of the steady state response may be remain unchanged but a considerable shift of the phase angle of the steady state response can be expected. We now compare the maximum amplitude of the response obtained from the linear and nonlinear analyses. Again, the effect of slider friction is neglected. A prudent observation shows that these two values are exactly the same. This implies that linear theory is sufficient to provide a good approximation of the amplitude of the steady-state response. However, as we compare the frequency at which the steady state response of the system reaches its maximum amplitude, there exists a considerable difference between the results from linear and nonlinear analyses. Linear analysis indicates that this peak amplitude can be observed when  $\Omega = 1$ . The nonlinear analysis show that the response achieves this amplitude when  $\Omega$  is at the value given by equations (4.92) and (4.93). This indicates that linear theory may offer a poor prediction of the frequency near which large amplitudes occur. Finally, let us consider the effect of  $\mu_{4_0}$  which represents the effect of slider friction. According the analysis,  $\mu_{4_0}$ 

has a favorable effect in reducing the amplitude of the response. This is caused by the foreshortening accompanying with the transverse deformation of the connecting rod. The existence of the slider friction will resist further deformation and hence has a tendency in reducing the amplitude of the response.

### 4.5 Superharmonic Resonance $(\Omega \approx \frac{1}{2})$

In analyzing the particular solution of  $v_2$  in section 4.2, we assumed that  $\Omega$  is away from 2 and  $\frac{1}{2}$  and proceeded to analyze the solution of  $v_3$ . When  $\Omega$  is near to  $\frac{1}{2}$ , a superharmonic resonance occurs. For  $\Omega$  near to  $\frac{1}{2}$ , the frequency ratio  $\Omega$  is expressed as

$$\Omega = \frac{1}{2}(1 + \epsilon \sigma_1) . \tag{4.100}$$

At the same time, the damping parameter  $\mu_2$  is rescaled according to  $\mu_2 = \epsilon \mu_{2_1}$  so that it will appear together with detuning parameter  $\sigma_1$  in the final resonant condition. Consequently, equation (4.29) reduces to

$$D_0^2 v_2 + v_2 = -2j(D_1 A_1) exp(jT_0) - 2j\mu_{2_1} A_1 exp(jT_0)$$

$$+ \mu_{4_0} \pi^2 \xi_1 \Omega \frac{\Lambda_4}{2} exp(2j\Omega T_0)$$

$$- (S + \frac{1}{2}) \xi_1 \Omega^2 \pi^2 (\frac{\Lambda_4}{4}) exp(2j\Omega T_0 - j\frac{\pi}{2})$$

$$+ \frac{1}{\pi} \xi_1^2 \Omega^2 exp(2j\Omega T_0 - j\frac{\pi}{2}) + N.S.T. + c.c. . \tag{4.101}$$

The elimination of the secular terms of the particular solution of the last equation requires

that

$$\frac{\mu_{4_0}}{6}\xi_1^2\pi exp(j\sigma_1T_1) - 2j(D_1A_1) - 2j\mu_{2_1}A_1 + \frac{\xi_1^2}{12\pi}(3-\Delta_4)exp(j\sigma_1T_1 - j\frac{\pi}{2}) = 0 \quad (4.102)$$

where  $\sigma_1$  is given in equation (4.100) and  $\Delta_4$  is defined by equation (4.42). Substituting  $A_1 = \frac{a}{2} exp(j\Psi)$  into equation (4.102), expanding and separating the resultant equation into real and imaginary parts, we obtain

$$a' = -\mu_{2_1} a + \frac{\mu_{4_0} \xi_1^2 \pi}{6} \sin \Phi_1 - \frac{\xi_1^2}{12\pi} (3 - \Delta_4) \cos \Phi_1 ,$$
 (4.103)

$$a\Phi_1' = \sigma_1 a + \frac{\mu_{4_0} \xi_1^2 \pi}{6} \cos \Phi_1 + \frac{\xi_1^2}{12\pi} (3 - \Delta_4) \sin \Phi_1$$
 (4.104)

where  $\Phi_1$  is given in equation (3.55). Therefore, when  $\Omega$  is near to  $\frac{1}{2}$ , the response equation takes the form

$$v(t) = \epsilon v_1(T_0, T_1, T_2) + O(\epsilon^2)$$

$$= \epsilon [\Lambda_4 \sin \Omega T_0 + a \cos(2\Omega T_0 - \Phi)] + O(\epsilon^2)$$
(4.105)

where  $\Lambda_4$  is given in equation (4.32), a and  $\Phi$  are given by equations (4.103) and (4.104), respectively. The steady state value of phase angle  $\Phi$  is given as

$$\Phi_s = \tan^{-1} \left[ \frac{\sigma_1(3 - \Delta_4) - 2\pi^2 \mu_{2_1} \mu_{4_0}}{2\pi^2 \sigma_1 \mu_{4_0} + (3 - \Delta_4) \mu_{2_1}} \right]$$
(4.106)

and the amplitude of the steady state response  $a_s$  is described by

$$(\mu_{2_1}^2 + \sigma_1^2)a_s^2 = \xi_1^4 \left[ \left( \frac{\mu_{4_0}\pi}{6} \right)^2 + \left( \frac{3 - \Delta_4}{12\pi} \right)^2 \right]. \tag{4.107}$$

Equation (4.107) represents the frequency response equation of this superharmonic resonance. Figure 4.4 provide an example of the frequency response equation associated with this superharmonic resonance. Equation (4.105) represents the first order approximation to

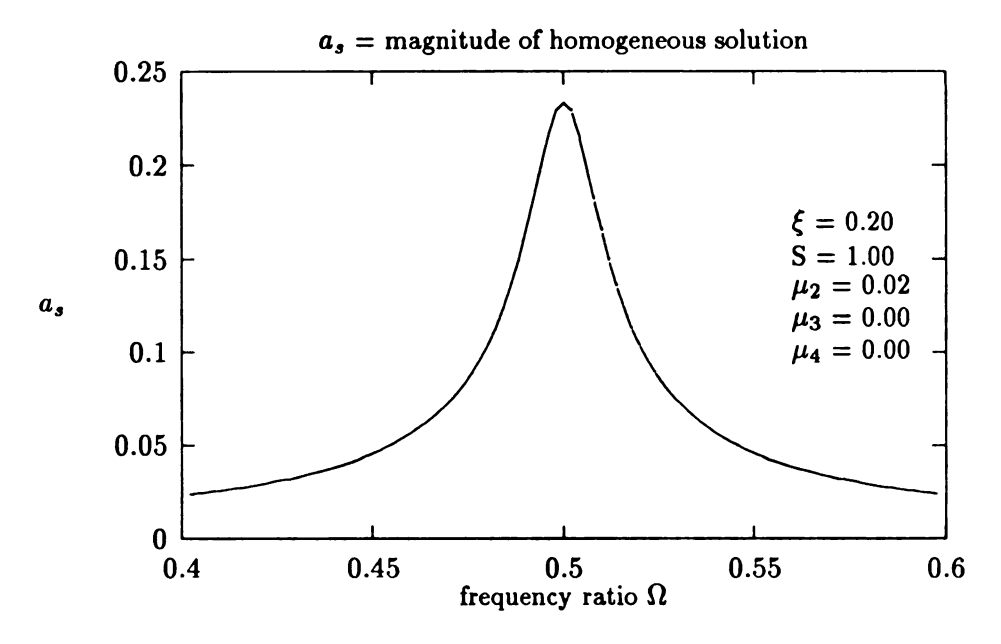


Figure 4.4: Frequency response equation for superharmonic resonance  $(\Omega \approx \frac{1}{2})$ 

the steady state response. Note that  $v_1$  consists of two parts, the first term is the particular solution and the second term is from the free oscillation term. Hence, the homogeneous solution does not decay to zero. This is caused by the last term in equation (4.29). Because of the existence of this oscillating term, resonance arises when  $\Omega \approx \frac{1}{2}$ . The amplitude of the particular solution is proportional to the length ratio  $\xi$ , while the second term is proportional to the square of length ratio. This implies that the second term vanishes more rapidly than the first one as the length ratio  $\xi$  approaches to zero. A simple calculation of the eigenvalues of the Jacobian matrix associated with equations (4.103) and (4.104) shows that this homogeneous solution is stable everywhere for  $\mu_{2_1} > 0$ . Hence, a steady state superharmonic resonance exists for all conditions and the response is composed by two terms with different frequencies. Certainly, the particular solution possesses the same frequency

as that of the external excitation, while, the homogeneous solution, which is included to improve the estimate, oscillates with twice the frequency of the external excitation. It should be noted that this result is simply an expansion of the *linear* response in terms of  $\xi$ .

Remark: An interesting observation about the influence of the mass ratio S on the amplitude of the homogeneous solution needs to be pointed out. Since the amplitude of the homogeneous solution is described by equation (4.107), a minimum value of this equation implies a minimum amplitude of the homogeneous solution. Based on this fact, we find that  $a_s$  reaches a minimum value when  $\Delta_4 = 3$ . This implies that a proper choice of the mass ratio can be used to suppress, but not eliminate, this superharmonic resonance. Furthermore, the existence of the damping parameter  $\mu_4$ , from the slider end, prevents us from having a homogeneous solution with a zero amplitude for this superharmonic resonance. This indicates that the damping parameter  $\mu_{40}$  has an adverse effect on the response of the system for this superharmonic resonance.

# 4.6 Superharmonic Resonance $(\Omega \approx \frac{1}{3})$

In the current section, we consider the superharmonic resonance case where  $\Omega$  is near to  $(\frac{1}{3})$ . In this case, equation (4.29) reduces to

$$D_0^2 v_3 + v_3 = -2j(D_2 A_1) exp(jT_0) - 2j\mu_{2_2} A_1 exp(jT_0) - j\mu_{4_0} \pi^4 A_1^2 \bar{A}_1 exp(jT_0)$$

$$+ \pi^4 S A_1^2 \bar{A}_1 exp(jT_0) + f_7 \xi_1^2 A_1 exp(jT_0) - j(\frac{\mu_{4_0}}{32}) \pi^2 A_1 \xi_1^2 exp(jT_0)$$

$$+ jf_8 \xi_1^3 exp(jT_0 + j\sigma_2 T_2) + (\frac{\mu_{4_0}}{1536}) \pi \xi_1^3 exp(jT_0 + j\sigma_2 T_2)$$

$$+ N.S.T. + c.c. \qquad (4.108)$$

where the coefficients  $f_7$  and  $f_8$  are given in Appendix E, and the detuning parameter  $\sigma_2$  is defined by

$$\Omega = \frac{1}{3}(1 + \epsilon \sigma_2) \ . \tag{4.109}$$

Therefore, in order to eliminate the secular term of  $v_3$ , we must have

$$-2j\mu_{2_{2}}A_{1} - 2j(D_{2}A_{1}) - j\mu_{4_{0}}\pi^{4}A_{1}^{2}\bar{A}_{1} - j(\frac{\mu_{4_{0}}}{32})\pi^{2}A_{1}\xi_{1}^{2} + \pi^{4}SA_{1}^{2}\bar{A}_{1}$$

$$+ (\frac{\mu_{4_{0}}}{1536})\pi\xi_{1}^{3}exp(j\sigma_{2}T_{2}) + f_{7_{1}}\xi_{1}^{2}A_{1} + jf_{8_{1}}\xi_{1}^{3}exp(j\sigma_{2}T_{2}) = 0. \quad (4.110)$$

Substituting  $A_1 = \frac{a}{2} exp(j\Psi)$  into equation (4.110), expanding and separating the resultant equation into the real and imaginary parts, we obtain

$$a' = -\mu_{2_2} a - (\frac{\mu_{4_0}}{8}) \pi^4 a^3 - (\frac{\mu_{4_0}}{64}) \pi^2 \xi_1^2 a + f_{8_1} \xi_1^3 \cos \Phi_2 + (\frac{\pi}{1536}) \xi_1^3 \mu_{4_0} \sin \Phi_2 , \qquad (4.111)$$

$$a\Phi_2' = \sigma_2 a + \frac{f_{7_1}}{2}\xi_1^2 a + \Delta_5 a^3 - f_{8_1}\xi_1^3 \sin\Phi_2 + (\frac{\pi}{1536})\xi_1^3 \mu_{4_0} \cos\Phi_2$$
 (4.112)

where  $\Phi_2$  is given in equation (3.71),  $\Delta_5$  is defined by equation (4.58), coefficients  $f_{7_1}$  and  $f_{8_1}$  are given in Appendix E. Because the coefficient of  $\mu_{4_0}\xi_1^3$  is small compared with the rest of terms in equations (4.111) and (4.112), we neglect the influence of this term in the following analysis. From these equations, we find that the frequency response equation takes the form,

$$a^{2}[(\mu_{2_{2}} + \frac{\mu_{4_{0}}}{8}\pi^{4}a^{2} + \frac{\mu_{4_{0}}}{64}\pi^{2}\xi_{1}^{2})^{2} + (\sigma_{2} + \frac{f_{7_{1}}}{2}\xi_{1}^{2} + \Delta_{5}a^{2})^{2}] = f_{8_{1}}^{2}\xi_{1}^{6}$$
(4.113)

and the frequency response curves are given by

$$\sigma_2 = -\frac{f_{7_1}}{2}\xi_1^2 - \Delta_5 a^2 \pm \sqrt{\frac{f_{8_1}^2 \xi_1^6}{a^2} - \left[\mu_{2_2} + \frac{\mu_{4_0}}{8}\pi^4 a^2 + \frac{\mu_{4_0}}{64}\pi^2 \xi_1^2\right]^2}.$$
 (4.114)

Figure 4.5 provides an example of the frequency response curve associated with this superharmonic resonance.

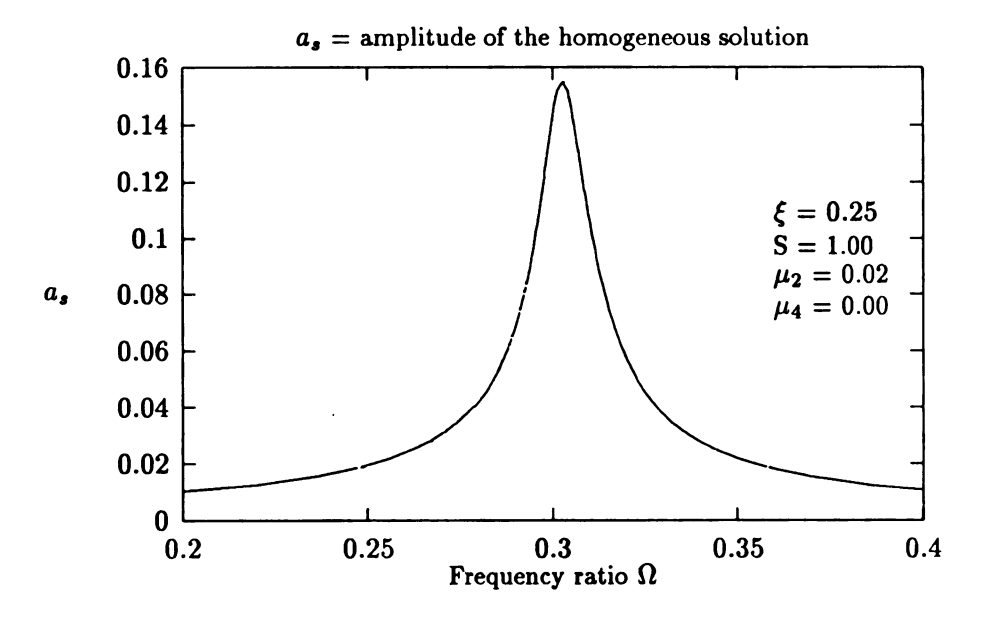


Figure 4.5: Frequency response equation for the superharmonic resonance  $(\Omega \approx \frac{1}{3})$ 

Despite the presence of the damping parameters, the homogeneous solution of  $v_1$  does not decay to zero. Moreover, the steady state response of the system can be approximated by

$$v(t) = \epsilon v_1(T_0, T_1, T_2) + O(\epsilon^2)$$

$$= \epsilon \left[ \Lambda_4 \sin \Omega T_0 + a \cos (3\Omega T_0 - \Phi) \right] + O(\epsilon^2)$$
(4.115)

where a and  $\Phi$  are described by equations (4.111) and (4.112), respectively. The steady

state value  $\Phi_s$  of the phase angle is defined by

$$\tan \Phi_{\bullet} = \left[ \frac{\sigma_2 + (f_{7_1}/2)\xi_1^2 + \Delta_5 a^2}{\mu_{2_2} + (\frac{\mu_{4_0}}{8})\pi^4 a^2 + (\frac{\mu_{4_0}}{64})\pi^2 \xi_1^2} \right]. \tag{4.116}$$

Note that equation (4.113) indicates that the homogeneous solution reaches its own maximum amplitude which is described by

$$(f_{8_1}^2 \xi_1^3)^2 - a_p^2 \left[ \left( \mu_{2_2} + \left( \frac{\mu_{4_0}}{8} \right) \pi^4 a_p^2 + \left( \frac{\mu_{4_0}}{64} \right) \pi^2 \xi_1^2 \right]^2 = 0$$
 (4.117)

when the frequency ratio is  $\Omega = (1 + \epsilon \sigma_p)/3$  with  $\sigma_p$  being defined by

$$\sigma_p = -(f_{7_1}/2)\xi_1^2 - \Delta_5 a_p^2 \,. \tag{4.118}$$

To determine the stability of each individual steady state response, we compute the Jacobian matrix associated with equations (4.111) and (4.112), which takes the form,

$$\begin{bmatrix} -\mu_{2_{2}} - (\frac{3}{8})\mu_{4_{0}}\pi^{4}a^{2} - (\frac{\mu_{4_{0}}}{64})\pi^{2}\xi_{1}^{2} & -(\sigma_{2} + (f_{7_{1}}/2)\xi_{1}^{2} + \Delta_{5}a^{2})a \\ (\sigma_{2} + (f_{7_{1}}/2)\xi_{1}^{2} + 3\Delta_{5}a^{2})/a & -\mu_{2_{2}} - (\frac{1}{8})\mu_{4_{0}}\pi^{4}a^{2} - (\frac{\mu_{4_{0}}}{64})\pi^{2}\xi_{1}^{2} \end{bmatrix} . \tag{4.119}$$

By computing the eigenvalues of this Jacobian matrix, we determine that these steady state responses are unstable when

$$[\mu_{2_{2}} + (\frac{3}{8})\mu_{4_{0}}\pi^{4}a^{2} + (\frac{\mu_{4_{0}}}{64})\pi^{2}\xi_{1}^{2}][\mu_{2_{2}} + (\frac{1}{8})\mu_{4_{0}}\pi^{4}a^{2} + (\frac{\mu_{4_{0}}}{64})\pi^{2}\xi_{1}^{2}]$$

$$+[\sigma_{2} + \xi_{1}^{2}(f_{7_{1}}/2) + \Delta_{5}a^{2}][\sigma_{2} + \xi_{1}^{2}(f_{7_{1}}/2) + 3\Delta_{5}a^{2}] < 0.$$
(4.120)

Otherwise, they are stable.

Remarks: First, the homogeneous solution does not decay to zero in spite of the existence of the damping parameters. Therefore, the steady state response is composed of two functions with two different frequencies. The particular solution oscillates with the same frequency as that of the external excitation, the homogeneous solution oscillates with a frequency that is three times the external frequency. Note that the amplitude of the particular solution given in equation (4.32), is proportional to the length ratio  $\xi_1$ , while the amplitude of the homogeneous solution (equation [4.113]) is proportional to the cube of the length ratio  $\xi_1$ . This implies that the homogeneous solution vanishes more rapidly than the particular solution as  $\xi$  approaches zero. Note that the linear approximation may be applicable when length ratio  $\xi$  is small, since the homogeneous solution may be insignificant.

Next, let us consider the frequency response equation (4.113), which is cubic in  $a_s^2$ . There exists more than one steady state responses in some parameter regions (Figure 4.5). Note that the value of  $\Delta_5$  is always positive, this implies that the backbone curve, which is the locus of the frequency responses, bends to the left. Moreover, the existence of  $f_{7_1}$  implies a shift of the origin of the backbone curve. In other words, the backbone curve associated with this superharmonic resonance does not originate from  $\Omega = \frac{\omega_n}{3}$ . Together with the stability results, we know that the frequency response curves bends to the left corresponding to a superharmonic resonance with a softening type of nonlinearity. However, the influence of  $\Delta_5 a_p^2$  may be insignificant so that the no bending of the backbone is observed. This indicates that, for small values of the length ratio  $\xi$ , there is no jump phenomenon.

Finally, let us discuss the influence of the mass ratio S on the amplitude of this superharmonic resonance. Since the amplitude of the free oscillation solution is governed by equation (4.113), it is possible to reduce the amplitude of this solution by reducing the value of coefficient  $f_{8_1}$ . In other words, we can suppress the contribution of the homogeneous so-

lution on the overall response by choosing a proper mass ratio. From a more physical point of view, we can select a mass ratio so that the external force is diminished. When such a mass ratio, which is about 1.40, is selected, equation (4.113) admits only the trivial solution, and hence the contribution of the free oscillation term is eliminated.

### 4.7 Subharmonic Resonance ( $\Omega \approx 3$ )

In order to analyze a subharmonic resonance for  $\Omega$  near to 3, we introduce the detuning parameter  $\sigma$  according to

$$\Omega = 3 + 3\epsilon^2 \sigma_2 \ . \tag{4.121}$$

Therefore, equation (4.36) reduces to

$$\begin{split} D_0{}^2v_3 &+ v_3 = -2j\mu_{2_2}A_1exp(jT_0) - j\mu_{4_0}\pi^4A_1^2\bar{A}_1exp(jT_0) - 2j(D_2A_1)exp(jT_0) \\ &- (\frac{81}{32})\mu_{4_0}\pi^2\xi_1^2A_1exp(jT_0) + \pi^4SA_1^2\bar{A}_1exp(jT_0) + f_7\xi_1^2A_1exp(jT_0) \\ &+ \left[ 2j\pi\Omega\xi_1\bar{A}_1^2 + (\frac{9}{8})\mu_{4_0}\xi_1\pi^3\bar{A}_1^2 \right]exp(jT_0 + 3j\sigma_2T_2) + N.S.T. + c.c. \end{split} \tag{4.122}$$

and we must have

$$-2j\mu_{2_{2}}A_{1}exp(jT_{0}) - 2j(D_{2}A_{1})exp(jT_{0}) + \pi^{4}SA_{1}^{2}\bar{A}_{1}exp(jT_{0})$$

$$-(\frac{81}{32})\mu_{4_{0}}\pi^{2}\xi_{1}^{2}A_{1}exp(jT_{0}) - j\mu_{4_{0}}\pi^{4}A_{1}^{2}\bar{A}_{1}exp(jT_{0}) + f_{7}\xi_{1}^{2}A_{1}exp(jT_{0})$$

$$+[2j\pi\Omega\xi_{1}\bar{A}_{1}^{2} + (\frac{9}{8})\mu_{4_{0}}\xi_{1}\pi^{3}\bar{A}_{1}^{2}]exp(jT_{0} + 3j\sigma_{2}T_{2}) = 0$$

$$(4.123)$$

in order to eliminate the secular terms from the particular solution of  $v_1$  and retain the periodicity of the solution. Expanding equation (4.123) with  $A_1 = \frac{a}{2} exp(j\Psi)$ , and separating

•

the resultant equation into real and imaginary parts, we obtain

$$a' = -\mu_{2_2}a - \frac{\mu_{4_0}}{8}\pi^4a^3 - \frac{81}{64}\mu_{4_0}a\pi^2\xi_1^2 + \frac{9}{32}\mu_{4_0}\pi^3a^2\xi_1\sin(3\Phi_2) + \frac{3}{2}\xi_1\pi a^2\cos(3\Phi_2),$$

$$a\Phi_2' = \sigma_2a + \frac{f_{7_2}}{2}\xi_1^2a + \Delta_5a^3 + \frac{9}{32}\mu_{4_0}\pi^3a^2\xi_1\cos3\Phi_2 - \frac{3}{2}\xi_1\pi a^2\sin3\Phi_2$$
 (4.125)

where  $\Phi_2$  is given in equation (3.71),  $f_{7_2}$  can be found in Appendix E, and  $\Delta_5$  is defined by equation (4.58). From the last two equations, we obtain the frequency response equation of the form,

$$a^{2} \left[ \left( \mu_{2_{2}} + \frac{\mu_{4_{0}}}{8} \pi^{4} a^{2} + \frac{81}{64} \mu_{4_{0}} \pi^{2} \xi_{1}^{2} \right)^{2} + \left( \sigma_{2} + \frac{f_{7_{2}}}{2} \xi_{1}^{2} + \Delta_{5} a^{2} \right)^{2} - \left[ \left( \frac{3}{2} \xi_{1} \pi \right)^{2} + \left( \frac{9}{32} \mu_{4_{0}} \pi^{3} \xi_{1} \right)^{2} \right] a^{2} \right] = 0.$$
 (4.126)

From equation (4.126), we see that the trivial solution is always a steady-state response of this specific resonance. Due to the complexity of equation (4.126), we only consider the case in which  $\mu_{40}$  is zero in the following analysis. After this simplification, equation (4.126) reduces to

$$a^{2}\left[\mu_{2_{2}}^{2}+\left(\sigma_{2}+\frac{f_{7_{2}}}{2}\xi_{1}^{2}+\Delta_{5}a^{2}\right)^{2}-\left(\frac{3}{2}\xi_{1}\pi\right)^{2}a^{2}\right]=0. \tag{4.127}$$

Now, besides the trivial response, we obtain the following nontrivial responses,

$$(a_2)^2, (a_3)^2 = \frac{1}{2\Delta_5^2} [-p \pm \sqrt{p^2 - q}]$$
 (4.128)

where coefficients p and q are given by

$$p = (2\sigma_2 + f_{7_2}\xi_1^2)\Delta_5 - (\frac{3}{2}\xi_1\pi)^2, \qquad (4.129)$$

$$q = \Delta_5^2 [(\mu_{2_2})^2 + (\sigma_2 + \frac{f_{7_2}}{2}\xi_1^2)^2]. \tag{4.130}$$

We note that q is always positive. Therefore, these nontrivial free oscillations exist only if  $p^2 \ge 4q$  and p < 0. These conditions imply that

$$\left(\frac{3}{2}\xi_1\pi\right)^4 - 2\left(\frac{3}{2}\xi_1\pi\right)^2\left(2\sigma_2 + f_{7_2}\xi_1^2\right)\Delta_5 - 4\Delta_5^2\mu_{2_2}^2 \ge 0, \qquad (4.131)$$

and

$$(3\xi_1\pi)^2 > 4(2\sigma_2 + f_{7_2}\xi_1^2)\Delta_5. \tag{4.132}$$

From equation (4.131), we solve for the values of  $\Delta_5$  for given values of  $\sigma_2$ ,  $\mu_{2_2}$  and  $\xi_1$ , and obtain the following inequality:

$$2\Delta_{5}\mu_{2_{2}} \leq -\frac{1}{\mu_{2_{2}}} (\frac{3}{2}\pi\xi_{1})^{2} (2\sigma_{2} + f_{7_{2}}\xi_{1}^{2})^{2} + \sqrt{(\frac{1}{\mu_{2_{2}}})^{2} (\frac{3}{2}\pi\xi_{1})^{4} (2\sigma_{2} + f_{7_{2}}\xi_{1}^{2}) + 4(\frac{3}{2}\xi_{1}\pi)^{4}}.$$
 (4.133)

This inequality provides the criterion regarding the existence of the nontrivial subharmonic response.

When these conditions hold, it is possible for the system to respond in such a way that the homogeneous oscillation (the  $A_1exp(jT_0)$  term in equation [4.31]) does not decay to zero, in spite of the presence of damping. Moreover, in the steady state, the nonlinear term adjusts the frequency of the free oscillation to one third that of the excitation. In this case,

the steady state response can be approximated by

$$v(t) = \epsilon v_1(T_0, T_1, T_2) + O(\epsilon^2)$$

$$= \epsilon \left[ a \cos\left(\frac{\Omega}{3}T_0 - \frac{\Phi}{3}\right) + \Lambda_1 \sin\Omega T_0 \right] + O(\epsilon^2)$$
(4.134)

where a is described by equations (4.128), where  $\Lambda_1$  is defined by equation (4.32), a and  $\Phi$  are described by equations (4.124) and (4.125), respectively. The steady state value of the phase angle is given as

$$\tan \Phi_s = \left(\frac{\sigma_2 + f_{7_2} \xi_1^2 / 2 + \Delta_5 a^2}{\mu_{2_2}}\right). \tag{4.135}$$

Note that the response of the system is dictated by the initial conditions as follow: When the initial conditions are selected in such a way that the nontrivial subharmonic resonance exists, then the response of the system can be approximated by equation (4.134). Otherwise, the system settles onto a steady state given by equation (4.134) with a = 0.

### 4.8 Summary and Discussion

In this section, we summarize the results obtained in the previous sections. Based on the observations of previous investigators [49], and the results from previous section, we select important system parameters and provide detailed discussions regarding their individual influence on the steady state response.

#### 4.8.1 Effect of the Length Ratio $\xi$

This problem is equivalent to a simply-supported beam subjected to both vertical and horizontal excitations coming from the same source. The magnitude of this excitation is proportional to the length ratio  $\xi$ . At the beginning of section 4.2, we solved a linearized

model to obtain a response whose amplitude is proportional to this parameter. In the primary resonance (section 4.4), although the amplitude of the steady state response can be predicted by using linear theory, the frequency at which the steady state response reaches its maximum amplitude also depends on the length ratio. Figure 4.6 shows the effect of the length ratio  $\xi$  on the amplitude of the primary resonance. From this figure, it is very clear that the amplitude of the primary resonance increases when  $\xi$  increases. In the parametric resonant case, the width of the frequency region in which the trivial solution becomes unstable is also proportional to the length ratio. Reconsidering Figure 4.1, the width between the two transition curves increases as  $\xi$  increases. Moreover, the amplitude of the nontrivial response depends upon  $\xi$  also. Figure 4.7 shows the effect of varying  $\xi$  on the nontrivial solutions for the principal parametric resonance. We note that, in Figure 4.7, the amplitude of the nontrivial solution increases as  $\xi$  increases. Moreover, points  $m_1$  and  $m_2$  in Figure 4.7, which are used to mark the origins of the branches of the nontrivial responses, represent the same points as those in Figure 4.1. Furthermore, the frequency region between points  $m_1$  and  $m_2$  corresponds to the region in which the trivial response is unstable. In all the superharmonic resonances, there exists an additional solution, besides the particular solution. The magnitude of these homogeneous solutions are proportional to a higher order power of the length ratio. To be specific, this non-zero homogeneous solution is of order  $O(\xi^2)$  in the case where  $\Omega$  is near to  $(\frac{1}{2})$ , and, is of order  $O(\xi^3)$  when  $\Omega$  is near to  $(\frac{1}{3})$ . These facts imply that the length ratio is the primary parameter, or in other words, the most important parameter, for the current problem.

### 4.8.2 Effect of the Frequency Ratio $\Omega$

The influence of this parameter on the response is not immediately obvious. In order

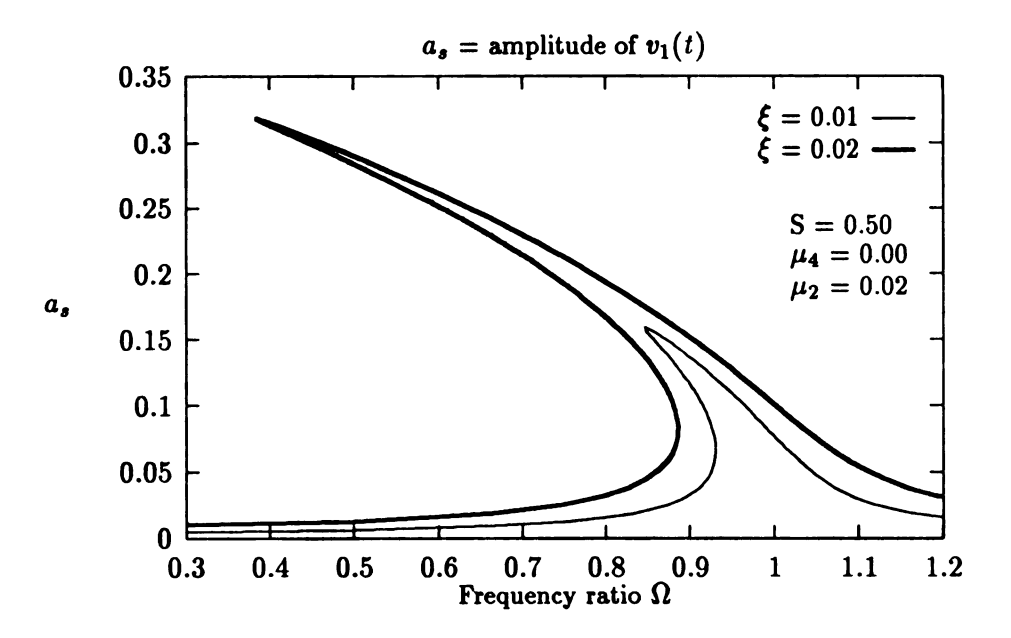


Figure 4.6: Influence of  $\xi$  on the primary resonance

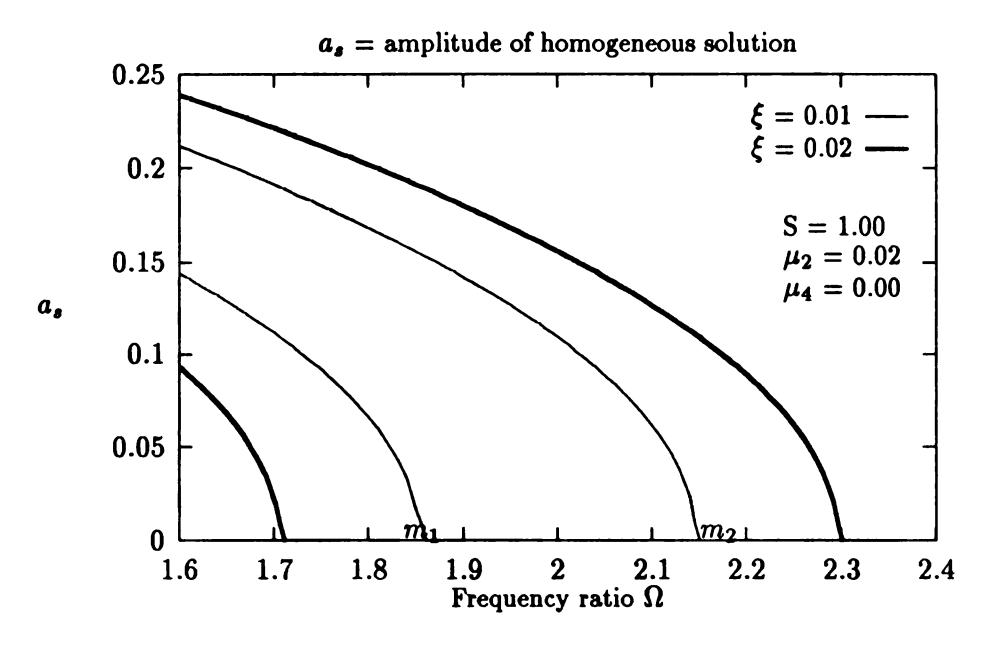


Figure 4.7: Influence of  $\xi$  on the principal parametric resonance

to understand the influence of  $\Omega$  on the response of the system, we need to separate our discussion in three categories: low frequency ratios, non-resonant frequency ratios and resonant frequency ratios.

First, let us begin our analysis in the low frequency ratio region. Let us consider the inertial force applied to the system. The accelerations  $a_x$  and  $a_y$  depend upon the square of  $\Omega$ . This implies that the inertial force is also proportional to the square of the frequency ratio, although this does not imply that the amplitude of the steady state response is overall proportional to the square of  $\Omega$ . However, in the region of low frequency ratio, the amplitude of the steady state response is proportional to the square of the frequency ratio. To show this, let us consider the amplitude of the linear response, i.e., equation (4.25),

$$X = \frac{2}{\pi} \frac{\xi \Omega^2}{\sqrt{(1 - \Omega^2)^2 + 4\mu_2^2 \Omega^2}} \approx \frac{2}{\pi} \xi \Omega^2$$
 (4.136)

for  $\Omega \ll 1$ . This implies that the amplitude of the response depends upon the length ratio as well as the frequency ratio. This point had been pointed out by previous investigators[30].

Next, let us consider the non-resonant case. When resonance is excited, the free oscillation term will decay to zero due to the presence of the damping. Consequently, the linear approximation will be sufficient to provide a good prediction. When a resonance is possible at a given operating frequency, we have to include an additional term in order to capture the effect of the homogeneous solution. Therefore, we may find that some additional peaks exist along the smooth profile of the linear response curve.

However, let us consider the asymptotic expansion of the geometrical relation, i.e. equation (4.22). From this expansion, it is clear that the external applied force is composed of multiple frequencies. Generally speaking, when  $\Omega$  is near to  $(\frac{1}{n})$ , we can expect a super-

harmonic resonance arising from the response of the system. It will be very difficult to verify these higher  $\operatorname{order}(n > 3)$  superharmonic resonances, since the magnitude of the homogeneous solution is proportional to the corresponding order of the length ratio. Unless the length ratio is large enough, the contribution of the homogeneous solution on the steady state response will be very small. This explains the reason why these homogeneous resonances do not appear in the simulation results.

#### 4.8.3 Effect of the Mass Ratio S

In the primary resonance case, the mass ratio S appears in the nonlinearity of the system and affects the response of the system by bending the backbone of the frequency response curve to the left. Figure 4.8 shows the effect of S on the frequency response equation (equation [4.92]). From this figure, it is very clear that S plays the role of nonlinearity in

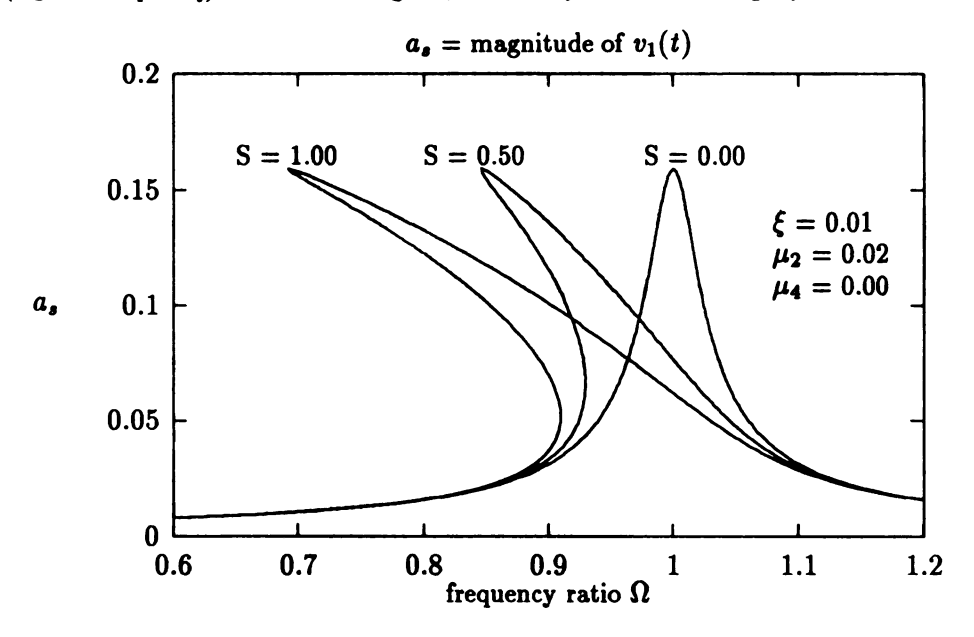


Figure 4.8: Influence of S on the primary resonance

the primary resonance. When S=0, there is no nonlinearity associated with the primary resonance, and hence no bending of the frequency response curve. When  $S\neq 0$  there exists some nonlinearity associated with the frequency response equation and the backbone curve

of the frequency response curve bend to the left.

In the principal parametric resonance, the influence of S is included in the terms  $\Delta_4$ and  $\Delta_5$ . According to the linear analysis, the main nose of instability, or in other words, the unstable regions on the  $\xi - \sigma_1$  domain, will be enlarged if the value of S is increased. To show this point, let us consider equations (4.62) to (4.69). From these equation we are aware of the following facts: (1) the width of the region in which the trivial solution is unstable increases when the mass ratio increases, (2) the amplitude of the nontrivial solutions  $a_2$  and a<sub>3</sub> change slightly when the mass ratio increases. With these two observations, we know that this parameter has both favorable and adverse effects on the principal parametric resonance. An increment of S will enlarge the unstable region, while this increment will also help to reduce the amplitude of the nontrivial solution. Figure 4.9 shows the effects of S on the width of the main nose of instability. From this figure, it is very clear that the distance between the two transition curves increases as S increases. Figure 4.10 shows the effect of S on the branches of the nontrivial responses of the principal parametric resonance (equation [4.92]). We use points  $m_1$ ,  $m_2$ ,  $m_3$  and  $m_4$  to mark the origins of different branches of nontrivial responses. We note that those two branches which originate from  $m_1$ and  $m_3$  correspond to the unstable responses, while those branches which originate from points  $m_2$  and  $m_4$  represent the stable responses.

In both of the superharmonic resonant cases, this parameter has a very interesting influence on the response curves. When the frequency  $\Omega$  is near to  $(\frac{1}{2})$ , the amplitude of the homogeneous solution depends upon the length ratio and the mass ratio. Equation (4.107) shows that the amplitude of the homogeneous solution is a linear function of the mass ratio. Figure 4.11 shows the effect of S on the amplitude of the non-zero homogeneous solution for the superharmonic resonance ( $\Omega \approx \frac{1}{2}$ ). The overall amplitude of this superharmonic

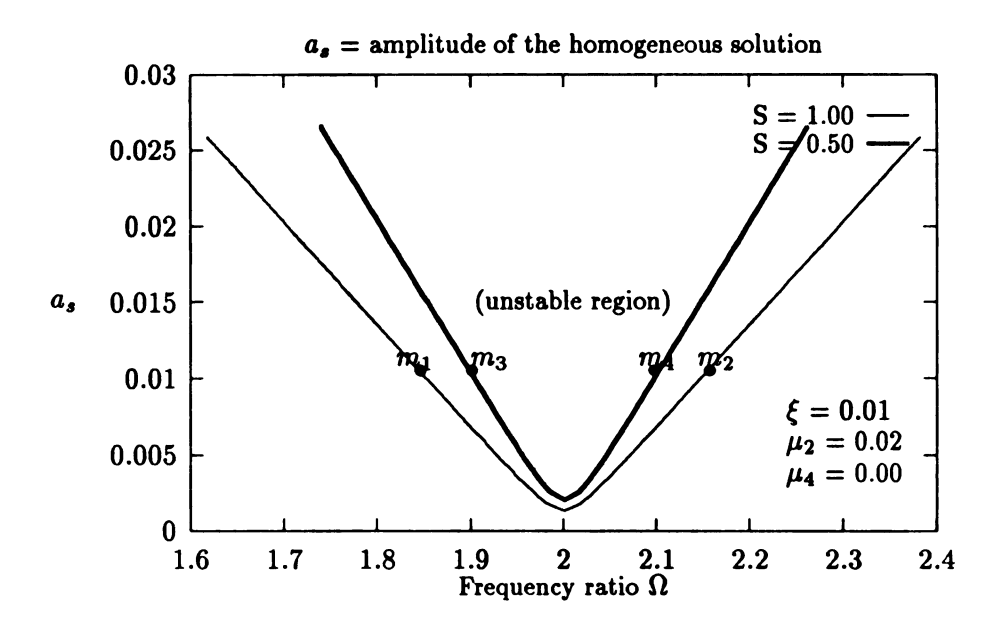


Figure 4.9: Influence of S on the main nose of instability

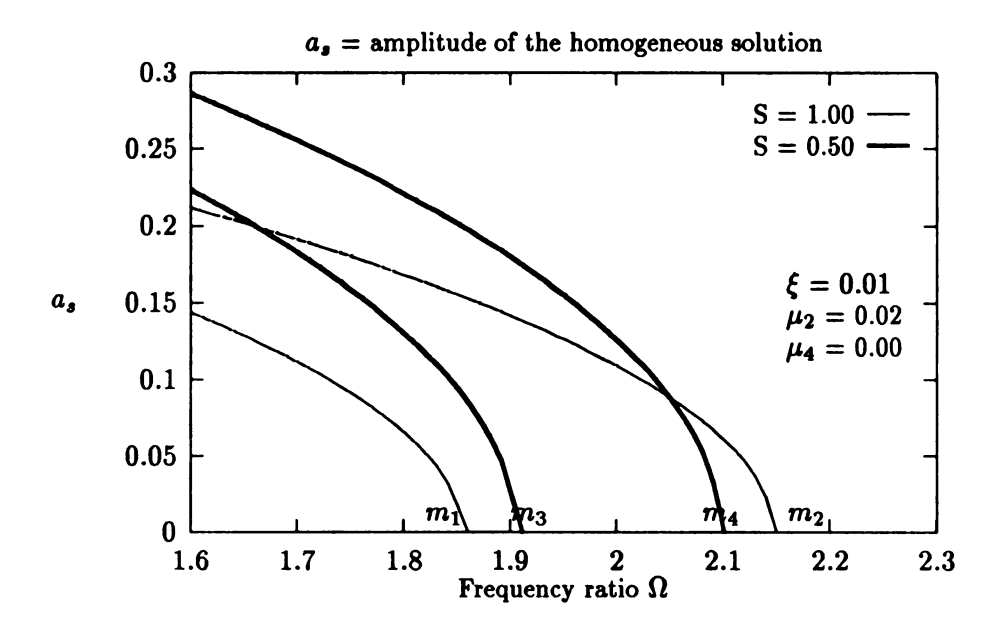


Figure 4.10: Influence of S on the principal parametric resonance

response first decreases as the mass ratio increases from 0 to a critical value which is about 0.11, while this amplitude will increase as the mass ratio increases beyond this critical value. We note that the existence of this resonance is independent of the mass ratio. Hence, it is possible to suppress the contribution of this resonance by choosing the mass ratio properly, i.e., near 0.11. The mass ratio has the same effect on the other superharmonic resonance,

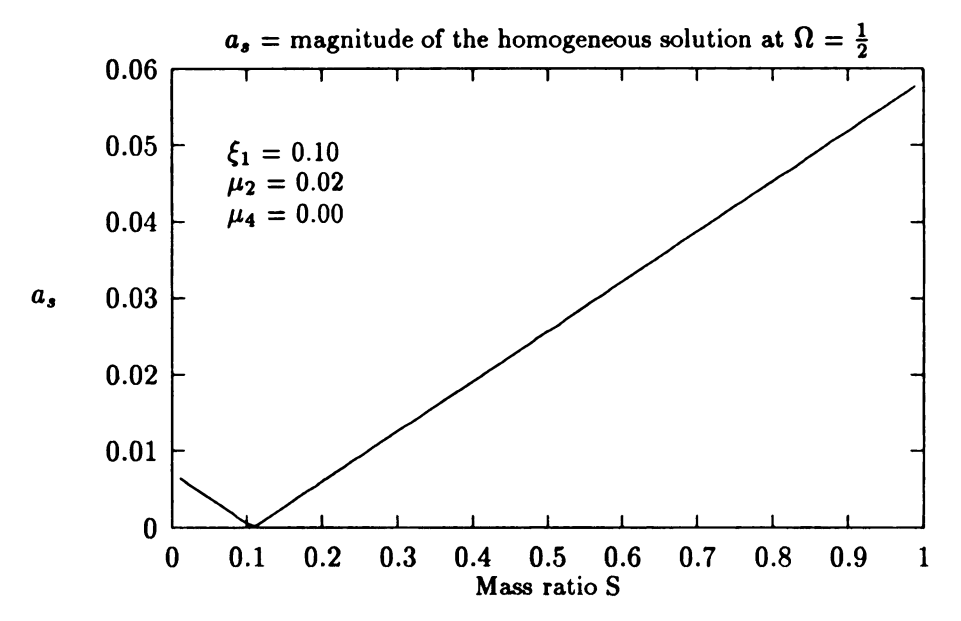


Figure 4.11: Influence of S on superharmonic resonance  $(\Omega \approx \frac{1}{2})$ 

i.e, when  $\Omega$  is near to  $(\frac{1}{3})$ . Figure 4.12 shows the effect of S on the superharmonic resonance in which  $\Omega \approx \frac{1}{3}$ . From this figure, we can observe the trace of the peak amplitude  $a_p$  associated with this superharmonic resonance. From this it is seen that a proper choice of the mass ratio will help us in reducing the amplitude of this resonance. A simple calculation of the roots of coefficient  $f_{8_1}$  show that the optimal value of S is about 1.44. Therefore, for this superharmonic resonance, we can diminish the contribution of the free oscillation term by letting S be near to 1.44.

### 4.8.4 Effect of the Damping Parameters $\mu_2$ and $\mu_4$

The internal material damping parameter  $\mu_2$  has favorable effect on the response of the

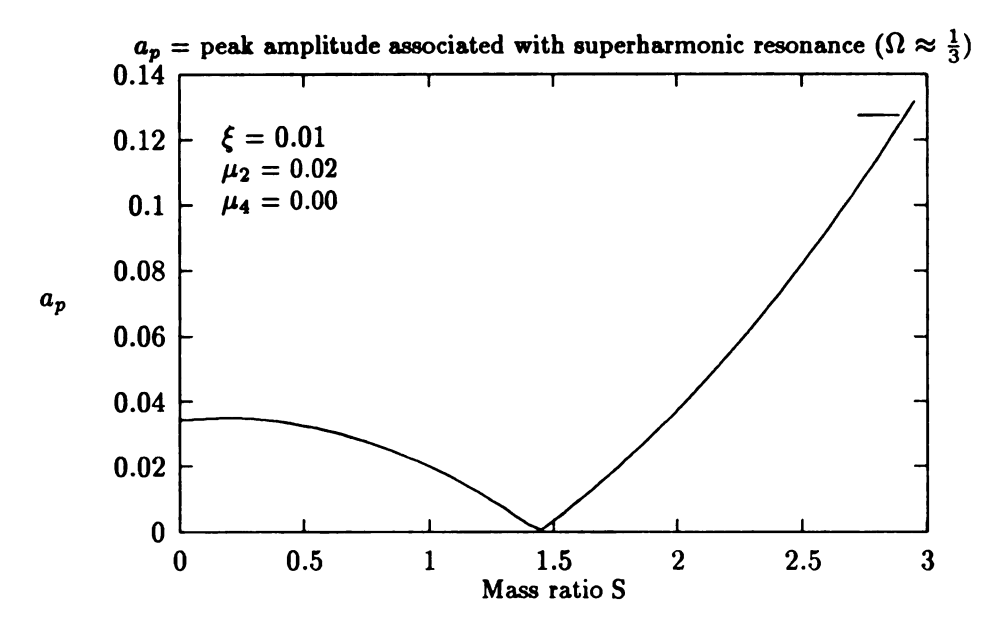


Figure 4.12: Influence of S on superharmonic resonance  $(\Omega \approx \frac{1}{3})$ 

system. For the region in which the linear approximation is valid, the amplitude of the particular solution decreases as  $\mu_2$  increases (equation [4.25]). As shown by the analysis, the peak amplitude associated with the primary resonance can be predicted by the linear approximation. Hence,  $\mu_2$  is expected to have the same effect on the primary resonance. Figure 4.13 shows the effect of  $\mu_2$  on the the primary resonance. From this figure, it is very clear that the amplitude of the primary resonance decreases as  $\mu_2$  increases. Moreover, the shift of the frequency associated with the primary resonance also decreases as  $\mu_2$  increases.

In the principal parametric resonance, this damping parameter decreases the region of the instability by lifting it from the  $\Omega$ -axis and narrowing its boundaries in the  $\xi\Omega$ - plane. Figure 4.14 shows the effect of  $\mu_2$  on the region in which the trivial response becomes unstable. From this figure, it is very clear that the main nose of instability associated with the principal parametric resonance shrinks as  $\mu_2$  increases. Figure 4.15 shows the effect of  $\mu_2$  on the branches of the nontrivial responses associated with the parametric resonance. Note that we use  $m_1$ ,  $m_2$ ,  $m_5$  and  $m_6$  to mark the origins of the nontrivial solutions. Those

branches originating from points  $m_1$  and  $m_5$  correspond to the unstable responses, while branches originating from points  $m_2$  and  $m_6$  represents the stable responses.

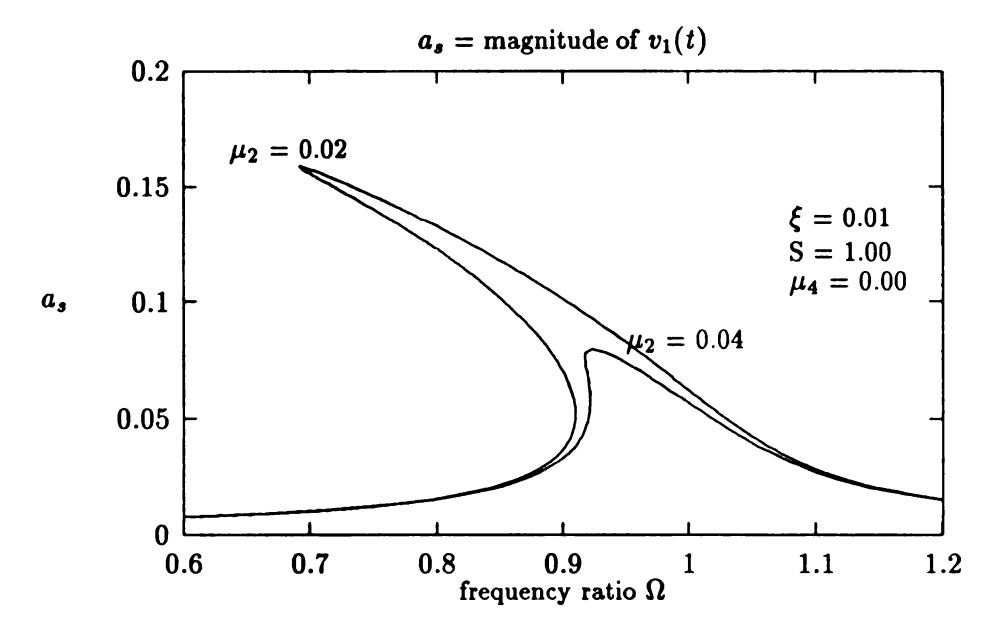


Figure 4.13: Influence of  $\mu_2$  on the primary resonance (equation [4.92])

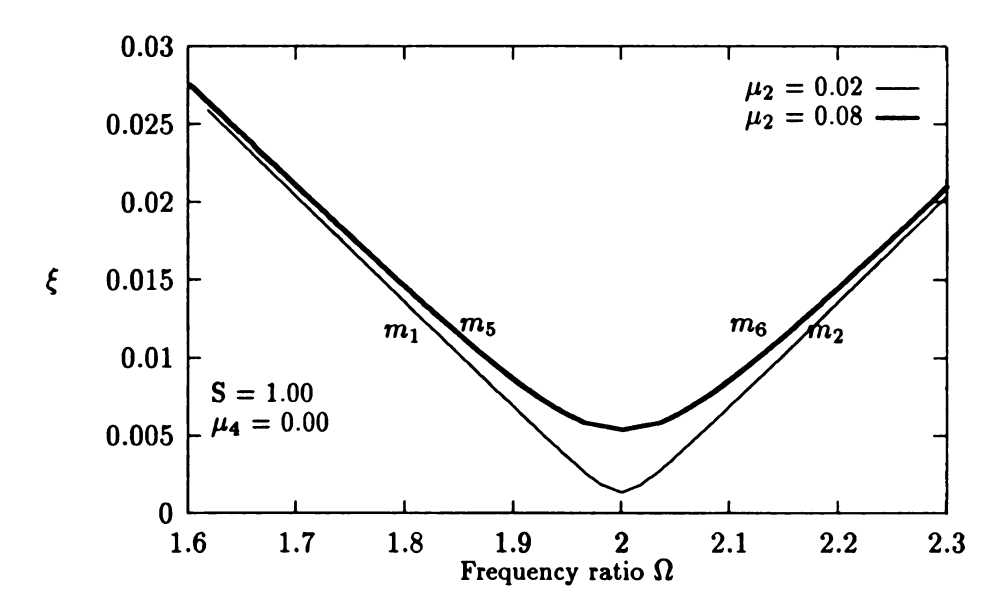


Figure 4.14: Influence of  $\mu_2$  on the main nose of instability

In deriving the equation of motion, we assumed that the bearing damping is very small compared to the transverse displacement. Based on this assumption, the bearing damping  $\mu_3$  is assumed to be of order  $O(\xi^2)$ . The analyses in previous sections show that this damping

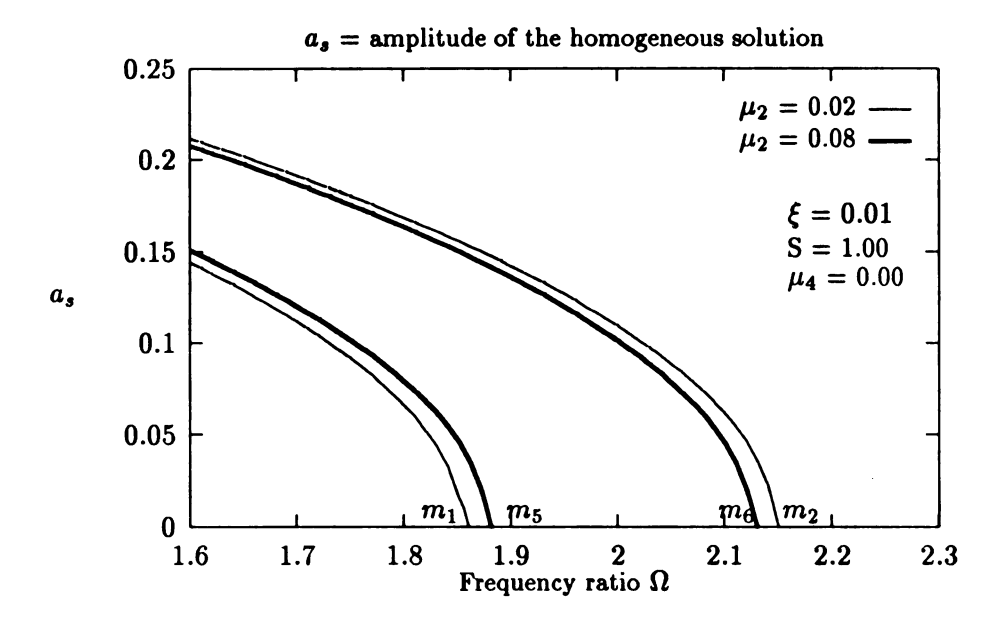


Figure 4.15: Influence of  $\mu_2$  on the principal parametric resonance

parameter has no influence on the response within the frequency region under investigation. This does not imply that  $\mu_3$  can be ignored. If we extend the path of this work, it will be very clear that this parameter can have influence on the higher-order (n > 3) superharmonic resonances.

The effect of the damping parameter  $\mu_4$ , which is used to model the friction between the slider mass and its contact surface, is complicated. This slider friction force is made up of two parts. The first part arises from the action of rigid body motion, while the second one is caused by foreshortening. The friction force introduced by rigid body motion can be treated as linear and has an adverse effect on the response. The slider friction introduced by foreshortening is nonlinear and has a favorable effect on the response of the system. When the response amplitude is small, the foreshortening introduced is small. In this case, the slider friction is mainly composed of friction introduced by rigid body motion. Hence, an increase of the value of  $\mu_4$  will be accompanied with an increase of the slider friction force. This corresponds to an increase of the axial force acting on the connecting rod and

hence an increase of the amplitude of the response. However, as the amplitude of the response increases, the friction force introduced by the elastic deformation increases also. This friction force acts as a resistance to prevent the connecting rod from further elastic deformation. Hence, the friction introduced by foreshortening has a favorable effect on the response of the system. Based on these observations, we now proceed to consider the effect of  $\mu_4$  in each individual resonance case.

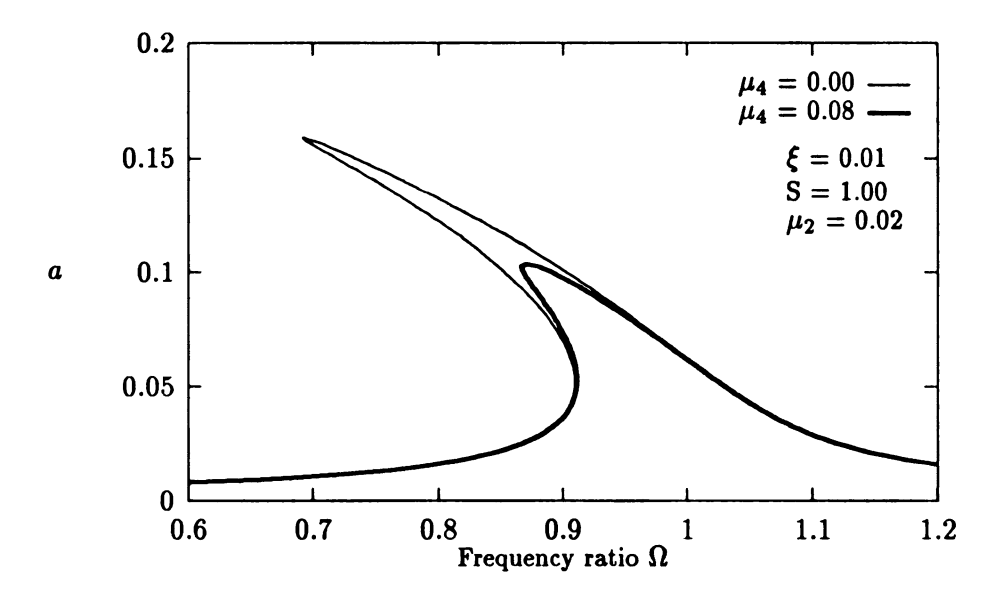


Figure 4.16: Influence of  $\mu_4$  on the primary resonance  $(\Omega \approx 1)$ 

In the cases of primary resonance ( $\Omega \approx 1$ ), third order superharmonic ( $\Omega \approx \frac{1}{3}$ ) and subharmonic ( $\Omega \approx 3$ ) resonances,  $\mu_4$  has a favorable effect. Figure 4.16 shows the effect of  $\mu_4$  on the primary resonance. As shown in this figure, it is very clear that  $\mu_4$  has a favorable effect on the response by reducing the amplitude of the response. In the superharmonic resonance, we can not reduce the amplitude of the free oscillation term to zero because of its existence. Figure 4.17 shows the effect of  $\mu_4$  on the superharmonic resonance in which  $\Omega \approx \frac{1}{2}$ . From this figure, it is very clear that the presence of  $\mu_4$  will increase the amplitude of the non-zero homogeneous solution and hence has an adverse effect. Figures 4.18 and 4.19

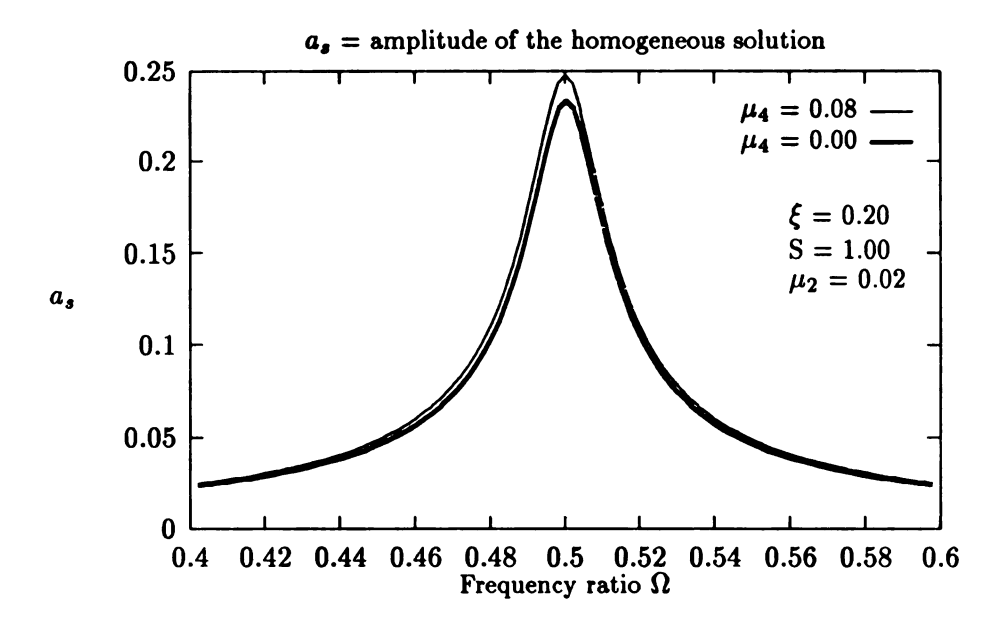


Figure 4.17: Influence of  $\mu_4$  on superharmonic resonance  $(\Omega \approx \frac{1}{2})$ 

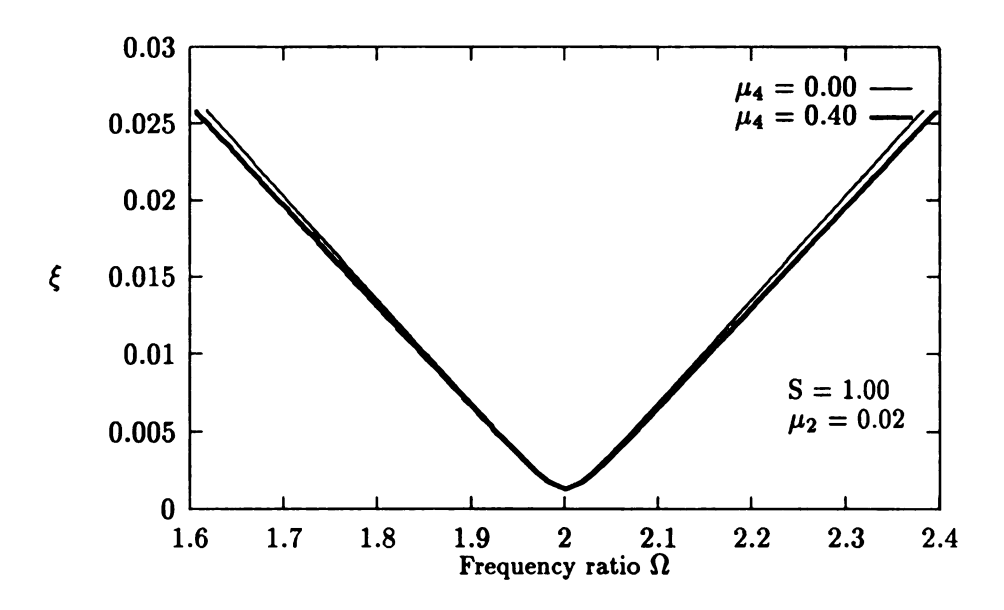


Figure 4.18: Influence of  $\mu_4$  on the main nose of instability  $(\Omega \approx 2)$ 

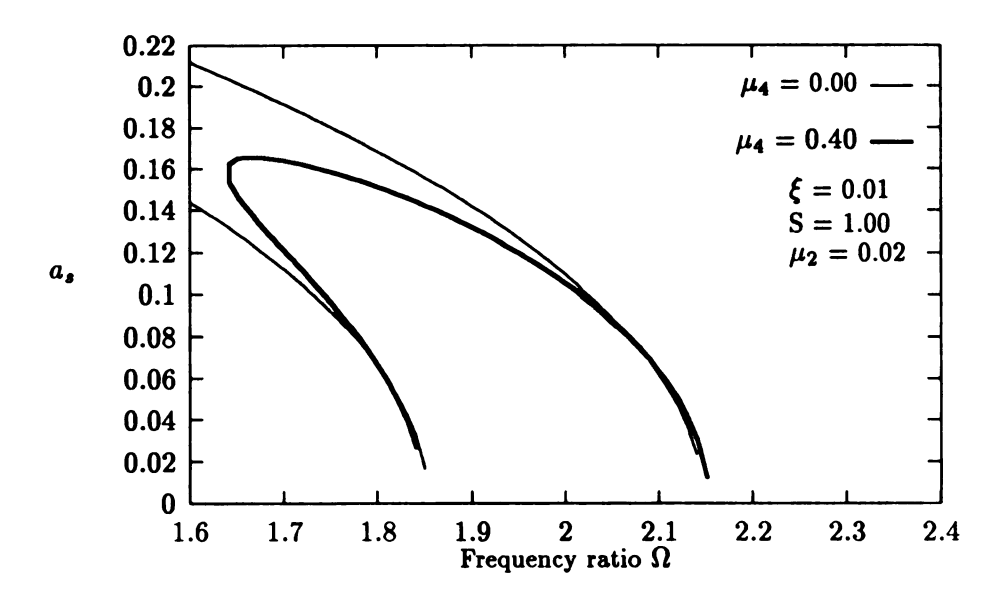


Figure 4.19: Influence of  $\mu_4$  on the principal parametric resonance  $(\Omega \approx 2)$ 

show the effect of  $\mu_4$  on the the principal parametric resonance. From Figure 4.18, we note that the distance between the transition curves increases as  $\mu_4$  increases. In other words, the presence of this damping parameter will increase the possibility for the existence of the nontrivial response and hence has an adverse effect. However, Figure 4.18 only reveals the effect of the friction force introduced by the rigid body motion. Hence, we conclude that  $\mu_4$  has an adverse effect of the principal parametric resonance by increasing the width of the main nose of instability associated with the principal parametric resonance. We now consider Figure 4.19 which shows the effect of  $\mu_4$  on the principal parametric resonance. From this figure, it is very clear that  $\mu_4$  has a favorable effect regarding response amplitudes. This implies that the friction force introduced by the elastic deformation can help in reducing the amplitude of the response.

# Chapter 5

# Comparisons between Distributed and Lumped

## **Parameter Models**

In the present chapter, we compare the analytical results obtained by using the distributed and lumped parameter models. Instead of examining the effects of each parameter on the overall response of the flexural vibration, this comparison proceeds by considering the resultant equations describing the resonance conditions. In order to make this comparison, the analytical results obtained in chapter 3 need to be modified. Since the effects of shear deformation and rotary inertia are not included in deriving equation (4.21), we delete these two effects by setting  $\alpha_2 = \alpha_3 = 0$  from the results obtained in chapter 3. Moreover, we substitute the value of n = 1 into the results from chapter 3, because only the first normal mode was used to convert equation (4.20) into a discrete system. After these modifications have been completed, we first consider the primary resonance case, and then the principal parametric resonance. After these resonances, we compare the results for the superharmonic resonances, and then the subharmonic resonance. We close this chapter by providing some summary points in the final section.

## 5.1 Primary Resonance $(\Omega \approx 1)$

In this section, we consider the case in which the operating frequency is near to the first

flexural natural frequency. We first consider the linear results obtained in sections 3.3 and 4.4. By letting n = 1 in equations (3.88) and (3.89)

$$a' = -\mu_{2_1} a - \frac{\xi_2}{\pi} \cos \Phi_1 , \qquad (5.1)$$

$$a\Phi_1' = \sigma_1 a + \frac{\xi_2}{\pi} \sin \Phi_1 \tag{5.2}$$

which are exactly the same as equations (4.75) and (4.76) in section 4.4. This implies that the continuous and discrete approaches will give us exactly the same result. Next, we consider the nonlinear results. After the effects of shear deformation, rotary inertia and bearing damping have been removed, we obtain the following equations:

$$a' = -\mu_{22}a - (\frac{\mu_{40}}{8})\pi^4 a^3 - \frac{\xi_3}{\pi}\cos\Phi_2, \qquad (5.3)$$

$$a\Phi_2' = \sigma_2 a + \Delta_2' a^3 + \frac{\xi_3}{\pi} \sin \Phi_2$$
 (5.4)

where

$$\Delta_2' = \left(\frac{\pi^2}{3} + \pi^2 S - \frac{15}{8}\right) \frac{\pi^2}{8} \tag{5.5}$$

from equations (3.112) and (3.113) by letting n=1. From the discrete analysis, we obtain

$$a' = -\mu_{2_2} - (\frac{\mu_{4_0}}{8})\pi^4 a^3 - \frac{\xi_3}{\pi} \cos \Phi_2 , \qquad (5.6)$$

$$a\Phi_2' = \sigma_2 a + \Delta_5 a^3 + \frac{\xi_3}{\pi} \sin \Phi_2 ,$$
 (5.7)

where

$$\Delta_5 = \frac{\pi^4}{8} S \tag{5.8}$$

in describing the resonance condition when  $\Omega \approx 1$ , which is repeated for convenience.

Basically, these two sets of equations are of the same form. The equations describing the variation of the amplitude function a are exactly the same. The only difference between these two sets of equations is the strength of nonlinear terms,  $\Delta'_2$  and  $\Delta_5$ , appearing in the equations describing the variation of the phase angle. As we compare the values of  $\Delta'_2$  and  $\Delta_5$ , we find that the difference between them is strongly dependent on the mass ratio S. Moreover, the distributed parameter approach will provide a slightly stronger nonlinearity than the lumped parameter one.

### 5.2 Principal Parametric Resonance ( $\Omega \approx 2$ )

In this section, we consider the principal parametric resonance. We first compare the linear results obtained in the first parts of section 3.2 and 4.3. After we set n = 1 and delete the effects of shear deformation, rotary inertia and bearing damping, we obtain the following equations:

$$a' = -\mu_{2_1}a - 2a\xi_1\Delta_1'\sin(2\Phi_1) + a\pi^2\mu_{4_0}\xi_1\cos(2\Phi_1), \qquad (5.9)$$

$$a\Phi_1' = \sigma_1 a - 2a\xi_1 \Delta_1' \cos(2\Phi_1) - a\pi^2 \xi_1 \mu_{4_0} \sin(2\Phi_1),$$
 (5.10)

where

$$\Delta_1' = (1 + 2S) \frac{\pi^2}{4} \tag{5.11}$$

from equations (3.53) and (3.54). From the discrete approach, we obtained

$$a' = -\mu_{2_1}a - 2a\xi_1\Delta_4\sin 2\Phi_1 + a\pi^2\mu_{4_0}\xi_1\cos(2\Phi_1), \qquad (5.12)$$

$$a\Phi_1' = \sigma_1 a - 2a\xi_1 \Delta_4 \cos 2\Phi_1 - a\pi^2 \mu_{4_0} \xi_1 \sin (2\Phi_1),$$
 (5.13)

where

$$\Delta_4 = (1+2S)\frac{\pi^2}{4} \ . \tag{5.14}$$

When we compare these two sets of equations, it is interesting to find that they are exactly the same. This implies that these two approaches will lead to the same linear results. In consequence, the main nose of instability for the principal parametric resonance will be the same. Next, we compare the nonlinear results obtained from the second part of sections 3.2 and 4.3. We obtain the following equations:

$$a' = -\mu_{2_2}a - (\frac{\mu_{4_0}}{8})\pi^4a^3 - 2a\xi_2\Delta_1'\sin(2\Phi_2) + a\mu_{4_0}\xi_2\pi^2\cos(2\Phi_2), \qquad (5.15)$$

$$a\Phi_2' = \sigma_2 a + \Delta_2' a^3 - 2a\Delta_1' \xi_2 \cos(2\Phi_2) - a\mu_{40} \xi_2 \pi^2 \sin(2\Phi_2)$$
 (5.16)

from equations (3.84) and (3.84) by letting n = 1,  $\alpha_2 = \alpha_3 = 0$  and deleting the effect of bearing damping,  $\mu_{3_2} = 0$ . From the discrete analysis, we obtained the following equations:

$$a' = -\mu_{2_2}a - (\frac{\mu_{4_0}}{8})\pi^4a^3 - 2a\xi_2\Delta_4\sin(2\Phi_2) + \xi_2\pi^2\mu_{4_0}a\cos(2\Phi_2), \qquad (5.17)$$

$$a\Phi_2' = \sigma_2 a + \Delta_5 a^3 - 2a\xi_2 \Delta_4 \cos(2\Phi_2) - \xi_2 \pi^2 \mu_{4_0} a \sin(2\Phi_2). \qquad (5.18)$$

We find that the equations describing the variation of the amplitude function are exactly the same. The difference between these two approaches is the strength of the nonlinearities  $(\Delta'_2 \text{ and } \Delta_5)$  appearing in the equations describing the variation of the phase angle. From these, we recognize that the distributed parameter and the lumped parameter models will provide the same result in determining the main nose of instability. Since the effects of the nonlinearities are again described by the parameters,  $\Delta'_2$  and  $\Delta_5$ , we obtain the same conclusion as that obtained in the last section. Briefly, the effect of nonlinearity is very

sensitive to the mass ratio, and the distributed parameter approach will provide a stronger nonlinearity than the lumped parameter one.

# 5.3 Superharmonic Resonance $(\Omega \approx \frac{1}{2})$

In this section, we consider the superharmonic resonance in which the operating angular speed is near to one half of the first flexural natural frequency. After we delete the effects of shear deformation, rotary inertia and the bearing damping, we obtain the following equations:

$$a' = -\mu_{2_1} a + \frac{\mu_{4_0} \xi_1^2}{6} \sin \Phi_1 - \frac{\xi_1^2}{12\pi} (3 - \Delta_1') \cos \Phi_1 , \qquad (5.19)$$

$$a\Phi_1' = \sigma_1 a + \frac{\mu_{4_0}\xi_1^2}{6}\cos\Phi_1 + \frac{\xi_1^2}{12\pi}(3-\Delta_1')\sin\Phi_1$$
 (5.20)

from equation (3.119) and (3.119) in section 3.4, where  $\Delta'_1$  is given in equation (5.11). From the lumped parameter model, we obtain

$$a' = -\mu_{2_1} a + \frac{\mu_{4_0} \xi_1^2}{6} \sin \Phi_1 - \frac{\xi_1^2}{12\pi} (3 - \Delta_4) \cos \Phi_1 ,$$
 (5.21)

$$a\Phi_1' = \sigma_1 a + \frac{\mu_{4_0} \xi_1^2}{6} \cos \Phi_1 + \frac{\xi_1^2}{12\pi} (3 - \Delta_4) \sin \Phi_1$$
 (5.22)

from equations (4.103) and (4.104), where  $\Delta_4$  is given in equation (4.42). As we compare these two sets of equations, we see that  $\Delta_4 = \Delta_1'$  and thus they are identical.

# 5.4 Superharmonic Resonance $(\Omega \approx \frac{1}{3})$

In this section, we consider the superharmonic resonance in which the the operating angular speed is near to one third of the first natural flexural frequency associated with the

connecting rod. We first compare the results obtained in sections 3.5 and 4.6. After we delete the effects of shear deformation, rotary inertia and bearing damping, we obtain the following equations:

$$a' = -\mu_{22}a - (\frac{\mu_{40}}{8})a^3\pi^4 - (\frac{\mu_{40}}{64})\xi_1^2\pi^2a - (\frac{\pi}{1536})\xi_1^3\mu_{40}\sin\Phi_2 + f_{21}'\xi_1^3\cos\Phi_2, (5.23)$$

$$a\Phi_2' = \sigma_2 a + \frac{f_{11}'}{2} a\xi_1^2 + \Delta_2' a^3 + (\frac{\pi}{1536})\xi_1^3 \mu_{40} \cos \Phi_2 - f_{21}'\xi_1^3 \sin \Phi_2$$
 (5.24)

where

$$f'_{1_1} = -\frac{251}{2304} + \frac{11\pi^2}{1728} + \frac{5}{144}\Delta'_1 - \frac{\Delta'_1^2}{63},$$
 (5.25)

$$f_{2_1}' = \frac{1559}{36864\pi} + \frac{17\pi}{27648} + \frac{91\Delta_1'}{11520\pi} - \frac{\Delta_1'^2}{360\pi}$$
 (5.26)

from equations (3.128) and (3.129). From the lumped parameter analysis, we obtained

$$a' = -\mu_{2_2}a - (\frac{\mu_{4_0}}{8})a^3\pi^4 - (\frac{\mu_{4_0}}{64})\xi_1^2\pi^2a - (\frac{\pi}{1536})\xi_1^3\mu_{4_0}\sin\Phi_2 + f_{8_1}\xi_1^3\cos\Phi_2, (5.27)$$

$$a\Phi_2' = \sigma_2a + \frac{f_{7_1}}{2}\xi_1^2a + \Delta_5a^3 + (\frac{\pi}{1536})\xi_1^3\mu_{4_0}\cos\Phi_2 - f_{8_1}\xi_1^3\sin\Phi_2$$

$$(5.28)$$

from equations (4.111) and (4.112), where

$$f_{7_1} = -\frac{17}{72} - \frac{\pi^4}{1008} + \frac{\pi^2 S}{32} - \frac{\pi^4 S}{252} - \frac{\pi^4 S^2}{252}$$

$$= -\frac{17}{72} - \frac{3}{64} \pi^2 + \frac{3}{16} \Delta_4 - \frac{\Delta_4^2}{63} , \qquad (5.29)$$

$$f_{8_1} = -\frac{5}{64\pi} + \frac{17\pi}{2160} - \frac{\pi^3}{5760} + \frac{461\pi S}{23040} - \frac{\pi^3 S}{1440} - \frac{\pi^3 S^2}{1440}$$

$$= -\frac{5}{64\pi} - \frac{59\pi}{27648} + \frac{461\Delta_4}{11520\pi} - \frac{\Delta_4^2}{360\pi} . \qquad (5.30)$$

For this superharmonic resonance, the results obtained from two approaches agree with each

other in a qualitative sense. However, the numerical values of each coefficient are different. Generally speaking, the magnitude of coefficient  $f_{8_1}$  is less than the magnitude of  $f'_{2_1}$  for 0.40 < S < 1.00. Otherwise, the magnitude of  $f_{2_1}$  is larger than that of  $f_{8_1}$ . This implies that the lumped parameter model predicts a larger response amplitude than the distributed parameter model for 0.4 < S < 1.0, while the lumped parameter model predicts a smaller response amplitude for either S > 1.0 or 0 < S < 0.4.

## 5.5 Subharmonic Resonance ( $\Omega \approx 3$ )

In this section, we consider the subharmonic resonance in which the frequency ratio is near to three times of the first natural flexural frequency associated with the connecting rod. After we neglect the effects of shear deformation, rotary inertia and bearing damping, we obtain the following equations:

$$a' = -\mu_{2_2} a - (\frac{\mu_{4_0}}{8}) \pi^4 a^3 - (\frac{81}{64}) \xi_1^2 \pi^2 \mu_{4_0} a$$

$$+ (\frac{9}{32}) \xi_1 \mu_{4_0} a^2 \sin(3\Phi_2) + \frac{f_{3_1}' \xi_1}{4} a^2 \cos(3\Phi_2) , \qquad (5.31)$$

$$a\Phi_2' = \sigma_2 a + \Delta_2' a^3 + \frac{f_{12}'}{2} \xi_1^2 a + (\frac{9}{32}) \xi_1 \mu_{40} a^2 \cos(3\Phi_2) - \frac{\xi_1}{4} f_{31}' a^2 \sin(3\Phi_2) \quad (5.32)$$

where

$$f_{12}' = -\frac{4761}{256} + \frac{201}{64}\pi^2 + \frac{117}{16}\Delta_1' - \frac{27}{5}\Delta_1'^2, \qquad (5.33)$$

$$f_{3_1}' = -\frac{45}{64}\pi + \frac{9}{8}\pi^3 + \frac{27}{8}\pi^3 S + \frac{3\Delta_1'}{8\pi}$$
 (5.34)

from equations (3.142) and (3.143) in section (3.6). While, for the lumped parameter model,

we obtain the following equations:

$$a' = -\mu_{2_2} a - (\frac{\mu_{4_0}}{8}) \pi^4 a^3 - (\frac{81}{64}) \xi_1^2 \pi^2 \mu_{4_0} a$$

$$+ (\frac{9}{32}) \xi_1 \mu_{4_0} a^2 \sin(3\Phi_2) + \frac{3}{2} \xi_1 \pi a^2 \cos 3\Phi_2 , \qquad (5.35)$$

$$a\Phi_2' = \sigma_2 a + \frac{f_{7_2}}{2} \xi_1^2 a + \Delta_5 a^3 + (\frac{9}{32}) \xi_1 \mu_{4_0} a^2 \cos(3\Phi_2) - \frac{3}{2} \xi_1 \pi a^2 \sin(3\Phi_2) \quad (5.36)$$

from equations (4.124) and (4.125), where

$$f_{7_2} = \frac{387}{8} - \frac{27\pi^4}{80} + \frac{243\pi^2 S}{32} - \frac{27\pi^4 S}{20} - \frac{27\pi^4 S^2}{20}$$
$$= \frac{387}{8} - \frac{243\pi^2}{64} + \frac{243\Delta_4}{16} - \frac{27\Delta_4^2}{5}. \tag{5.37}$$

From the results obtained by these two different approaches, we observe that they give the same qualitative behavior, although the numerical values of the coefficients are different. Generally speaking, the magnitude of coefficient  $f'_{12}$  is less than that of coefficient  $f_{72}$ . The magnitude of coefficient  $f'_{31}$  is larger than 1.5. These implies that the distributed parameter model predicts a larger nontrivial homogeneous solution.

## 5.6 Summary

In this chapter, we compared the results obtained by using two different models in investigating the flexural vibration associated with the flexible connecting rod. Instead of discussing the effects of each parameter on the overall response, we proceeded by considering the resulting equations which describe the resonance conditions. The following conclusions are drawn: (1) these two models provide the same results in the linear part, and (2) the distributed parameter model will provide a stronger nonlinearity than the lumped parameter

model. It can be seen from the value of  $\Delta'_2$  that in the distributed parameter model the mass ratio is not the only source of nonlinearity, and that the geometric nonlinearity (associated with finite deformations) is more significant in the distributed parameter model than in the lumped parameter model.

The absence of the bearing damping parameter  $\mu_3$  in the lumped parameter model is caused by assuming that it is of order  $O(\epsilon^2)$ . Although the same assumed order is applied in the distributed parameter analysis, the effect of this parameter has been recovered from the final equation describing the resonance conditions, since the expansions included term beyond  $O(\epsilon^2)$ . However, because of the nature of the lumped parameter model, the effect of bearing damping was neglected from the very beginning of the analysis, since its presence would require modification of the assumed mode shape employed. Actually, this parameter can be included in the lumped parameter analysis by following the analysis pattern outlined in Appendix A.

### Chapter 6

# **Numerical Solutions and Comparisons**

In the present chapter, we present some numerical simulation studies of equation (4.21). The main purpose is to verify the analytical work with these numerical solutions. In order to take a systematic approach and obtain a clear picture of the results, we identify the various cases considered with the help of a table, Table 6.1. In obtaining the numerical solutions, we use the programs LSODE[22] and AUTO[14]. The former is a numerical solution package for solving initial value problems for ordinary differential equations, and the latter is a software package capable of tracking steady state response curves and, simultaneously providing stability information. AUTO is used to obtain the global picture for the response curves, and LSODE to provide time traces for specific parameter values.

In Figure 6.1 we demonstrate that the general features of the response of the nonlinear lumped paramter model are well predicted by our asymptotic results. This is done by comparing the analytically predicted frequency response curve with that computed by AUTO and with simulations from LSODE at several frequencies for a specific set of parameter values.

In Figure 6.1 we show the frequency response generated by the three methods described above. We note that the agreement is very good, and that the improtant features are captured by the analysis. In particular, the bending of the primary resonance near  $\Omega = 1$ , and the parametric resonance near  $\Omega = 2$  all appear in the simulations and in both response

curves. We now turn to the details of how the individual parameters affect the overall response, and describe the accuracy of the analysis.

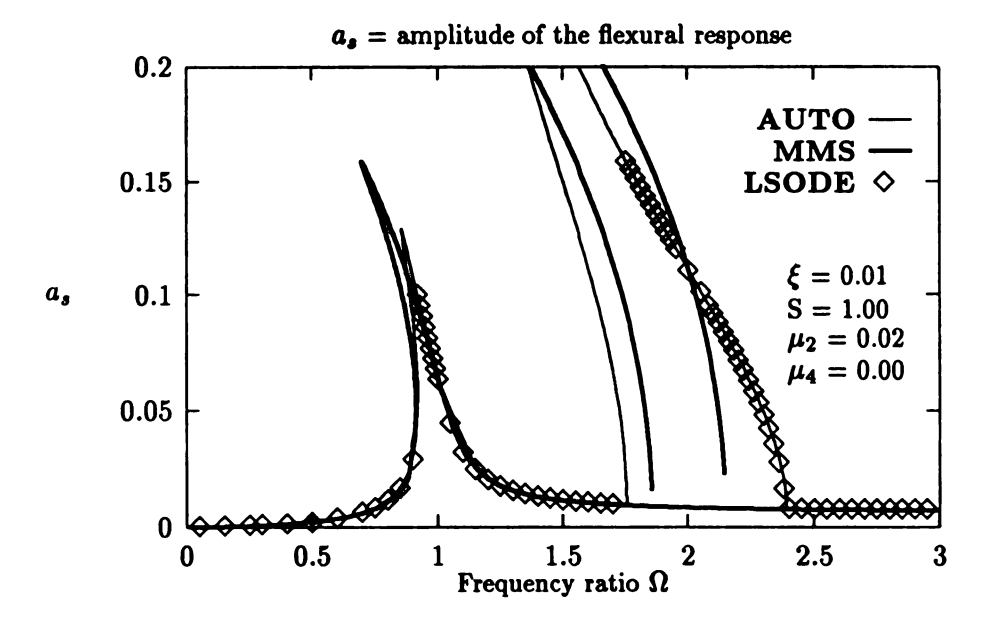


Figure 6.1: Frequency response curves from MMS, LSODE and AUTO

In section 6.1, we consider the effect of the length ratio  $\xi$  on the overall response of equation (4.21). In section 6.2, the effect of the mass ratio on the overall response is considered. We examine the effects of the damping parameters  $\mu_2$ ,  $\mu_3$  and  $\mu_4$  on the overall response in section 6.3. In section 6.4, we summarize the observations to close this chapter.

### 6.1 Influence of the Length Ratio $\xi$

In this section, we consider the the effect of the length ratio  $\xi$  on the overall response of the model given by equation (4.21). It is the purpose of this section to verify the predictions from the nonlinear approximation in chapter 4 with the help of the numerical tools **LSODE** and **AUTO**. We use Table 6.1 to identify the various cases considered for different parameters combinations.

We first compare the frequency response curves obtained in chapter 4 with the results

Case	ξ	S	$\mu_2$	$\mu_3$	$\mu_4$	Case	ξ	S	$\mu_2$	$\mu_3$	$\mu_4$
1	0.005	0.00	0.02	0.00	0.00	2	0.005	0.50	0.02	0.00	0.00
3	0.005	1.00	0.02	0.00	0.00	4	0.010	0.00	0.02	0.00	0.00
5	0.010	0.50	0.02	0.00	0.00	6	0.010	1.00	0.02	0.00	0.00
7	0.050	0.00	0.02	0.00	0.00	8	0.050	0.50	0.02	0.00	0.00
9	0.050	1.00	0.02	0.00	0.00	10	0.100	0.00	0.02	0.00	0.00
11	0.100	0.50	0.02	0.00	0.00	12	0.100	1.00	0.02	0.00	0.00
13	0.010	0.00	0.04	0.00	0.00	14	0.010	0.50	0.04	0.00	0.00
15	0.010	1.00	0.04	0.00	0.00	16	0.050	0.00	0.04	0.00	0.00
17	0.050	0.50	0.04	0.00	0.00	18	0.050	1.00	0.04	0.00	0.00
19	0.010	0.00	0.02	0.00	0.40	20	0.010	0.50	0.02	0.00	0.40
21	0.010	1.00	0.02	0.00	0.40	22	0.050	0.00	0.02	0.00	0.40
23	0.050	0.50	0.02	0.00	0.40	24	0.050	1.00	0.02	0.00	0.40
25	0.010	0.00	0.02	0.08	0.00	26	0.010	0.50	0.02	0.08	0.00
27	0.010	1.00	0.02	0.08	0.00						

Table 6.1: Identification of Combinations of Parameters

from AUTO. After this, we focus our attention on qualitative observations. Figure 6.2 shows the frequency response curves obtained from the analytical work and AUTO for case 5. Figure 6.3 shows the frequency response curves for case 6. From these two figures, it is clear that the nonlinear approximation matches the numerical results quite well when & is small. When the length ratio  $\xi$  is larger than 0.10, the analytical result can provide only qualitative consistency with the numerical results. According to the analytical results, when  $\xi$  is larger than 0.10, the detuning associated with the primary resonance becomes so large that the peak amplitude occurs at negative values of the frequency ratio. This is physically impossible. Based on this observation, we would like to use results from AUTO to carry out a qualitative investigation regarding the effect of the length ratio  $\xi$  on the overall response and verify the analytic predictions. Figure 6.4 shows frequency response curves for S =0.0 with different  $\xi$  values (cases 1, 4 and 7). According to the analytical results, S=0corresponds to a linear oscillator, because S plays the role of nonlinearity in equation (4.21). This implies that there is no nonlinearity associated with equation (4.21), and hence there is no detuning associated with the primary resonance. Moreover, the amplitude of the

response is proportional to  $\xi$ . The main nose of instability does exist, because its existence is independent of the nonlinearity. Both of these two points are verified by Figure 6.4. We note that, in Figure 6.4, the peak amplitude increases from 0.06 to 0.39 when  $\xi$  increases from 0.005 to 0.05.

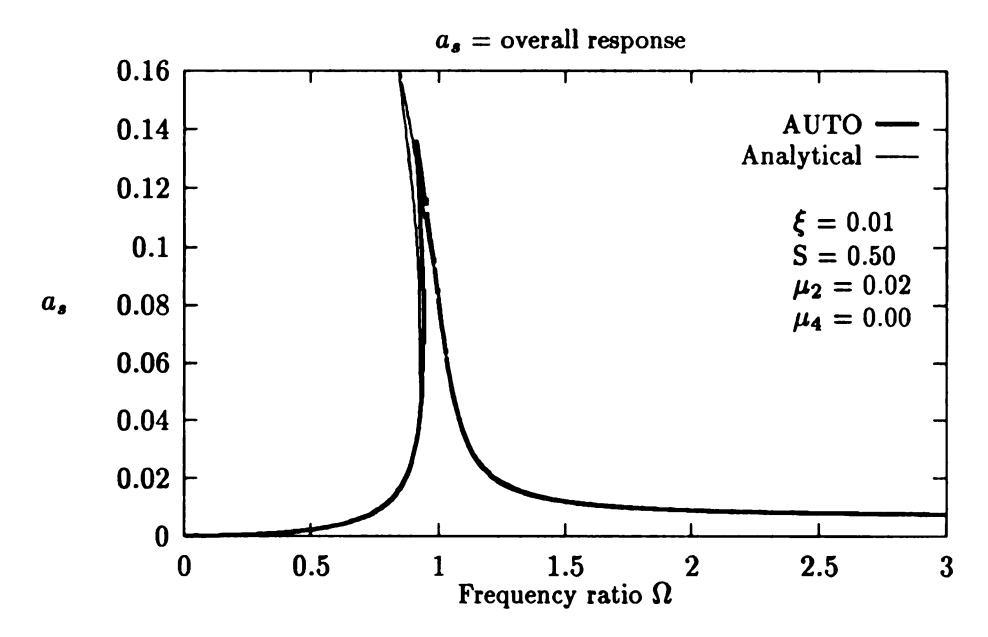


Figure 6.2: Comparison between Analytical result with AUTO (case 5)

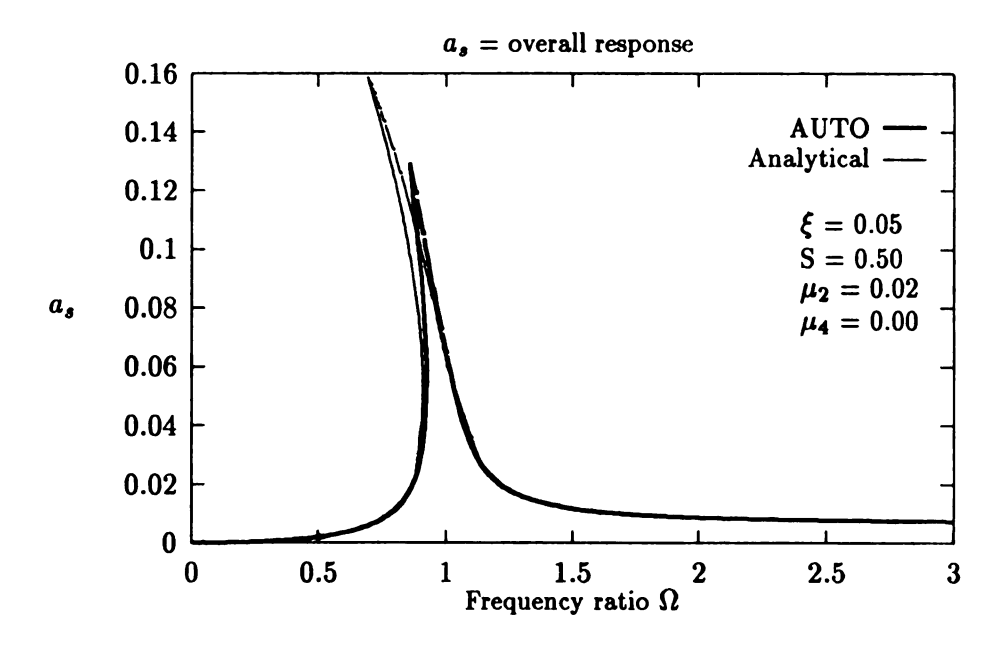


Figure 6.3: Comparison between Analytical result with AUTO (case 6)

Next, we consider cases in which  $S \neq 0$ . According to the analytical predictions, the

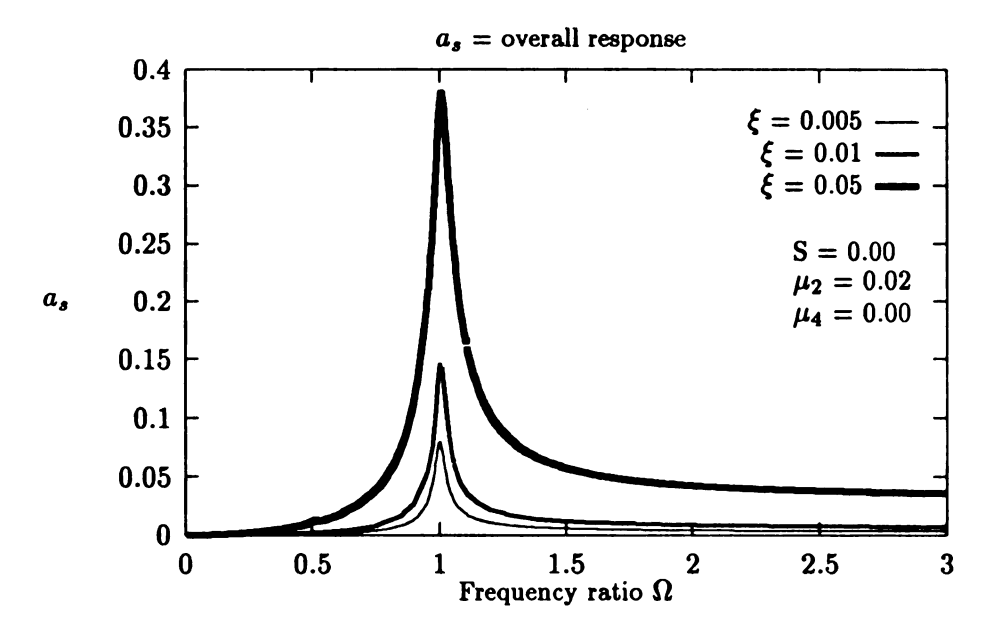


Figure 6.4: Frequency response for cases 1, 4 and 7

cases in which S>0 correspond to systems with a softening type of nonlinearity. Moreover, the strength of nonlinearity depends on the value of S. The peak amplitude of the response shall be the same as that given in the linear approximation, while the detuning associated with the primary resonance  $(\sigma_p)$  is proportional to the square of  $\xi$ . Figure 6.5 shows the numerical results for different  $\xi$  values with S=0.50 (cases 2, 5 and 8), and the results for S=1.00 (cases 3, 6 and 9) are given in Figure 6.6. From these figures, we observe that the analytical work does provide results which are consistent with the numerical solution. It is interesting to note that as  $\xi$  increases, the superharmonic resonance near  $\Omega \approx \frac{1}{2}$  begins to appear in Figures 6.5 and 6.6. This is as predicted by the analysis of section 4.5. When  $\xi$  is smaller than 0.10, the analytical approximation provides very good results. When  $\xi$  is larger than 0.10, the analytical prediction again provides only qualitative information. Table 6.1 contains bifurcation information obtained from analytical results and AUTO. In this table, we use  $PD_1$  and  $PD_2$  to mark the points at which principal parametric resonance instabilities occur, while we mark the turning point associated with the primary resonance

by  $LP_1$  and  $LP_2$ . In other words, the region between points  $PD_1$  and  $PD_2$  represents the main nose of instability, and the response curve between points  $LP_1$  and  $LP_2$  represents the unstable response near the nonlinear primary resonance. The readers should refer to Figure 6.7 for the locations of these points. For the sake of clearness in the figures, the branches of the nontrivial response associated with the parametric resonance are generally not included. However, the bifurcation points listed in table 6.1 are sufficient to provide the important information. From Table 6.1, we draw the following conclusions. When the length ratio  $\xi$  increases, (1) the detuning associated with the primary resonance (the shift of point  $LP_2$ ) increases, and (2) the width of the main nose of instability (the distance between points  $PD_1$  and  $PD_2$ ) increases, and (3) the superharmonic resonance near  $\frac{1}{2}$ appears. We note that, when the length ratio  $\xi$  is larger than 0.10, the analytical results predict a considerable detuning associated with the primary resonance and the value of  $LP_1$ becomes negative. Since the Method of Multiple Scales can only provide local analysis, this prediction becomes unreliable. Based on this fact, the bifurcation points for large  $\xi$  values are not provided. As a matter of fact, AUTO also fails to provide the overall response curve when  $\xi$  is larger than 0.10. We note that, in some cases, there may exist no limit points  $LP_1$  and  $LP_2$  associated with the frequency response curves either from the analytical approximations or from AUTO. This will be explained in section 6.2.

Figures 6.8 to 6.11 show comparisons between analytical approximations and simulation results for time traces at the  $\Omega = \frac{1}{2}$  superharmonic resonance. From these figures, it is very clear that the analytical approximations match the simulation results quite well.

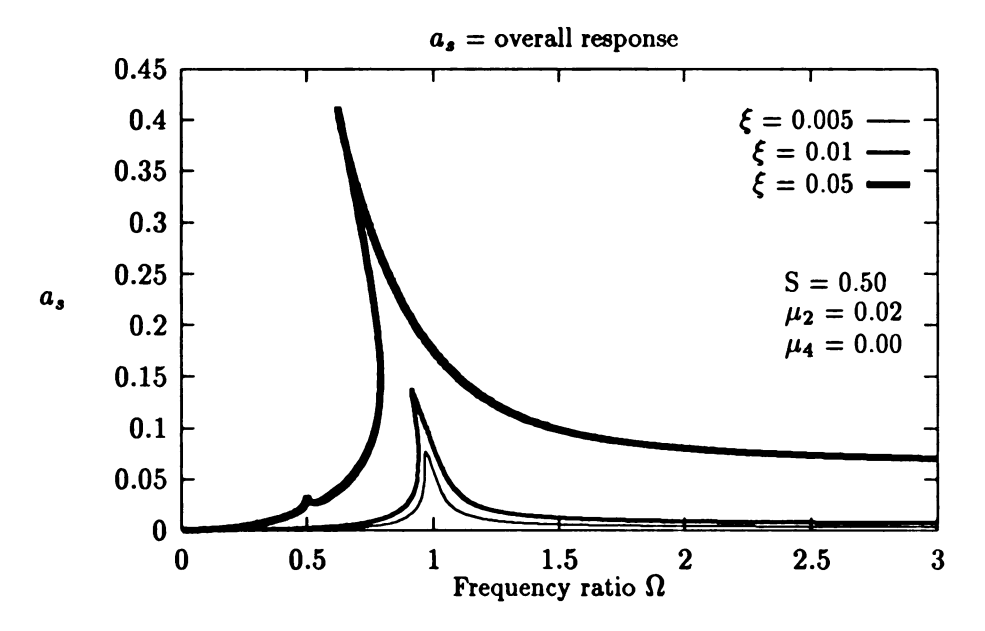


Figure 6.5: Frequency response for cases 2, 5 and 8

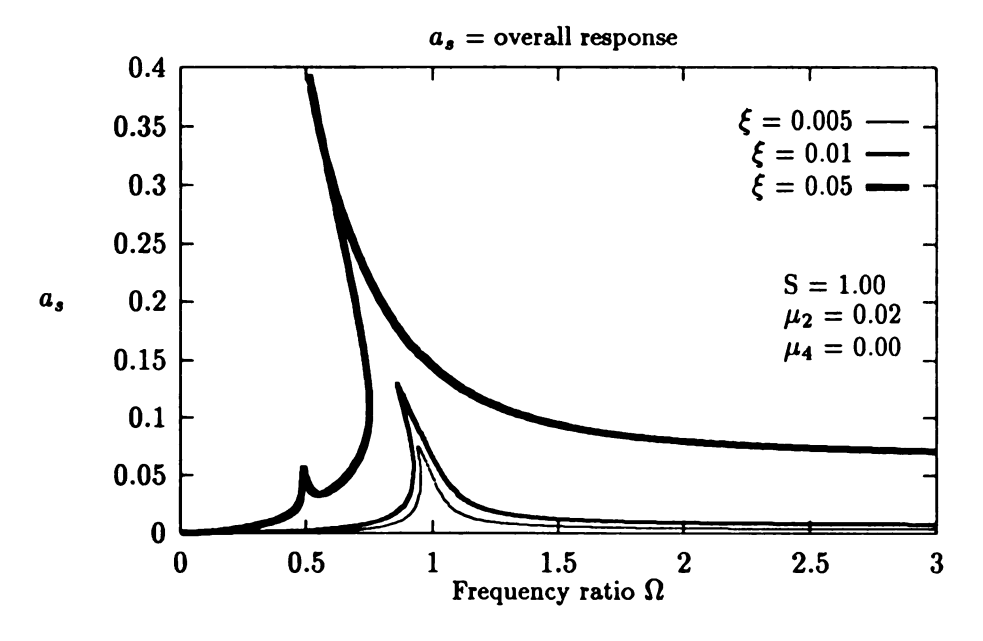


Figure 6.6: Frequency response for cases 3, 6 and 9

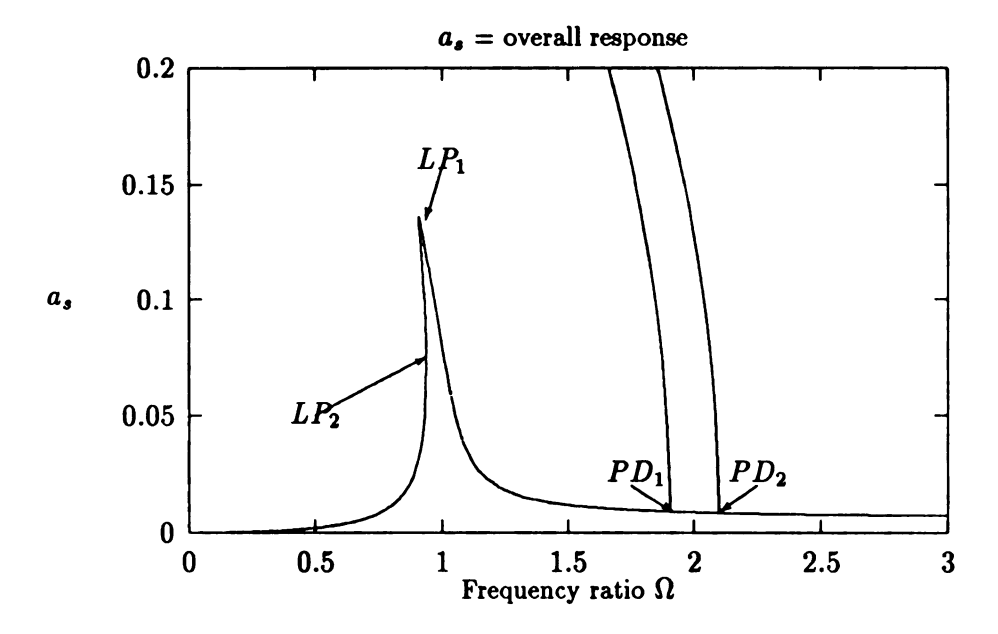


Figure 6.7: Location of points  $PD_1$ ,  $PD_2$ ,  $LP_1$  and  $LP_2$ 

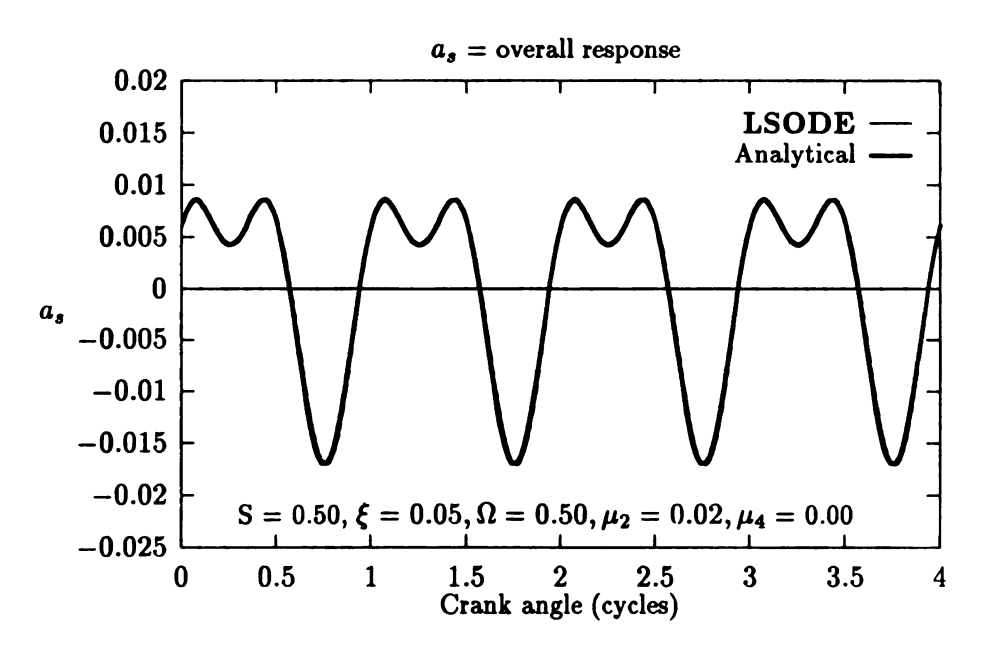


Figure 6.8: Comparison between simulation and analytical approximation for case 8

Case	Anal	ytical	AUTO			
1	$PD_1=1.9855$	$PD_2=2.0145$	$PD_1 = 1.9700$	$PD_2 = 2.0330$		
2	$LP_1 = 0.9711$	$LP_2=0.999$	$LP_1 = -$	$LP_2 = -$		
	$PD_1=1.9549$	$PD_2=2.0451$	$PD_1=1.9131$	$PD_2=2.1013$		
3	$LP_1=0.9270$	$LP_2=0.9643$	$LP_1=0.9505$	$LP_2=0.9390$		
	$PD_1=1.9287$	$PD_2=2.0713$	$PD_1=1.8680$	$PD_2 = 2.1670$		
4	$PD_1 = 1.9549$	$PD_2=2.0450$	$PD_1 = 1.9153$	$PD_2=2.0996$		
5	$LP_1=0.8477$	$LP_2=0.9296$	$LP_1=0.9353$	$LP_2 = 0.9104$		
<u> </u>	$PD_1 = 1.9034$	$PD_2=2.0966$	$PD_1 = 1.8290$	$PD_2 = 2.2312$		
6	$LP_1=0.6925$	$LP_2=0.9092$	$LP_1=0.8582$	$LP_2=0.9215$		
	$PD_1 = 1.8533$	$PD_2=2.1467$	$PD_1 = 1.7564$	$PD_2 = 2.3909$		
7	$PD_1 = 1.7541$	$PD_2=2.2459$	$PD_1 = 1.6354$	$PD_2 = 2.8600$		
8	$LP_1=0.7830$	$LP_2 = -2.8534$	$LP_1=0.8430$	$LP_2=0.7003$		
	$PD_1 = 1.5067$	$PD_2=2.4931$	$PD_1=1.3593$	$PD_2 > 3.00$		
9	$LP_1 = -$	$LP_2 = -$	$LP_1 = 0.8133$	$LP_2=0.5956$		
	$PD_1 = 1.2600$	$PD_2=2.7400$	$PD_1=1.0936$	$PD_2 > 3.00$		
13	$PD_1 = 1.9711$	$PD_2=2.0289$	$PD_1 = 1.9460$	$PD_2=2.0664$		
14	$LP_1 = -$	$LP_2 = -$	$LP_1 = -$	$LP_2 = -$		
	$PD_1 = 1.9098$	$PD_2=2.0902$	$PD_1 = 1.8406$	$PD_2 = 2.2169$		
15	$LP_1 = 0.94222$	$LP_2=0.9985$	$LP_1 = -$	$LP_2 = -$		
	$PD_1 = 1.8575$	$PD_2=2.1425$	$PD_1 = 1.7637$	$PD_2 = 2.3811$		
16	$PD_1 = 1.7565$	$PD_2=2.2435$	$PD_1 = 1.6382$	$PD_2 = 2.8602$		
17	$LP_1=0.7873$	$LP_2 = -$	$LP_1 = 0.8473$	$LP_2=0.7799$		
	$PD_1 = 1.5081$	$PD_2 = 2.4919$	$PD_1 = 1.3625$	$PD_2 > 3.0$		
18	$LP_1=0.7293$	$LP_2 = -$	$LP_1 = 0.8150$	$LP_2 = -$		
	$PD_1 = 1.2609$	$PD_2=2.7391$	$PD_1 =$	$PD_2 =$		
19	$PD_1 = 1.9542$	$PD_2=2.0458$	$PD_1 = 1.8882$	$PD_2 = 2.1314$		
20	$LP_1=0.8477$	$LP_2 = -$	$LP_1 = 0.9376$	$LP_2 = 0.9120$		
	$PD_1 = 1.9030$	$PD_2=2.0970$	$PD_1 = 1.8156$	$PD_2 = 2.2493$		
21	$LP_1=0.6925$	$LP_2 = -$	$LP_1 = 0.8612$	$LP_2=0.9202$		
	$PD_1 = 1.8531$	$PD_2=2.1469$	$PD_1 = 1.7481$	$PD_2=2.4045$		
22	$PD_1 = 1.7509$	$PD_2=2.2491$	$PD_1 = 1.5537$	$PD_2 = -$		
23	$LP_1 = 0.7830$	$LP_2 = -$	$LP_1 = -$	$LP_2 = -$		
	$PD_1 = 1.5053$	$PD_2=2.4947$	$PD_1 = 1.3400$	$PD_2 = -$		
25	$PD_1 = 1.9549$	$PD_2=2.0450$	$PD_1 = 1.9141$	$PD_2=2.1009$		
26	$LP_1=0.8477$	$LP_2=0.9296$	$LP_1 = 0.9376$	$LP_2 = 0.9088$		
	$PD_1 = 1.9034$	$PD_2=2.0906$	$PD_1 = 1.8283$	$PD_2=2.2319$		
27	$LP_1 = 0.6925$	$LP_2=0.9092$	$LP_1 = 0.8554$	$LP_2=0.9210$		
L	$PD_1 = 1.8533$	$PD_2=2.1467$	$PD_1 = 1.7560$	$PD_2=2.3915$		

Table 6.2: Comparison of Bifurcation Data

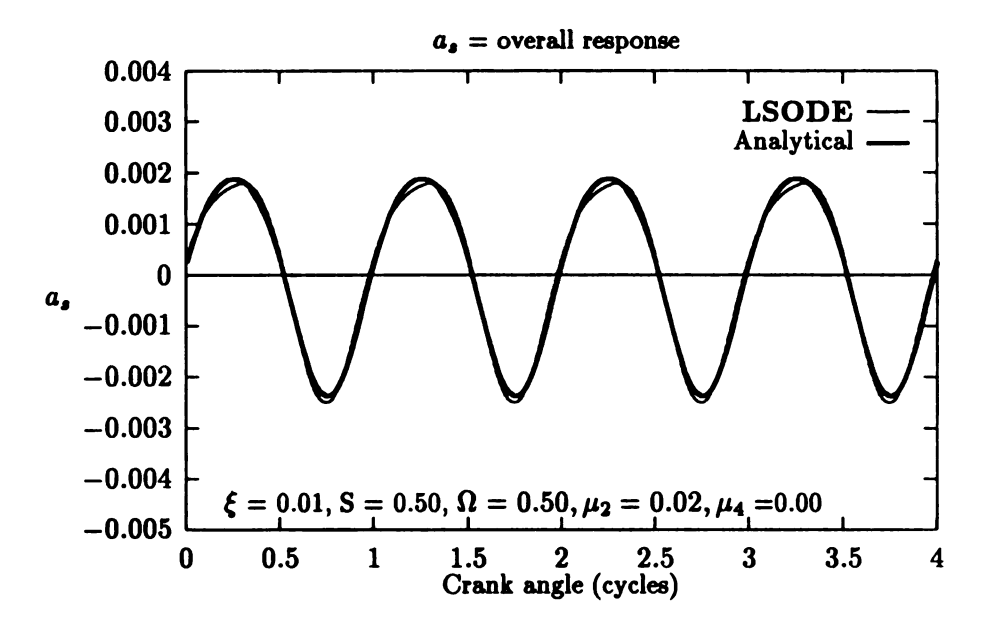


Figure 6.9: Comparison between simulation and analytical approximation for case 5

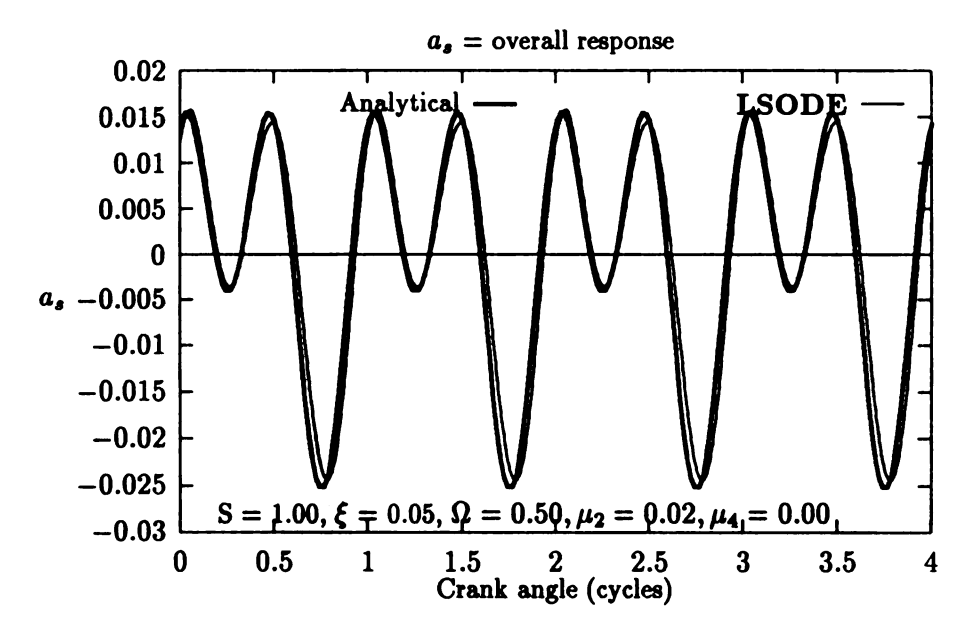


Figure 6.10: Comparison between simulation and analytical approximation for case 9

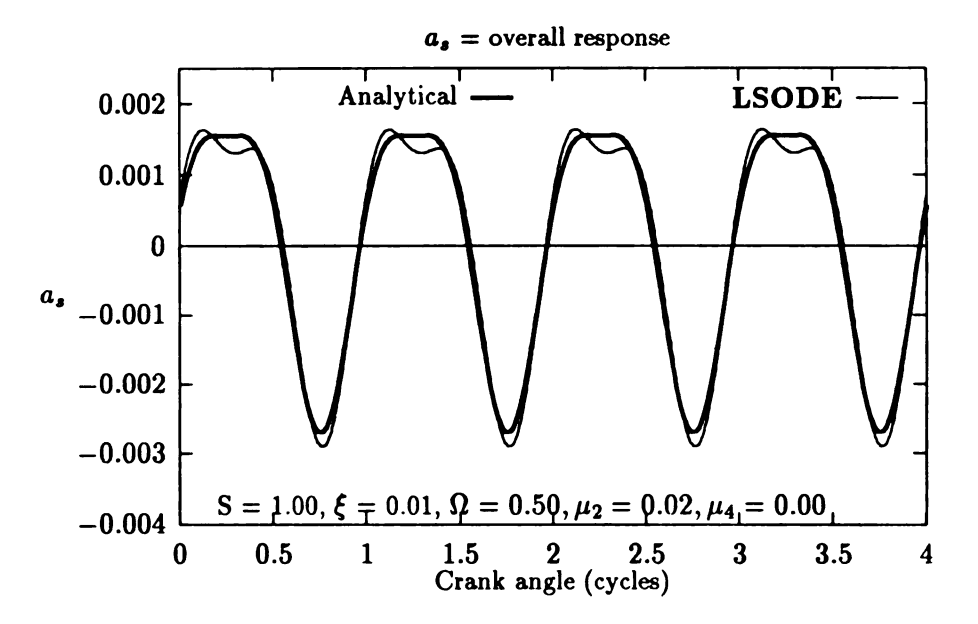


Figure 6.11: Comparison between simulation and analytical approximation for case 6

#### 6.2 Influence of the Mass Ratio S

In this section, we investigate the effect of the mass ratio S on the overall response predicted by equation (4.21). According to the analytical work, the mass ratio S plays the role of the nonlinearity in equation (4.21). Moreover, the strength of the nonlinearity depends in a complicated way on the mass ratio. In section 6.1, it was shown that the linear approximation matches the nonlinear approximation as well as the numerical solutions for case in which S is zero. For the primary resonance, the detuning associated with the primary resonance increases linearly as S increases, while the peak amplitude remains unchanged. There will be no detuning associated with the primary resonance when S = 0. Hence, when S = 0, there is no bifurcation associated with the primary resonance. In the principal parametric resonance, the width of the main nose of instability increases as S increases. Moreover, the amplitude of the responses changes as the mass ratio changes. In the superharmonic resonance in which  $\Omega$  is near to one half, the mass ratio affects the

response in a very interesting way. The amplitude of the response decreases as S increases from zero to a critical value, while the amplitude increases after S increases beyond this critical value. Figure 6.12 contains the frequency response curves for cases 4, 5 and 6. Figure 6.13 shows the frequency response curves associated with cases 7, 8 and 9.

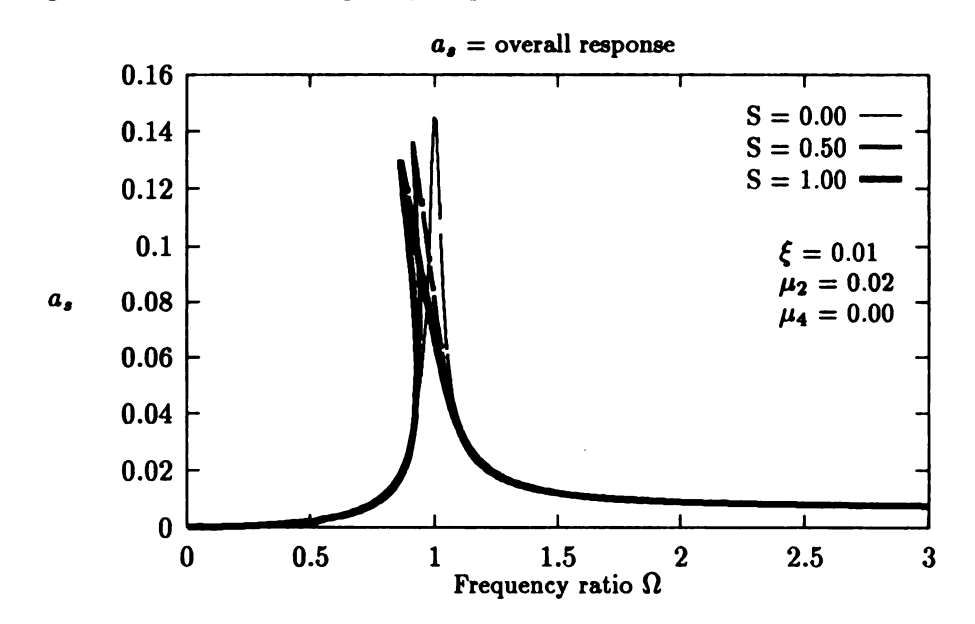


Figure 6.12: Frequency response curves from AUTO (cases 4, 5 and 6)

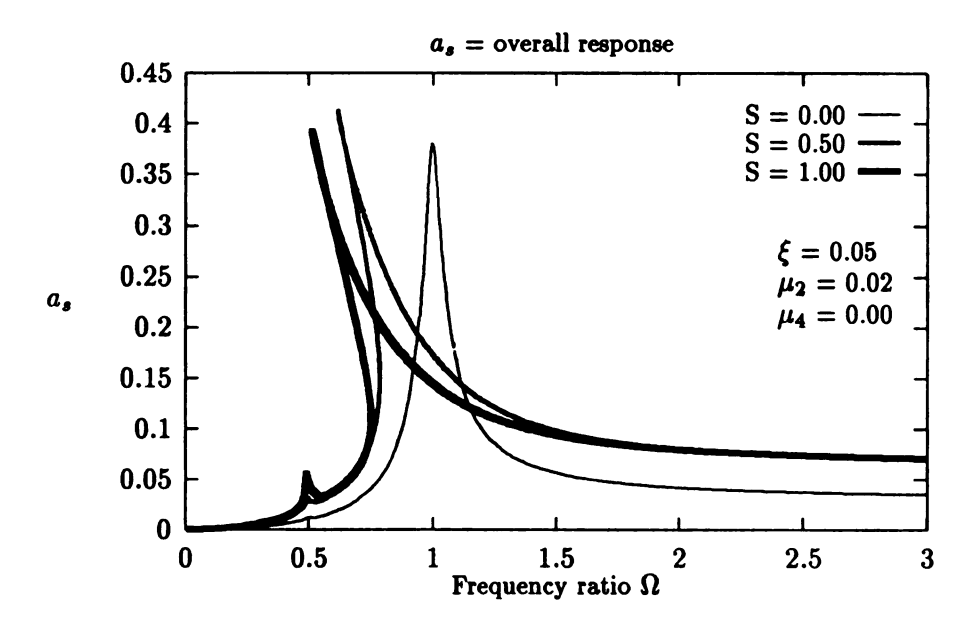


Figure 6.13: Frequency response curves from AUTO (cases 7, 8 and 9)

We first consider the primary resonance. As these figures show, the peak amplitude of the response remains essentially unchanged while the detuning  $\sigma_p$  increases as S increases from zero to one. This in turn enlarges the instability region associated with the primary resonance. From the numerical results listed in Table 6.1, we know that the width of the instability region increases from zero (case 4) to 0.0633 (case 6) as S increases from zero to one. Figure 6.14 contains the simulation results for cases 7 and 8 with  $\Omega = 1.00$ . From this figure, we observe that the larger the mass ratio is, the smaller the peak amplitude of the response will be. This is caused by the bending of the frequency response curves associated with the primary resonance (Figure 6.12 and Figure 6.13). Next, let us consider the principal parametric resonance. The width of the main nose of instability, as shown in Table 6.1, increases from 0.2338 (case 4) to 0.6409 (case 6) when S increases from zero (case 4) to one (case 6). (In order to keep Figures 6.12 and 6.13 as clear as possible, the branches of the nontrivial solution are not shown in these figures.) Figure 6.15 shows the branches of parametric response for cases 5 and 6. From this figure, it is very clear that as S is increased these response branches bend more, and the main nose of instability is enlarged.

In order to consider the effect of the mass ratio S on the amplitude of the superharmonic resonance, we need to consider the response curves when  $\Omega$  is near to one half. Figure 6.16 shows the amplitude of the response at  $\Omega = 0.50$ . Comparing this figure with Figure 4.11, it is very clear that the numerical solution agrees the analytical prediction.

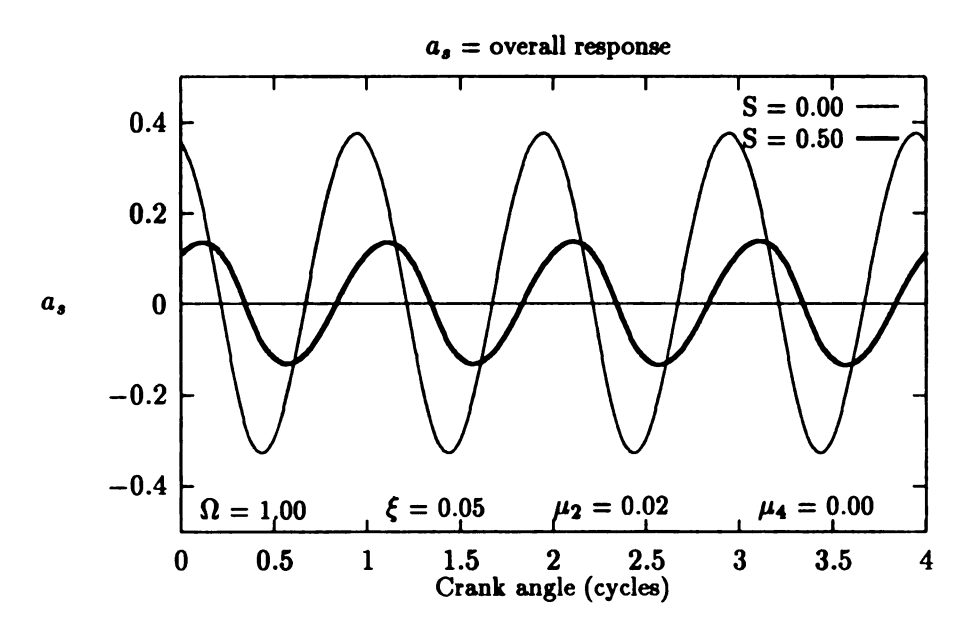


Figure 6.14: Simulation results for cases 7 and 8

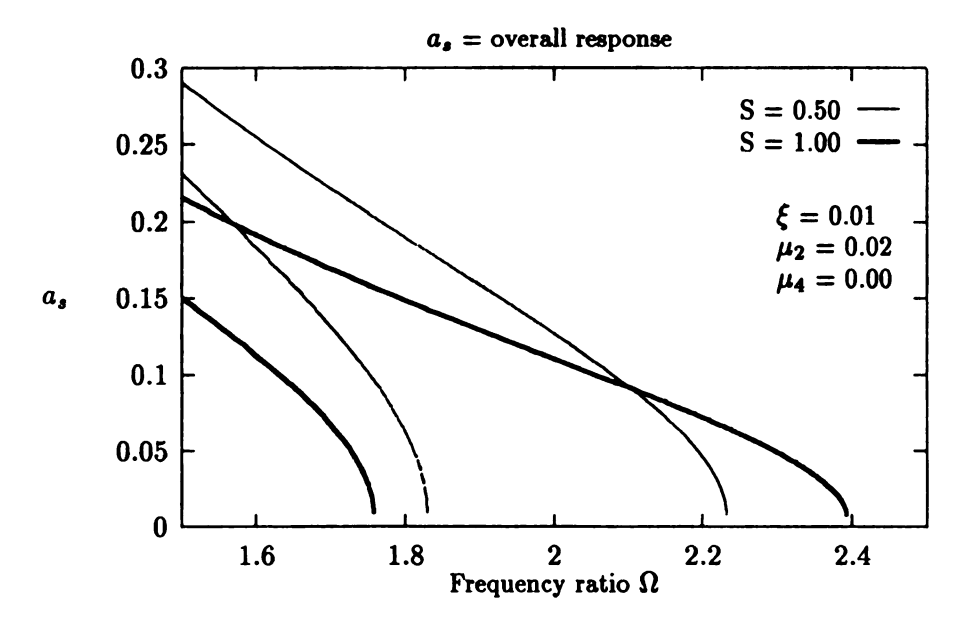


Figure 6.15: Nontrivial responses associated with the principal parametric resonance (cases 5 and 6)

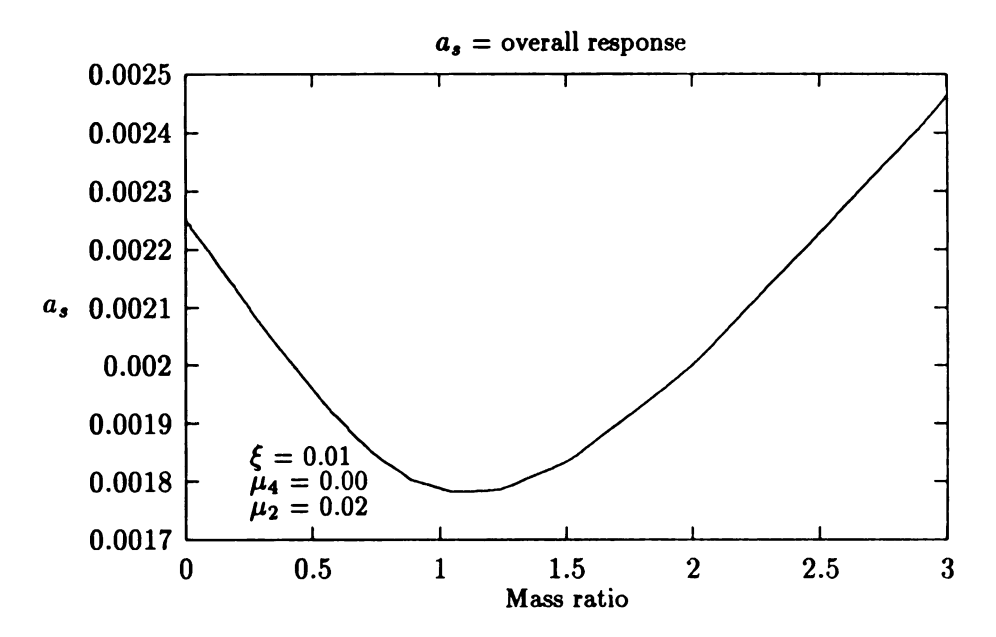


Figure 6.16: Amplitude of the response at  $\Omega = \frac{1}{2}$ 

#### 6.3 Influence of the Friction Parameters $\mu_2$ and $\mu_4$

In this section, we consider the effects of the damping parameters  $\mu_2$ ,  $\mu_3$  and  $\mu_4$  on the overall response of equation (4.21). The parameter  $\mu_2$  corresponds to the internal material damping associated with the connecting rod. The parameter  $\mu_3$  represents the damping effect of the bearings at the joints between members. The parameter  $\mu_4$  is used to model the friction force acting at the slider end. We focus our attention on the qualitative behavior of the response as each of these parameters is changed.

#### 6.3.1 Effect of the Damping Parameter $\mu_2$

The analytic results indicate that this parameter has a favorable effect on the overall response curves. According to the analytical results, this parameter affects the response by reducing the amplitude of the response and the width of the instability region associated with each resonance case. Near the primary resonance, the amplitude of the response

decreases as  $\mu_2$  increases. Therefore, the detuning of the frequency  $(\sigma_p)$  decreases. This implies that the unstable region associated with the response curves (region between points  $LP_1$  and  $LP_2$ ) will shrink as  $\mu_2$  increases. In the principal parametric resonance, the

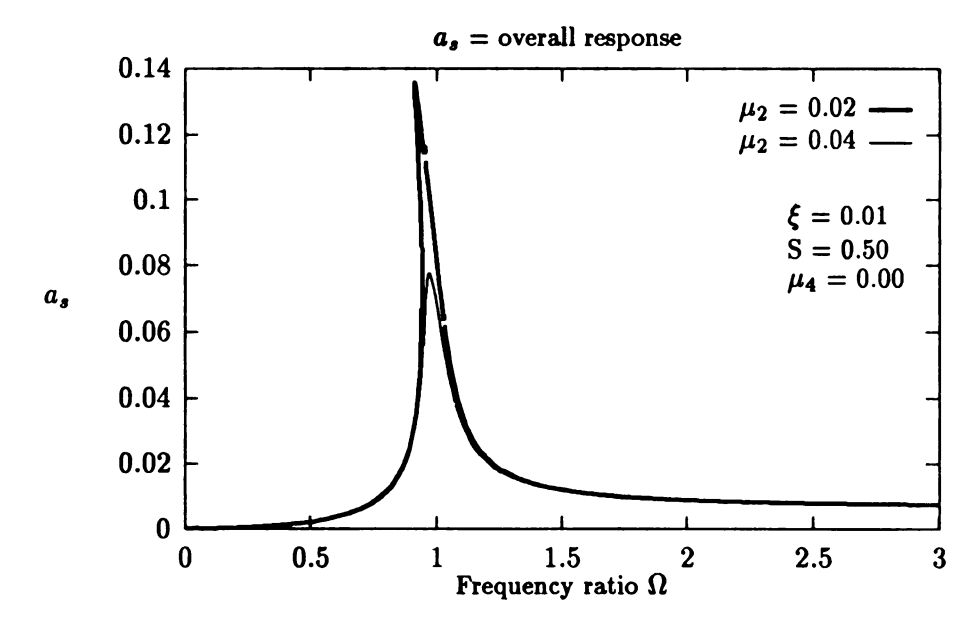


Figure 6.17: Frequency response curves from AUTO (case 5 and 14)

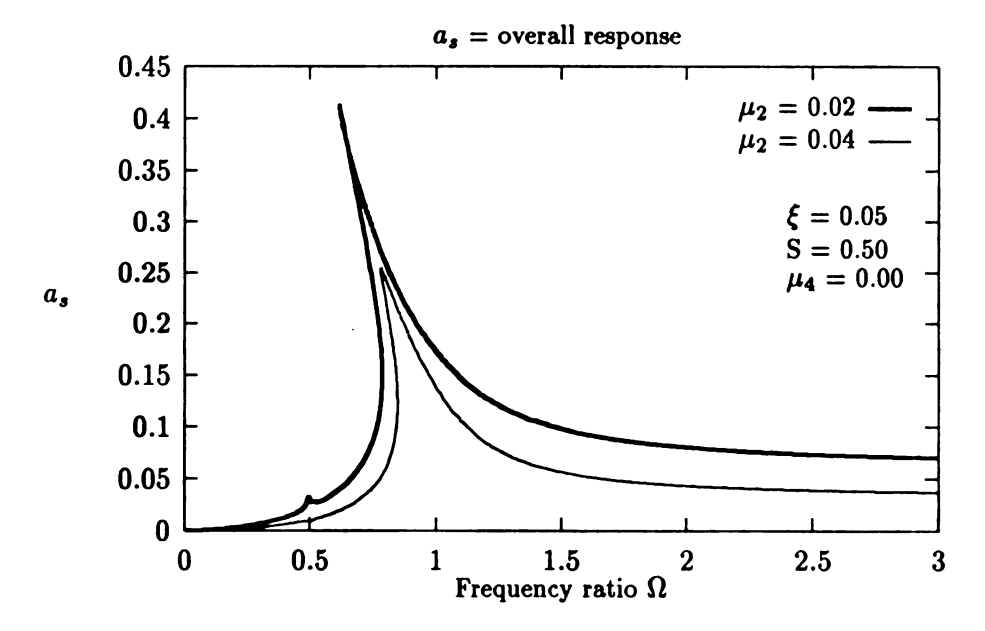


Figure 6.18: Frequency response curves from AUTO (case 8 and 17)

main nose of instability also shrinks as  $\mu_2$  increases. Moreover, the amplitude of response which originates from the main nose of instability also deceases as  $\mu_2$  increases. Figure 6.17

shows the response curves for cases 5 and 14. Figure 6.18 shows the response curves for cases 8 and 17. Figure 6.19 shows the simulation results for cases 8 and 17. From these figures, it

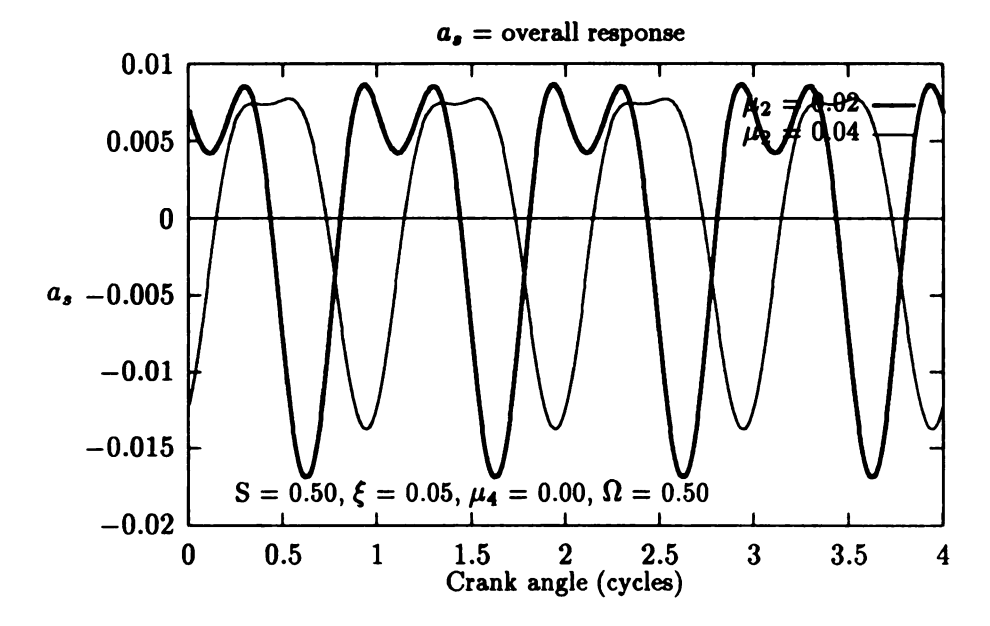


Figure 6.19: Simulation results from LSODE (case 8 and 17)

is very clear that  $\mu_2$  does have a favorable effect on the response. Moreover, all the trends predicted by the analytical work are verified. Figure 6.17 and Figure 6.18 show that the amplitude of response decreases as  $\mu_2$  increases. This in turn reduces the contribution of the nonlinearity on the overall response. In consequence, the response curve is smoother for larger values of  $\mu_2$ . This point is clearly shown from Figure 6.19 which demonstrates how the second harmonic is reduced as  $\mu_2$  is increased near the  $\Omega = \frac{1}{2}$  superharmonic resonance. Regarding the instability region associated with the primary resonance, let us consider the locations of  $LP_1$  and  $LP_2$ . From Table 6.1, we find that the width of the instability region decreases from 0.1427 (case 8) to 0.0674 (case 17) as  $\mu_2$  increases from 0.02 to 0.04.

Next, let us consider the principal parametric resonance. Figure 6.20 shows branches of response originating from the main nose of instability for cases 5 and 14, that is near  $\Omega = 2.0$  with different  $\mu_2$  values. Figure 6.21 shows the simulation results for cases 5 and

14 associated with the principal parametric resonance. From Figure 6.20, it is clear that  $\mu_2$  has a small but favorable effect on the principal parametric resonance. The width of the main nose of instability associated with the principal parametric resonance decreases from 0.4022 (case 5) to 0.3763 (case 14), as  $\mu_2$  increases from 0.02 to 0.04.

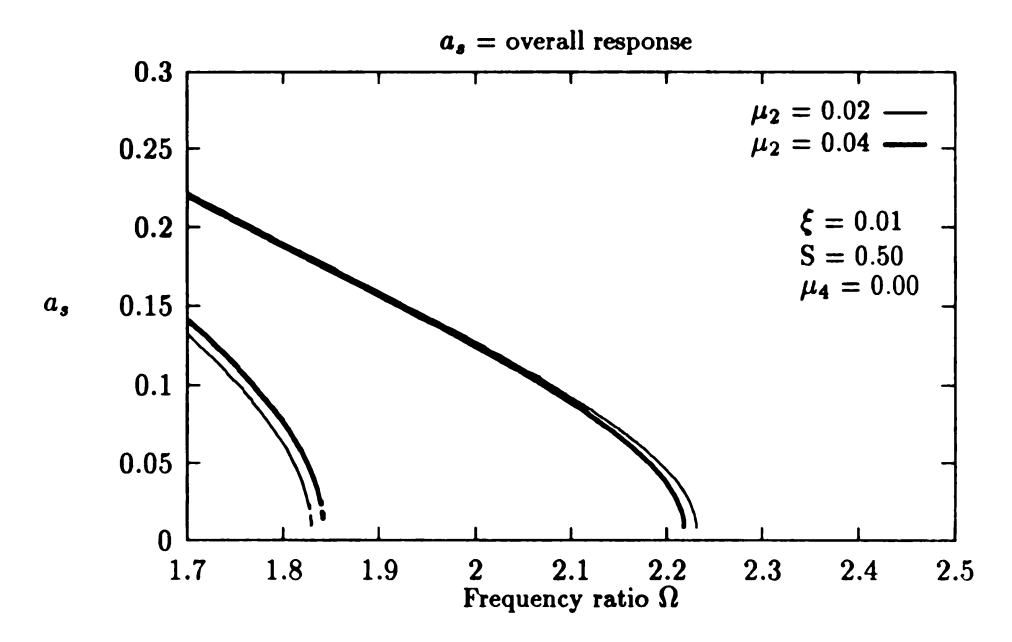


Figure 6.20: Nontrivial responses associated with the principal parametric resonance (case 5 and 14)

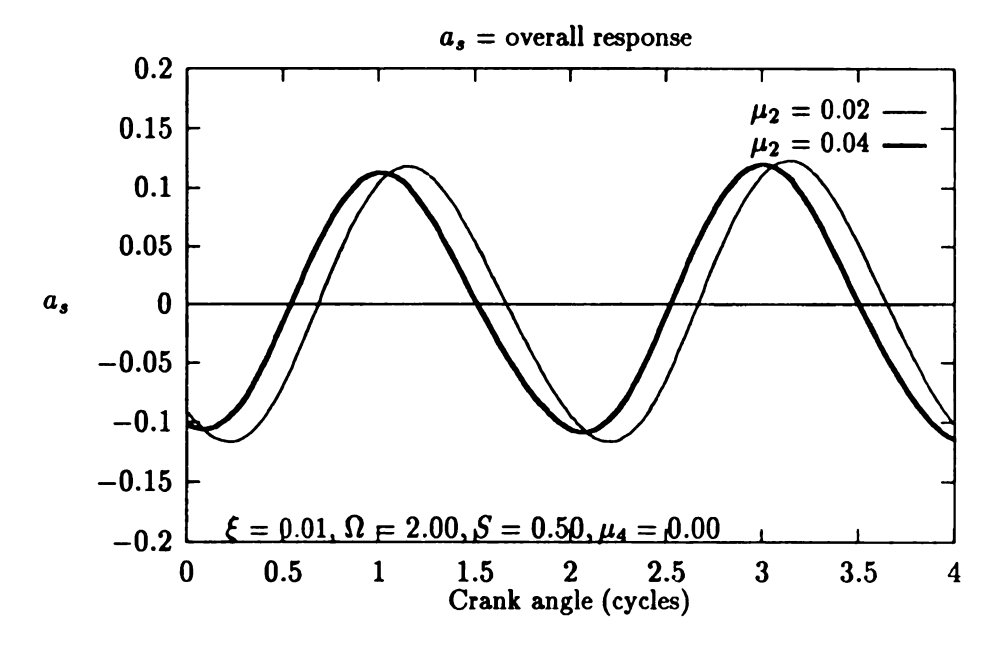


Figure 6.21: Simulation results for cases 5 and 14

#### 6.3.2 Effect of the Friction Parameter $\mu_4$

According to the analytical results, the friction parameter  $\mu_4$  has a favorable effect on all the resonances, except the second order superharmonic resonance ( $\Omega \approx \frac{1}{2}$ ) and the main nose of instability associated with the principal parametric resonance ( $\Omega \approx 2$ ). Figure 6.22 shows the overall frequency response curves for cases 6 and 21. Figure 6.23 shows that the

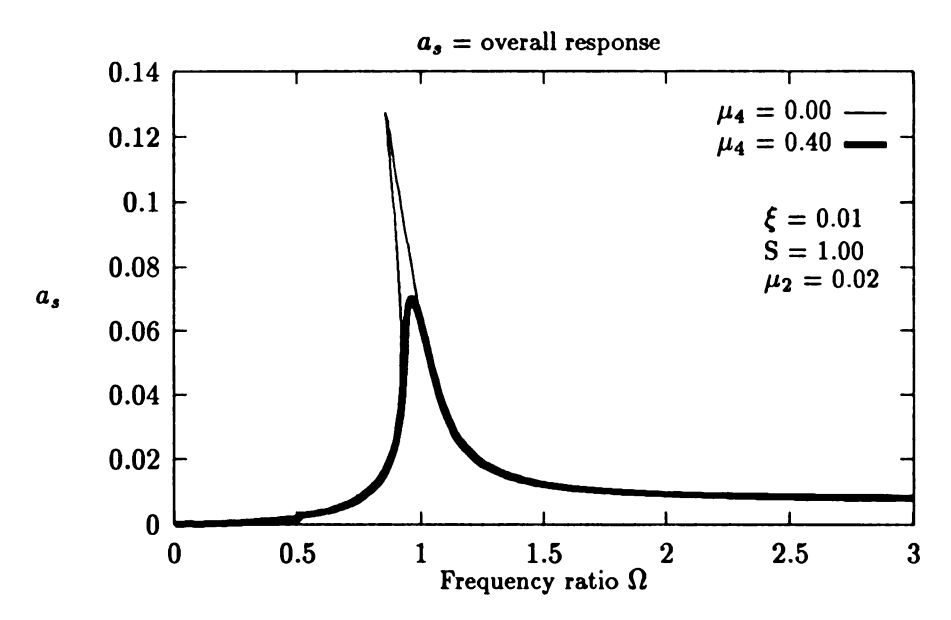


Figure 6.22: Frequency response curves from AUTO (cases 6 and 21)

overall frequency response curves for cases 8 and 23. As shown in these figures, the friction parameter  $\mu_4$  affects the responses by reducing the peak amplitudes of the responses and hence has a favorable effect. However, it should be noted that relative magnitude of the superharmonic resonance near  $\Omega=0.5$  is increased due to an increase ion the amplitude of the second harmonic. Figure 6.24 depicts branches of response originating from the main nose of instability associated with the principal parametric resonance ( $\Omega\approx 2$ ) for cases 5 and 20. Figure 6.25 shows branches of response originating from the main nose of instability for cases 6 and 21. From these figures, it is very clear that the friction parameter  $\mu_4$  has a favorable on the principal parametric resonance. Form the bifurcation data contained in

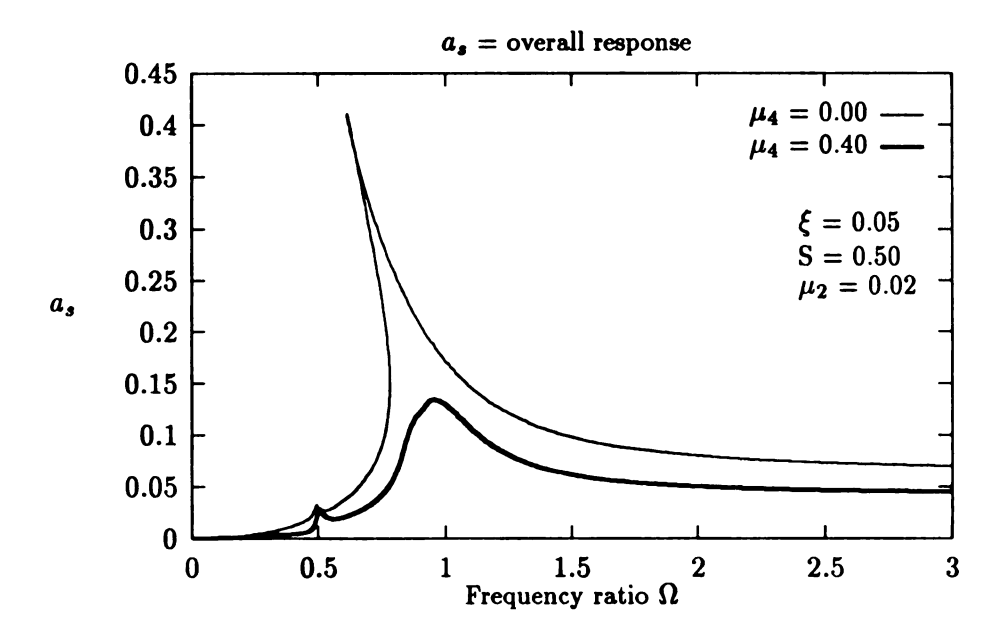


Figure 6.23: Frequency response curves from AUTO (cases 8 and 23)

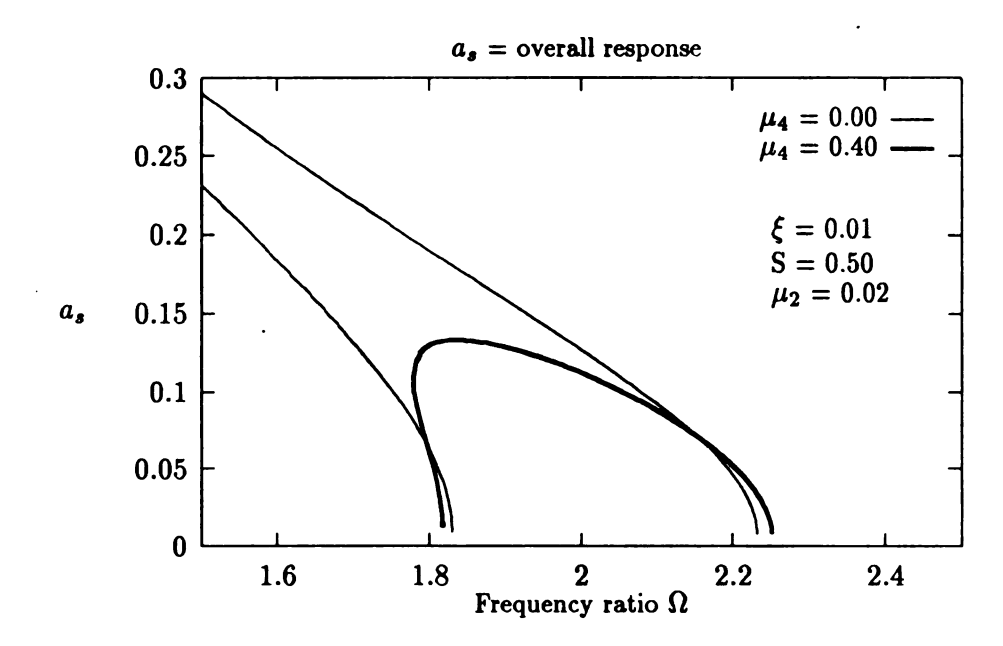


Figure 6.24: Nontrivial responses associated with the principal parametric resonance from AUTO (cases 5 and 20)

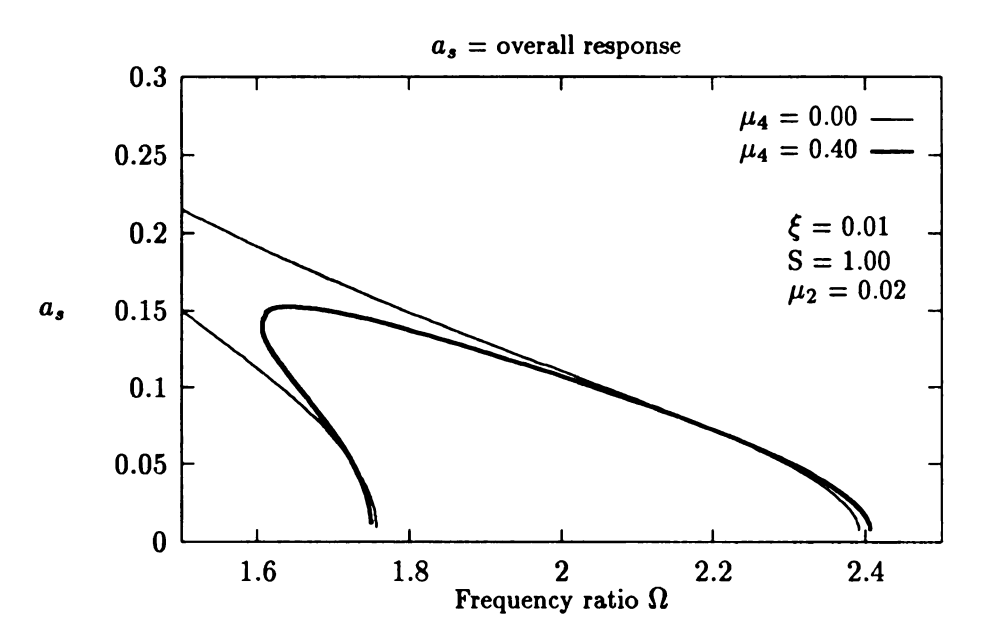


Figure 6.25: Nontrivial responses associated with the principal parametric resonance from AUTO (cases 6 and 21)

Table 6.1, we find that the width of the main nose of instability increases from 0.2934 in case 6 to 0.6564 in case 21. This indicates that  $\mu_4$  has a tendency to increase the width of the main nose of instability and hence has an adverse effect. Figure 6.26 shows the response for  $\Omega \approx \frac{1}{2}$  for cases 7 and 22. Figure 6.27 and Figure 6.28 show the analytical approximations and simulation results for case 7 and case 22, respectively. From these figures, it is clear that the amplitude near the superharmonic resonance in which  $\Omega$  is near to  $\frac{1}{2}$  increases as  $\mu_4$  increases, as predicted. This increase of the amplitude is due to the increasing influence of the nonlinearity on the overall response. Near this resonance, as  $\mu_4$  is increased, the amplitude of the second harmonic, which comes from the free oscillation in this case, also increases. In comparing Figures 6.26 and 6.27, we find that the perturbation approach can provide very accurate results compared with the numerical solutions. This point is shown from the profile of the responses given in Figures 6.26 and 6.27.

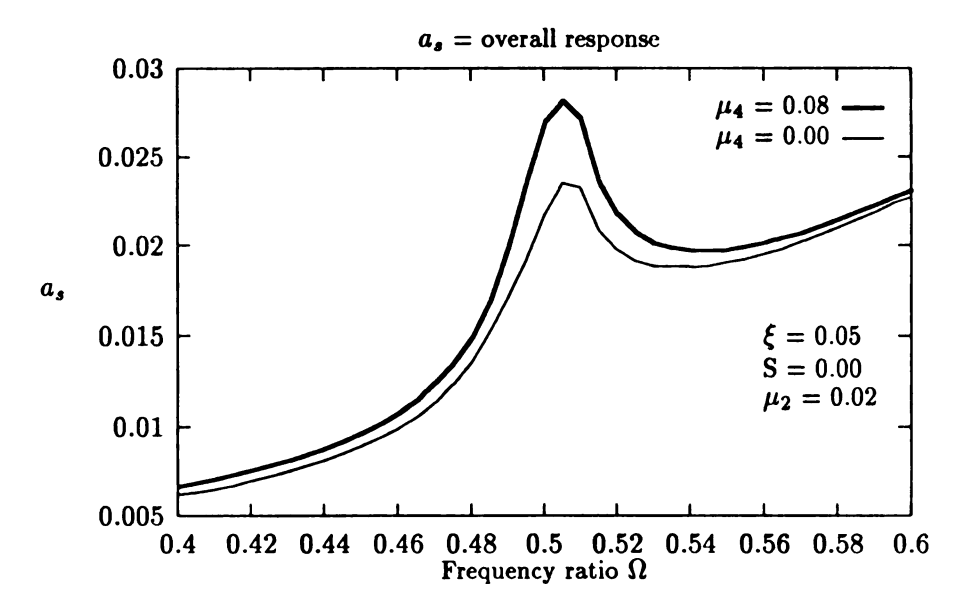


Figure 6.26: Frequency response for cases 7 and 22 from LSODE

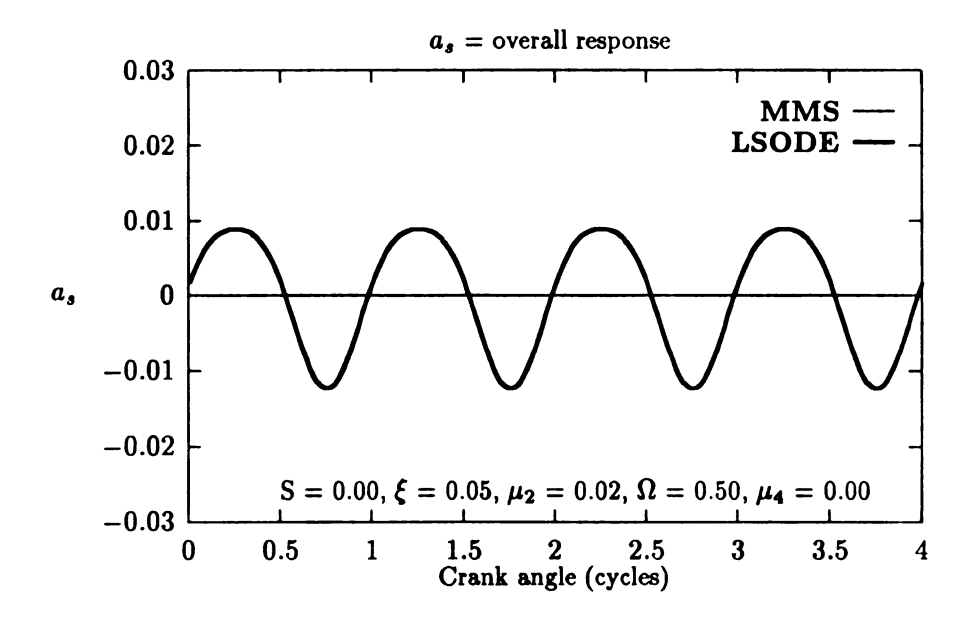


Figure 6.27: Analytical approximation and simulation results for case 7

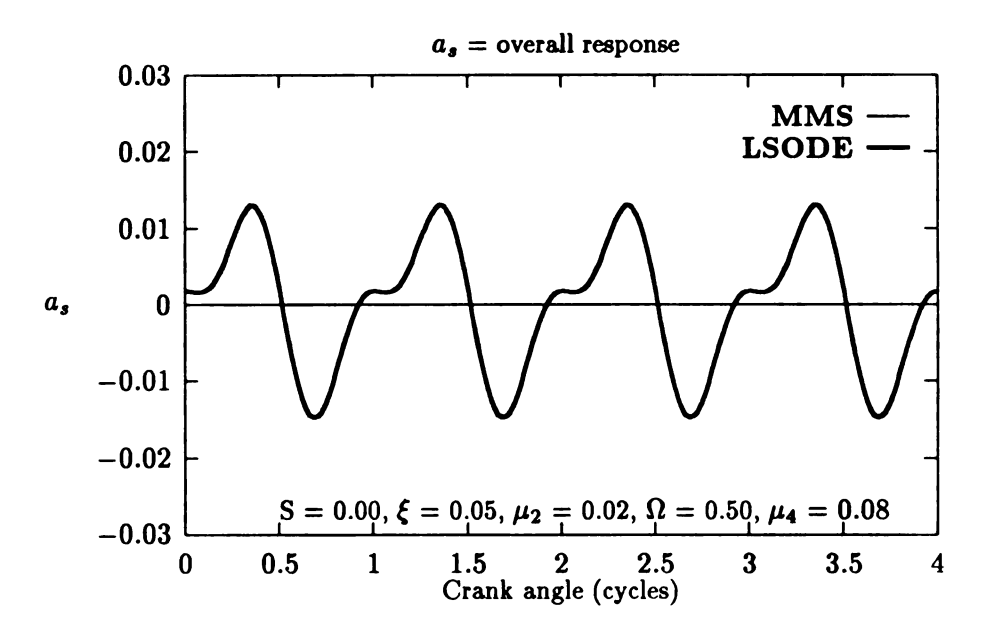


Figure 6.28: Analytical approximation and simulation results for case 22

#### 6.4 Conclusions

In this chapter, we considered the lumped parameter model with the help of the software packages LSODE and AUTO. The main aim was to verify the qualitative predictions from the analytical work. Instead of quantitative accuracy, we focused our attention of the qualitative behavior associated with the analytical work. To achieve this goal, we conducted these numerical studies by considering the effect of each parameter on the overall response predicted from equation (4.21). As the results show, there are remarkable agreements between the analytical and numerical results. However, these numerical studies were restricted to small length ratios  $\xi \ll 1$ . As we mentioned in the previous sections, the length ratio  $\xi$  serves as the primary parameter for the current problem. The length ratio  $\xi$  represents not only the magnitude of the inertia force, but also contributes to the strength of the nonlinearity. When the length ratio  $\xi$  increases, the amplitude of the response increases. At some value of  $\xi$ , the original equation develops an overly strong nonlinearity, which the method of multiple scales is not able to handle. Although, according to the analytical

approximation, the mass ratio S is the only source of nonlinearity, the numerical results show that, for large  $\xi$ , there exists a nonlinearity in addition to the one arising from the inertia of the end mass  $m_4$  attached to the slider end. In order to demonstrate this, let us consider the frequency response curve plotted in Figure 6.29. Note that there is a very small frequency shift associated with the primary resonance in Figure 6.29. This frequency shift implies that even without any mass attached to the slider end, there exists a small nonlinearity of the softening type associated with the primary resonance. Because this detuning of the frequency associated with the primary resonance is very small compared with case 7, the nonlinearity associated with case 10 is very weak. Another interesting observation arises from the type of nonlinearity associated with the principal parametric resonance. To show this, let us consider Figures 6.30 and 6.31 which contain the branches of the nontrivial responses associated with the principal parametric resonance for cases 4 and 7, respectively. From these figures, we find that these branches bend slightly to the

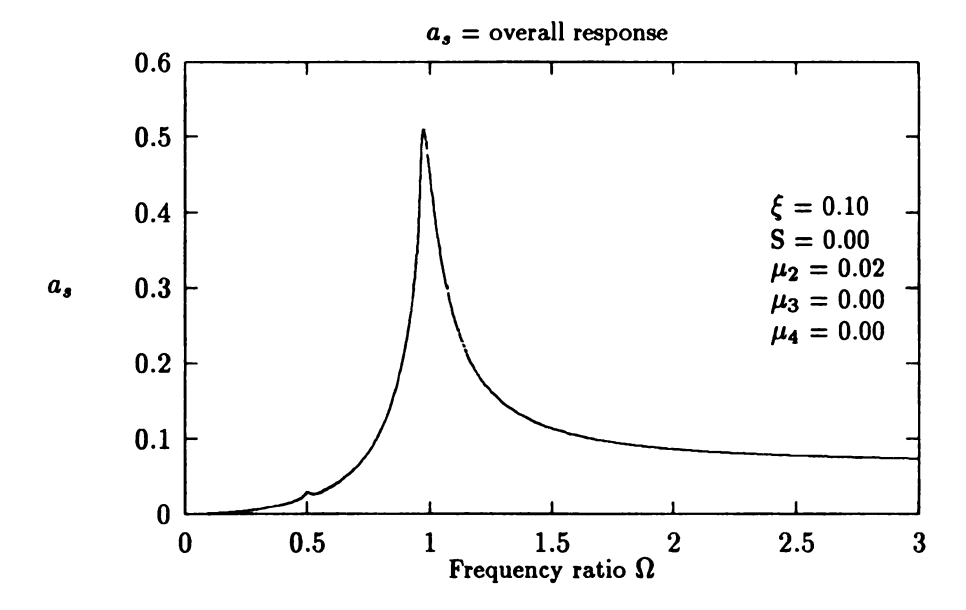


Figure 6.29: Frequency response curve for case 10

right. This corresponds to a hardening nonlinearity. By considering the slopes associated

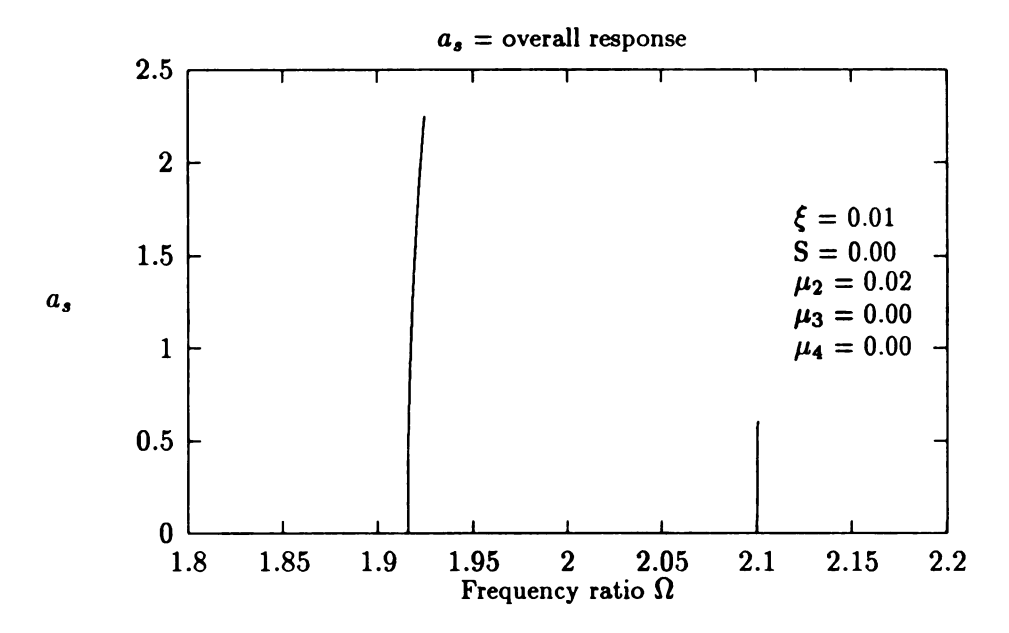


Figure 6.30: Nontrivial responses associated with the principal parametric resonance (case 4)

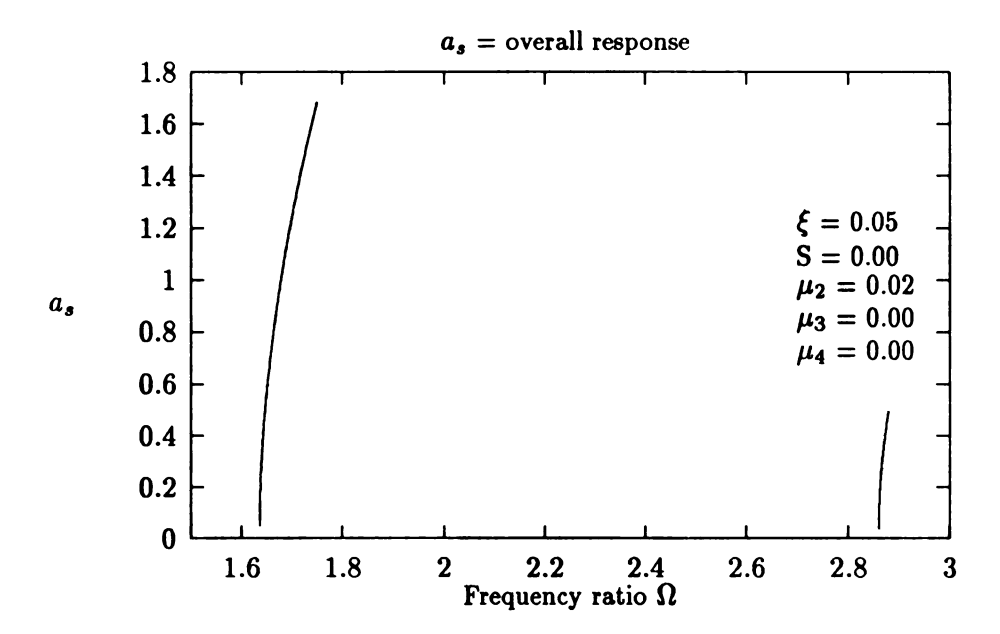


Figure 6.31: Nontrivial responses associated with the principal parametric resonance (case 7)

with these branches, we conclude that the effects of the nonlinearity is very weak. Hence, we know that equation (4.21) possesses a hardening type nonlinearity when there is no end mass  $m_4$  attached to the slider end. In the distributed parameter approach, the mass ratio S is not the only source of nonlinearity. The geometric nonlinearity does share this role with the mass ratio S. Despite these disagreements, the analytical work does provide a reasonable prediction regarding the qualitative behavior of equation (4.21), especially when S is nonzero.

	S	ξ	$\mu_2$	S	ξ	$\mu_2$
AUTO	0	0.35	0.04	0	0.25	0.02
	0.5	0.25	0.04	0.5	0.20	0.02
	1.0	0.15	0.04	1.0	0.10	0.02
MMS	0	no limit	0.04	0	no limit	0.02
	0.5	0.05	0.04	0.5	0.025	0.02
	1.0	0.036	0.04	1.0	0.018	0.02

Table 6.3: Limits of MMS and AUTO

Both the analytical method and the numerical simulations have difficulties in obtaining the overall response curves over a wide range of frequencies ( $\Omega=0.005$  to 3.00). Table 6.3 contains information concerning the limitations for both the analytical method MMS and the numerical tool AUTO. Since the effect of friction parameters  $\mu_3$  and  $\mu_4$  are not significant, we let  $\mu_3=\mu_4=0$  in generating Table 6.3. Since the length ratio  $\xi$  is the primary parameter, we select it as the key parameter to monitor the limits of these two approaches. Regarding the limits of AUTO, the data provided in the table indicate the maximum length ratio  $\xi$  for which AUTO will generate the overall frequency response curves. For the analytical solutions MMS, the data are the maximum values of  $\xi$  which will not produce a detuning associated with the primary resonance, larger than unity so that the peak amplitude of the response can be observed for a positive operating frequency  $\Omega$ . It should

be noted that significantly larger values of  $\xi$  can be handled by **AUTO** if one restricted attention to a smaller frequency range.

### Chapter 7

## **Summary and Conclusions**

High operating speeds, superior reliability and accurate performance are major characteristics of modern industrial machinery and commercial equipment. The traditional rigid body analysis which presumes low operating speeds becomes insufficient for describing the performance of such high speed machinery. A thorough understanding of the dynamic behavior of machine elements undergoing high speed operations is necessary in these situations. It is the purpose of this dissertation to present an analytical approach for describing the elastic mechanism problem and provide a theoretical explanation for some of the dynamic phenomena observed in both numerical and experimental works. One of the simplest and most popular mechanisms, the slider-crank mechanism, is selected as the prototype system to demonstrate this analytical work.

In this dissertation, we study the flexural vibration associated with the elastic connecting rod of an otherwise rigid slider crank mechanism by using the Method of Multiple Scales and the numerical techniques. Similar perturbation methods, such as the regular expansion method[8, 9] and the Method of Averaging[30, 31], have been applied to study this problem. However, up to the present time, all these investigations have provided only linear results. In particular, analyses of the stability associated with the steady state response and detailed studies of the nonlinear response have not been carried out.

This problem is equivalent to the flexural vibration of a simply supported beam subjected to (1) inertia force and the motion of its foundation, arising from the motion of the crank shaft, (2) axial loads which come from the presence of the friction force on the slider mass and the inertia force associated with the slider mass, (3) concentrated frictional moments which come from the presence of bearing friction on the joints between links. The single mode flexural response of the connecting rod can be approximated by a single ordinary differential equation with multi-frequency harmonic excitations and time-varying coefficients which are also of multi-frequency. These frequencies are composed of the crank speed plus harmonics of it.

Several different types resonances can arise in this problem. The first type is caused by the time-varying coefficients, and is referred to as the parametric resonances. The second type occurs when one of the harmonic excitation terms has the same frequency as one of the natural flexural frequencies, and correspond to as the primary and/or superharmonic resonances. A third type, the subharmonic resonances can occur when a natural frequency is a multiple of one of the excitation frequencies.

Two different models are used to study this problem. In the first model, the dynamic response of the elastic connecting rod is described by a set of partial differential equations. The dynamic behavior is studied by obtaining approximate solutions of these partial differential equations using the Method of Multiple Scales and Galerkin truncations. In second model, the dynamic behavior of the connecting rod is described by a single nonlinear differential equation obtained by direct modal truncation of the partial differential equations. This latter procedure follows the works by Viscomi et al.[49] and Badlani[9], although we have included the effects of bearing and slider friction. We analyze the response predicted by this model by obtaining approximate solutions of the governing ordinary differential equa-

tion using the Method of Multiple Scales. In both of these two models, several resonances, such as the primary resonance, the principal parametric resonance and superharmonic resonances, were studied in detail and compared. In addition, extensive numerical studies were carried out, including direct simulation as well as the generation of frequency response curves using path following software.

The major features of this work are outlined here. The length ratio  $\xi$  turns out to be the parameter which has the most direct influence on the response. The magnitude of the response and the strength of the nonlinearity both depend on the this parameter. The reordering of the length ratio is the essential step needed to extend the analysis to include nonlinear effects. Since the external force is expressed as an asymptotic expansion in  $\xi$ , the validity of the application of the asymptotic method in studying this problem relies on the order of length ratio  $\xi$ . The mass ratio S is proved to be the strongest source of nonlinearity. When there is no end mass attached to the slider, there exists only a very weak geometrical nonlinearity associated with the geometrical effects of flexure. This point is clearly shown by the numerical studies and the analysis of the distributed parameter system. The presence of the end mass makes the system behave like a system possessing a softening type of nonlinearity. As a consequence, the frequency response curve will bend to the left. Regarding this parameter, our analysis is in conflict with previous investigations [30, 31]. Our results, which are confirmed by the numerical studies, indicates that the peak amplitude of the response is independent of the mass ratio. Moreover, the amplitude of the superharmonic resonances can be slightly reduced by choosing a proper end mass. The effects of three damping mechanisms are included in the model, these are represented by the parameters  $\mu_2$ ,  $\mu_3$  and  $\mu_4$ . The internal material damping  $\mu_2$ , as expected, has a favorable effect on the overall response. This parameter affects the response by reducing the amplitude of the response and shrinking the width of the instability regions. The bearing friction,  $\mu_3$ , has an adverse effect on the overall response. Although, the effect of bearing friction is not as significant as that of  $\mu_2$ , the presence of  $\mu_3$  will increase the amplitude of the response and increase the parameter regions where instabilities occur. This occurs since the bearing friction at the connection acts like a constant bias moment plus a fluctuating moment which adds a constant bias to the response in addition to providing an additional source of periodic input. The slider friction parameter  $\mu_4$  shows a variety of effects. The slider friction force is composed of two actions: rigid body motion and elastic deformation. Friction based on the rigid body motion has an adverse effect on the response. Friction based on the elastic deformation has a favorable effect on the response. Although the effect of  $\mu_4$  may not as significant as  $\mu_2$ , it has a not favorable effect on the overall response. The effects of shear deformation and rotary inertia, included in the distributed parameter system analysis, affect the response by shifting the entire frequency response curves leftward in frequency.

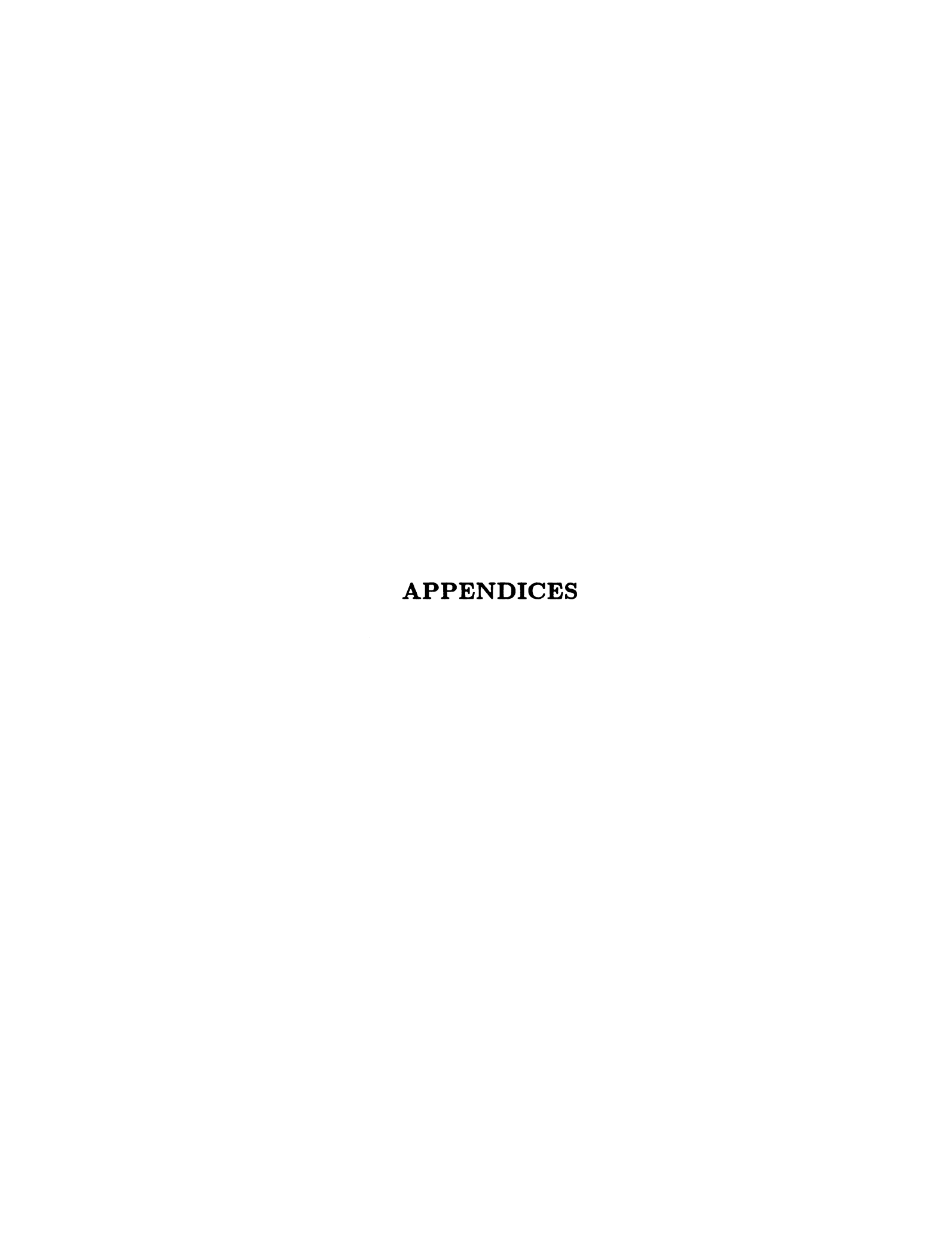
The results presented in this dissertation represents a successful extension of previous efforts in that the effects of nonlinearities have been analyzed in a systematic manner. The major drawback of this approach is that tedious manipulations are involved in analyzing the higher order resonances. This difficulty may be overcame with more advanced symbolic manipulation programs. Also, with the advent of high speed computers, the finite element approach becomes more and more favorable for specific design purposes. However, like most numerically based approaches, the finite element approach can only provide pointwise information in parameter space regarding the response. A recent finite element study[12] used more than one hundred simulations with a commercially available package to obtain a response curve. We must admit that the finite element approach will provide more reliable and accurate solutions. However, this analytical approach provides important information

useful for the prediction of the influence of various parameters, and a theoretical explanation for the nonlinear phenomena associated with these systems.

Future works in this area can be separated into several distinct directions. First, this analysis can be directly extended to study the elastic behavior associated with the flexible coupler of an otherwise rigid four-bar mechanism. Second, for a more complete understanding of the elastic behavior of the slider crank mechanism, the flexibility of the crank shaft needs to be included. Moreover, the effects of off-set, clearances in the bearings, piston cylinder clearances, external force on the slider mass, and out-of-pane deformation should also be included. An application of Hsu's method[24] to study the linearized model, with multi-degree-of-freedom, should also be considered. A detailed study to the slider crank mechanism with low frequency ratio  $\Omega$  and large length ratio  $\xi$  is recommended.

As for the general improvement in the analysis techniques for elastic mechanism problems, a more thorough understanding of the inertia force is required. In all previous analytical works, the dynamics of the flexible link is formulated relative to a coordinate system that follows the rigid body motion of the beam. This approach presumes an infinitesimal strain and is sometimes referred to as the shadow beam approach. In future work, it is intended to include large overall motion and strains by employing geometrically exact formulations. Recent results from Simo and Vu-Quoc[38, 39] may prove useful for this extension.

In addition, future work should include careful systematic experiments to verify the modeling assumptions and to examine the nature and consequences of the behaviors predicted in this study.



## Appendix A

#### Construction of the Linear Operator

In this appendix, we consider the flexural vibration of a simply supported beam subjected to the following conditions: (1) a distributed force is applied along the span of this beam, (2) concentrated bending moments are applied at both ends, and (3) motion of the supporting foundation. This is modeled by a linear partial differential equation subjected to nonhomogeneous boundary conditions. Because of the linear nature of the partial differential operator, it can be converted into a partial differential equation with homogeneous boundary conditions. In this appendix, we solve this problem by using concepts from vibration theory [16, 46] rather than rigorous mathematical arguments. Therefore, the transverse deflection will be described by a linear partial differential equation subjected to a set of homogeneous boundary conditions, which can then be truncated by Galerkin's method with the usual linear mode shape functions. To achieve this goal, we first convert the nonhomogeneous kinematical (or rigid) boundary conditions[16] into homogeneous ones by considering the motions of the foundation. Next, we consider the natural boundary conditions and obtain the equivalent partial differential equation with homogeneous boundary conditions. Based on this equivalent equation, and its associated boundary conditions, we then apply Galerkin's procedure to transform the continuous system into a discrete system. After this procedure has been presented completely, we then provide an example problem to demonstrate this procedure.

The transverse deflection of this simply supported beam is described by

$$\alpha_1 \pi^4(D_0^2 v) + \alpha_1 v_{xxxx} = Q_1(x, t), \tag{A.1}$$

with the following boundary conditions:

$$v(0,t) = Q_2(t), \qquad (A.2)$$

$$v(1,t) = Q_3(t), \qquad (A.3)$$

$$v_{xx}(0,t) = Q_4(t), (A.4)$$

$$v_{xx}(1,t) = Q_5(t), (A.5)$$

where  $D_0$  represents derivative with respect to the time variable,  $Q_1(x,t)$  represents a distributed load applied along the span of the beam,  $Q_2(t)$  and  $Q_3(t)$  stand for the motion of the left and right points, respectively, and  $Q_4(t)$  and  $Q_5(t)$  represent the bending moments applied to the left and right ends, respectively. We note that the first two boundary conditions are referred to as the kinematical boundary conditions, while, equations (A.4) and (A.5) are referred to as the natural boundary conditions. Our goal is to find an equivalent ordinary differential equation which takes the form,

$$\alpha_1 \pi^4 (D_0^2 w_n) + \omega_n^2 w_n = q_n(t) \tag{A.6}$$

describing the amplitude of the transverse deflection of this simply supported beam. First, we compensate for the motion of the foundation by letting

$$v(x,t) = \bar{w}(x,t) + Q_2(t)(1-x) + Q_3(t). \tag{A.7}$$

Substituting this expression into equation (A.1) and its associated boundary conditions (A.2) to (A.5), we obtain

$$\alpha_1 \pi^4 D_0^2 \bar{w} + \alpha_1 \bar{w}_{xxxx} = Q(x, t) = Q_1(x, t) - \alpha_1 \pi^4 D_0^2 [Q_2(1 - x) + Q_3]$$
(A.8)

and the following boundary conditions:

$$\bar{w}(0,t) = 0, \qquad (A.9)$$

$$\bar{w}(1,t) = 0, \tag{A.10}$$

$$\bar{w}_{xx}(0,t) = Q_4(t),$$
 (A.11)

$$\bar{w}_{xx}(1,t) = Q_5(t)$$
. (A.12)

This procedure transforms the kinematical boundary conditions to zero, and replaces the effect of the beam motion by a modification of the distributed force acting on the beam. We note that equation (A.8) and its associated boundary conditions (A.9) to (A.12) correspond to a simply supported beam subjected to concentrated bending moments applied at each end. Next, we apply the principle of virtual work to handle the nonhomogeneous bending moments (A.11) and (A.12). First, we compute the virtual work done by the inertial force,

$$\delta U_1 = -\alpha_1 \pi^4 \int_0^1 (D_0^2 \bar{w}) \delta w ds \tag{A.13}$$

and the virtual work done by the elastic force and the external loads

$$\delta U_2 = -\delta \left( \int_0^1 \alpha_1 \bar{w}_{xx}^2 dx \right) + \int_0^1 Q(x,t) \delta \bar{w} dx$$

$$= -\alpha_1 \bar{w}_{xx} \delta \bar{w}_x + \alpha_1 \bar{w}_{xxx} \delta \bar{w} - \alpha_1 \int_0^1 \bar{w}_{xxxx} \delta \bar{w} dx + \int_0^1 Q(x,t) \delta \bar{w} dx . \quad (A.14)$$

From the principle of virtual work, we must have

$$\delta(U_1 + U_2) = 0 \tag{A.15}$$

which yields

$$\int_0^1 \alpha_1 \pi^4 D_0^2 \bar{w} \delta \bar{w} dx = -\int_0^1 \bar{w}_{xxxx} \delta \bar{w} dx + \int_0^1 Q(x, t) \delta \bar{w} dx$$
$$- \alpha_1 \bar{w}_{xx} \delta \bar{w}_x + \alpha_1 \bar{w}_{xxxx} \delta \bar{w} . \tag{A.16}$$

We now assume  $\bar{w} = w_n(\sin n\pi x)$  and employ the boundary conditions for equation (A.16). After carrying out all the integrations, we obtain

$$\alpha_1 \pi^4 D_0^2 w_n + \omega_n^2 w_n = q_n(t) - \alpha_1 \frac{n\pi}{2} [Q_5(t) \cos n\pi - Q_4(t)]$$
 (A.17)

where

$$q_n(t) = 2 \int_0^1 Q(x,t) \sin n\pi x ds$$

$$= 2 \int_0^1 Q_1(x,t) \sin n\pi x dx - 2\alpha_1 \pi^4 D_0^2 \int_0^1 [Q_2(1-x) + Q_3] \sin n\pi x dx (A.18)$$

represents the component of the external force projected onto the n-th mode.

To demonstrate the procedure described above, let us consider the following equation, from section 3.1:

$$\alpha_1 \pi^4 (D_0^2 v_3) + \alpha_1 v_{3xxx} = Q_1(x, t) \tag{A.19}$$

$$Q_{1}(x,t) = -\alpha_{1}^{2}\alpha_{2}v_{1xxxxx} - 2\alpha_{1}\mu_{2}D_{0}v_{1xxx} + (e_{0_{3}}v_{2x})_{x}$$

$$- \alpha_{1}(v_{1x}v_{1xx}^{2})_{x} + (e_{0_{4}}v_{1x})_{x} + \alpha_{1}^{2}\alpha_{3}\pi^{4}D_{0}^{2}v_{1xx}$$

$$- \alpha_{1}\pi^{4}(2D_{0}D_{2}v_{1} + 2D_{0}D_{1}v_{2} + D_{1}^{2}v_{1}) + \alpha_{1}\pi^{4}\xi_{1}^{2}\Omega^{2}v_{1}\cos\Omega T_{0}$$

$$+ 2\alpha_{1}\pi^{4}\xi_{1}\Omega(D_{0}u_{2})\cos\Omega T_{0} - \alpha_{1}\pi^{4}\xi_{1}\Omega^{2}u_{2}\sin\Omega T_{0}$$

$$- \alpha_{1}\pi^{4}\xi_{1}^{3}\Omega^{2}\frac{(1+x)}{2}\sin^{3}\Omega T_{0} + \alpha_{1}\pi^{4}\xi_{1}^{3}\Omega^{2}x\cos^{2}\Omega T_{0}\sin\Omega T_{0}$$
(A.20)

with the following boundary conditions:

$$v_3(0,t) = Q_2(t) = 0, (A.21)$$

$$v_3(1,t) = Q_3(t) = \frac{1}{4} (n\pi)^2 \hat{v}_n^2 \xi_1 \sin \Omega T_0 , \qquad (A.22)$$

$$v_{3xx}(0,t) = Q_4(t) = -(\frac{v_{1x}^3}{6} + \alpha_1 \alpha_2 v_{1xxx})_x - 2\mu_{3_2} D_0 \hat{v}_{1n} - 2\mu_{3_2} \xi_1 \Omega \cos \Omega T_0, (A.23)$$

$$v_{3xx}(1,t) = Q_5(t) = -(\frac{v_{1x}^3}{6} + \alpha_1 \alpha_2 v_{1xxx})_x + 2\mu_{3x} D_0 \hat{v}_{1n} - 2\mu_{3x} \xi_1 \Omega \cos \Omega T_0 . (A.24)$$

After applying the procedure, we obtain

$$\begin{split} D_0{}^2\hat{v}_{3n} &+ \omega_n^2\hat{v}_{3n} = -2j\omega_n(D_2A_n + \mu_{2_2}n^4A_n)exp(j\omega_nT_0) \\ &- j\mu_{4_0}(n\pi)^4\omega_nA_n^2\bar{A}_nexp(j\omega_nT_0) - j(\frac{\mu_{4_0}}{2})(n\pi)^4\omega_nA_n\Lambda_1^2exp(j\omega_nT_0) \\ &+ 2A_n(\alpha_1\alpha_2 + \alpha_1\alpha_3)(n\pi)^2n^4exp(j\omega_nT_0) \\ &- [\frac{15}{8} - (\frac{1}{3} + S)(n\pi)^2]n^4(n\pi)^2A_n^2\bar{A}_nexp(j\omega_nT_0) \\ &+ \frac{2}{\pi^2}jn^4\mu_{3_2}A_nexp(j\omega_nT_0) + (\frac{1}{8})\mu_{4_0}(n\pi)^4\Omega\Lambda_1^3exp(3j\Omega T_0) \\ &+ jf_2\xi_1^3exp(3j\Omega T_0) + f_1\xi_1^2A_nexp(j\omega T_0) + jf_3\bar{A}_n^2\xi_1exp(j\Omega T_0 - 2j\omega_nT_0) \end{split}$$

+ 
$$\mu_{4_0}\bar{A}_n^2(n\pi)^4\Lambda_1(\frac{\Omega}{2}-\omega_n)exp(j\Omega T_0-2j\omega_n T_0)+N.S.T.+c.c.$$
 (A.25)

$$f_{1} = \frac{\Omega^{2}}{8} + \frac{\pi^{2}n^{2}\Omega^{2}}{12} - \frac{27n^{4}\Omega^{4}}{8(\omega_{n}^{2} - \Omega^{2})^{2}} - \frac{\pi^{2}n^{6}\Omega^{4}}{6(\omega_{n}^{2} - \Omega^{2})^{2}}$$

$$- \frac{3\Omega^{6}}{8(\omega_{n}^{2} - \Omega^{2})^{2}} - \frac{\pi^{2}n^{2}\Omega^{6}}{6(\omega_{n}^{2} - \Omega^{2})^{2}} + \frac{n^{2}\Omega^{3}\cos n\pi}{(\omega_{n}^{2} - \Omega^{2})} + \frac{2\Omega^{4}\cos n\pi}{(\omega_{n}^{2} - \Omega^{2})}$$

$$+ \frac{2\Omega^{6}\Delta_{1}}{n^{2}(\omega_{n}^{2} - \Omega^{2})^{2}} + \frac{2n^{2}\Omega^{4}\Delta_{1}}{(\omega_{n}^{2} - \Omega^{2})^{2}} + \frac{\Omega^{4}\Delta_{1}^{2}}{n^{4}(\omega_{n}^{2} - (\Omega + \omega_{n})^{2})}, \qquad (A.26)$$

$$f_{2} = -\frac{\Omega^{2}}{8n\pi} - \frac{n^{3}\Omega^{6}}{2n\pi(\omega_{n}^{2} - \Omega^{2})^{3}} - \frac{3\Omega^{8}}{8n\pi(\omega_{n}^{2} - \Omega^{2})^{3}} - \frac{n\pi\Omega^{8}}{6(\omega_{n}^{2} - \Omega^{2})^{3}}$$

$$-\frac{\Omega^{4}}{16n\pi(\omega_{n}^{2} - \Omega^{2})} - \frac{n\pi\Omega^{4}}{24(\omega_{n}^{2} - \Omega^{2})} + \frac{\Omega^{2}\cos n\pi}{4n\pi} - \frac{3\Omega^{6}\cos n\pi}{n\pi(\omega_{n}^{2} - \Omega^{2})}$$

$$-\frac{\Omega^{4}\Delta_{1}}{2n\pi(\omega_{n}^{2} - 4\Omega^{2})} + \frac{2\Omega^{8}\Delta_{1}}{n^{3}\pi(\omega_{n}^{2} - \Omega^{2})^{3}} + \frac{\Omega^{4}\Delta_{1}}{n^{3}\pi(\omega_{n}^{2} - \Omega^{2})}$$

$$+\frac{\Omega^{4}\Delta_{1}\cos n\pi}{2n^{3}\pi(\omega_{n}^{2} - 4\Omega^{2})} + \frac{\Omega^{6}\Delta_{1}^{2}}{n^{5}\pi(\omega_{n}^{2} - \Omega^{2})(\omega_{n}^{2} - 4\Omega^{2})}, \qquad (A.27)$$

$$f_{3} = \frac{3\pi n^{5}\Omega^{2}}{2(\omega_{n}^{2} - \Omega^{2})} + \frac{3\pi n\Omega^{4}}{16(\omega_{n}^{2} - \Omega^{2})} - \frac{\pi^{3}n^{3}\Omega^{4}}{6(\omega_{n}^{2} - \Omega^{2})} - \frac{\pi^{3}Sn^{3}\Omega^{4}}{2(\omega_{n}^{2} - \Omega^{2})}$$

$$- \frac{3\pi n\Omega^{3}\omega_{n}}{8(\omega_{n}^{2} - \Omega^{2})} + \frac{\pi^{3}n^{3}\Omega^{3}\omega_{n}}{3(\omega_{n}^{2} - \Omega^{2})} + \frac{\pi^{3}Sn^{3}\Omega^{3}\omega_{n}}{(\omega_{n}^{2} - \Omega^{2})} + \frac{9n\pi\Omega^{2}\omega_{n}^{2}}{16(\omega_{n}^{2} - \Omega^{2})}$$

$$- \frac{\pi^{3}n^{3}\Omega^{2}\omega_{n}^{2}}{2(\omega_{n}^{2} - \Omega^{2})} - \frac{3(n\pi)^{3}S\Omega^{2}\omega_{n}^{2}}{2(\omega_{n}^{2} - \Omega^{2})} - \frac{n\pi\Omega^{2}\cos n\pi}{4}, \qquad (A.28)$$

and N.S.T. represents those terms which have no effects in considering the secular terms of the particular solution of  $v_{3n}$ . When the frequency ratio  $\Omega$  is near to  $\frac{\omega_n}{3}$ , the superharmonic resonance takes place. Under this condition, equation (A.25) reduces to

$$D_0^2 \hat{v}_{3n} + \omega_n^2 \hat{v}_{3n} = -2j\omega_n(D_2 A_n + \mu_{2_1} n^4 A_n) exp(j\omega_n T_0)$$

$$+ (\alpha_{1}\alpha_{3} + \alpha_{1}\alpha_{2})(n\pi)^{2}n^{4}exp(j\omega_{n}T_{0}) + j\frac{2}{\pi^{2}}n^{4}\mu_{3_{2}}A_{n}exp(j\omega_{n}T_{0})$$

$$- (n\pi)^{2}n^{4}\left[\frac{8}{15} - (\frac{1}{3} + S)(n\pi)^{2}\right]A_{n}^{2}\bar{A}_{n}exp(j\omega_{n}T_{0})$$

$$+ f_{1_{1}}\xi_{1}^{2}A_{n}exp(j\omega_{n}T_{0}) + jf_{2_{1}}\xi_{1}^{3}exp(3j\Omega T_{0})$$

$$- j\mu_{4_{0}}(n\pi)^{4}A_{n}^{2}\bar{A}_{n}exp(j\omega_{n}T_{0}) - j(\frac{\mu_{4_{0}}}{32})(n\pi)^{2}\omega_{n}\xi_{1}^{2}A_{n}exp(j\omega_{n}T_{0})$$

$$+ \frac{\mu_{4_{0}}}{1536}(n\pi)\omega_{n}\xi_{1}^{3}exp(3j\Omega T_{0}) + N.S.T. + c.c.$$
(A.29)

$$f_{1_1} = \frac{-91n^4}{2304} + \frac{11\pi^2n^6}{1728} + \frac{5n^4\cos n\pi}{72} + \frac{5n^2\Delta_1}{144} - \frac{\Delta_1^2}{63}$$
 (A.30)

and

$$f_{2_1} = -\frac{583n^3}{36864\pi} - \frac{17\pi n^5}{27648} + \frac{61n^3 \cos n\pi}{2304\pi} + \frac{37n\Delta_1}{11520\pi} + \frac{n\Delta_1 \cos n\pi}{90\pi} + \frac{\Delta_1^2}{360n\pi} . \tag{A.31}$$

This case is fully investigated in section 3.5.

Next, we consider the case in which the frequency ratio  $\Omega$  is near to  $3\omega_n$ . Under this condition, a subharmonic resonance takes place and equation (A.25) reduces to

$$D_{0}^{2}\hat{v}_{3n} + \omega_{n}^{2}\hat{v}_{3n} = -2j\omega_{n}(D_{1}A_{n} + \mu_{2}n^{4}A_{n})exp(j\omega_{n}T_{0})$$

$$+ A_{n}(\alpha_{1}\alpha_{2} + \alpha_{1}\alpha_{3})(n\pi)^{2}n^{4}exp(j\omega_{n}T_{0})$$

$$- \left[\frac{15}{8} - (\frac{1}{3} + S)(n\pi)^{2}\right]n^{4}(n\pi)^{2}A_{n}^{2}\bar{A}_{n}exp(j\omega_{n}T_{0})$$

$$+ \frac{2}{\pi^{2}}jn^{4}\mu_{3}A_{n}exp(j\omega_{n}T_{0}) + f_{1}^{2}\xi_{1}^{2}A_{n}exp(j\omega T_{0})$$

$$+ jf_{3}\bar{A}_{n}^{2}\xi_{1}exp(j\Omega T_{0} - 2j\omega_{n}T_{0}) - j\mu_{4}(n\pi)^{4}\omega_{n}A_{n}^{2}\bar{A}_{n}exp(j\omega_{n}T_{0})$$

$$- j(\frac{81}{32})(n\pi)^{2}\omega_{n}\mu_{4}\xi_{1}^{2}A_{n}exp(j\omega_{n}T_{0})$$

$$+ (\frac{9}{8})(n\pi)^{3}\omega_{n}\mu_{4}\xi_{1}\bar{A}_{n}^{2}exp(j\Omega T_{0} - 2\omega_{n}T_{0}) + N.S.T. + c.c.$$
(A.32)

$$f_{1_2} = -\frac{1899n^4}{256} - \frac{87\pi^2n^6}{64} - \frac{189n^4\cos n\pi}{8} + \frac{405n^2\Delta_1}{16} - \frac{27\Delta_1^2}{5}$$
 (A.33)

and

$$f_{3_1} = -\frac{189}{64}\pi n^5 - \frac{9}{16}\pi^3 n^7 + \frac{27}{16}n^3\pi^3 + \frac{27}{8}\pi^3 S n^3 - \frac{9}{4}\pi n^5 \cos n\pi . \tag{A.34}$$

This case is studied in detail in section 3.6.

## Appendix B

## Superharmonic and Principal Parametric

# Resonances for $\xi = \epsilon \xi_1$

Recalling that in analyzing the particular solution of  $\hat{v}_{2n}$ , we need to distinguish between the following cases: (1)  $\Omega$  is near to  $2\omega_n$ , (2)  $\Omega$  is near to  $\frac{\omega_n}{2}$ , and (3)  $\Omega$  is away from  $2\omega_n$  and  $\frac{\omega_n}{2}$ . The first case corresponds to the principal parametric resonance, while the second one corresponds a superharmonic resonance. When these two resonances take place, it is necessary to reorder the damping parameters  $\mu_2$  and  $\mu_4$  so that they will appear, together with the detuning parameter  $\sigma_1$ , in the final resonant condition. To achieve this goal, we rescale the damping parameters  $\mu_2$  and  $\mu_4$  according to equations (3.49) and (3.10), and then redo all the relevant computations. In this appendix, we provide a detailed solution procedure for obtaining the final resonant condition.

Expanding equations (2.51), (2.52) and (2.53) with these newly reordered damping parameters, and equating the corresponding coefficients of the like-power terms in  $\epsilon$ , we obtain the following equations:

#### Order $\epsilon^3$

$$(u_{3x} + v_{1x}v_{2x})_x = (e_{0x})_x = -\alpha_1 \pi^4 \xi_1 \Omega^2 \cos \Omega T_0, \qquad (B.1)$$

$$\alpha_1 \pi^4 D_0^2 v_1 + \alpha_1 v_{1_{xxxx}} = \alpha_1 \pi^4 \xi_1 \Omega^2 (1 - x) \sin \Omega T_0 , \qquad (B.2)$$

Order  $\epsilon^4$ 

$$\alpha_1 \pi^4 D_0^2 v_2 + \alpha_1 v_{2xxxx} = (e_{0_3} v_{1x})_x - 2\alpha_1 \pi^4 (D_0 D_1 v_1)$$

$$+ \alpha_1 \pi^4 \xi_1^2 \Omega^2 \cos \Omega T_0 \sin \Omega T_0 - 2\alpha_1 \mu_{2_1} D_0 v_{1xxxx}. \quad (B.3)$$

Applying the same procedure to the associated boundary conditions, we obtain the following boundary conditions:

Order  $\epsilon$ 

$$v_1 = v_{1xx} = 0$$
, at  $x = 0$ , (B.4)

$$v_1 = v_{1xx} = 0$$
, at  $x = 1$ , (B.5)

Order  $\epsilon^2$ 

$$v_2 = v_{2xx} = 0$$
, at  $x = 0$ , (B.6)

$$(u_{2x} + \frac{v_{1x}^2}{2}) = v_2 = 0, v_{2xx} = -2\mu_{3_2}\Omega$$
, at  $x = 1$ , (B.7)

Order  $\epsilon^3$ 

$$u_{3x} + v_{1x}v_{2x} = \alpha_1 \pi^4 \xi_1 \Omega^2 S \cos \Omega T_0 + 2\alpha_1 \pi^4 \mu_{4_0} \xi_1 \Omega \sin \Omega T_0 . \text{ at } x = 1,$$
 (B.8)

Note that we have dropped all the terms involved in products with  $e_{0_2}$  in obtaining the equations, since we have already shown that  $e_{0_2} = u_{2x} + \frac{v_{1x}^2}{2} = 0$  in section 3.1. We first project equation (B.2) onto the n-th mode by setting  $v_1 = \hat{v}_{1n}(\sin n\pi x)$  and integrating from x = 0 to x = 1, resulting in equation (3.29). The general solution of  $\hat{v}_{1n}$  is then given

in equation (3.30). Now, we solve the expression for  $e_{0_3}$  and obtain

$$e_{0_3} = (u_{3x} + v_{1x}v_{2x})$$

$$= \alpha_1 \pi^4 \xi_1 \Omega^2 (1 - x + S) \cos \Omega T_0 + 2\alpha_1 \pi^4 \mu_{4_0} \xi_1 \Omega \sin \Omega T_0.$$
 (B.9)

Hence, equation (B.3) reduces to

$$D_{0}^{2}\hat{v}_{2n} + \omega_{n}^{2}\hat{v}_{2n} = -2j\mu_{2_{1}}\omega_{n}n^{4}A_{n}exp(j\omega_{n}T_{0})$$

$$- 2j\omega_{n}(D_{1}A_{n})exp(j\omega_{n}T_{0})$$

$$+ (\frac{1-\cos n\pi}{2n\pi})\xi_{1}^{2}\Omega^{2}exp(2j\Omega T_{0} - j\pi/2)$$

$$- \frac{1}{4}(1+2S)(n\pi)^{2}A_{n}\xi_{1}\Omega^{2}exp(j\omega_{n}T_{0} + j\Omega T_{0})$$

$$- \frac{1}{4}(1+2S)(n\pi)^{2}\bar{A}_{n}\xi_{1}\Omega^{2}exp(-j\Omega T_{0} + j\omega_{n}T_{0})$$

$$- \frac{1}{4}(1+2S)(n\pi)^{2}\Lambda_{1}\xi_{1}\Omega^{2}exp(2j\Omega T_{0} - j\pi/2)$$

$$- \mu_{4_{0}}(n\pi)^{2}\xi_{1}\Omega\bar{A}_{n}exp(j\Omega T_{0} - j\omega_{n}T_{0} - j\pi/2)$$

$$+ \frac{(n\pi)^{2}}{2}\mu_{4_{0}}\xi_{1}\Omega\Lambda_{1}exp(2j\Omega T_{0}).$$
(B.10)

Note that the difference between this equation and equation (3.34) in section 3.1. When  $\Omega$  is near to  $2\omega_n$ , we describe  $\Omega$  as  $\Omega = 2(\omega_n + \epsilon \sigma_1)$ , then equation (B.10) reduces to

$$D_0^2 \hat{v}_{2n} + \omega_n^2 \hat{v}_{2n} = -2j\omega_n (D_1 A_n) exp(j\omega_n T_0) - 2j\omega_n n^4 \mu_{2_1} A_n exp(j\omega_n T_0)$$

$$-(1+2S)(n\pi)^2 \bar{A}_n \xi_1 \omega_n^2 exp(j\omega_n T_0 + 2j\sigma_1 T_1)$$

$$-2\mu_{4_0} (n\pi)^2 \xi_1 \omega_n \bar{A}_n exp(j\omega_n T_0 + 2j\sigma_1 T_1 - j\pi/2)$$

$$+N.S.T. + c.c.$$
(B.11)

which is equation (3.51) in section 3.2. When  $\Omega$  is near to  $\frac{\omega_n}{2}$ , we express  $\Omega$  as  $\Omega = \frac{1}{2}(\omega_n + \epsilon \sigma_1)$  in equation (3.51). In that case, we obtain

$$\begin{split} D_0^2 \hat{v}_{2n} &+ \omega_n^2 \hat{v}_{2n} = -2j(D_1 A_n) \omega_n exp(j\omega_n T_0) - 2j\omega_n n^4 \mu_{2_1} A_n exo(j\omega_n T_0) \\ &+ (n\pi)^2 \mu_{4_0} \xi_1 \Omega \Lambda_1 exp(2j\Omega T_0) + \frac{1 - \cos n\pi}{2n\pi} \xi_1^2 \Omega^2 exp(2j\Omega T_0 - j\pi/2) \\ &- \frac{1}{4} (1 + 2S)(n\pi)^2 \Lambda_1 \xi_1 \Omega^2 exp(2j\Omega T_0 - j\pi/2) + N.S.T. + c.c. \end{split} \tag{B.12}$$

which is equation (3.117) in section 3.4.

## Appendix C

# Solution Procedure for the Case $\xi = \epsilon^2 \xi_2$

In this appendix, we present a complete solution procedure for the case in which the length ratio  $\xi$  is scaled by  $\xi = \epsilon^2 \xi_2$ . Moreover, in order to have the damping parameters  $\mu_2$ ,  $\mu_3$  and  $\mu_4$  included in the final resonant equation, we scale these parameters according to equations (3.8), (3.9) and (3.10). Expanding equations (2.51), (2.52) and (2.53) with these ordering relations, and equating the coefficients of the like-power terms, we obtain the following equations:

Order  $\epsilon$ 

$$u_{1xx} = (e_{0_1})_x = 0 , (C.1)$$

Order  $\epsilon^2$ 

$$(u_{2x} + \frac{v_{1x}^2}{2})_x = e_{02} = 0 , (C.2)$$

Order  $\epsilon^3$ 

$$(u_{3x} + v_{1x}v_{2x})_x = (e_{0_3})_x = 0, (C.3)$$

$$\alpha_1 \pi^4 D_0^2 v_1 + \alpha_1 v_{1xxxx} = \left[ \left( u_{2x} + \frac{v_{1x}^2}{2} \right) v_{1x} \right]_x,$$
 (C.4)

Order  $\epsilon^4$ 

$$\left[u_{4x} + \frac{v_{1x}^4}{8} + \frac{v_{2x}^2}{2} + v_{1x}v_{3x}\right]_x + \alpha_1(v_{1x}v_{1xxx})_x = \alpha_1\pi^4(D_0^2u_2 - \xi_2\Omega^2\cos\Omega T_0), \quad (C.5)$$

$$\alpha_1 \pi^4 D_0^2 v_2 + \alpha_1 v_{2xxxx} = \alpha_1 \pi^4 \xi_2 \Omega^2 (1 - x) \sin \Omega T_0 - 2\alpha_1 \pi^4 D_0 D_1 v_1 , \qquad (C.6)$$

Order  $\epsilon^5$ 

$$\alpha_{1}\pi^{4}D_{0}^{2}v_{3} + \alpha_{1}v_{3xxxx} = -\alpha_{1}\pi^{4}(D_{1}^{2}v_{1} + 2D_{0}D_{2}v_{1} + 2D_{0}D_{2}v_{2})$$

$$+ \alpha_{1}^{2}\alpha_{3}\pi^{4}(D_{0}^{2}v_{1xx}) + (e_{0_{4}}v_{1x})_{x} - \alpha_{1}(v_{1x}v_{1xx}^{2})_{x}$$

$$- \alpha_{1}^{2}\alpha_{2}v_{1xxxxxx} - 2\alpha_{1}\mu_{2_{2}}D_{0}v_{1xxxx}, \qquad (C.7)$$

subjected to the following boundary conditions:

Order  $\epsilon^1$ 

$$u_1 = v_1 = v_{1xx} = 0,$$
 at  $x = 0,$  (C.8)

$$u_{1x} = v_1 = v_{1xx} = 0,$$
 at  $x = 1$ , (C.9)

Order  $\epsilon^2$ 

$$u_2 = v_2 = v_{2xx} = 0,$$
 at  $x = 0$ , (C.10)

$$(u_{2x} + \frac{v_{1x}^2}{2})_x = v_2 = 0, v_{2xx} = -2\mu_{3x}\Omega, \quad \text{at } x = 1,$$
 (C.11)

Order  $\epsilon^3$ 

$$u_3 = v_3 = 0 ,$$

$$v_{3xx} = -\left(\frac{v_{1x}^3}{6} + \alpha_1 \alpha_2 v_{1xxx}\right)_x + 2\mu_{3x} D_0 v_{1x}, \quad \text{at } x = 0 ,$$
(C.12)

$$(u_{3x}+v_{1x}v_{2x})=v_3=0,$$

$$v_{3xx} = -\left(\frac{v_{1x}^3}{6} + \alpha_1 \alpha_2 v_{1xxx}\right)_x + 2\mu_{3x} D_0 v_{1x}, \quad \text{at } x = 1,$$
 (C.13)

Order  $\epsilon^4$ 

$$(u_{4x} + \frac{v_{1x}^4}{8} + \frac{v_{2x}^2}{2} + v_{1x}v_{3x}) + \alpha_1(v_{1x}v_{1xxx}) = -2\alpha_1\pi^4\mu_{4_0}(D_0u_2)$$

$$- S\alpha_1\pi^4(D_0^2u_2) + S\alpha_1\pi^4\xi_2\Omega^2\cos\Omega T_0 - 2\alpha_1\pi^4\mu_{4_0}\xi_2\sin\Omega T_0, \text{ at } x = 1.(C.14)$$

Because we have already shown that  $e_{0_2} = (u_{2x} + \frac{v_{1x}^2}{2}) = 0$  in section 3.1, all terms involving products with this quantity have been dropped in obtaining these equations. Moreover, all terms involving products with  $e_{0_3} = (u_{3x} + v_{1x}v_{2x})$  are dropped also, because  $e_{0_3} = (u_{3x} + v_{1x}v_{2x}) = 0$  for the current case. To show this, we solve equations (C.3) and obtain its general solution which is

$$(u_{3x} + v_{1x}v_{2x}) = c_0 (C.15)$$

where  $c_0$  is a function independent of the spatial variable x and it must be equal to zero, because of the boundary condition (C.13). We now proceed to solve the first order equation for flexural vibration which is described by equation (C.4). Equation (C.4) becomes

$$D_0^2 \hat{v}_{1n} + \omega_n^2 \hat{v}_{1n} = 0 \tag{C.16}$$

after being discretized by Galerkin's procedure with  $v_1 = \hat{v}_{1n}(\sin n\pi x)$ . Hence, the general solution of  $\hat{v}_{1n}$  takes the form

$$\hat{v}_{1n} = A_n(T_1, T_2) \exp(j\omega_n T_0) + c.c.$$
 (C.17)

We then solve for  $u_2$  from the expression  $(u_{2x} + \frac{v_{1x}^2}{2}) = 0$  to obtain

$$u_2 = -\frac{1}{4}(n\pi)^2 \hat{v}_{1n}^2 \left(x + \frac{\sin 2n\pi x}{2n\pi}\right)$$
 (C.18)

where  $\hat{v}_{1n}$  is given in equation (C.17). With the solution of  $u_2$ , we next solve the expression for  $e_{0_4}$  and obtain

$$e_{0_4} = \left(u_{4x} + \frac{v_{1x}^4}{8} + \frac{v_{2x}^2}{2} + v_{1x}v_{3x}\right)$$

$$= \alpha_1 \pi^4 (\xi_2 \Omega^2) (1 - x + S) \cos \Omega T_0 - \alpha_1 v_{1x} v_{1xxx} - 2\alpha_1 \pi^4 \mu_{4_0} \xi_2 \Omega \sin \Omega T_0$$

$$+ \frac{1}{8} \alpha_1 \pi^4 (D_0^2 \hat{v}_{1n}^2) [-\sin n\pi x^2 + (n\pi)^2 (1 + 2S - x^2)]$$

$$+ \alpha_1 \pi^4 (n\pi)^4 \mu_{4_0} (D_0 \hat{v}_{1n}) \hat{v}_{1n} . \tag{C.19}$$

We can then convert equation (C.6) into

$$D_0^2 \hat{v}_{2n} + \omega_n^2 \hat{v}_{2n} = -2j\omega_n (D_1 \hat{v}_{1n}) exp(j\omega_n T_0) + \frac{2}{n\pi} \xi_2 \Omega^2 \sin \Omega T_0$$
 (C.20)

which is equation (3.66). In analyzing the particular solution of this equation, we need to distinguish the following cases: (1)  $\Omega$  is near to  $\omega_n$  and (2)  $\Omega$  is away from  $\omega_n$ . The case in which  $\Omega$  is near to  $\omega_n$  will be investigated in section 3.3. At the present time, we assume that  $\Omega$  is away from  $\omega_n$  and continue to consider the higher order equations. With all the information obtained up to the present, equation (C.7) becomes

$$\alpha_{1}\pi^{4}D_{0}^{2}v_{3} + \alpha_{1}v_{3xxxx} = -2\alpha_{1}\pi^{4}(D_{0}D_{2}v_{1}) + \alpha_{1}^{2}\alpha_{3}\pi^{4}(D_{0}^{2}v_{1xx}) - \alpha_{1}(v_{1x}v_{1xx}^{2})_{x}$$

$$- \alpha_{1}^{2}\alpha_{2}v_{1xxxxxx} - 2\alpha_{1}\mu_{2}D_{0}v_{1xxxx} - 2\alpha_{1}\pi^{4}\mu_{4_{0}}\xi_{2}\Omega v_{1xx}\sin\Omega T_{0}$$

$$- \alpha_{1}(v_{1x}^{2}v_{1xxx})_{x} + \alpha_{1}\pi^{2}[\xi_{2}\Omega^{2}(1-x+S)v_{1x}\cos\Omega T_{0}]_{x}$$

$$+ \alpha_{1}\pi^{2}[\frac{1}{8}(D_{0}^{2}\hat{v}_{1n}^{2})[-(\sin n\pi x)^{2} + (n\pi)^{2}(1-2S-x^{2})]v_{1x}]_{x}$$

$$+ \alpha_{1}\pi^{4}\mu_{4_{0}}(n\pi)^{2}(D_{0}\hat{v}_{1n})\hat{v}_{1n}v_{1xx}$$
(C.21)

subject to boundary conditions (C.12) and (C.13). This represents the flexural vibration of a simply-supported beam subjected to a distributed load and to concentrated moments applied at each end. This is a simplified case of the more general case handled in the Appendix A. Therefore, by applying the results obtained in the Appendix A, equation (C.21) can be converted into

$$D_0^2 \hat{v}_{3n} + \omega_n^2 = -2(D_0 D_2 \hat{v}_{1n}) - \alpha_1 \alpha_3 n^2 (D_0^2 \hat{v}_{1n}) + \frac{1}{4} n^6 \pi^2 \hat{v}_{1n}^3$$

$$+ \alpha_1 \alpha_2 \pi^2 n^4 \hat{v}_{1n} - 2\mu_{22} n^4 (D_0 \hat{v}_{1n}) - (\frac{1}{2} + S) \pi^2 n^2 \omega_n^2 \xi_2 \hat{v}_{1n} \cos \Omega T_0$$

$$- \frac{3}{4} n^4 \pi^2 \hat{v}_{1n}^3 (\frac{1}{16} - \frac{(n\pi)^2}{12} - \frac{S(n\pi)^2}{4}) + (n\pi)^2 \xi_2 \hat{v}_{1n} \mu_{4_0} \Omega \sin \Omega T_0$$

$$- j\mu_{4_0} (n\pi)^2 A_n^2 \bar{A}_n exp(j\omega_n T_0)$$
(C.22)

by Galerkin's procedure with  $v_3 = \hat{v}_{3n} \sin n\pi x$ . This equation is the equation describing the resonance condition for the principal parametric resonance. We note that the there are two friction type forces in this equation, both arise from slider friction. The  $[(n\pi)^2 \xi_2 \hat{v}_{1n} \mu_{40} \Omega \sin \Omega T_0]$  term arises because the action of rigid body motion; while the  $[-j\mu_{40}(n\pi)^2 A_n^2 \bar{A}_n exp(j\omega_n T_0)]$  represents the contribution of elastic deformation.

## Appendix D

# Solution Procedure for the Case $\xi = \epsilon^3 \xi_3$

In this appendix, we present a detailed solution procedure for equations (2.51), (2.52) and (2.53) expanded with  $\xi = \epsilon^3 \xi_3$ ,  $\mu_2 = \epsilon^2 \mu_{2_2}$ ,  $\mu_3 = \epsilon^2 \mu_{3_2}$  and  $\mu_4 = \mu_{4_0}$ . We expand equations (2.51), (2.52) and (2.53) with these new ordering relations and solve them sequentially. After application of the procedure in Appendix A to the partial differential equation describing the third order flexural vibration, we obtain the ordinary differential equation which is used in section 3.3.

Expanding equation (2.51), (2.52), (2.53) and their associated boundary conditions with these ordering relations, and equating the coefficients of the like-powered terms in  $\epsilon$ , we obtain the following equations:

Order  $\epsilon$ 

$$u_{1xx} = (e_{0_1})_x = 0 (D.1)$$

Order  $\epsilon^2$ 

$$(u_{2x} + \frac{v_{1x}^2}{2})_x = (e_{02})_x = 0,$$
 (D.2)

Order  $\epsilon^3$ 

$$(u_{3x} + v_{1x}v_{2x})_x = (e_{0_3})_x = 0, (D.3)$$

$$\alpha_1 \pi^4 D_0^2 v_1 + \alpha_1 v_{1xxxx} = \left[ \left( u_{2x} + \frac{v_{1x}^2}{2} \right) v_{1x} \right]_x, \qquad (D.4)$$

Order  $\epsilon^4$ 

$$u_{4x} + \frac{v_{1x}^4}{8} + \frac{v_{2x}^2}{2} + v_{1x}v_{3x} + \alpha_1(v_{1x}v_{1xxx})_x = \alpha_1\pi^4(D_0^2u_2), \qquad (D.5)$$

$$\alpha_1 \pi^4 D_0^2 v_2 + \alpha_1 v_{2xxxx} = -2\alpha_1 \pi^4 D_0 D_1 v_1 , \qquad (D.6)$$

Order  $\epsilon^5$ 

$$\alpha_{1}\pi^{4}D_{0}^{2}v_{3} + \alpha_{1}v_{3xxxx} = -\alpha_{1}\pi^{4}(D_{1}^{2}v_{1} + 2D_{0}D_{2}v_{1} + 2D_{0}D_{2}v_{2})$$

$$+ \alpha_{1}^{2}\alpha_{3}\pi^{4}D_{0}^{2}v_{1xx} + (e_{0_{4}}v_{1x})_{x} - \alpha_{1}(v_{1x}v_{1xx}^{2})_{x} - \alpha_{1}^{2}\alpha_{2}v_{1xxxxx}$$

$$- 2\alpha_{1}\mu_{2_{2}}D_{0}v_{1xxxx} + \alpha_{1}\pi^{4}\xi_{3}\Omega^{2}(1-x)\sin\Omega T_{0}, \qquad (D.7)$$

subjected to the following boundary conditions:

Order  $\epsilon$ 

$$u_1 = v_1 = v_{1xx} = 0$$
, at  $x = 0$ , (D.8)

$$u_{1x} = v_1 = v_{1xx} = 0$$
, at  $x = 1$ , (D.9)

Order  $\epsilon^2$ 

$$u_2 = v_2 = v_{2xx} = 0$$
, at  $x = 0$ , (D.10)

$$(u_{2x} + \frac{v_{1x}^2}{2}) = v_2 = 0, v_{2xx} = -2\mu_{3x}\Omega, \quad \text{at } x = 0,$$
 (D.11)

Order  $\epsilon^3$ 

$$u_3 = v_3 = 0 ,$$

$$v_{3xx} = -(\frac{v_{1x}^3}{6} + \alpha_1 \alpha_2 v_{1xxx})_x + 2\mu_{3x} D_0 v_{1x} , \quad \text{at } x = 0 , \qquad (D.12)$$

$$(u_{3x} + v_{1x}v_{2x}) = v_3 = 0 ,$$

$$v_{3xx} = -(\frac{v_{1x}^3}{6} + \alpha_1\alpha_2v_{1xxx})_x + 2\mu_{3x}D_0v_{1x} , \quad \text{at } x = 1 ,$$
 (D.13)

Order  $\epsilon^4$ 

$$(u_{4x} + \frac{v_{1x}^4}{8} + \frac{v_{2x}^2}{2} + v_{1x}v_{3x}) + \alpha_1(v_{1x}v_{1xxx}) = -S\alpha_1\pi^4(D_0^2u_2)$$
$$- 2\alpha_1\pi^4\mu_{40}(D_0u_2), \text{ at } x = 1.$$
(D.14)

Note that in obtaining these equations and boundary conditions, we have dropped all those terms involving products with  $e_{0_2}=(u_{2x}+v_{1x}^2/2)$  and  $e_{0_3}=(u_{3x}+v_{1x}v_{2x})$ , since these two quantities are zero. Equation (D.4) can be truncated with  $v_1=\hat{v}_{1n}(\sin n\pi x)$  to obtain

$$D_0^2 \hat{v}_{1n} + \omega_n^2 \hat{v}_{1n} = 0 \tag{D.15}$$

which admits the following solution:

$$\hat{v}_{1n} = A_n(T_1, T_2) exp(j\omega_n T_0) + c.c.$$
 (D.16)

where c.c. stands for the complex conjugate term of the preceding terms. Substituting this solution of  $\hat{v}_{1n}$  into  $u_{2x} + \frac{v_{1x}^2}{2} = 0$  and solving for  $u_2$ , we obtain

$$u_2 = -\frac{1}{4}(n\pi)^2 \hat{v}_{1n}^2 \left(x + \frac{\sin 2n\pi x}{2n\pi}\right)$$
 (D.17)

where  $\hat{v}_n$  is given in equation (D.16). Now, we solve equation (D.5) and obtain

$$u_{4x} + \frac{v_{1x}^4}{8} + \frac{v_{2x}^2}{2} + v_{1x}v_{3x} = -\alpha_1(v_{1x}v_{1xxx}) + \alpha_1\pi^4\mu_{40}(n\pi)^4(D_0\hat{v}_{1n})\hat{v}_{1n}$$

$$+ \frac{1}{8}\alpha_1\pi^4(D_0^2\hat{v}_{1n}^2)[(n\pi)^2(1+2S-x^2)-(\sin n\pi x)^2]$$
 (D.18)

which is the forth order relative elongation along the median line. In obtaining the solution of  $\hat{v}_{2n}$ , we need to consider the following equation:

$$D_0^2 \hat{v}_{2n} + \omega_n^2 \hat{v}_{2n} = -2j\omega_n (D_1 A_n) exp(j\omega_n T_0) - \frac{2}{n\pi} \mu_{3_2} \Omega \cos n\pi + c.c.$$
 (D.19)

where  $-\frac{2}{n\pi}\mu_{3_2}\Omega\cos n\pi$  comes from the nonhomogeneous boundary condition. To remove the secular term from the particular solution of  $\hat{v}_{2n}$ , we must have  $(D_1A_n)=0$ . This implies that  $A_n$  must be independent of the time scale  $T_1$ . Collecting this information, equation (D.7) reduces to

$$\alpha_{1}\pi^{4}(D_{0}^{2}v_{3}) + \alpha_{1}v_{3xxx} = \alpha_{1}\pi^{4}\xi_{3}\Omega^{2}(1-x)\sin\Omega T_{0} - \alpha_{1}\pi^{4}(2D_{0}D_{2}v_{1})$$

$$+ \alpha_{1}^{2}\alpha_{3}\pi^{4}(D_{0}^{2}v_{1xx}) - \alpha_{1}(v_{1x}v_{1xx}^{2})_{x} - \alpha_{1}^{2}\alpha_{2}v_{1xxxxx}$$

$$- 2\alpha_{1}\mu_{2_{2}}D_{0}v_{1xxxx} - \alpha_{1}(v_{1x}^{2}v_{1xxx})_{x} + \alpha_{1}\pi^{4}\mu_{4_{0}}(n\pi)^{4}(D_{0}\hat{v}_{1n})\hat{v}_{1n}v_{1xx}$$

$$+ \frac{1}{8}\alpha_{1}\pi^{4}(D_{0}^{2}\hat{v}_{1n}^{2})[[(n\pi)^{2}(1+2S-x^{2})-\sin n\pi x^{2}]v_{1x}]_{x}$$
 (D.20)

subjected to boundary conditions (D.12) and (D.13). This equation and its associated boundary conditions correspond to a simply supported beam subjected to distributed load applied along its span and concentrated moments applied to each end. By using the procedure described in Appendix A, equation (D.20) and its associated boundary conditions can be transformed into the following equivalent system:

$$D_0^2 \hat{v}_{3n} + \omega_n^2 \hat{v}_{3n} = -2j\omega_n (D_1 A_n) exp(j\omega_n T_0) - j\mu_{4_0} (n\pi)^4 A_n^2 \bar{A}_n exp(j\omega_n T_0)$$
$$+ A_n (n\pi)^2 n^6 (\alpha_1 \alpha_2 + \alpha_1 \alpha_3) exp(j\omega_n T_0)$$

$$-2j\omega_{n}n^{4}\mu_{2}A_{n}exp(j\omega_{n}T_{0}) + 2j\frac{n^{4}}{\pi^{2}}\mu_{3}A_{n}exp(j\omega_{n}T_{0})$$

$$-\left[\frac{15}{8} - (\frac{1}{3} + S)(n\pi)^{2}\right](n\pi)^{2}n^{4}A_{n}^{2}\bar{A}_{n}exp(j\omega_{n}T_{0}) + N.S.T. + c.c. \quad (D.21)$$

which is the resonant equation considered in section 3.3. We note that the term involving with the friction parameter  $\mu_4$  in the last equation represents the slider friction force due to the foreshortening. We note that the  $\left[\mu_{4_0}(n\pi)^4A_n^2\bar{A}_n\right]$  term in the last equation represents the contribution of the slider friction acting on the connecting rod.

#### Appendix E

## Coefficients $f_7$ and $f_8$

In this appendix, the values of  $f_7$ ,  $f_8$  and  $f_9$  in equation (4.36) are given. First, we present the function  $f_7$ , which is the coefficient multiplying  $exp(jT_0)$ ,

$$f_7 = \frac{5\Omega^2}{8} + \frac{6\pi^2 S\Omega^4}{(1 - \Omega^2)^2} - \frac{2\Omega^2}{1 - \Omega^2} - \frac{4\Omega^4}{1 - \Omega^2} + \frac{\pi^4 \Omega^4}{16(1 - (1 + \Omega)^2)} + \frac{\pi^4 S\Omega^4}{4(1 - (1 + \Omega)^2)} + \frac{\pi^4 S^2 \Omega^4}{4(1 - (1 + \Omega^2)^2)}.$$
 (E.1)

For the superharmonic resonance occurring at  $\Omega \approx (\frac{1}{3})$ , the coefficient  $f_7$  becomes

$$f_{7_1} = -\frac{17}{72} - \frac{\pi^4}{1008} + \frac{3\pi^2 S}{32} - \frac{\pi^4 S}{252} - \frac{\pi^4 S^2}{252} . \tag{E.2}$$

For the subharmonic resonance taking place at  $\Omega \approx 3$ , the coefficient  $f_7$  becomes

$$f_{7_2} = \frac{387}{8} - \frac{27\pi^4}{80} + \frac{243\pi^2 S}{32} - \frac{27\pi^4 S}{20} - \frac{27\pi^4 S^2}{20} . \tag{E.3}$$

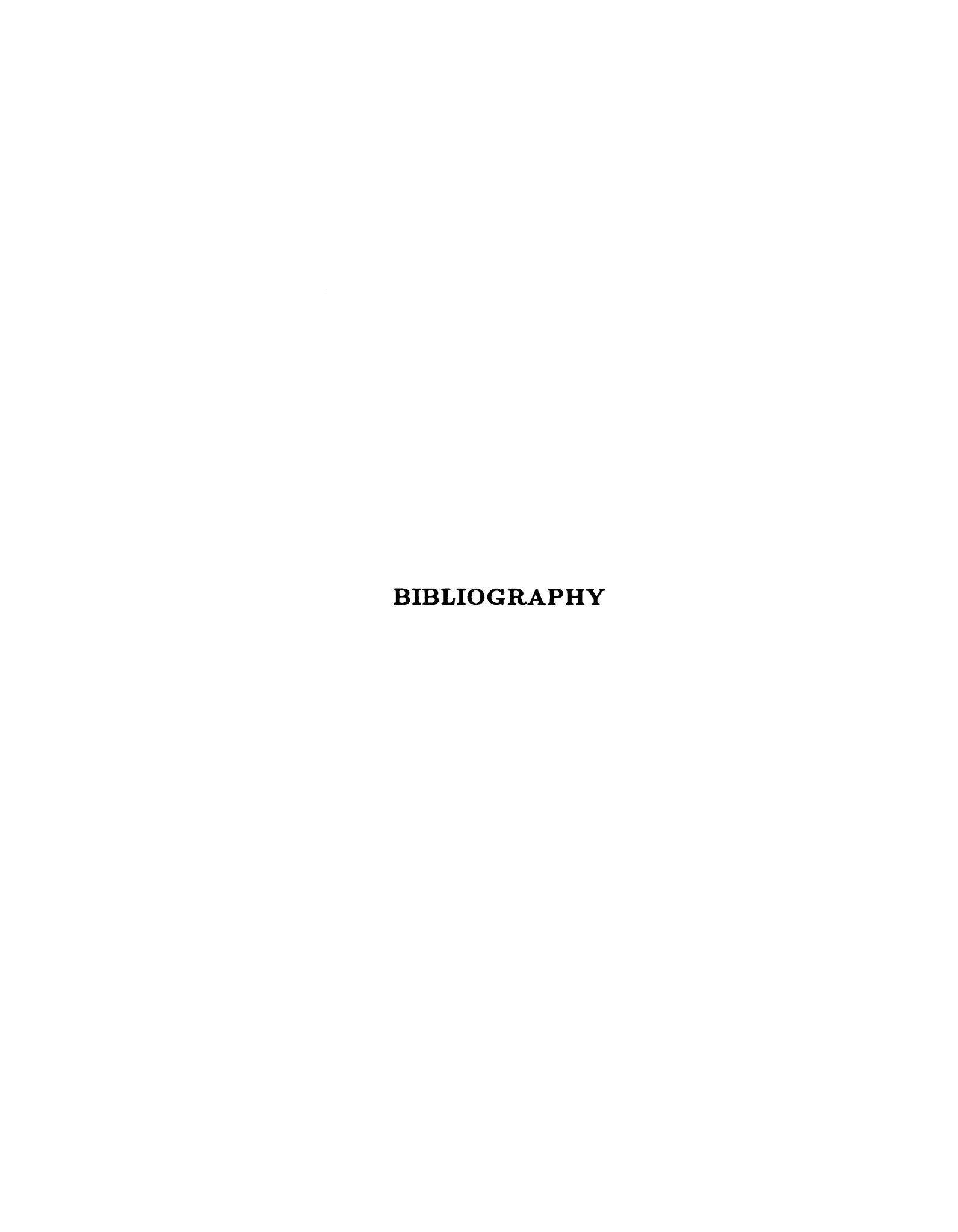
Next, let us consider the coefficient function  $f_8$ . The coefficient multiplying  $exp(3j\Omega T_0)$  is given by

$$f_8 = \frac{-5\Omega^2}{8\pi} + \frac{\pi\Omega^4}{4(1-4\Omega^2)} + \frac{\pi S\Omega^4}{2(1-4\Omega^2)} + \frac{9\pi S\Omega^8}{(1-\Omega^2)^3} - \frac{5\Omega^6}{2\pi(1-\Omega^2)^2}$$

$$-\frac{5\Omega^{4}}{16\pi(1-\Omega^{2})} + \frac{\pi\Omega^{4}}{6(1-\Omega^{2})} + \frac{\pi S\Omega^{4}}{2(1-\Omega^{2})} - \frac{\pi^{3}\Omega^{6}}{16(1-4\Omega^{2})(1-\Omega^{2})} - \frac{\pi^{3}S\Omega^{6}}{4(1-4\Omega^{2})(1-\Omega^{2})} - \frac{\pi^{3}S^{2}\Omega^{6}}{4(1-4\Omega^{2})(1-\Omega^{2})}.$$
(E.4)

This coefficient function becomes active only when the superharmonic resonance  $\Omega \approx (\frac{1}{3})$  occurs. Under this condition, it becomes

$$f_{8_1} = \frac{-5}{64\pi} + \frac{17\pi}{2160} - \frac{\pi^3}{5760} + \frac{461\pi S}{23040} - \frac{\pi^3 S}{1440} - \frac{\pi^3 S^2}{1440} \,. \tag{E.5}$$



#### Bibliography

- [1] A.G. Erdman A. Midha and D.A. Frohrib. An approximate method for the dynamic analysis of elastic linkage. *Mechanisms. Trans. ASME, Journal of Engineering for Industry*, 99(B):449-455, 1977.
- [2] A.G. Erdman A. Midha and D.A. Frohrib. Finite elemet approach to mathematical modeling of high-speed elastic linkages. *Mechanism and Machine Theory*, 13:603-618, 1978.
- [3] G.N. Sandor A.G. Erdman and R.G. Oakberg. A general method for kinetoelastodynamics analysis of mechanisms. *Mechanisms. Trans. ASME, Journal of Engi*neering for Industry, 94(B):1193-1205, 1972.
- [4] I. Imam A.G. Erdman and G.N. Sandor. Applied kineto-elasto-dynamics. Proceedings of the second OSU Applied Mechanisms Conference, Stillwater, Oklahoma, 1971.
- [5] R. Cohen A.H. Neubauer Jr. and Jr. A.S. Hall. An analytical study of the dynamics of an elastic linkage. Trans. ASME Journal of Engineering for Industry, 88(B):311-317, August 1966.
- [6] R.M. Alexander and K.L. Lawrence. An experimental investigation of the dynamic response of an elastic mechanism. *Trans. ASME Journal of Engineering Industry*, 96(1), Feburary 1974.
- [7] R.M. Alexander and K.L. Lawrence. Experimentally determined dynamic strains in an elastic mechanism. Trans. ASME Journal of Engineering Industry, 97(3), August 1975.
- [8] M. Badlani and W. Kleirlenz. Dynamic stability of elastic mechanisms. Trans. ASME Journal of Mechanical Design, 101:149-153, 1979.
- [9] M. Badlani and A. Midha. Effect of internal material damping on the dynamics of a slider-crank mechanism. Trans. ASME Journal of Mechanisms, Transmission, and Automation Design, 105(3):452-459, 1983.
- [10] S. Chow. Nonlinear Effects of Large Deflection and Material Dampings on the Steady State Vibrations of Beam. PhD thesis, University of Minnesota, 1965.
- [11] S. Chu and K.C. Pan. Dynamic responses of a high-speed slider-crank mechanism with an elastic connecting rod. Trans. ASME Journal of Engineering for Industry, 97:542-550, 1975.
- [12] D.L. Cronin and H. Liu. Finite element analysis of the steady-state behavior of flexible mechanisms. In The First National Applied Mechanisms and Robotics Conference, Cincinnati, Ohio, November 1989.

- [13] A. Midha D.A. Turcic and J.R. Bosnik. Dynamic analysis of elastic mechanism system: Part 2: Experimental results. Trans ASME Journal of Dynamic Systems, Measurement and Control, 106:255-260, 1984.
- [14] E. Doedel. Auto: A program for the automatic bifurcation analysis of autonomous systems. Congressus Numerantium, 30, 1981.
- [15] S. Dubowsky and J. Maatuk. The dynamic analysis of elastic spatial mechanisms. Proceedings of the IV World Congress on Machines and Mechanisms, University of Newcastle-Upon-Tyne, England, 1975.
- [16] Clive L. Dym and Irving H. Shames. Solid Mechanics, A Variational Approach. McGraw-Hill, New York, 1973.
- [17] A.G. Erdman and G.N. Sandor. Kineto-elastodynamics a review of the state of the art trends. Mechanism and Machine Theory, 7(1):19-33, 1972.
- [18] M.V. Gandhi and B.S. Thompson. The finite element analysis of flexible components of mechanical systems using a mixed variational principle. *Mechanisms. Trans. ASME*, *Journal of Engineering for Industry*, 1980. ASME Paper No. 80-DET-64.
- [19] E.P. Golebiewski and J.P. Sadler. Analytical and experimental investigation of elastic slider- crank. *Mechanisms. Trans. ASME, Journal of Engineering for Industry*, 93(B):1266-1271, 1976.
- [20] Donald T. Greenwood. Principles of Dynamics. Prentice-Hall, Inc., Englewood Cliffs, N.J., 1969.
- [21] J. Guckenheimer and P. Holmes. Nonlinear Oscillations, Dynamical Systems, and Bifurcations of Vector Fields. Springer-Verlag, New York, Heidelberg, Berlin, 1983.
- [22] Alan C. Hindmarsh. Odepack, a systematized collection of ode solvers. In R. S. Stepleman et al., editor, Scientific Computing, pages 55-64. North-Holland, Amsterdam, 1983.
- [23] Housner-Hudson. Applied Mechanics-Dynamics. Van Nostrand, Princeton, N.J., 1959.
- [24] C.S. Hsu and Chen W.H. Steady-state response of a dynamical system under combined parametric and forcing excitations. *Journal of Applied Mechanics*, 1974.
- [25] G.N. Sandor I. Imam and S.N. Kramer. Deflection and stress analysis in high speed planar mechanisms with elastic links. *Mechanisms. Trans. ASME, Journal of Engineering for Industry*, 95(B):541-548, 1973.
- [26] G.G. Lowen and C. Chasssapis. The elastic behavior of linkages: An update. Mechanism and Machine Theory, 21:33-42, 1982.
- [27] G.G. Lowen and W.G. Jandrasits. Survey of investigation into the dynamic behavior of mechanisms containing links with distributed mass and elasticity. *Mechanism and Machine Theory*, 7(1):3-17, 1972.
- [28] P.K. Nath and A. Ghosh. Kineto-elastodynamic analysis of mechanisms by finite element method. Mechanism and Machine Theory, 15:179-197, 1980.

- [29] A.H. Nayfeh and D.T. Mook. *Nonlinear Oscillations*. Wiley Interscience, New York, 1979.
- [30] H.C. Lee P.W. Jasinski and G.N. Sandor. Stability and steady-state vibrations in a high-speed slider- crank mechanism. *Journal of Applied Mechanics*, 1970. ASME Paper No. 70-APM-UUU.
- [31] H.C. Lee P.W. Jasinski and G.N. Sandor. Vibration of elastic connecting rod of a high-speed slider- crank mechanism. *Trans. ASME, Journal of Engineering for Industry*, 93B:636 644, 1971.
- [32] F. Reuleaux. Theoretische kinematik: Grunduge einer theorie des maschinewesens (1985). Kinemtics of Machinery, English translation by A.B.W. Kennedy, (1876). Reprinted by Dover Publication, New Yrok (1963).
- [33] R. R. Ryan. Flexibility Modeling Methods in Multibody Dynamics. PhD thesis, Stanford University, 1986.
- [34] J.P. Sadler. On the analytical lumped-mass model of an elastic four-bar mechanism. Trans. ASME, Journal of Engineering for Industry, 97(2):561-565, May 1975.
- [35] J.P. Sadler and G.N. Sandor. A lumped approach to vibration and stress analysis of elastic linkages. Trans. ASME, Journal of Engineering for Industry, 95(2):549-557, May 1973.
- [36] J.P. Sadler and G.N. Sandor. Nonlinear vibration analysis of elastic four-bar linkage. Trans. ASME, Journal of Engineering for Industry, 96(2):411-419, May 1974.
- [37] G.N. Sandor and Xirong Zhuang. A linearized lumped parameter approach to vibration and stress analysis of elastic linkages. machanism and Machine Theory, 20(5), 1985.
- [38] J.C. Simo and L. Vu-Quoc. On the dynamic of flexible beam under large overall motions- the plane case: Part i. Trans. ASME Journal of Applied Mechanics, 53, december 1986.
- [39] J.C. Simo and L. Vu-Quoc. On the dynamic of flexible beam under large overall motions- the plane case: Part ii. *Trans. ASME Journal of Applied Mechanics*, 53, december 1986.
- [40] G.H. Sutherland. Analytical and experimental investigation of a high-speed elastic-member linkage. Trans. ASME Journal of Engineering for Industry, 98(3), August 1976.
- [41] I.G. Tadjbakhsh. Stability of motion of elastic planar linkage with application to slider-crank mechanism. Trans. ASME Journal of Mechanical Design, 104(4):698-703, 1982.
- [42] B.S. Thompson. The analysis of an elastic four-bar linkage on a vibrating foundation using a variational mehtod. *Trans. ASME Journal of Mechanical Design*, 102(2):320-328, 1980.
- [43] B.S. Thompson and R.P. Ashworth. Resonance in planar linkage mechanism mounted on vibrating foundations. *Journal of Sound and Vibration*, 7(3):403-414, 1976.

- [44] B.S. Thompson and A.D.S. Barr. A variational principle for the elastodynamics motion of planar linkages. SAME Transc. Journal of Engineering Industry, 98(4):541-548, 1976.
- [45] B.S. Thompson and C.K. Sung. A survey of finite element techniques for mechanism design. *Mechanism and Machine Theory*, 21(4):351-359, 1986.
- [46] S. Timoshenko. Vibration Problem in Engineering. Van Nostrand, Princeton, N.J., 1990.
- [47] D.A. Turcic and A. Midha. Dynamic analysis of elastic mechanism system: Part 1: Applications. Trans ASME Journal of Dynamic Systems, Measurement and Control, 106:249-254, 1984.
- [48] D.A. Turcic and A. Midha. Generalized equations of motion for the dynamic analysis of elastic mechanism systems. *Trans ASME Journal of Dynamic Systems, Measurement and Control*, 106:243-248, 1984.
- [49] B.V. Viscomi and R.S. Ayre. Nonlinear dynamics response of elastic slider crank mechanism. Trans. ASME, Journal of Engineering for Industry, 93(B):251-262, 1971.
- [50] S. Wiggins. Intorduction to Applied Nonlinear Dynamical Systems and Chaos. Springer-Verlag, New York, Heidelberg, Berlin, 1990.
- [51] R.C. Winfrey. Elastic linkage mechanism dynamics. Trans. ASME, Journal of Engineering for Industry, 93:268-272, 1971.
- [52] R.C. Winfrey. Dynamical analysios of elastic link mechanism by reduction of coordinates. Trans. ASME, Journal of Engineering for Industry, 94(B):577-582, 1972.
- [53] Hong Hee Yoo. Dynamic Modeling of Flexible Bodies in Multibody Systems. PhD thesis, University of Michigan, 1988.
- [54] Z.G. Zhu and Y. Chen. The stability of the motion of a connecting rod. Trans. ASME Journal of Mechanisms, Transmission, and Automation Design, 105(4):637-640, 1983.

MICHIGAN STATE UNIV. LIBRARIES
31293007663598